The Synthesis of Polymeric Materials as Living and Self-healing Systems.

E. B. SHARP

PhD

2022

The Synthesis of Polymeric Materials as Living and Self-healing Systems.

Elliot Bryce Sharp

A thesis submitted in partial fulfilment of the requirement of the University of Northumbria at Newcastle for the degree of Doctor of Philosophy.

Research undertaken in the Department of Applied Sciences.

June 2022

In loving memory

Robert Andrew Downs

(1986-2020)

Mathew Robinson

(1994-2019)

Stan Collingwood

(1947-2019)

To my loving family,

Thank you for your support, guidance and reassurance throughout this journey, you are the key reason to my success.

“It always seems impossible until it’s done.”

- *Nelson Mandela*

Acknowledgements

Firstly, I would like to thank Professor Justin Perry for giving me the opportunity to embark upon this project along with his knowledge, support, and patience throughout this research. I would also like to thank Dr Robert Downs and Bradley Thomas for their contributions in numerous aspects throughout this project. Thanks to Dr Matthew Unthank for his vast knowledge in polymer and surface substrate chemistry.

I would like to also say thank you to all Northumbria University staff in their help and support. A special thankyou to Gordon Forrest and Dr Karen Haggerty for their knowledge and time in contributing to numerous tasks in the lab.

As for my friends, a special thank you to Lee McCarron for being there for me in all my long days training and studying, and for always being a truly inspirational role model. Your motivation and encouragement have guided me through, helping me until the very end. I would also like to thank Thomas Hutchinson for his guidance in sport and studying through the final parts of my PhD. Your kindness and generosity is something I aspire to and cannot thank you enough.

Special thankyou to all my colleagues who worked with me in EBA510A and EBA606, who helped me make this project full of joyful experiences. I would like to extend my gratitude to Joe Watson for his help and laughter both inside and outside of university hours.

A huge contribution goes to my partner Laura Marriott who has not left my side throughout my final year. Her love and appreciation have helped me through challenging times along with her patience and understanding. I would truly not be here if it was not for you Laura, so thank you.

Finally, I would like to thank my family and friends who have been there with love and support whenever needed. Your generosity and kindness have allowed me to be who I am today and the key reason to my success. To my Mum, Dad, and sister Philippa, to whom I owe a great deal, thank you.

Declaration

I declare that the work contained in this thesis has not been submitted for any other award and that it is all my own work. I also confirm that this work fully acknowledges opinions, ideas, and contributions from the work of others.

Elliot Sharp

Signature:

Date: 08/05/2022

Abstract

Advancements in smarter materials will play a major role in reducing materials, energy use, pollution, and carbon emissions. This creates a need for research to devise new composite materials incorporating the latest technologies in fields such as whole-cell catalysts and self-healing methods to create biocomposite materials. Functional biocomposite materials can be produced by depositing immobilised microorganisms onto a surface of a substrate material in a flexible, non-porous polymer which can sustain living cells. Ideally these biocoatings should be easy to apply using manual draw down techniques or by ink-jet printing for well-defined patterns and show activity rates at least comparable with free-floating cells.

The focus of this thesis was to create a method for the development of multichannel 3D substrates, embedding immobilised cells within a polymer matrix to create a multifunctional bioactive coating. To achieve this, a latex polymer coating was synthesised using styrene, butyl acrylate and acrylic acid. This composition was adjusted to create several latex polymer samples with varying physical properties. Increases in styrene content correlated directly to increasing glass transition temperature and hardness. Latex polymers were subject to coalescing agents to enhance film formation and reported small changes in coating properties. Several feasible substrates were coated and analysed for adhesion and surface coverage, the highest performing were implemented into biocatalysis reaction assays. Assays when compared to equivalent cell suspension systems reported reaction rates up to five times that of suspended yeast cells.

Distribution of cells were analysed using fluorescent *E. coli* under confocal and scanning electron microscopes. The development of these techniques enabled the analysis of BL21 (DE3) competent *E. coli* cells containing a pOPINF plasmid to be immobilised into the co-polymer coating and cell survival measured through expression of a green fluorescent protein.

Latex polymer composites were used to immobilise two strains of cyanobacteria. *S. elongatus* PCC 7942 and CCAP 1479/1A were tested on loofah substrates for toxicity, adhesion, net CO_2 fixation rates and biological responses. CO_2 uptake was found to increase by 19 - 22 and 4 - 7-fold for CCAP 1479/1A and PCC 7942 for the best performing biocomposites relative to their suspension controls. While immobilized, CCAP biocomposites survived in excess of 12 weeks, however PCC 7942 biocomposites experienced cell leaching after 4 weeks.

A complex and high-resolution piezoelectric ink-jet printer was used to deposit small (<50 µm) latex-cell droplets onto a 3D laser-cut scaffold of a polyacrylic material which created a channeled network reactor. A continuous flow circuit was created and tested using a standard cell assay.

In parallel, a suite of self-healing polyurethane samples were synthesised and the optimal composition of alcohols and diisocyanate monomers investigated. To measure self-healing capabilities polyurethane samples were cut and rejoined after 1 and 24 hours. Samples were analysed using tensile strength testing and compared to identical uncut samples. The polymer was found to retain between of 63 - 98 % (after 24 h) and 33 - 61 % (after 1 h) of its uncut strength.

Contents

List of Abbreviations

AA	Acrylic acid
BA	Butyl Acrylate
°C	Celsius
CMC	Critical Micelle Concentration
DOD	Drop on demand
DSC	Differential scanning Calorimetry
g	Grams
GFP	Green Fluorescent Protein
GPC	Gel permeation chromatography
FDA	Fluorescein diacetate
FTIR	Fourier-transform infra-red spectroscopy
h	Hours
HV	Vickers Pyramid Number
IPAM	Imaging pulse amplitude modulation
ITPG	Isopropylthiogalactoside
Kg	Kilogram
LR	Low resolution
µg	Microgram
µL	Microlitre
µm	Micrometre
MFFT	Minimum film Formation Temperature
mL	Millilitres
mm	Millimetre

mmol	Millimole
nm	Nanomatre
M_n	Number average molecular weight
M_p	Molecular weight of highest peak
M_w	Weight average molecular Weight
M_z	Z-average molecular weight
NMR	Nuclear magnetic resonance
PD	Polydispersity index
PLA	Polylactic acid
ppb	Parts per billion
ppm	Parts per million
PU	Polyurethane
RPM	Rotations per minute
RT	Retention time
SEM	Scanning electron microscopy
Sty	Styrene
SD	Standard deviation
T_g	Glass transition temperature
THF	Tetrahydrofuran
UV	Ultra violet
V	Volts
VH	Vickers Hardness
WVTR	Water Vapour Transmission Rate
Wt %	Weight percent

1 Introduction

1.1 Overview

The aim of this project is to develop a biocomposite coating that immobilises microorganisms in a nanostructured porous water-borne polymer latex while maintaining their active components to enable biocatalysis reactions. To achieve this, a range of biocatalysis assays that can measure cell activity using different techniques require investigation. From this, successful candidates can be taken forward into immobilising into a synthesised latex polymer coatings to assess and compare activity levels to their suspended counterparts. With the aid of 3D printing to build scaffolds capable of supporting the biocomposite, and ink-jet printing enabling the deposition of the biocomposite coating at the micrometer scale, this will enable an alternative method for biocatalysis reactions using more advanced and efficient technologies. In addition to this, a polyurethane material was investigated, a bioinspired idea capable of self-healing at a molecular scale with the aim to synthesise different formulations and analyse self-healing capabilities using analytical techniques.

1.2 Whole cell biocatalysis

With recent advances in genomic and genetic engineering, research into biocatalysis for industrial synthetic chemistry is expanding rapidly. Biocatalysts can be single enzymes or whole living cells and both formats have a wide range of catalytic industrial applications. In correlation to this, the number of enzymes being engineered and analysed for biocatalysis is also increasing. [1] Biocatalysis has become a key tool for the production of pure small organic molecules due to the high stereospecificity and selectivity these enzymes possess. In particular, whole-cell catalysts containing specific enzymes have gained a lot of attention for industrial processes. A microbially-based process offers protection for the enzyme by virtue of the cell's structure, hence increasing its operational stability. Despite this advantage, industry continues to use largely isolated enzymes. [2] This is due to their high purity, reducing the potential for unwanted side reactions and minimising the potential for

biological contamination in the output of a reaction. Extensive research into biocatalysis has created applications in biological processes, textiles, health and disease, and food processing. [3, 4] Enzymes possess the ability to catalyse reactions under mild conditions in multiple formats. The most popular modes of use are suspended singular enzymes, in aggregates with other entities, or attached to surfaces. However, the majority of enzymes are unstable, and hard to recover when used as a singular enzyme in the suspension phase making this an expensive process. The incorporation of immobilised enzymes into industrial processes has in some cases increased both technical performance and economy. [5] Further development of immobilisation techniques has seen applications grow into areas in diagnostics, biosensors and bioaffinity chromatography, indicating there are a range of methods to connect a protein to a solid support and retain activity. [6] A successful enzyme system requires a combination of an enzyme, a support, and a mode of attachment. There is no single dominant form in regards to the type of support used for biocatalysts, however the support characteristics usually desired are physical resistance to pressure, hydrophilicity, minimal inter-reactivity with enzymes, bio-compatibility, microbial resistance and low cost. [7]

Biocatalysis is usually defined as the use of natural substances such as enzymes from biological sources to increase the rate of which a reaction occurs. Enzymes as catalysts in chemistry have been developed and studied from the early 1900's and have now developed into an important alternative to nonbiological catalysts. Biocatalysts offer a more sustainable approach to industry, often offering reduced by-products and energy consumption. Additionally, enzymes have been shown to be stable in a range of different conditions and can be used for extended periods before replacement is needed. [8, 9] This makes them ideal for batch reactions where the reliability of the catalyst is a direct variable to the cost of purchase. Biocatalytic reactions have the option to be performed in aqueous environments offering lower solvent expenses, and potentially a safer working environment. Despite this, there has been an increase in the number of reactions incorporating organic solvents into biocatalyst systems in the past 10 years. This is because organic solvents allow a higher substrate

loading and prevent the hydrolysis of water-sensitive compounds. [10] Engineered enzymes have been produced that can catalyse reactions in organic solvents with partial aqueous conditions. Protein engineering has also provided solutions to problems such as level of expression, stability, specificity, and activity by providing tailored alterations in amino acid sequencing.

Selecting the correct biocatalyst is often decided by selectivity, stability, and activity, of which are all highly important in all types of catalysts. Enzymes are highly active and stable in moderate temperatures and pH values and are often very specific in selectivity which allows a clean step conversion but can limit the range of substrates. Enzymes contain a highly complex chiral 3D structure which can confer high stereoselectivity leading to complex chiral molecules. It is this inherent chirality that has driven adoption of enzyme-based synthesis in the pharmaceutical and fragrance industries. The food and beverage industry has also seen an increase in the use of enzyme biocatalysis due to the potential lower toxicity and hazard to health in comparison to chemocatalysis.

1.2.1 Applications

Biocatalysis has developed into a viable alternative to chemical synthesis with research focused on the synthesis and resolution of optically active intermediates. [11, 12, 13] Rapid advances in biocatalysis are mainly due to the discovery of new enzyme variants which is possible by bioinformatics or computational modelling. [14] Despite an immense range of naturally occurring microbial enzymes, it is very rare to find a naturally occurring enzyme in possession of all the desired features for immediate use in industrial applications, and so methods for optimisation of biocatalytic methods are common in research literature.

Chiral amines are present in more than 90 % of the world's top-selling and newly approved small molecules found in the pharmaceutical industry. One of the most versatile methods for the synthesis of optically pure chiral amines is the amine transaminase (ATA) reaction in which the conversion of a carbonyl to an amine is observed (Scheme 1.2.1). Transaminases are of interest due to their ability to use a broad range of amine donors and acceptors. An example of this is the production of the anti-hyperglycemic drug sitagliptin (Janumet®) (Figure 1.2.1) worth $6 billion in revenue in 2016. [15] Other examples include the antiretroviral drug lopinavir (Figure 1.2.2), the adrenergic antagonist dilevalol (Figure 1.2.3), and the Alzheimer's drug rivastigmine (Figure 1.2.4). [16, 17] Previous chemical synthetic routes for these compounds reported low chiral selectivity along with low efficiency and considerable environmental impact. [18] However, there are still some challenges to be overcome for transaminase biocatalysis including unfavorable thermodynamic reaction equilibria, limited substrate bonding and inhibition by substrate or product. Efforts have been made in order to combat these problems by increasing the size of the ATA active site and hence reducing steric constraints to accept bulky substrates. [19] There is no doubt that ATA's hold huge potential in the development of innovative routes for the synthesis of chiral amines using engineered enzyme variants that combat substrate challenges and stability and allow the integration into industrial syntheses.

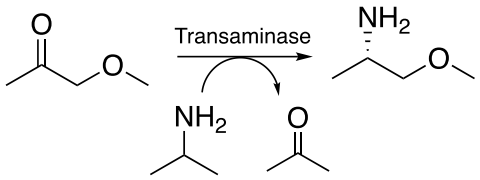

Scheme 1.2.1- Transaminase-catalysed reductive amination.

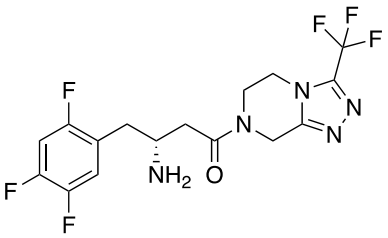

Figure 1.2.1 - Sitagliptin

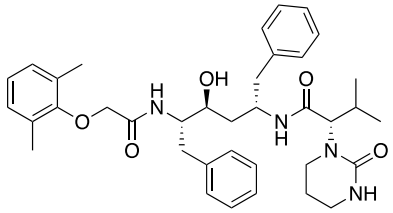

Figure 1.2.2 - Lopinavir

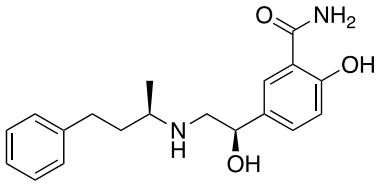

Figure 1.2.3 - Dilevalol

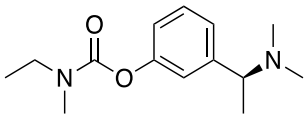

Figure 1.2.4 - Rivastigmine

1.2.2 Immobilisation techniques

Using enzymes as a catalyst can be uneconomic on the basis of the cost implications of their use. Their high purchase costs due to their extensive purification and isolation techniques can make them more expensive than chemocatalysts. Their sensitivity to pH, temperature and substances at trace levels can denature or inhibit the active site making them more fragile than chemocatalysts. To overcome these challenges, enzymes can be fixed within or onto a solid structure which mimics the protection of an organelle. This process is commonly called immobilisation, and can offer robustness, while still allowing the enzyme to perform the same reactions as suspended enzymes. Furthermore, immobilised enzymes allow easy separation of products and enzymes with the additional bonus of multiple uses (making their use more economical). There are few reported drawbacks when considering enzyme activity when comparing immobilised to suspended enzymes. Enzyme access to substrates can be reduced if there is difficulty with the substrate penetrating the immobilisation matrix. [20]

Immobilisation techniques have developed with the aid of reversible and irreversible methods (Figure 1.2.5). Reversible techniques refer to the complete desorption of the enzyme away from the support when the immobilised derivative becomes inactivated (enzyme cannot be further used). The supports can then be recovered fully intact and can be ready to be used again for a fresh enzyme. This not only reduces production costs and materials, but eliminates the difficult task of waste disposal (specifically enzyme immobilised polymer resins). [21] Other reversible methods include the reversible covalent bond of disulfides. This is a popular method when the enzyme to be immobilised contains exposed thiol groups enabling immobilisation onto thiol reactive supports under mild conditions. However, applications for this are not limited to thiol enzymes as enzymes containing unreactive or no thiol groups can be modified chemically or engineered in order to provide them with the necessary functionality. [22]

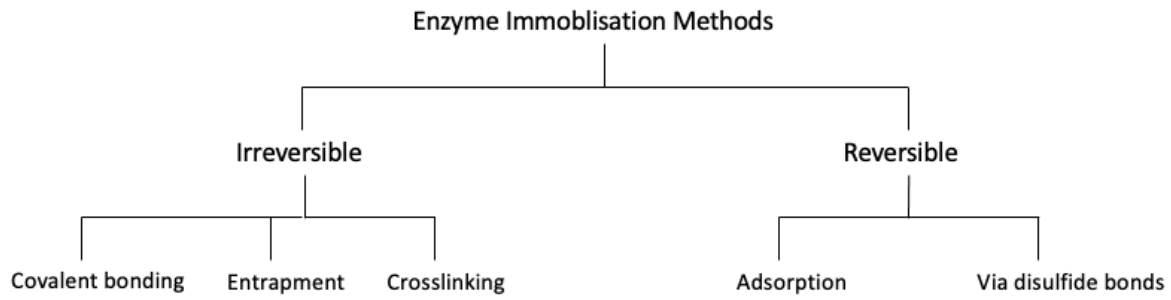

Figure 1.2.5- Enzyme immobilisation methods.

Although reversible methods seem to offer all the necessary advantages for immobilisation, some enzyme applications may not require such complicated and costly methods. Covalent binding of an enzyme to a carrier enables a tightly fixed immobilisation. Because of this, enzyme leaching is low, and contamination of product is rarely observed. Covalent immobilisation can be used in any medium, unlike adsorbed enzymes that are usually applied in organic solvents to avoid leaching. An extreme type of covalent binding is crosslinking of enzymes with the aid of a di-functional agent to make cross-linked enzyme aggregates (CLEAs). This technique consists of first aggregating the enzymes, which involves the addition of a precipitant such as acetone and ethanol followed by a

crosslinking agent such as glutaraldehyde. CLEAs show significantly enhanced shelf-life and stability and are easy to recover and reuse. [23] Other irreversible methods include entrapment, involving the capture of enzymes within a polymeric network that allows the substrate and products to pass through the network whilst retaining the enzyme. The process requires the enzyme to be trapped rather than previous methods of being bound to the matrix. One of the most popular routes for entrapment is through the encapsulation of enzyme in calcium alginate beads which is instantaneous, nontoxic, inexpensive, and versatile. Because enzymes are not bound or chemically bonded to the matrix (and less likely to cause direct changes to the cell or enzymes functions), it is one of the least disruptive immobilisation methods.

1.3 Biofilms

Biofilms are densely packed surface-associated communities of microbial cells that grow on living or inert substrates. Microbial communities use immobilisation in biofilms to anchor themselves in specific locations and offer a model for immobilisation across 3D surfaces. An established biofilm structure contains not only microbial cells but an extracellular polymeric substance and an optimum environment for exchange of genetic material between cells. [24] A primary example of a naturally occurring biofilm is dental plaque. Plaque contains about 80 – 90 % water (w/w) with 70 % of the remaining dry weight being various bacteria, and 30 % consisting of polysaccharides and glycoproteins. [25] Microorganisms that form the biofilm in plaque are mostly *Streptococcus mutans* (60 – 90 %) and other anaerobes such as fusobacterium and actinobacteria. These early colonisers adhere to the clean surface of the tooth almost instantly and allow secondary colonisers to then grow. Biofilm organisms develop on a wide range of interfaces and are embedded in a self-produced extracellular polymeric substance in which they live within “pockets”. These microbial systems are governed by the structure, diffusion and physiological activity of the community. [26] Organisms with the ability to create biofilms are often spatially well-structured, are usually self-regenerating and more resistant to toxic reagents. Their durability makes them ideal biocatalysts for applications. [27]

Not all bacteria are able to create a biofilm themselves, some microorganisms live in symbolic cell/matrix pairs such as lichens (Figure 1.3.1). Lichens are composite organisms whereby a stable symbiotic relationship between a fungus and algae/cyanobacteria occur. [28] The algae or cyanobacteria can produce simple sugars by photosynthesis, unlike fungi that require external food source. In return, the algae or cyanobacteria benefit from an optimum living environment which enables them to survive as a stable long-term association. If the microorganism cannot achieve this, their use in a biofilm will need an alternative matrix, this has led to extensive research to find synthetic alternatives capable of supporting these bacteria. These synthetic alternatives are usually a composite material based on a porous polymer film. Commonly used polymer latexes are synthesised by radical polymerisation and have had a great deal of attention due to their wide range of coating applications including household emulsion paint and adhesives. A wide range of synthetic polymers have been developed as components of coatings and are suited for artificial biofilms. Comparing the material properties of biofilms and those available from synthetic polymers, there is clear potential to integrate the two areas of research.

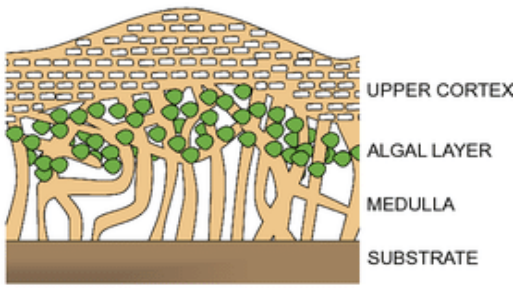

Figure 1.3.1- Structure of a lichen biocomposite. [28]

1.4 Radical Polymerisation

Radical polymerisation remains one of the most widely used types of polymerisation. It involves the addition of monomer molecules *via* radical species, whereby the growing chain radical attacks the π bond of a monomer causing it to break homolytically. One electron from the π bond forms a bond with the unpaired electron from the terminal carbon group of the chain radical. The remaining π bond electron moves to the other carbon double bond which becomes the new active radical site. This process is repeated during the addition of monomer molecules until they are depleted. A typical radical polymerisation reaction can be divided into three main stages: initiation, propagation, and termination with the addition of chain transfer reactions that occur in most chain polymerisations.

1.4.1 Initiation

There are two ways in which initiation can occur, the first is through the formation of free radicals sourced from an initiator, the second involves the addition of one of these free radicals to a monomer molecule. Free radicals can be formed from homolytic scission or a transfer of an electron to an ion or molecule. Homolytic scission involves a single bond in which the two bonding electrons split either side of the original bond towards either atom associated to the bond. This creates two radical species and can be due to the application of heat (Scheme 1.4.1). The same process can also be done using ultraviolet light as a source of activation energy (Scheme 1.4.2). Redox reactions can also be used in the creation of free radicals for polymerisations at low temperatures (<50 °C). The reaction requires a charged ion and a molecule containing a peroxide bond. In most cases the ion will donate an electron to the peroxide molecule. This splits the peroxide bond creating a radical and other ions. [29]

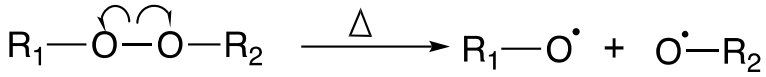

Scheme 1.4.1- Homolytic scission to create two free radical species.

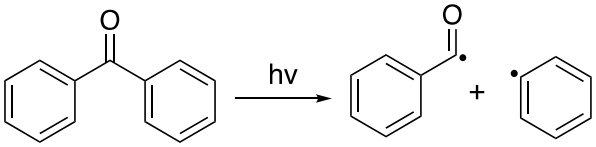

Scheme 1.4.2-Radical formation from benzophenone using UV light.

1.4.2 Propagation

In the propagation stage, monomer is added to promote the growth of a polymer chain. In this growth two types of addition can occur (Scheme 1.4.3). The predominant addition is called head-to-tail, however the addition reaction is decided through which part of the molecule the radical will attack. This is decided by steric hindrance. On the rare occasion head-to-head addition occurred, it would be immediately followed by a tail-to-tail addition to generate the more stable active centre to continue the predominant head-to-tail addition.

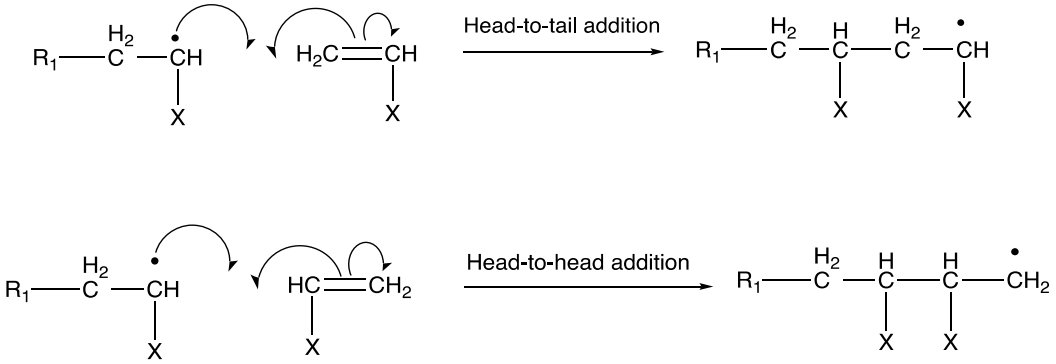

Scheme 1.4.3- Head-to-head and head-to-tail addition steps.

1.4.3 Termination

The termination step involves the irreversible coupling of two growing chains. This occurs when both radicals react with one another to create a single polymer chain. This polymer chain is subject to a

head-to-head linkage and corresponding R groups at either end of the polymer chain (Scheme 1.4.4) Other forms of termination include disproportionation which involves the abstraction of a hydrogen atom from a carbon atom from one of the growing chain radicals. The remaining electron joins with the unpaired electron to create a π-bond. Disproportionation creates shorter chains compared to the previous termination step due to both radical chains terminating without joining together (Scheme 1.4.5). Both types of termination take place in polymerisation but the extent of each one depends on factors such as temperature and monomer choice. The excess of alkyl chains in some polymers can provide hydrogens for disproportionation to occur more readily.

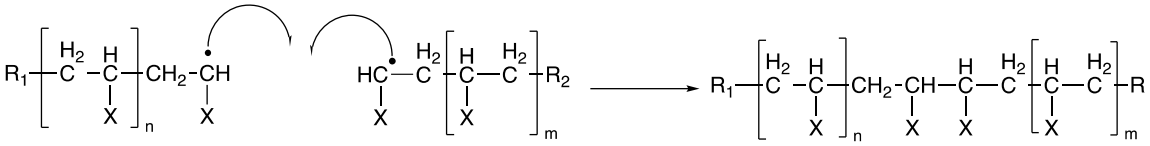

Scheme 1.4.4- Termination step consisting of two radical chains forming a single polymer chain (m/n represents the repeating unit for the polymer chain).

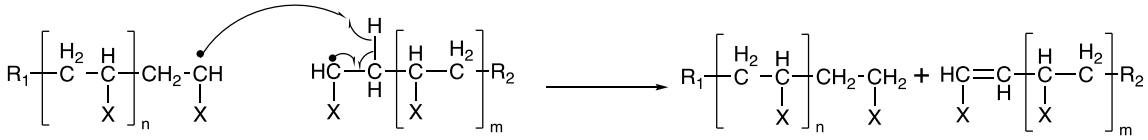

Scheme 1.4.5- Termination step using disproportionation (m/n represents the repeating unit for the polymer chain).

1.4.4 Emulsion polymerisation

Emulsion polymerisation is a heterogeneous polymerisation process. The process requires the initiator solution to be soluble in the aqueous dispersion medium but not in the monomer. A latex is defined as a colloidal suspension of polymer particles stabilised by dispersing agents in an aqueous medium. The dispersing agents used are usually ionic, non-ionic or copolymer surfactants that are made from monomers with different hydrophobicities. [30] When using the word latex, it often

becomes interchangeable with emulsion due to emulsion polymerisation being the most common technique to formulate a latex. This technique is one type of heterophase polymerisation involving organic and aqueous phases. Polymers prepared via heterophase polymerisation can then be synthesised into a polymer dispersion in water with the addition of surfactant. These anionic surfactants (1-5 wt % of monomer solution) consist of two parts. One part contains a hydrophilic hydrocarbon chain and the other a hydrophobic anionic head group with an associated counterion (Figure 1.4.1). Surfactants usually possess a low molecular solubility in water due to their hydrophobic tails. This is due to the structure they form once critical micelle concentration (CMC) is exceeded. When the CMC limit is reached, the surfactant molecules position themselves into spheres known as micelles measuring 5 nm in diameter (depending on the surfactant). In most cases, micelles position themselves so that hydrophilic heads are facing on the outside of the sphere and hydrophobic tails are based within the inside. This means hydrophilic heads are in contact with the dispersion medium (usually water) and allows micelles to absorb considerable quantities of insoluble substances. [31] This property has made them considerably effective in the use of detergents and soaps through the absorbance of grease and oil. Emulsion polymerisation processes can be inconsistent, producing varied molecular weights and functional distributions. Acrylate, styrene and diene based latexes are a common copolymer system in industry due to their cost-effective formulations and adhesion capabilities on substrates.[32, 33, 34] Polymer to solvent mass ratios are typically 50 : 50, with surfactants usually being added to ensure stability of finely dispersed particles. [35]

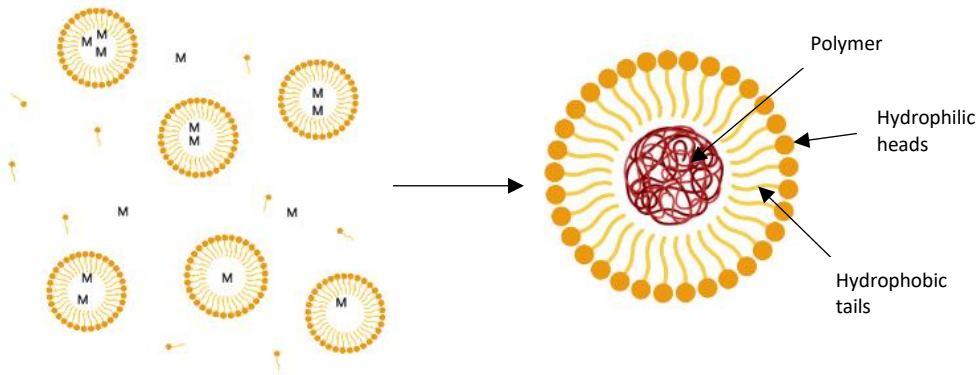

Figure 1.4.1- Micelle, surfactant, and monomer formations within emulsion polymerisation.

1.4.5 Particle nucleation

The start of the emulsion polymerisation process begins with particle nucleation. This process is only feasible once the concentration of the surfactant is above the critical micelle concentration. In this stage, depending on the monomer used, one mechanism predominates the other. Monomer molecules that are dissolved in the aqueous phase react with free radicals produced by the initiator solution to produce oligomeric radical species. These species will propagate multiple times in the aqueous phase. At this stage several different situations can occur. Firstly, termination in the aqueous phase can produce small species similar to the surfactant. Secondly, chains may continue to grow until they reach a critical degree of polymerisation. [36] Exceeding this point, chains will become surface active and grow further until reaching another critical degree of polymerisation. Eventually precipitation will occur due to the radicals becoming insoluble in the aqueous phase. Oligomeric radicals can absorb and diffuse in monomer swollen micelles and can initiate polymerisation. [37] The monomer swollen micelles continue to grow due to being supported by absorption of monomer from the aqueous phase. When the polymer exceeds the size of the original micelles, the surfactant becomes absorbed and is aided by additional surfactant to maintain stability. The surfactant sourced from unreacted micelles, and the monomer inside these micelles is redistributed throughout the system. Eventually all surfactant molecules will be consumed, ending particle nucleation.

Hydrophobic monomers that possess low solubility in water usually control this process. [37] Monomers such as methyl acrylate have high solubilities in water and undergo homogeneous nucleation. Different to micellar nucleation, the oligomeric radical continues to propagate in the aqueous phase until at which point the chain radical collapses and becomes a primary particle whilst retaining the radical site at the end of the chain. The primary particles continue to absorb surfactant and monomer due to the other end of the chain derived from the initiator. The chain continues to propagate, creating latex particles. Nucleation is only terminated once the number of formed particles is high enough to ensure that all radicals will be captured. [31]

1.4.5.1 Particle growth

Particle growth continues by the diffusion of monomer through the aqueous phase from the monomer droplets. To ensure the concentration of monomer within a particle remains the same, the rate of monomer diffusion needs to be higher than the rate of polymerisation. Once the process exhausts all monomer droplets, the rate of polymerisation declines as the last monomer droplets are polymerised.

1.4.5.2 Miniemulsion polymerisation

Emulsion polymerisation and miniemulsion polymerisation undergo the same process in which the formation of droplets is dispersed in medium. However, in miniemulsion, the number of particles in the solution is controlled via the addition of a miniemulsion prior to the polymerisation. This comprises of small (50-300 nm) monomer droplets in larger numbers to efficiently capture all radicals. The particle nucleation process is then subject to miniemulsion monomer droplets. Polymerisation continues inside the miniemulsion droplet until the particle becomes swollen where the process proceeds the same way as in emulsion polymerisation. The development of miniemulsion polymerisation methods have also helped to create hydrophobic and hydrophilic latexes which would be hard to synthesise under standard emulsion polymerisation.

1.4.6 Applications of emulsion polymerisation

Emulsion polymerisation offers several advantages over polymerisation techniques. Excellent heat transfer is observed, and high polymer concentrations can be synthesised easily. Due to the little use of volatile organic compounds used in this method, emulsion polymerisation is also seen as an environmentally friendly alternative due to its water-borne properties. Because of these factors, latexes are becoming widely used in applications such as paints, adhesives, binders, thermal plastics, and synthetic rubbers.

1.5 Latex polymers systems

The coatings industry has benefitted extensively from the development of latex systems. They can be synthesised with high precision and with engineered properties for desired applications. Latexes have taken the interest of recent research in the paints, paper coating, adhesives, textile sizing and inks industries. [38] Particular interest are the blends of small and large particles and film forming and non-film forming particles. [39]

Waterborne latex polymer coatings have become ideal scaffolds due to their cheap production rates and film forming capabilities, making them perfect for immobilising and sustaining larger organic materials. The entrapment of various compounds within coatings has already been introduced with a range of metals and additives being analysed. The research led to applications in areas such as antimicrobial paints. [40] These systems are an important tool to reduce and remove any biological colonization from bacteria that can influence human health. Mould growing in an indoor environment can contribute significantly to air contamination and hence human health deterioration. These paints usually contain silver or copper, especially when they are added in the form of monodispersed particles. However stability of these particles can be aided by the addition of silica microspheres containing immobilised silver and copper particles. [41] Coatings can be conditioned to become resistant to microbes such as fungi, viruses, and bacteria. These coatings are now used in hospitals to maintain sterile equipment and high use areas. Bellotti *et al*. reports the

study of silver, copper, and zinc oxide nanoparticles upon the growth of *C. globosum* and *A. alternata* using agar plate assays. The effects were seen to inhibit growth proportional to the concentration of silver and copper nanoparticles tested. [42]

1.5.1 History of latex polymer integrated systems

Studies involving latex microbial coatings began in the 1980's by Lawton, Bunning and Flanagan who described the successful use of bioactive polymer latex to coat solid particles, nylon mesh, membranes, and silica. They reported the use of acrylate and vinyl acetate monomers that were polydispersed using a particle size of 260 nm and a glass transition temperature of 13 °C. To create a porous texture, calcium carbonate was used as an additive to increase porosity within the coating. Once dry, the calcium was removed from the coating using dilute aqueous acid. Once washed to neutral pH, the pores created spaces required for microbial sustainability. [43] Since this, a range of different latex compositions, additives and bacteria have been reported to be successfully immobilised to form latex polymer coatings. [38, 44, 45]

Cantwell *et al.* reported the use of polymer blends ranging in glass transition temperature from -60 to 60 °C using a polymer matrix to create a stable enzyme system. Coatings were applied to a range of different substrates with a coating of 1 - 2 mm flocculates, thicker than the thin films that are being developed today. However, no data was published on cell viability following entrapment. Following this research, Flanagan *et al.* immobilised *Penicillium chrysogenum* in a range of film thicknesses. Using this technique enabled a bioreactor that was capable of producing *penicillin G* in a system that was 3-6 times the productivity of the standard free-cell fermentation process. [46]

Martens *et al.* prepared thin films using a methacrylate and acrylate copolymer to allow photosynthetic *Synechocoous* to be immobilised into polymer films. In doing so they produced a photoreactive biocoating on a carbon electrode. Activity rates were close to 100 % (compared to isolated cells), like those encapsulated in calcium alginate. Long term stability was also similar to that of the alginate matrixes when stored in buffer or as a dry state. [47] However, limitations in coating

porosity, poor coating thickness, lack of method to quantify the concentration of cell survival rates, and the response of cells from film formation demonstrated the level of complexity of biohybrid systems. Prior to these reports, little knowledge was known on the characteristics and mechanism of waterborne film formation. Since then, research has seen developments in polymer coatings, cell adhesion methods, and cell survival methods with the advancements in cell engineering.

1.5.2 Glass transition temperature

The glass transition temperature (T_g) is the temperature at which an amorphous polymer material changes from a glass rigid state to a rubbery flexible state. It is a term used to describe changes in thermodynamic properties such as heat capacity and thermal expansivity and can be used as a useful factor in determining a materials application. The glass transition temperature relates directly to polymer cohesive energy and its packing density, which is subsequently related to chain flexibility, intermolecular interactions, and molecular weight. Below the T_g in an amorphous polymer, the molecules remain fixed in place causing a rigid material. Above the T_g, the polymer chains can move and become flexible and soft (Figure 1.5.1). However, this process cannot be integrated with melting points which happens in crystalline polymers. Melting is the process of polymer chains falling out of their crystalline structures into a disordered liquid. Amorphous polymers, depending on their applications can be used above or below their T_g. For example, plastics such as acrylic and polystyrene can be used below their T_g in their glassy state to create hard materials, while materials such as elastomers are highly rubbery and flexible due to their low T_g. However, in most applications it is not just one polymer that is utilised. To produce the desired physical properties usually a copolymer blend is employed. It is important to create a coating that has the correct copolymer composition to produce a polymer with the desired T_g. The T_g must be low enough to permit coalescence at the lowest application temperature but high enough to ensure coating durability. [48] It is not favorable for coalescence to occur unless the T_g is lower than the temperature at which they are formed. Typically, latex T_g's range from 0 – 25 °C so they can be formed and coalesced easily at

room temperature. If the desired T_g needs to be altered, the addition of a known hard or soft copolymer can influence the T_g. [49] The use of a cross-linker can also dramatically enhance hardness, block resistance and adhesion. [50]

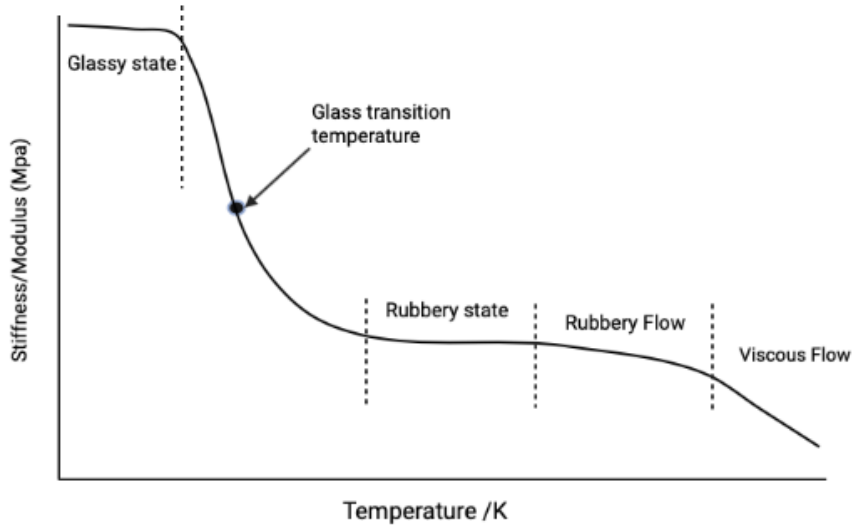

Figure 1.5.1- State changes in amorphous polymers.

1.5.3 The Fox Equation

Several approaches have been proposed for estimating the theoretical glass transition temperature in an amorphous polymer. One of the most widely used methods is the Fox equation (Equation 1.5.1), in which a calculation of a theoretical T_g can be established using properties of the pure components. The Fox equation represents the relationship in molecular weight upon glass transition temperature. This is also relevant to the addition in small molecule weight additives (plasticisers) to the polymer. The increase in small molecules increase the free volume hence lowering T_g.

$$\frac{1}{T_g} = \frac{w_1}{T_{g,1}} + \frac{w_2}{T_{g,2}}$$

w_1 Mass fraction 1

w_2 Mass fraction 2

$T_{g,2}$ Glass transtion temperature 1

$T_{g,1}$ Glass transtion temperature 2

T_g Glass transtion temperature

Equation 1.5.1- The Fox equation.

1.5.4 Alteration of polymer properties

Polymer blends (copolymers) are receiving increasing attention in literature due to their industrial possibilities. Finding a homogeneous polymer (a polymer with a single repeated chain) with multiple desired properties for applications can be challenging. To combat this, other monomer chains can be introduced into the polymer blend. This can not only change glass transition temperature, but can influence dry time, coalescence, hydrophobicity, and adhesion properties. Creating blends of polymers while conserving their individual properties in the final mixture is seen as an efficient and cost-effective way to develop new structural materials that can be synthesised for challenging applications.

The strength of forces between polymer chains are dictated by the interactions between polymer chains. This can involve hydrogen bonds, dipole forces and Van der Waals interactions. These interactions increase the rigidity of the polymeric material and hence increase the glass transition temperature. The strength and number of interactions found between chains depends on functional groups and chain lengths present. Polymer chains consisting of amide and polyamide function groups are more subject to hydrogen bonding. Numerous latex polymer coatings have been engineered using variations of acrylate/vinyl acetate based monomers. [51] These monomers are of low T_g and hence lose permeability due to wet coalescence. To solve this, harder T_g monomers such as styrene can be added to increase the polymer T_g and hence improve polymer particle wet

coalescence. This monomer ratio can be altered depending upon the necessary desired film forming characteristics. [52] Winnik *et al.* describes how soft and hard latex blends can be used to create films with reduced diffusion rates by the alteration in physical properties. The diffusion of poly(butyl methacrylate) (PBMA) was monitored using fluorescence energy transfer in films formed from poly(methyl methacrylate) (PMMA) and a high T_g shell made from styrene and acrylic monomers. In both cases the presence of these hard particles were found to have reduced diffusion of the PBMA. Further reductions in diffusion coefficient could be seen when increasing polymer concentration and reducing particle size.

Eckersely *et al.* investigated the combinations of hard/soft and small/large ratios of particle size to create desired film formation properties, resistance and mechanical properties. [49] Block resistance was significantly improved with the addition of a hard latex to a soft film forming latex even in ratios of 70:30. This was seen in addition of up to 50 % hard concentrations. Block resistance was widely altered with changing hard to soft ratios, however film properties remained constant. The best performance from each latex blend was the highest R_{soft} / R_{hard} value tested. Both hard and soft particles contributed to the properties of the film. Small hard particles were thought to be responsible in reinforcing the film's structure. When testing high size particle ratios, it was found the concentration of hard particles upon the surface of the film was also higher when analysed by SEM. Results concluded that blending the hard and soft polymer latexes can improve block resistance without compromising other chemical or physical properties.

1.5.5 Additives in polymer latex coatings

Coalescence is a vital part in creating a uniform film coating. The process involves changing from a liquid to a solid state, which can be difficult if not prepared effectively. The emulsified polymer that will become a latex film exists as tiny, suspended droplets of solid particles dispersed in water. During the drying process, water will evaporate from the solution and doing so will force the remaining latex particles closer to one another. When particle charges are no longer sufficiently

strong enough to repel each other, the particles collapse together creating a solid film. However, this is only likely to happen if polymer particles are soft enough to promote film formation. The coating will most likely crack or flake if latex particles are found to be too hard for coalescence, usually due to high friction between particles. Film formation is dependent on polymer composition. The temperature at which the polymer can no longer form a film is called the minimum film formation temperature (MFFT). Polymers that formed films easily have low MFFT values. These polymers do not usually show promising properties for applications such as paints due to their low durability and high tack adhesive properties. To create a paint with desirable properties, often a high minimum film formation temperature would be required (15 – 45 °C). However, in some cases it might be required for a coating to have a lower MFFT (near 0 °C) in this case a coalescing agent would be required. The purpose of a coalescing agent is to soften the latex polymer particles before the drying process to promote a uniform film. After this, the agent is required to evaporate slowly over time to maximise the film's physical strength. One of the most popular coalescing agents is Citroflex™ from Vertellus. These citric acid esters offer improved resistance to grease and are used as a plasticiser and film strengthening agent in hairsprays and nail polishes.

1.5.6 Film formation

Polymeric solutions possess a simple approach to film formation. The formulation of latex films involves three main processes; 1) consolidation- the evaporation of water to form a packed latex particle network, 2) compaction- particle deformation begins to eliminate areas between latex particles, and 3) coalescence- the coming together of nearby latex particles to create a uniform film. Figure 1.5.2 shows the film formation process in a latex polymer. The latex droplets are dispersed onto the substrate surface in suspension whereby the solvent starts to evaporate causing clumping and compaction forming a gel-state. This polymer chain interpenetration occurs at a specific concentration and varies upon solvent and polymer concentrations. This increased viscosity is called intrinsic viscosity and is an indication of the interactions between the solvent and polymer particles.

The rate of solvent evaporation is critical for good film formation and is affected by temperature, pressure, movement of air and humidity. [53] If evaporation is too slow the substrate becomes overwetted in which extreme cases lead to substrates becoming dissolved. If evaporation happens too quickly the remaining polymer particles might not have had time to spread onto the surface, leading to peeling. To promote the optimum rate of solvent evaporation, external conditions can be altered. The easiest and most influential is the drying temperature. Mesic *et al.* investigated the effects of drying temperature on film formation and barrier performance of a latex-based coating formulation. Coatings were deposited using a flexographic printing press onto paper absorbent substrates and dried at 25, 40, 50 and 75 °C. Samples were evaluated using water vapour transmission rate (WVTR) and water absorption at the substrate-coating interface. SEM imaging reported visible differences in the three samples. Fractures and cracking (100 µm) were observed in samples dried at room temperature and 40 °C. This is thought to be due to the slow evaporation of water allowing free movement of polymer particles to follow the receding waterfront during evaporation. High drying temperatures (50 and 75 °C) saw the formation of a closely packed system followed by high particle diffusion. This process led to no visible cracking at 75 °C. The report concludes film formation is highly dependent on drying temperature relative to rates of viscous deformation. Temperatures below 75 °C were found to be insufficient to ensure complete coalescence resulting in cracking and fracturing. [54]

Other conditions such as humidity can influence drying time. If humidity is too high during drying, evaporation rates decrease, causing defects to develop such as flash corrosion. [55, 53] For example, in industrial paints, iron salts can extract into the paint film before particle coalescence, which leads to the final coating becoming spoiled. [56, 57] Surfactant leaching can also be seen in paint drying under high humidity. Furthermore, the risks of reintroducing water into a dry coating film are high leading to coating defects.

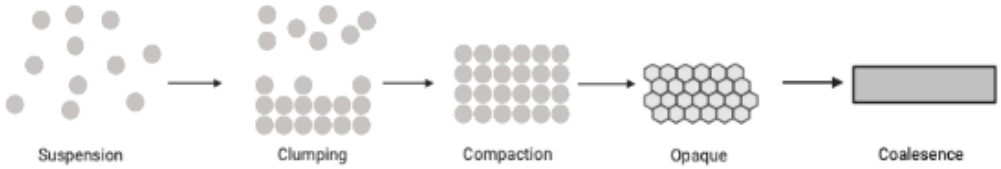

Figure 1.5.2- latex polymer film formation process.

1.5.7 Coating methods

Many film coatings used in modern day applications aim for a minimum thickness approach. This approach creates a cost-effective method with minimum waste and reduced total volume. Thin films (<100 µm) are considered vital in electronic devices, environmental applications, and energy storage devices. The most important factor when synthesising and depositing a thin film is its morphology and stability. Methods of deposition can be divided into two main techniques, physical and chemical (Figure 1.5.3). In the case of radical polymerised latex coatings, evaporation techniques are favoured due to their low VOC content and fast evaporation rates at room temperature (when using water). Other coatings require more extensive deposition methods, often with the aid of thermal vacuums, electron, or laser beams to enhance vaporization. More complex physical deposition techniques such as spluttering can be used when introducing the deposition of metal oxide films by controlling the crystalline structure and surface roughness. The process is subject to bombardment of ions to a target holding the coating molecules with a specific kinetic energy. This leads to the transfer of the required molecules to the substrate in a dense thin film. [58] Spluttering has several advantages over evaporation techniques including the use of high melting point materials, and the use of high vacuum processes. Applying this technique can be difficult to use when depositing uniformly onto complex substrate shapes.

Physical techniques for the deposition of thin films onto substrates as described previously create high quality and efficient methods. However, these methods can be costly in purchasing and machine maintenance, and often require a large target substrate surface area. The need for a cost-effective approach for the use in industry is therefore important. The sol-gel technique is popular in the synthesis of oxide materials and often requires cheaper and more accessible equipment. In this case the sol-gel technique is the transmission from a colloidal suspension to a viscous gel or solid material. This method is often used in metal alkoxides with the reaction of alcohols following a hydrolysis and condensation to create a hydroxyl or oxo bridge. [59]

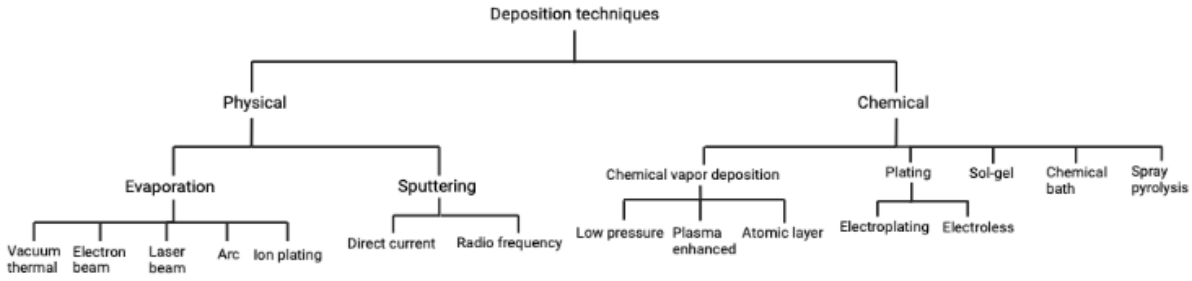

Figure 1.5.3- Possible coating methods for thin film formation.

Further advancements in deposition extend to not only coatings but immobilised coatings whereby bioactive films can be deposited onto substrates with the incorporation of living bacteria. Bernal *et al.* describes the method in which an external electric field-driven cellular assembly aids a deposition of concentrated sample of cyanobacteria onto flexible polyester substrates. To achieve this, the substrate was activated using layer-by-layer polyelectrolyte deposition. The cells were assembled using AC-electric field-induced long-range interactions producing linear chains of cells above the substrate. Normal to the substrate plane, dielectrophoretic forces localize the cells onto the polyelectrolyte surface maintaining their immobilised state when electric fields were removed. When compared to equivalent gravity settled samples coverage increased from 40 to 60 %. [60]

1.6 Microorganism Immobilisation

Numerous approaches have been established to prolong the lifetime of whole-cell biocatalysts, however any methods which use “free-floating" or suspended organisms involve extra costs because of filtration and purification. As a result, numerous immobilisation methods have been created involving physical confinement and/or chemical attachments. These techniques have both advantages and drawbacks. Overall, physical bonding provides a weaker method of immobilisation when used in industrial environments. Chemical techniques such as entrapment introduce the inclusion of an enzyme in a gel lattice and requires the synthesis of a polymer/gel network alongside the enzyme. However, complexes can be subject to diffusion rate issues whereby reagents are prevented from diffusing or conversely diffuse too quickly. This can be detrimental when using enzyme rate-dependent systems. Adsorption immobilisation can be a cheap and effective route, but it is too easily reversible in most cases. Covalent attachments and cross-linking are durable in the use of industrial applications but are expensive and risk effective enzyme performance. It is therefore clear the method of immobilisation is highly dependent on enzyme properties, industrial methods and their associated practicality and cost.

A modern-day route to creating a viable process of immobilisation capable of supporting and sustaining enzymes is through their integration within a synthetic latex polymer (Figure 1.6.1). The polymer matrix can be synthetic, bio-based or even inorganic, as these have been shown to support enzyme activity and contain as high as 50 % by volume of viable cells. [61, 62, 63] How the enzymes can be used is determined by the interactions between the enzyme and the synthetic polymer support (Figure 1.6.2).

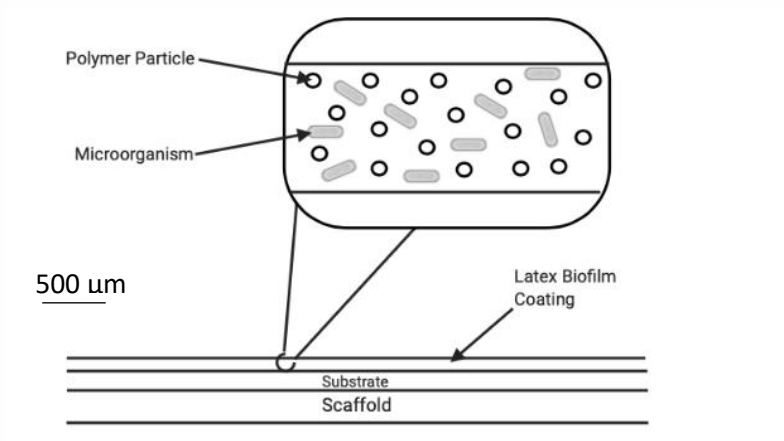

Figure 1.6.1- A bioactive coating structure.

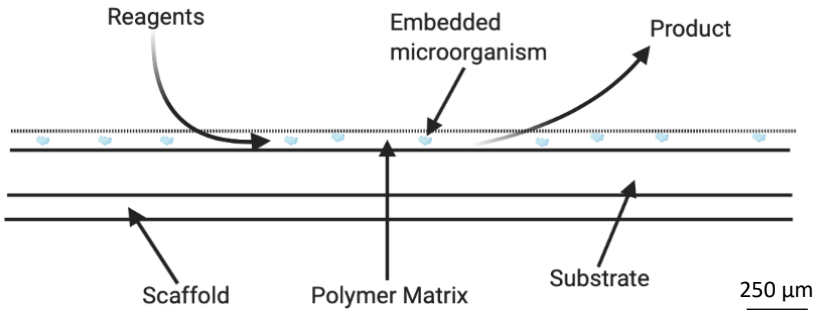

Figure 1.6.2- Basic bioactive coating method.

Biocatalytic coatings consist of nonporous voids produced by partially coalesced polymer particles. These spaces between particles allow entrapment and sustainability of microorganisms in a wet habitat, even once the external polymer coatings are dry. Deposition of these coatings can vary using methods such as ink-jetting, spreaders or aerosol sprays producing thin films of 2 - 200 µm containing 10^{10} to 10^{12} per m^2 of non-growing microorganisms. [38]

Over the past 30 years, biocoatings have seen extensive research due to their wide range of possible applications. Biocoatings combine the selective functionality of highly concentrated microorganism communities with nanostructured soft materials and water-borne adhesive coating technologies. [64]

The increase in interest is due to not only biocatalysis, but their ability to control gas adsorption due

to their large porous surface area. The immobilisation of a high concentration of microorganisms onto a surface is an efficient and cost-effective way of converting what would be an inert substrate into a bioactive platform. Synthetic biocoatings allow a means to concentrate enzyme activity in a desired area while utilising hosts to synthesise and then maintain these biochemical systems. [44] The formation of coating microstructure and adhesion in waterborne latex coatings relies upon the nanostructure of the films, which in turn determines their physical and mechanical properties. Nanostructure can be manipulated via altering component ratios, coating methods, drying times and substrates. In addition, non-toxic waterborne latexes can withstand high cell loading limits of 500 - 1000 fold greater than an equivalent suspension culture. [62, 63, 65] These limits can be reached with the aid of osmoprotectants (which increase porosity) such as glycerol and sucrose. [66, 38, 64]

It is widely understood latex coatings allow microorganisms such as *E. coli* to be dried and frozen for months with the ability to be reused following a simple rehydration step. [62] In comparison to naturally grown biofilms, water-born latex adhesive coatings, applied with modern printing technologies, allow deposition of a thin, concentrated, and sustainable biofilm. Such synthetic biofilms allow the possibility of entrapping non-growing functional microorganisms in a partially sealed protective coating. [61] Their nanoporous microstructure, large diffusion capabilities and ability to entrap high cell densities along with being able to be stored partially desiccated allow a significant advantage over more traditional techniques such as monoliths, crosslinked gels and membranes. [67] The observable properties of a latex such as film formation, stability, adhesion and tensile strength are mostly determined by the polymeric properties of the individual emulsion particles. [68]

1.6.1 Challenges facing latex immobilisation

Although the idea behind immobilisation using a polymer film is achievable, there are setbacks regarding the reliability, stability, and longevity of these biocoatings. Current challenges faced include the longevity of the guests' activity. One way to overcome this problem is to extend the

lifetime of immobilised cells using a starved environment. In this environment, bacteria lack at least one vital nutrient, resulting in limited growth, combined with brief periods where excess nutrients are given to enable extensive growth for short periods. [69, 70, 71] Other problems in polymer immobilisation methods include gas and liquid transfer limitations, cell immobilisation, cell concentration, poor control of film thickness and the ability to only support organisms that colonize and form an extracellular matrix. In comparison, natural biofilms habitually release cells from their extracellular matrix which in some cases leads to reactor plugging. One example of a synthetic matrix type are hydrogel polymers. Hydrogels have been shown to shed cells as the pores become unstable over time and with changing conditions. Once dried, they exhibit decreased stability resulting in release or outgrowth of cells. [72] Other limitations of soft hydrogels and some cryogel matricies for entrapment of viable microbial cells are well known: Poor mass transfer (in and out of the system), poor stability and limited specific reactivity. These gels have been investigated for rates of immobilisation using *Caldariella acidophila, Sporotrichum thermophile*, *Bacillus stearothermophilus* and *Acetogenium kivui.* [73, 74, 75, 76] Mass transfer is highly limited by polymer film thickness, whereby a greater coating thickness increases restrictions regarding transfer in and out of the matrix system. In order to minimise this, coatings are kept between 10 - 500 µm to ensure structural integrity to maintain immobilised cells and high transfer rates. [65, 77] To solve transfer limitations, coatings have been developed that no longer require drying time to adhere to paper substrates. [72] Additionally, application methods have been created to deliver multilayered coatings that increase transparency without compromising cell viability. [60] An alternative to this is the use of non-film forming components (usually glycerol) inserted into the coating in order to increase the porosity of the coating. [66] Chen *et al.* reported the use of rigid tubular nanoclays known as halloysite to tune the required porosity (Figure 1.6.3). The halloysite dictated an increase in the permeability of the composite coating of up to 1 x 10^{-4} m h^{-1}. Bacteria encapsulated in a halloysite composite coating was also found to have statistically significant higher metabolic activities using the expression of a yellow fluorescent protein when compared to the same bacteria encapsulated in a

non-optimised coating made from latex particles alone. This activity was confirmed via confocal laser scanning microscopy. [78] Although the addition of non-film forming particles has shown to increase activity, it is necessary that the particles allow sufficient transparency as the addition of particles may decrease light transmission and hence decrease microorganism activity. In addition to this, the additive needs to have low toxicity towards the immobilised microorganism, to be inert to the polymer latex, and to be larger than the latex polymer particles but smaller than any immobilised guests. [64] This method also means higher costs of production and begins to add to its environmental impact, especially when using additives such as non-biodegradable plastics and inherently hazardous chemicals. Properties of the polymer can also influence cell activity. Monomer toxicity, particle size, glass transition temperature (T_g), drying time, substrate, and biomass loading can effect polymer film formation, drastically changing the host environment. [44, 79, 80, 81]

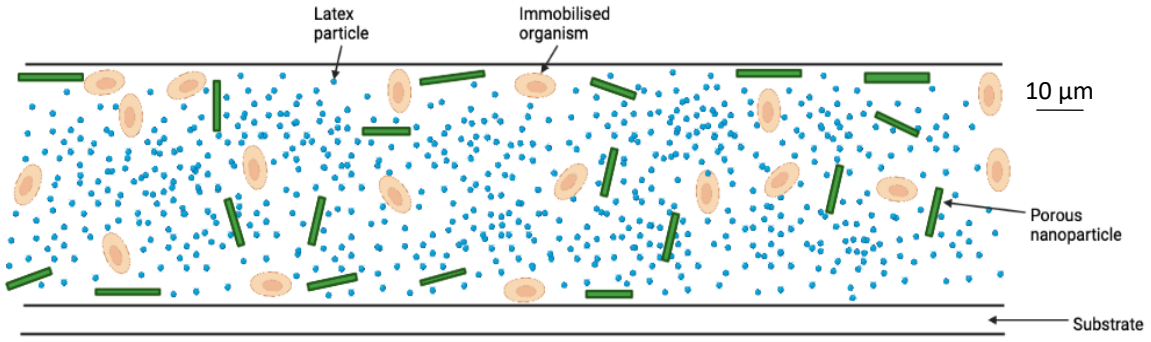

Figure 1.6.3- Increasing porosity in a microorganism embedded latex polymer coating.

1.6.2 History of bioactive polymer latex systems

Bioactive coatings incorporated with microorganisms were first developed by Eastman Kodak for use in layered dry reagent clinical chemistry. [82] Synthetic biocatalytic coatings most simply allow the intensification of hydrolytic enzymes but are less able to carry out oxidations or reductions due to the need to provide cofactors for the reaction to proceed. [82, 83, 84, 85]

Swope and Flickinger revolutionised latex biocoatings by embedding several different microorganisms into nanoporous systems. Starved *Escherichia coli* was successfully entrapped in a 10-80 µm thick latex film composed of acrylic and vinyl acetate monomers. The cells were kept in place via a top coating of latex sealant. [86] Embedded *E. coli* was given no nitrogen or carbon source and only induced using isopropylthiogalactoside (IPTG). When compared with suspended cells, the induced IPTG agent in the immobilised cells had similar induction kinetics. When the induced agent was replaced with lactose, the suspended cells kinetics indicated a lag phase but not when *E. coli* was immobilised within the biofilm. In this stationary phase, *E. coli* continued to synthesise *β-galactosidase* for weeks after immobilisation under drying conditions. Additional work researched by Lyngberg *et al*. developed *E. coli* coatings using trehalose with glycerol or sucrose mixed with the standard latex binder as a top coating to increase coating porosity. [87] From this, a patch coating method was designed using a polyester substrate and vinyl mask setup. Coatings were developed with thicknesses ranging from 2 to 75 µm which enabled a higher mass transfer overcoming previous methods used such as hydrogels. [61, 62]

Although living organisms have now been the focus of latex immobilised systems, previous studies have incorporated various compounds to create functional anticorosion coatings. Danková *et al.* describes a two-step emulsion polymer latex procedure with the addition of 1.5 wt % zinc oxide nanoparticles. Effects of the additive on the physicomechanical properties, chemical anticorrosion and antimicrobial resistance were studied. Results reported improved anticorrosion capabilities when compared to a polymer lacking the zinc oxide additive. With the incorporation of zinc oxide during synthesis, the latex demonstrated improved stability in polymeric dispersion exhibiting physicochemical, mechanical, and anticorrosion properties superior to those of the initial standard and commercial latex binder used previously. The zinc binder also provided possibilities in interior applications with reduced biocide contents. The addition of zinc oxide created a coating that can be applied for environments with moderate corrosion burden. [33]

Lyngberg *et al.* reported a novel method for the immobilisation of *Escherichia coli* HB101 into a latex copolymer film to create a single-use mercury patch biosensor. The latex consisted of two layers of vinyl acetate copolymers coated onto a polyester substrate. Mercury levels were detected ranging from 0.1 nM to 10 000 nM $HgCl_2$ in buffer. [62] Activity remained for 78 hours post exposure and induction increased more than 100-fold with the addition of 1 mM D-cysteine to the buffer in immobilised cells and 3.5 times in suspended cells. Once immobilised, cells were desiccated and stored for 2 weeks. Activity was still present, however the lowest detection levels of luciferase induction as a function of mercury concentration had decreased in this time from 0.1 nM to 1 nM when compared to freshly prepared samples. Interestingly, the concentration of mercury detection had increased to 1 – 10,000 nM $HgCl_2$ from their previous 0.1 - 100 nM. The mercury detection method could be prolonged by freezing the newly immobilised cells immediately with PBS buffer and glycerol for at least 3 months before being used for testing. This research revolutionised latex coatings, developing the first generation of biocoatings that could maintain their adhesive properties once rehydrated with cell concentrations as high as 50 % by volume. [62]

The first report of the embedment of microorganisms with a half-life of more than 2000 hours was in 1995, using several different hard to soft polymer blends ranging in T_g from -60 °C to 60 °C. The research however focused mainly on spherical masses, not thin film coatings. Rates of immobilised enzyme activity was reported; however, no data was present involving cell viability following cell entrapment. Non-growing bacteria such as *Rhodopseudomonas palustris* CGA009 (half-life 3000 hours) have been incorporated into biocoatings which have been shown to produce hydrogen gas from acetate at a rate of 2.08 mM H_2 m^{-2} h^{-1} over a 4000-hour period. This same study reports under complete nitrogen starvation the long term rate of hydrogen production was not affected. [88, 89]

Flickinger *et al*. describes a method to create a multiple uniform strip coating using a polyester substrate which in turn can be adapted easily to create different combinations of biocoatings. The coating foundations consists of a substrate polymer blend mixed with an embedded microorganism and a protective layer. In previous research, the most common substrates were glass, stainless steel,

photographic paper, plastic and polyester due to their appropriate surface energy for polymer adhesion. [90] In order for this substrate to remain in place and flat, an additional support scaffold is used; this is crucial to provide a consistent coating thickness and distribution. In addition to this, the same coating method was successfully reported on non-growing *Thermotoga maritima* at temperatures of 80 °C in artificial seawater. [76]

Successful immobilisations using a synthetic biocoating was reported using a methyl methacrylate, butyl acrylate and methacrylic acid- based latex polymer. The monomer composition was altered to create a glass transition temperature of 34 °C. The emulsion polymerisation method consisted of anionic surfactants (sodium dodecyl sulfate and Lakeland PAE 136) due to their solubilization of proteins. [91] The reported latex polymer coating had no toxicity towards the embedded *E. coli* and was tested using both a latex toxicity test and colony-forming unit analysis. Morphology of cells inside the coating was tested using SEM imaging of a frozen cross-sectional area. Metabolic activity was confirmed for *E. coli* biocoatings using confocal laser scanning microscopy. [78]

The range of microorganisms tested within these active coatings remains small with the majority of cell types uninvestigated, in particular microalgae. Immobilised organisms that have been researched are laboratory and chemically robust in structure with the ability to withstand extreme changes in stress and environment. Advancements in this area of research would see the immobilisation of more vulnerable cells. However, the success rate of this will be inevitably low during the first stages of immobilisation testing. Once this can be achieved, it may provide higher levels of support and protection to the immobilised guest from external environments, improving cell longevity.

1.7 Self-healing Materials

1.7.1 Introduction

The expansion of manufactured man-made polymers has seen environmental waste levels increase and hence threaten human health, oceans, and landfills. To combat this issue, polymer experts are

forced to create more sustainable and smarter material alternatives. One of those ways is to increase a materials longevity. Polymeric materials are now considered the technological advancement of recent times in which high demand is matched by strong research. [92] The structural properties possessed by most polymers eventually lead to damage in the form of cracks and breakages which then leads over time to create mechanical degradation. [93] In the case of electronic polymeric components, such as wire protection, this can lead to electrical failure. Polymers can also undergo microcracking, usually induced by thermal and mechanical fatigue. When this occurs, the polymer structure and strength is greatly reduced. One way to prevent this is to create a self-healing polymer capable of healing at a molecular level instantaneously.

1.7.2 Healing in biosystems

Self-healing is a property found in most living systems permitting them to deal with damaged areas with no external aid. In natural biological systems healing of wounds follows three main steps (Figure 1.7.1). The first induces an inflammatory response, an immediate action to terminate further bleeding which includes blood clotting from platelets and proteins in blood plasma. This process is followed by cell proliferation and matrix deposition which can last for a period of days. The last step is the matrix remodeling which can take several months to complete. This then activates the transport of chemicals to the affected area and can therefore be repaired. [94] Of course biologically this has evolved over millions of years to allow some creatures to not only repair but regrow and replace damaged limbs and tails. This process is also seen in bones and skin in which damaged areas are constantly being removed and replaced by new material. [95]

Synthetic alternatives possess a slightly different method to self-healing. The chemical overall process is usually much quicker (less than days) than that of the biological response seen in most living organisms. The synthetic route begins with actuation which starts the self-healing process followed by the transport and chemical repair of this material.

Self-healing materials are already abundant in the modern-day world. When damaged through thermal or mechanical actions, these materials have the ability to heal or restore to their original properties. [96] However, to do so often requires an external factor (such as extreme heat). It is no surprise that research has made several attempts to mimic this process, the aim of which is to create synthetic self-healing materials that are not only able to self-heal but with no additional aid or support. An efficient self-healing system would be capable of not only rapid healing but being able to maintain 100 % of its original mechanical properties. [97] Numerous polymers have now been developed and studied to meet these aims using various techniques. Research has developed faster repair methods under ambient temperatures and pressures.

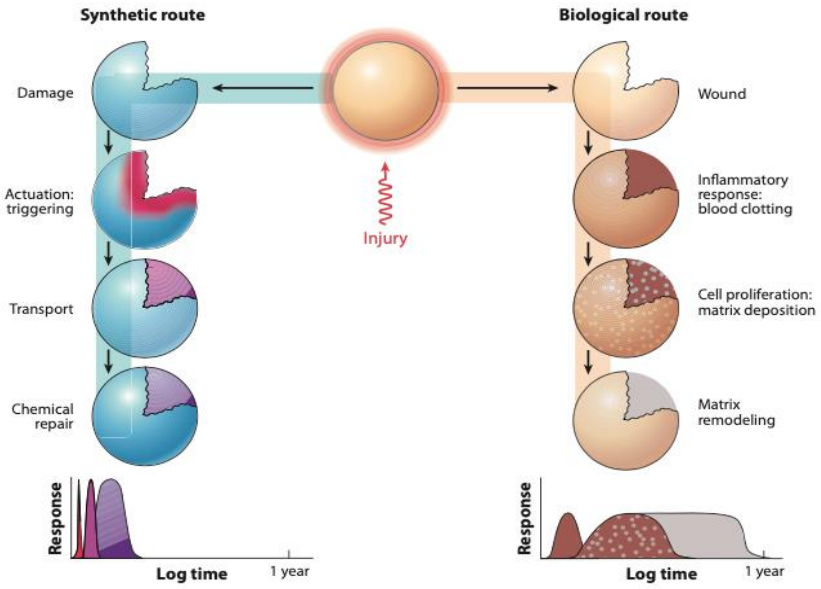

Figure 1.7.1- Synthetic and biological responses to healing. [94]

1.7.3 Approaches to self-healing

The development in self-healing materials over the past 20 years has seen various successful mechanisms reported and analysed. The main mechanisms used can be subcategorised into 5 areas.

1.7.3.1 Microencapsulated healing agents

One of the first developments in synthetic self-healing requiring no external intervention was reported by White *et al.* in 2001. [98] The process involved the integration of small encased fluid into the polymer system which can break upon damage, releasing their contents to fill and repair cracks (Figure 1.7.2). The material incorporates microencapsulated healing agents that are released upon crack intrusion. Reagents selected consisted of dicyclopentadiene (DCPD) monomer microcapsules (50 - 200 μm) encased within a urea-formaldehyde shell. A metal-based catalyst (Grubbs' catalyst) was embedded within the epoxy prepolymer to promote a ring opening metathesis polymerisation. When these results were compared to 3 controls which included 1; neat epoxy containing no Grubbs' catalyst or microspheres, 2; epoxy with microspheres but no catalyst and 3; catalyst but no microspheres, all three of these materials showed no self-healing properties. [98] Polymers containing both microspheres and catalyst were found to repair up to 75 % and averaging 60 % strength recovery across four samples tested. Polymer engineering is vital in this method of self-healing. For example, if capsule walls are too thick, they will not rupture during the cracking process, however if walls are too thin, they will break and release agent when no cracks are displayed. Other design properties are required such as toughness of the microcapsules and properties relating to the microcapsule and polymer matrix integration. It is therefore important to engineer a capsule with the correct properties to ensure effective sufficient self-healing. Microencapsulation shows promising research into developing the next generation of materials; however this method generates drawbacks. The influence of the microspheres can cause interruptions in material strength and hence reduce the strength even before damage is even inflicted. Other factors such as the importance of engineering spheres that are strong enough to withhold themselves embedded within the material but weak enough to break under impact or cutting. Furthermore, choosing a viable healing agent-catalyst combination that work at a rapid rate without compromising the material is a challenging subject.

It is inherent that microencapsulated healing systems are a viable option for the future of modern-day materials providing these factors are met. The incorporation of this technique has already been reported in anti-corrosion paints, epoxy coatings and even the development of biodegradable microcapsules. [99, 100, 101]

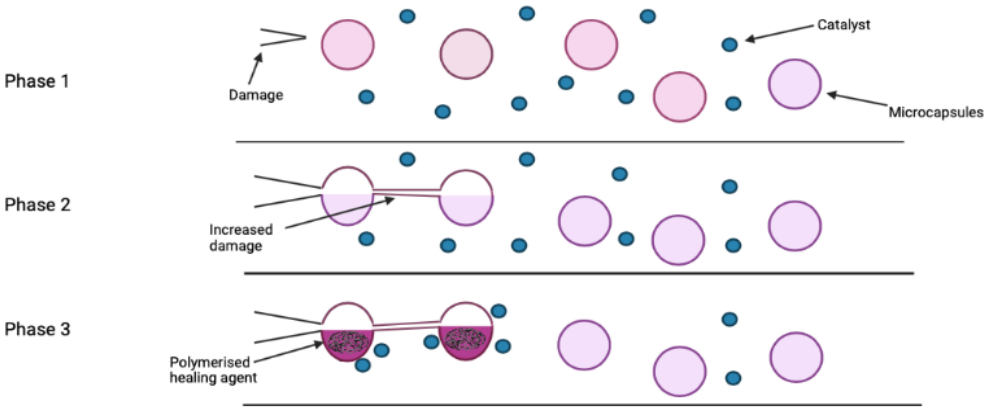

Figure 1.7.2- Microencapsulated self-healing concept

1.7.3.2 Microvascular self-healing materials

This method of self-healing is based on the naturally occurring self-healing found in living things. Most living species depend on the transport of blood through veins and arteries as a fast response to heavy skin damage. This method of self-healing materials mimics this approach with polymers containing their own individual vascular systems composed of tiny tubes (100 µm) capable of pumping healing agents around the material to the site of damage. The transport of healing agent is subject to pressure drop (from the pressure being released at the break point). The agent is pushed towards the required site and repairs the damage. This technique has seen promising levels of healing when compared to a microencapsulated approach. Repairs ten times the size of encapsulated healing agent can be achieved, however the time taken for healing to be completed can be a great deal longer due to the time taken for the healing agent to enter the site of interest. To be a viable option for rapid self-healing, response times would need to be increased dramatically. Furthermore, the engineering required to create strong and efficient vascular networks is extensive.

Not only this, but the network also demands the catalyst or healing agent to be liquid to ensure efficient transport. Solid catalysts and healing-agents have reported slower rates of healing due to transportation issues such as the use of Grubbs' catalyst. [102] Never-the-less there are some applications that would benefit from this technique such as building structures or vehicles where degradation may occur at a slower rate. The theory behind this model brings promise in respect to material healing with possibilities of repair without the interruption of material strength. Although this is the case, when considering the complex engineering required to develop microchannels and ensuring the successful development of a pressure system within these channels, the practicality of this model seems challenging and complex.

1.7.3.3 Shape memory materials

The first shape memory effect was seen in a gold-cadmium alloy in the 1930's, however practical shape-memory alloys started to become popular in the 1960's after the development of nitinol (nickel-titanium alloy). In the 1990's research began into developing polymers with the same memory-shape properties (shape-memory polymers). These materials were cheaper, lighter, more flexible and didn't fatigue after repeated deformations. Since then, metals have been popular shape-memory materials for many years in the uses of eyeglasses or alloys. These materials can be programmed to remember an original shape and when deformed and applied under heat, the material can reform back into its original shape. This shape-memory effect can be exploited using hot and cold temperatures to create different forms known as two-way shape-memory effect. [103] Such materials like nitinol and several copper, zinc and aluminum-based alloys are capable of shape memory. The reasoning behind these properties lies in the materials' crystalline structure. Shape memory is the transition between two types of crystalline forms. In the case of heat induced materials one state requires heat to rearrange the crystalline structure. The two states of crystalline structure are austenite (high temperatures) and martensite (low temperatures). Similar to shape memory, shape changing polymers were developed that show gradual changing in shape when

heated or cooled. [104] Recently, shape-memory and shape-changing polymers have been developed from biodegradable polymers, crystal elastomers and both synthetic and natural hydrogels. [105] These materials have been developed and used in applications such as crease free fabrics, skin care products, wound dressings, and electronic devices.

1.7.3.4 Reversible materials

The development of self-healing materials does not always need to be a highly challenging and complex process. In this case some materials already pose the ability to self-heal using properties such as functionality and low melting points. Thermoplastics are easy to melt, recyclable and can be molded into new forms with ease. These plastics can be designed to break down under heat to leave the original monomers from which the polymer was formed (depolymerisation). When cooled, the monomer polymerises and creates a polymer. The process does require heat in a specific area for this to be achieved. [106, 107] This technique has been applied to bullets due to their small impact area and high temperature characteristics. New bullet proof materials are being researched using this type of reversible mechanism. [108]

1.7.3.5 Other methods

Other mechanisms for self-healing have been developed such as incorporating covalent and supramolecular bonds so when cut or damaged, have the ability to reform polymer networks between each side of the affected area. [109, 110, 111, 112] The dispersal of nanomaterials within the polymer matrix which when subject to a magnetic field can enable repair. [113, 114] The potential for materials to self-heal using biological aids has also been reported. Henk *et al*. reported the incorporation of alkali-resistant spore forming bacteria added to cement paste mixtures proved promising candidates for applications in self-healing.[115, 116, 117]

1.7.4 Future of self-healing materials

Multiple methods have been developed with moderate success to create materials capable of repair for modern day world uses. However, further research is needed to ensure fast responses, efficient transport of aid and maintaining structural integrity. To understand the principles behind the mechanisms of self-healing is still a challenging area and will undoubtably be the success to achieving efficient and sustainable self-healing materials.

1.8 Ink-Jetting technologies

1.8.1 Introduction

Ink-jetted substrates create reactive surfaces capable of a high surface to volume ratio. Ink-jetting is a well-known established technique in surface printing and 3D printing. The deposition of droplets is usually controlled via electronic pulses at a specific voltage to allow generation of droplets of a known size, shape and location onto substrates. A desired height and thickness of coating can be applied through jetting parameters with the ease of multiple runs. In addition to the above, ink-jet printing is a non-contact process meaning dispensing does not affect the fluid/surface dynamics such as unwanted interactions, wetting or contamination. Furthermore, the ability to free-fly dispensed droplets over millimetres, and the addition of multiple jetting devices, allows the deposition of numerous fluids into plate-wells solely from an ink-jet device to create compact, sterile, accurate reactions without the need for additional equipment and materials.

Recently, the field of applications has been directed at bioengineering with the obvious advantages of high throughput and cost-effective methods. Commercial thermal inkjet printers have been adapted to deposit biomolecules onto target substrates with small or no reduction in activity. [118] Furthermore, the method of printing can be finely tuned to suit the applications needs.

1.8.2 Inkjet printing methods

There are two types of inkjet methods depending on the rate and duration at which the flow of fluid is applied.

1.8.2.1 Drop-on-demand printing

Drop-on-demand (DOD) printing generates a droplet with each pulse initiated and are only injected when required. Two main types of drop-on-demand systems are available thermal and piezo. Thermal drop-on-demand printing systems are mostly used in the office printer market and have no need for a recyclable system for wasted fluids due to only jetting when instructed. Droplets are formed by rapidly heating a resistive element in a small chamber containing the printing fluid. The fluid causes a thin film once heated to vaporise into a rapidly expanding bubble which causes a pulse of pressure to eject a droplet (Figure 1.8.1). The system is simple and can give extremely high fluid dispensing performance through thermal demand at low cost. High nozzle density also leads to compact and smaller devices. Although the purchase cost of a DOD printer is low, the specialized ink that is required can be expensive. This is mainly due to the ink having specific surface tension and viscosity to allow it to be vapourised by a heater for the printing process to be successful. If other alternative inks are used, printing performance and longevity can be drastically reduced. The second type of drop-on-demand printing is piezo drop-on-demand which involves a piezo crystal in the printhead that acts in response to an applied voltage causing a change in pressure in the reservoir leading to a droplet formation. [119] This is currently the most abundant and promising inkjet system. This is due to its ability to jet a wide range of fluids with reliable printing devices with a long printing lifetime. Because of this, print heads can be expensive and very prone to breakages, which limits the number of low-cost applications this method could be applied to. Drop-on-demand printers have recently dominated the office printer market due to their straightforward and high efficiency fluid deposition.

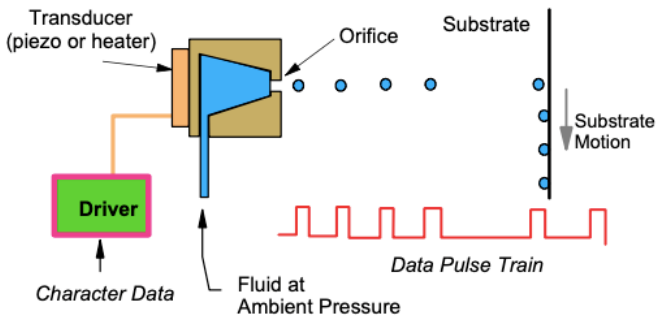

Figure 1.8.1- Drop-on-demand ink-jet printing set up

1.8.2.2 Continuous printing

Continuous inkjet printing technology ejects droplets continuously from the printhead. Once ejected the droplets are either directed to the substrate or directed to a collector for recirculation (Figure 1.8.2). Continuous printing systems can be used in a range of applications, most commonly used in the labelling of food and medicines due to their capability to cope with high duty cycle applications. [120, 121] The system usually requires the capture of wasted or unused droplets to be recycled back into the jetting system to prevent wastage. A pump directs the printing fluid from a reservoir to the required nozzle for printing. Printing is produced in a continuous stream at high frequency using a vibrating piezoelectric crystal. Each droplet becomes charged once passing through an electrode followed by a deflection plate which uses an electric field to decide which droplets are printed and which are reused. Continuous inkjet printing has found advantages over other techniques due to its ability to use volatile solvents allowing fast dry times and aiding adhesion. However, high maintenance costs and specific requirements for chargeable fluids mean continuous printing systems may not be a viable option for some applications.

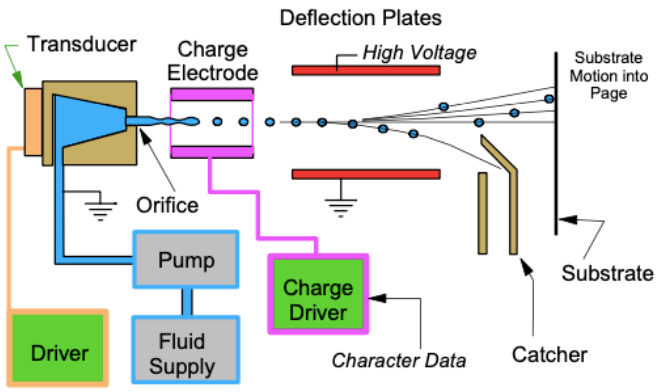

Figure 1.8.2- Continuous ink-jet printing set up

1.8.3 Droplet formation

In the case of a piezo drop on demand printer, a voltage is applied to the piezo crystal whereby the electrical energy is converted into kinetic energy causing fluctuations in the volume within the printhead along with pressure change which together can lead to the dispersion of a droplet. When a voltage is applied to the piezoelectric actuator, an acoustic wave is generated in the piezoelectric printhead. This creates a flow of fluid that proceeds in the direction of the nozzle of the device using several different pulses. A droplet is generated from the device when the kinetic energy exceeds that of the surface energy. The larger the different between the energies, the greater the velocity of the droplet being released. The viscosity and surface tension are highly important factors when deciding the required parameters for jetting. High viscosity solutions require more kinetic energy hence more electrical energy to break the surface energy of the droplet. The voltage applied to the jetting device is also important. If the voltage is too high the acoustic waves formed will not have disappeared completely before the following wave has been initiated. This then leads to an uncontrolled stream of droplets being dispersed or a constant stream of fluid being ejected from the orifice. If the voltage is too low, waveforms will not overcome the surface tension and no droplet formation will be seen.

Factors such as surface tension, viscosity and density are all significant in creating a successful print. These physical properties can be expressed as three numbers. Using Equation 1.8.1, the relationship between the Ohnesorge (Oh), Reynolds (Re) and Weber (We) numbers can be calculated to a Z value. This Z number corresponds to the solutions properties in printing, fluidity, and droplet formation. For successful printing, Z values are required to be between 1 and 10. If Z values are calculated to be less than one, droplets can be formed, however the probability of satellite formation and problematic droplet velocity usually to increase. The deterioration in these properties leads to the reduction in printing accuracy and resolution. If Z values are calculated higher than 10 the fluid will be unable to form droplets. High surface tension and viscosity result in high Z values. Additives such as isopropanol alcohol and acetone can be introduced to the printing fluid to decrease the Z value. However, in doing so biologically active fluids may be hindered due to risks in toxicity.

$$z = \frac{\mathrm{Re}}{\sqrt{\mathrm{We}}} = \frac{1}{\mathrm{Oh}} = \frac{\sqrt{\rho\gamma l}}{\mu}$$

z	Z number
Re	Reynolds number
We	Weber number
Oh	Ohnesorge number
ρ	Liquid density (mg/mm^3)
γ	Surface tension (dyne/com)
l	Drop diameter (mm)
μ	Liquid viscosity (cP)

Equation 1.8.1- Formulation to create a Z ink value

1.8.4 Substrate interactions

Once successful jetting has been achieved, droplet interactions (once in contact with the substrate) can significantly change print quality. Properties such as fluid drying time can be heavily influenced by substrate choice. Dilute solutions may require several layered prints which require fast drying times under time constrained methods. Some temperature or chemical sensitive inks can be subject

to a change in phase once deposited onto a substrate. The change in phase from liquid to solid can be caused by factors such as drying temperature, solvent evaporation, and external chemical reactions.

1.8.5 Evolution of Inkjet applications

Inkjet applications have seen a great deal in advancement since their development 60 years ago. One of the applications that benefited from this advancement is bioprinting. This is the use of an inkjet printer to deposit biological based components onto 2D surfaces. 3D bioprinting has become the subject of interest due to the successful printing of active cells. Saunders *et al*. report the successful print of a HT1080 fibrosarcoma derived cell line. [122] Driving voltages were increased from 40 V to 80 V with only a slight drop-in cell survival rate from 98 % to 94 %. Other studies reported similar findings with survival rates of 97 % in the printing of Chinese Hamster Ovary (CHO) cells and embryonic motorneuron cells. [123] The migration to introduce printing of human living tissue to mimic organs and artificial internal systems has always been an ambitious step. The challenge of not only printing cells but creating tissues that fill the complexity and function of their native counterparts remains the most demanding test. [124] Recently, Negro *et al*. reported the jetting of complex cell-laden hydrogel structures containing living cells. [125] The bioprinting of cells have all been researched in the structure of biosensors and diagnostic devices. [126] Despite this research, the fabrication of 3D scaffold tissues remains challenging due to the encapsulating of cells. Recent research has found a solution to this in creating self-folding 3D prints (4D patterns). The 4D printed pattern creates a 3D scaffold capable of cell encapsulation. Cells embedded within these 4D microtubes were human umbilical vein endothelial cells (HUVECs) to mimic micro vessels. Cells reported high viability and engrafted onto the inner microtubes walls mimicking the native cells. [127]

The evolution of inkjet technology looks promising for the technological advancement in tissue engineering. Research has proved that the generation of 3D printed scaffolds are possible, however mimicking complex cell properties have chosen to be challenging. The fundamental needs of

bioprinting are still being decoded to this day. Simple structures have successfully been accomplished and this alone is a promising step forward in the research to creating 3D engineered bioprinted cell systems capable of mimicking cell properties.

1.9 Objectives and Strategy

The aims for this thesis are as follows:

1 Develop a synthesis for latex polymer with the required properties to host microorganisms

2 Successfully immobilise living microorganisms into a latex polymer coating

3 Develop and analyse self-healing polyurethane formulations using tensile strength testing

4 Develop a method for the deposition of complex latex-cell microdroplets onto 2D-, self-healing and 3D surfaces

Chapter 2 details numerous whole cell biocatalysis reactions that will be used in further chapters to demonstrate cell activity.

Chapter 3 reports the synthesis and composition of a synthetic polymer latex and the alterations in monomer ratios to create different physical properties.

Chapter 4 details the incorporation of microorganisms into a latex polymer coating. Baker's yeast, *E. coli* and cyanobacteria were all tested using assays, microscope imaging and net CO_2 absorption testing.

Chapter 5 describes a method for the development and polymerisation of a self-healing polyurethane. A further method was developed to analyse strength retention after short and long durations of healing.

Chapter 6 reports a method for deposition of latex-cell complexes onto 3D laser cut surfaces using piezoelectric ink-jet printing.

2 Assay development for the assessment of immobilisation methodology

2.1 Introduction

Baker's yeast (*Saccharomyces cerevisiae*) is one of the most researched organisms used as a tool for biocatalysis. Its low cost, zero pathogenicity and inherently high stereoselectivity across several reaction types has made it an ideal first choice biocatalyst for chemists looking to develop synthetic methods with high yields of a specific enantiomer. One example reaction is the reduction of phenoxyacetone using Baker's yeast to create single enantiomer (S)-1-phenoxy-2-propanol (Scheme 2.1.1) and this has been studied extensively over the past 30 years. [128, 129, 130] Another is the enantioselective reduction which has been shown to be both synthetically useful and as an analytical methodology of acetophenone to (S) 1-phenylethanol (Scheme 2.1.2). [131] The chemo- and enantioselectivity of these reactions has been shown to be adaptable through genetic engineering to produce alternative pathways. Adaptations to substrates, changes in growing conditions and the use of inhibitors have all been used as viable methods for increasing selectivity. [132] However, research has led to more complex methods to improve and optimize yeast biocatalysis such as recombinant DNA techniques to develop yeast with predictable, reversible, and higher yielding stereoselectivity. [133]

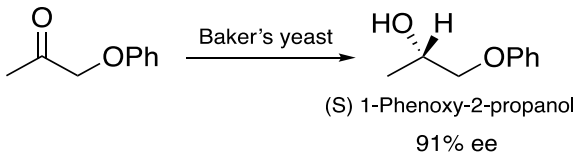

Scheme 2.1.1- The selective reduction of phenoxyacetone to (S) 1-phenoxy-2-propanol using Baker's yeast.

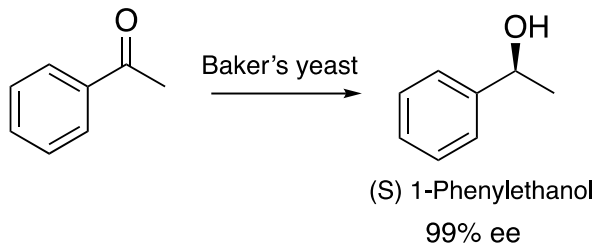

Scheme 2.1.2-Selective reduction of acetophenone to (S) 1-phenylethanol.

S. cerevisiae can perform a wide range of reactions where there are clear advantages over abiotic methods, in particular for the asymmetric reduction of carbonyl groups to alcohols. Reactions such as the reduction of α-methyleneketones can see not only the reduction of the carbonyl group but the carbon-carbon double bond of an alkene may be reduced, in this case to obtain the corresponding saturated compounds with high enantiomeric excess. (Scheme 2.1.3). [134] Other reactions such as reducing aromatic nitrocompounds to amines have also seen a great deal of success over alternative chemical methods. In comparison, *S. cerevisiae* can perform selective reactions with little or no waste produced, and often requires no organic solvents and possesses relatively high activities in mild conditions. Most Baker's yeast reductions have been conducted as fermentation-like processes in aqueous systems. Fermentation only requires nutrients (such as sucrose or glucose) to be added to the reaction to promote activity. These conditions allow the yeast to be living and reproducing with the substrate conversion usually generating a high level of stereoselectivity. [135] It is this selectivity that is seen in most biochemical systems such as sugars and amino acids whereby one enantiomer predominates in nature.

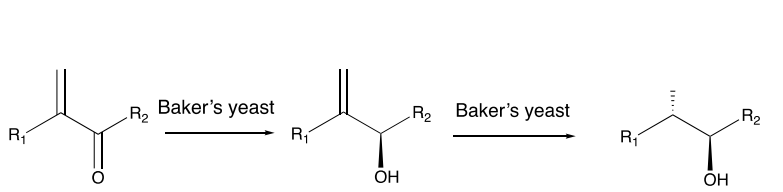

		ee (%)
R_1= Me	R_2=*n*-Pr	92
R_1= Me	R_2=*n*-Hexyl	>99
R_1= Me	R_2=Bn	88
R_1= Me	R_2=Ph	88

Scheme 2.1.3- Baker's yeast reduction on α-methyleneketones. [134]

In this chapter, investigations into biotransformations using free microorganisms and isolated enzymes were reported to provide experimental and analytical protocols to use as test beds for new systems. These protocols involve the use of chromogenic assay experiments and analytical methods such as NMR spectrometry. Specifically immobilised organisms and enzymes such as Baker's yeast and lipase were investigated as biocatalysts in two model reactions: reduction of the nitro group and ester hydrolysis. These experiments provide rapid data collection and analysis, without the necessary need for additional equipment such as a Fyrite® gas chamber to measure changes in oxygen and carbon dioxide. Furthermore, these reactions are important steps in pharmaceutical and food industry models.

2.2 Reduction of 3, 4-dinitrobenzoic acid using suspended Baker's yeast

Baker's yeast has been shown to be particularly capable of reducing nitro compounds to amino derivatives using nitroreductase. [129] One of the most effective is the reduction of aromatic nitro compounds to their corresponding amines. This success is due to high chemoselectivity, a property that makes yeast superior to other reduction methods which may reduce other functionality or cause overreduction. In this chapter, Baker's yeast is used (Scheme 2.2.1) for the reduction of 3, 4-dinitrobenzoic acid (DNB) to 3-amino, 4-nitrobenzoic acid (2.1) and 4-amino, 3-nitrobenzoic acid (2.2). When nitro groups in this compound are successfully reduced to amino derivatives, the reaction displays a colour change from colourless to yellow/orange. This chromogenic reaction was used to monitor cell survival and activity through the progression of the reaction.

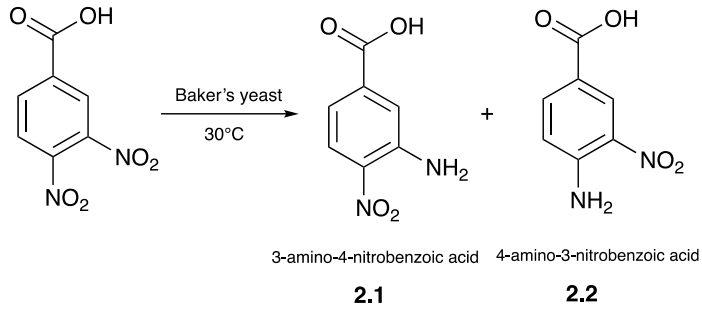

Scheme 2.2.1- 3, 4-Dinitrobenzoic acid reduction to 3-nitro,4-aminobenzoic acid and 3-amino,4-nitrobenzoic acid.

To create an optimum standard reaction method for the rest of this project, preliminary investigations into reduction of nitroaromatic compounds were undertaken. The desired substrate, 3, 4-dinitrobenzoic acid, is poorly soluble in most solvents but can be sufficiently dissolved in ethanol for the reaction to proceed, however there was some concern that ethanol might poison *S. cerevisiae*. To investigate ethanol's toxicity towards this yeast, a trio of reactions were run in parallel to assess the effect of various levels of ethanol. Figure 2.2.1 shows the three reactions undertaken. Each reaction was placed into a beaker, each containing 3,4-dinitrobenzoic acid, yeast, phosphate buffer, and ethanol. A beaker containing DNB, yeast, and buffer without the presence of ethanol was used as a comparison to measure changes in yeast activity. These reactions were run alongside a blank containing DNB and buffer to ensure yeast was responsible for the reduction. The presence of 2 % v/v ethanol in the reaction system showed a clear detrimental effect on the yeast's activity when compared to non-ethanolic systems. Although yeasts naturally produce ethanol (mainly as a final product of anaerobic fermentation of sugars which prevents overload when their metabolic operation reaches a critical level), excess ethanol is toxic to yeast and induces stress responses such as the synthesis of heat shock proteins and the accumulation of trehalose. [136] The addition of ethanol to this system would appear to have exceeded this critical level and hence reduce the yeast's reductive capacity. Therefore, future reactions involving yeast as biocatalyst were studied in the absence of ethanol.

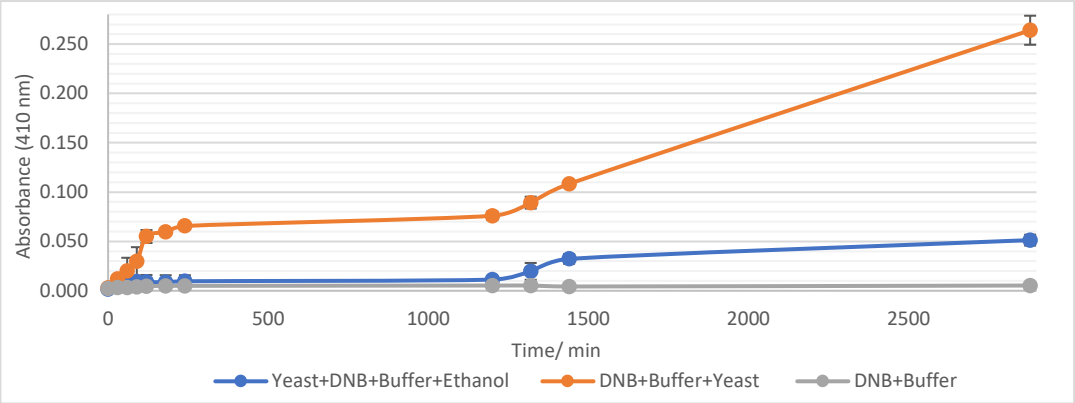

Figure 2.2.1-Average absorbances for 3, 4-dinitrobenzoic acid (DNB) using formulation testing.

2.2.1 Baker's yeast calibration

Once conditions were established which gave an optimal chromogenic response to progress of a reaction, a calibrated set of reactions were screened to determine activity levels. To create an absorbance calibration for the reduction of 3,4-dinitrobenzoic acid, five reaction conditions containing different masses of Baker's yeast were investigated. From the results obtained in Figure 2.2.2 increasing the mass of yeast in the system increases the final absorbance after 24 hours. It is known that increasing sugar concentrations increase cell activity (until a maximum point whereby sugar concentrations start inhibiting activity due to water transport out of the cell). [137] Similar conclusions can be drawn for suspended yeast cell concentrations.

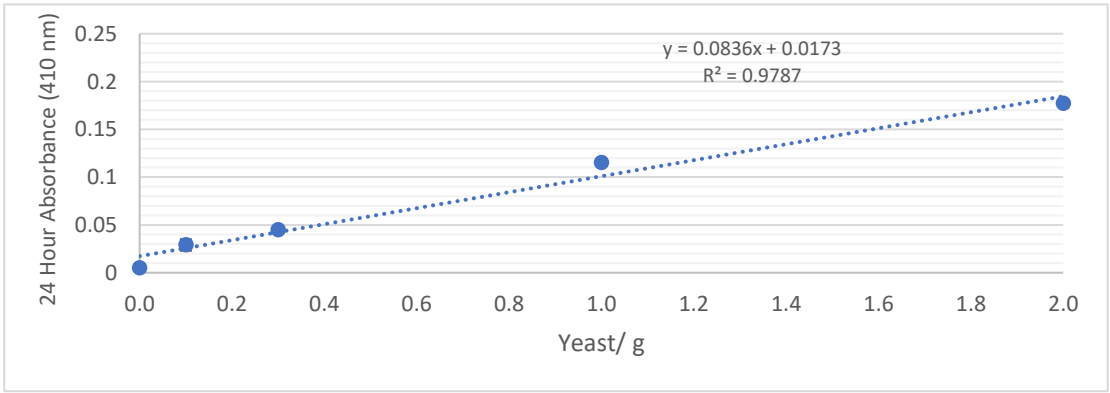

Figure 2.2.2-Absorbance calibration of 3, 4-dinitrobenzoic acid reduction using Baker's yeast.

From the results in this investigation, it is clear that higher masses of yeast correlate directly to an increase in 24-hour absorbance. This reaction will be used as a calibration standard to compare how immobilised cells compared to that of those in a suspended system.

2.3 Catalysis of 4-nitrophenyl octanoate using suspended lipase (*Thermomyces lanuginosa*)

Lipases are active enzymes that catalyse the hydrolysis of ester bonds and constitute prime candidates for industrial and biotechnological applications ranging from the detergent industry to organic synthesis. *Thermomyces langinosa* lipase has been extensively studied in industrial and biotechnological research because of its potential for triacylglycerol transformation, specifically in an organism's biochemistry to hydrolyse glycerol esters both at high water content and transesterification in quasi-anhydrous conditions without any additional co-factors. This makes it an attractive alternative to not just biological applications, but a viable alternative for chemical synthesis. This isolated enzyme was investigated for its ability to hydrolyse ester bonds by using a substrate that can be easily cleaved to generate a product that can be easily detected. The substrate prior to ester cleavage needs to be non-toxic and give a clear indication to the extent of conversion. Keeping this in mind, the hydrolysis of 4-nitrophenyl octanoate, an ester when hydrolysed gives rise to 4-nitrophenol, a compound that appears a bright green/yellow colour was selected (Scheme 2.3.1). This slow colour change will hopefully report a direct correlation to the progress of the reaction.

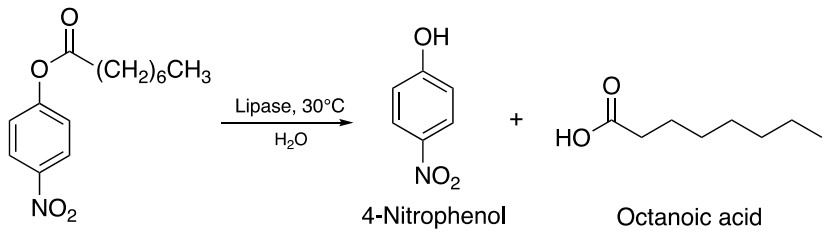

2.3

Scheme 2.3.1- Lipase catalysis of 4-nitrophenol octanoate

In this section, 4-nitrophenyl octanoate is studied under lipase catalysed hydrolysis to produce 4-nitrophenol and octanoic acid. This chromogenic reaction which shows a colour change from a colourless 4-nitrophenol octanoate to coloured 4-nitrophenol, could provide as a sensitive assay for lipase activity when it is immobilised either *in vitro* or *in vivo* and provide a quantitative assessment of enzymatic rates.

After some optimisation by experiment, a lipase catalysed hydrolysis reaction of 4-nitrophenyl octanoate was successful in synthesising 4-nitrophenol. The product was a strong absorber in the UV'/VIS spectrum and the enzymes concentration gave a measurable extent of activity within 7 days. From Figure 2.3.1 the absorbance is characteristically larger in the presence of lipase when compared to a control of suspended 4-Nitrophenol in buffer solution (pH 7.4). However, after analysing the absorbance of the control, it was found to show significant activity without the presence of the enzyme. After 7 days, suspended lipase samples reported absorbances of 1.805. This appears to show significant activity, however following the subtraction of the control reading (1.055 after 7 days), enzyme final absorbance (grey line in Figure 2.3.1) was much lower than the raw results suggest. Furthermore, absorbances reported little change in activity after 6 hours, most likely due to the increasing presence of the by-product octanoic acid, which would lower the pH of the buffer solution (hence why a slightly basic buffer was used), reducing the absorbance of the 4-nitrophenol product to a colourless compound. Although the pH was not measured after the reaction, this could be a factor as to why no increases in absorbance was seen.

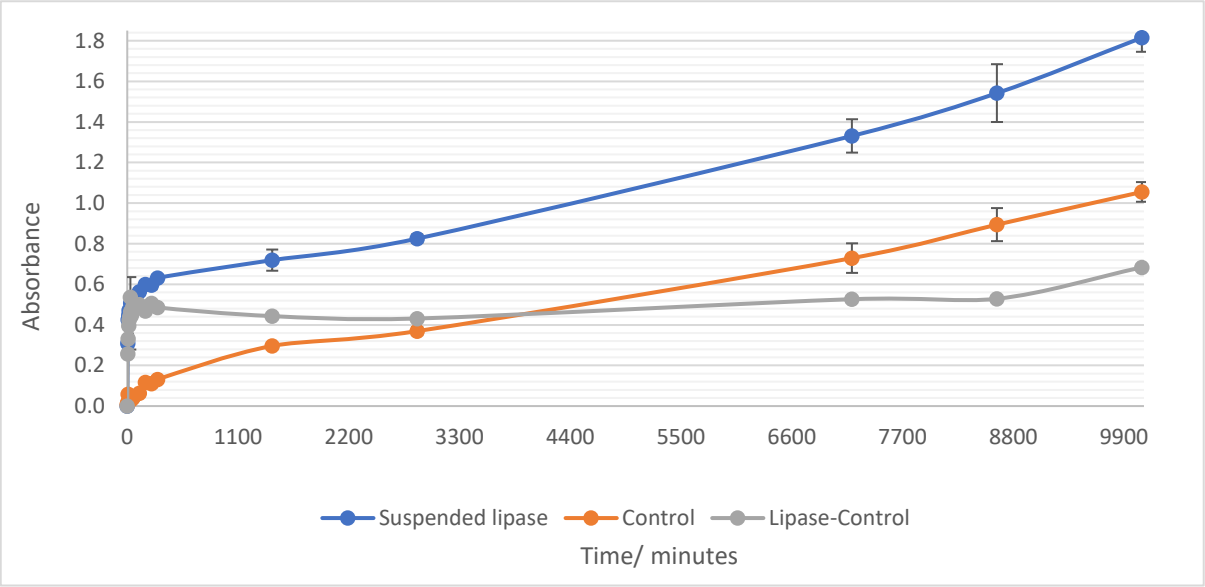

Figure 2.3.1- Average absorbance of lipase catalysed 4-nitrophenol

In this section an assay of lipase activity using 4-nitrophenyl octanoate was reported which tracked the generation of 4-nitrophenol by UV/vis spectroscopy. Although this reaction was straightforward, the high levels of activity found in the control sample and the products pH sensitivity bring unnecessary challenges. Furthermore, the lipase studied in this investigation is a liquid lipase (lipozyme®) which in suspended systems enable good reaction rates and few unwanted by-products. The liquid state could cause problems in future work when changing the format of biocatalyst to be immobilised into solid biocomposite systems.

2.4 Ethyl acetoacetate reduction using Baker's yeast [128]

Previously, the use of Baker's yeast to reduce aromatic nitro compounds to the corresponding amines was reported (section 2.2). Baker's yeast is also well known to reduce other multiply bonded functional groups. [134] The reduction of a 1,3 ketoester to a hydroxyalkanoate ester has been described and has also been shown to work well in extreme reaction conditions e.g. very low levels of water, and such could be a good indicator for activity of biocatalysts in similarly challenging environments. [138] In this section a model reaction was developed which sees the stereoselective reduction of ethyl acetoacetate to (S)-ethyl-3-hydroxybutyrate in 95 % ee using Baker's yeast. [139] This compound has found to be incredibly useful as a chiral starting precursor for many natural products. [128]

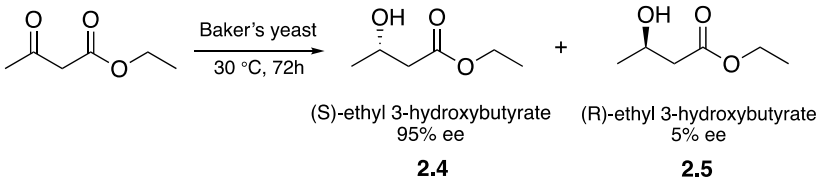

Scheme 2.4.1- Baker's yeast reduction of ethyl acetoacetate to (S/R)-ethyl 3-hydroxybutyrate

A solution comprising of water, Baker's yeast, sucrose, and ethyl acetoacetate was ran for 72 hours at 30 °C. The reaction set up previously had no sucrose present, however very low product yields were obtained without the sugar. The presence of sucrose saw an increase in product yield from 11 % to 59 %. After every 24 hours, additional sucrose was necessary as cell nutrient to promote cell activity as without it, cell activity decreased dramatically. Additionally, samples were extracted every 24 hours, filtered and analysed using NMR spectroscopy to measure the progress of the reaction. Figure 2.4.1 shows the 72-hour crude reaction mixture following aqueous work up and drying. The NMR spectrum shows the formation of the OH peak (B) at 4.7 ppm and the transformation of the methyl group (A) from a singlet to a doublet at 1.05 ppm. From the NMR analysis, the starting material was consumed, however impurities were present in the crude reaction mixture.

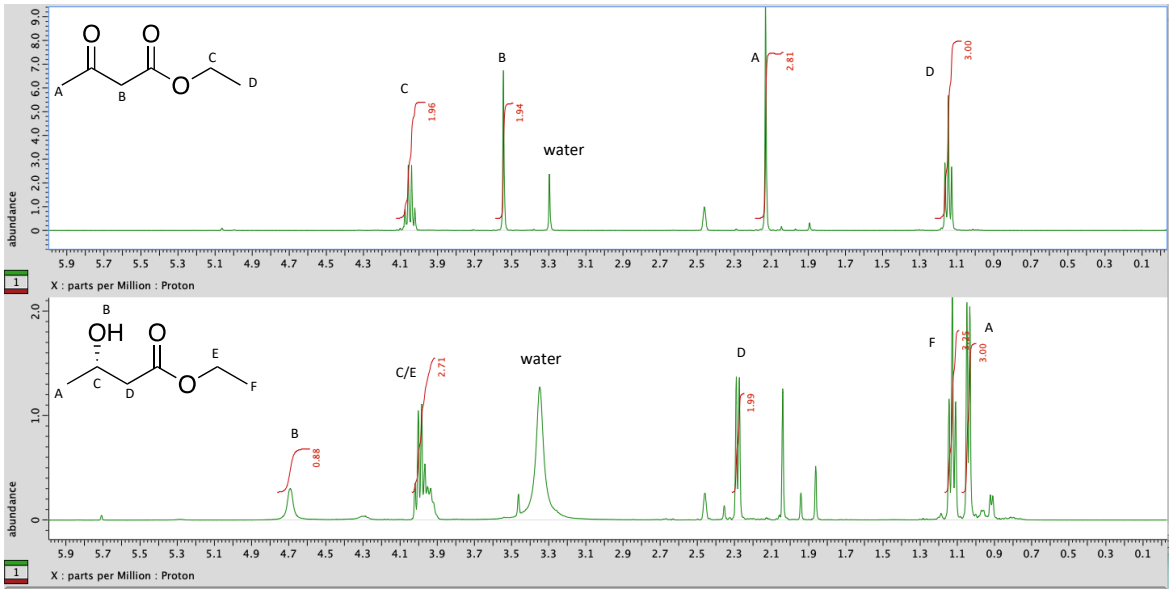

Figure 2.4.1- H^1 NMR spectra of ethyl acetoacetate (top) and crude (S/R)-ethyl 3-hydroxybutyrate (bottom) in DMSO

The reduction of ethyl acetoacetate appeared to be a viable method to prove the activity of a biocatalyst. However, the sheer quantity of sucrose and biocatalyst that was required to be added every 24 hours and the time-consuming filtration process for product analysis proved this reaction to be an unreasonable model for tracking biocatalysts. This model will not be taken forward into future work.

2.5 Fluorescein diacetate hydrolysis using Baker's yeast [140]

The hydrolysis of fluorescein diacetate (FDA) is an established fluorogenic technique used as a viability probe that measures both enzymatic activity and cell-membrane integrity (Scheme 2.5.1). [140, 141, 142] Upon interaction with intracellular and extracellular esterase (from the extrusion from cells) this ester yields fluorescein, a highly fluorescent (λ_{max} 485 - 530 nm) compound. This substrate offers the potential to report on an organism as part of a sensitive and simple reaction which can be viewed under a fluorescence microscope as well as using numerical measurements using spectroscopy or chromatography. [143]

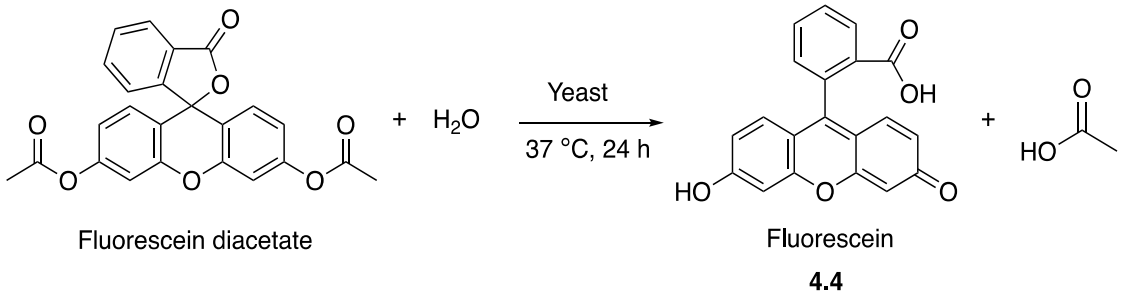

4.4

Scheme 2.5.1- Baker's yeast catalysed fluorescein diacetate hydrolysis

To assess this, two beakers containing buffer (pH 7.4) and fluorescein diacetate were warmed to 37 °C. To one of the beakers, baker's yeast was added and stirred in suspension. Samples (100 μl) were taken every hour for the first 6 hours, and a final 24-hour time point. These samples were diluted with 900 μl of water and measured using fluorescence spectrometry. A total of four masses of yeast were analysed ranging from 0.1 g - 2.0 g. Fluorescein diacetate in the presence of Baker's yeast reported a clear detectable change in fluorescence over a 24-hour period (Figure 2.5.1). In the presence of no catalyst, the control hydrolysis (light blue data point) was comparatively negligible in comparison to lipase-catalysed reactions showing enzymatic hydrolysis is responsible for the conversion and not water. Furthermore, the amount of yeast used in the reaction is a determining factor in the conversion rate and final fluorescence. The reaction is determined through the availability of the enzyme to convert the substrate. Increasing yeast mass indicates a greater mass of lipase within the cell biomass, and hence increases the number of catalytic sites for substrate-enzyme reactions.

In this experiment, the hydrolysis of fluorescein diacetate proved to be a useful tool to probe Baker's yeast as a biocatalyst. Although dead yeast cells can hydrolyse FDA as they show tendencies to lyse (pop open releasing their enzymes into the environment), the main aim was to develop a biocatalyst assay that can be implemented into future work. The experiment provided a simple detection method for the analysis of conversion from substrate to product. The use of a highly fluorogenic

product made it easy to detect and measure reaction activity with the aid of a fluorescence spectrometer.

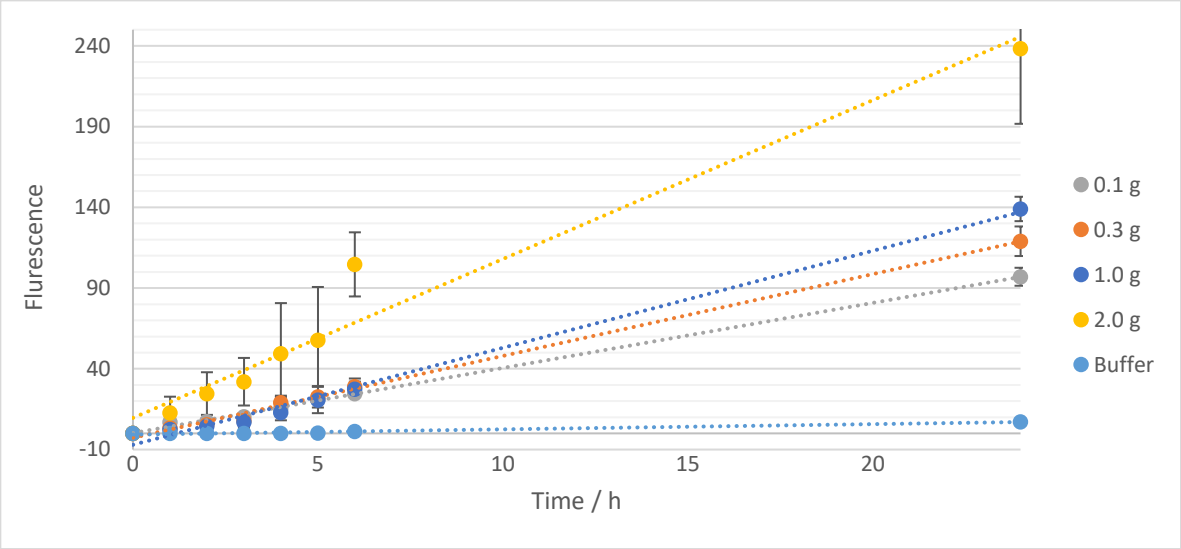

Figure 2.5.1-FDA hydrolysis using suspended Baker's yeast as a function of mass of enzyme

2.6 Summary

This chapter details a set of assays which were developed to monitor and measure both whole-cell and isolated enzyme biocatalyses which are the target reactions for this thesis. These reactions proved able to demonstrate and at least semi quantitatively monitor a microorganism such as Baker's yeast and a purified enzyme such as lipase as they acted to reduce or hydrolyse relevant compounds. Quantitative assays were demonstrated and tested in addition to controls to ensure cells and enzymes made a significant contribution to the rate of reaction for accurate measurement. Although the reduction of ethyl acetoacetate reported a successful change in functionality, this needed large masses of yeast and sucrose to see acceptable levels of conversion (>40 %). This led to problems post reaction in which extreme filtering was necessary to remove large quantities of yeast and sugars from the reaction mixture. Mimicking this level of sucrose in an immobilised system would require an incorporation of sucrose into the biocomposite which can blemish mechanical and porosity coating properties. In addition, the product needed to be removed and washed (all time-

consuming processes) to confirm conversion had taken place. The crude NMR spectrum also gave rise to by-products which would require further purification methods. Because of this, the reaction will not be taken forward into future immobilisation investigations.

The simplest biocatalysis reaction proved to be the hydrolysis of fluorescein diacetate. The chromogenic reaction provided an excellent assay to test the progress of a reaction and reported suitable fluorescence values to replicate in an analogous method for assaying an immobilised biocomposite biocatalyst. Additionally, the reactions reported in this chapter can be used to compare the activity of biocatalysis reactions where the biocatalyst is immobilised versus in suspension in the reaction medium.

3 Synthesis of latex polymer coating formulations

3.1 Introduction

Latexes are colloidal dispersions of polymer nanoparticles suspended in water and have played important roles in applications such as coatings, adhesives, sensors and biomedicines. [144, 145, 146, 62] More recently, emulsion polymers have moved beyond providing the basis of paints, elastomers and coatings, to be viable environments to host living organisms due to their low toxicity and high porosity. [65, 147] Polymer latexes have been particularly studied for their potential to be porous scaffolds for microorganism immobilisation.[148, 78] The aim is to investigate this by immobilising a range of microorganisms into a latex polymer to create a biocomposite coating. To achieve this, a latex polymer needs to be synthesised that can be easily formulated, has low toxicity, and a low manufacturing cost.

In this chapter, the synthesis of an acrylic-styrene latex co-polymer capable of drying under ambient temperatures on various surfaces to create a translucent polymer film is reported. Monomer compositions are manipulated to achieve varying physical properties such as T_g, hardness and dry time. Following synthesis, an additive was incorporated (Texanol™) into films in varying volumes to increase the rate of particle coalescence in film formation (Figure 3.1.1). These coatings were analysed using spectroscopic and analytical techniques to determine polymer properties. The successful synthesis of this latex provided the beginning of an immobilised system consisting of a biocomposite coating capable of biocatalysis.

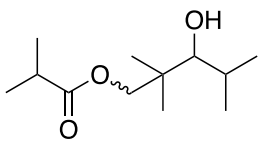

Figure 3.1.1- Structure of Texanol™ (mixture of isomers).

3.2 Latex polymer synthesis

A co-polymer was chosen to be synthesised with monomers that are commonly used in industry in the manufacture of commodity polymers. Styrene and acrylate based compounds are the most used monomers due to their low cost and high stability within a polymer chain. [149] Monomers that were chosen consisted of styrene (S), butyl acrylate (BA) and acrylic acid (AA) (compound 3.1) using radical polymerisation. A 1 litre reaction scale was chosen due to the cheap cost of reagents, and the necessary use of an overhead stirrer.

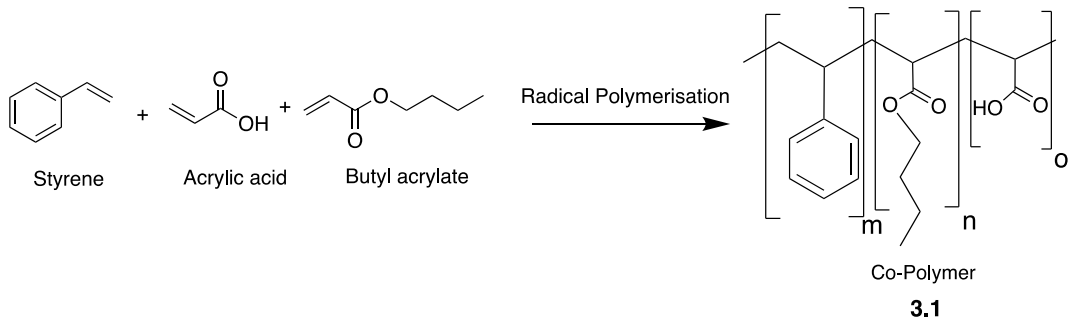

Scheme 3.2.1- Radical polymerisation synthesis of styrene, acrylic acid, and butyl acrylate co-polymer.

The process involved a dropwise addition of ammonium persulfate (initiator) at a rate of 26 mL / hr and monomer emulsion (styrene, acrylic acid and butyl acrylate) at a rate of 144 mL / hr over a 4-hour period using a remote syringe pump. Not only were dropping speeds essential to maintain a steady and even addition of monomer and initiator solution to the reaction mixture, but they also provided a consistent amount of unreacted monomer so that the rate of chain growth was kept constant. Syringe pumps were found to be the most efficient equipment to use for the addition procedure due to their precise, numerical, and highly controlled lever system. Other methods of drip feeding were tested, such as separating funnels, pipettes and burettes. However, this equipment was found to prompt inconsistencies in drop rate depending on the volume of solution held within the funnel. During the reaction period, intense stirring (>650 rpm) was found to be essential in creating a colloidal suspension of latex polymer particles. The use of a water jacketed reaction vessel attached to a water bath provided a greater distribution of heat around the reaction mixture when

compared to a heating block. Polyethylene balls were added to the water bath to slow the evaporation of water during synthesis.

Following the synthesis of the polymer latex, the pH of the reaction mixture was measured by pH meter. The pH was reported to be 2.5 ± 0.3 depending on the batch. This highly acidic environment will be unfavourable to the majority of cells when immobilised. To overcome this, all formulations were neutralised using 0.1 M NaOH. Once cooled, the polymer became a white thick solution (50 % solid particles). This chapter describes the analysis of this latex using gel permeation chromatography, differential scanning chromatography, Vickers hardness testing and dynamic light scattering.

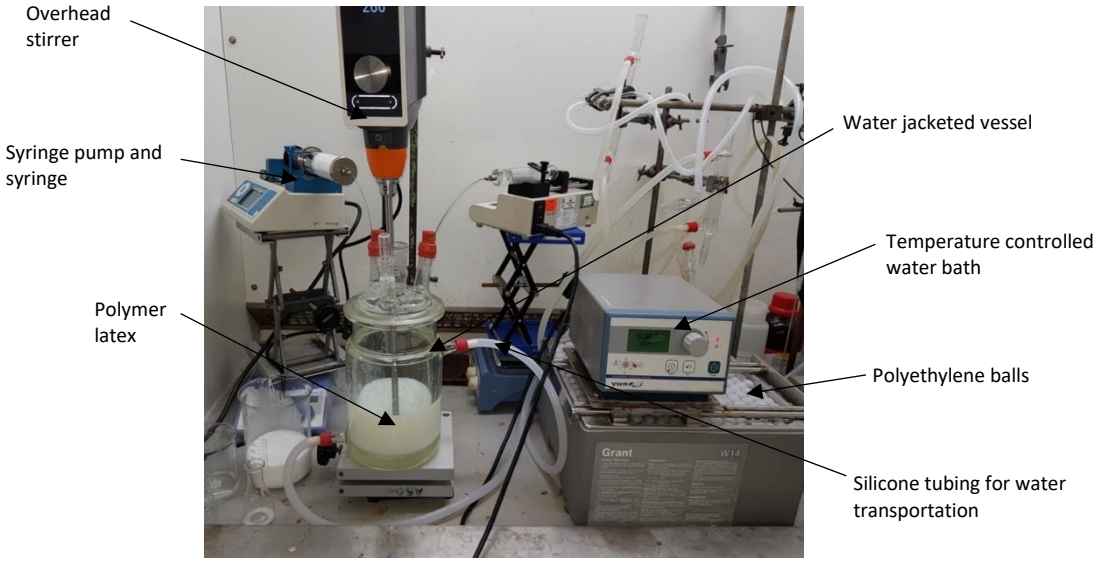

Figure 3.2.1- 1L latex polymerisation set up.

3.2.1 Monomer reactivity ratios [150]

The reactivity ratio is a measure of the tendency for a co-monomer to show a preference for insertion into a growing chain in which the last inserted unit was the same, rather than the other co-monomer. Ratios that are under 1 show potential to create an alternate block polymer which show alternative monomers in the chain. Ratios equal to 1 are said to be random order with some monomers forming alternate monomer blocks and some forming single monomer chains. Ratios that

are higher than 1 are more likely to show blocks of identical monomers. Demonstrations for each polymer composition are shown in Figure 3.2.2. Monomer reactivity ratios are important as they are responsible for the overall composition and sequencing of the copolymer structure.

$r_S : r_B = 1$ (random) SBSBSBBBSBSSSBS

$r_S : r_B < 1$ (alternate) SBSBSBSBSBSBSBS

$r_S : r_B > 1$ (block) SSSSSBBBSBBBSSS

Figure 3.2.2- Monomer reactivity ratio values and their corresponding copolymer structures for butyl acrylate (B) and styrene (S) polymers

Although this was not investigated explicitly within this chapter, a literature search discovered what had been concluded previously on this topic. Research reported by Ziaee *et al*. describes the process for the determination of monomer reactivity ratios for a styrene-butyl acrylate co-polymer. [150] Ziaee *et al*. describes the monomer ratios calculated at 15 % conversion and above 15 % conversion. Table 3.2.1 shows the monomer reactivity ratios using various calculative methods for styrene (r_S) and butyl acrylate (r_B). Each method used to calculate activity ratios involved a combination of calculations and experimental procedures. The reaction whereby conversion meets 15 % reported r_S to have an average calculation of 0.884 and r_B of 0.207. Due to both r_S and r_B being <1, 15 % conversion causes an azeotropic composition. This is a variation in the instantaneous mole fraction of monomer where feed and copolymer composition are the same and are directly affected by the reactivity ratios of each monomer. Although small masses of acrylic acid (1 % w/w) were used in the formulation specified in this chapter, the quantities in comparison to other monomers were thought to have a negligible effect on chain ratios. Since the synthesis in this work is a controlled drip feed of monomer and initiator, and the ratio values are below 1, styrene and butyl acrylate will form an alternating copolymer structure.

The monomer reactivity ratio for the styrene-butyl acrylate copolymerisation system was seen to vary with increasing the percentage of conversion. When analysing conversion over 15 %, monomer

reactivity ratios shift whereby the styrene ratios increase from 0.884 to 1.032. This increase means $r_S > 1 > r_{B,}$ creating a composition drift in where styrene is incorporated faster into the chain causing the copolymer to be rich in styrene. When styrene becomes depleted, an increasing amount of butyl acrylate is incorporated into the polymer chain. The reasons following the change in monomer reactivity can be explained due to an enhancement of viscosity of the reaction media when increasing the percentage of reaction. Ziaee *et al*. also investigated calculating values for the monomer ratios at 80 °C (Table 3.2.2), which is close to the reaction temperature of this latex polymer syntheses. The table below follows similar values to that previously calculated in Table 3.2.1. Although reactivity ratios were not measured in this procedure, similar values would expect to be similar to Zaiee *et al*.

Method (15 % conversion)	**r_S**	**r_B**
Finemann-Ross	0.884	0.208
Mayo-Lewis	0.883	0.208
Kelen-Tüdós	0.883	0.207
Extended Kelen-Tüdós	0.886	0.196
Mao-Huglin	0.887	0.216
Tidwell-Mortimer	0.882	0.206
Method (>15 % conversion)		
Extended Kelen-Tüdós	1.058	0.239
Mao-Huglin	1.006	0.232

Table 3.2.1- Conversion monomer reactivity ratios calculated using various methods [150]

Experimental method	**Markov Reaction Order**	**Reaction temperature**	**r_s**	**r_B**
Ziaee *et al*.	First-order Markov	80 °C	0.883	0.207
	Second-order Markov		0.892	0.208

Table 3.2.2- Experimental comparison of reactivity ratios obtained from Ziaee et al. [150]

3.2.2 Surface coatings

Following the synthesis of the polymer latex, a surface material was needed that will maximise the coating performance by ensuring excellent coverage with the minimum number of coatings. To investigate this, a range of materials were coated with the polymer latex using a 100 µm draw down cube. Contrasting materials were tested for adhesion and coalescence properties using visual inspection. Materials that gave promising surface properties were glass, aluminium and foamed polyvinyl chloride (PVC). These materials offered full coating coverage with no surface pooling or reduced adhesion. However, although foamed plastics such as PVC gave successful coating properties, this is thought to be due to the porosity of the material (the coating absorbing into the air pockets within the material), rather than functional group interactions to material surface (Figure 3.2.3). As for the other materials tested, promising properties are most likely due to surface functional group characteristics. The glass used in this investigation was soda-lime glass. This specific glass predominantly contains SiO_2 (73 %), Na_2O (14 %), CaO (9 %) and MgO (4 %) (reported as oxides). Such compounds provide opportunities for potential bonding between coating and surface through various intermolecular interactions (Figure 3.2.4 A). In the case of an acrylate-styrene based polymer, OH groups in glass have the greatest potential to form hydrogen bonding with the acid groups in the latex, along with Van der Waals interactions between various CH_2 groups in the acrylate chain. Once coatings had dried, cracking was seen in coated glass samples (Figure 3.2.3 B). This is most likely due to a high drying temperature and not because of material-latex interactions. Surprisingly, Perspex (polymethyl methacrylate) gave poor coating adhesion and surface coverage (Figure 3.2.3 D). This observation was unexpected since the polymer possess potential areas for hydrogen bonding. This is due to two reasons; the material's composition could be a mixture of multiple plastics (or an additional plastic coating), some of which maybe unfavourable for this latex coating. The second could be due to the high contents of water being present in the latex which

makes it unsuitable for hydrophobic materials, affecting surface spreading before the polymer can dry. Acrylics' hydrophobicity will be analysed in future chapters to confirm this.

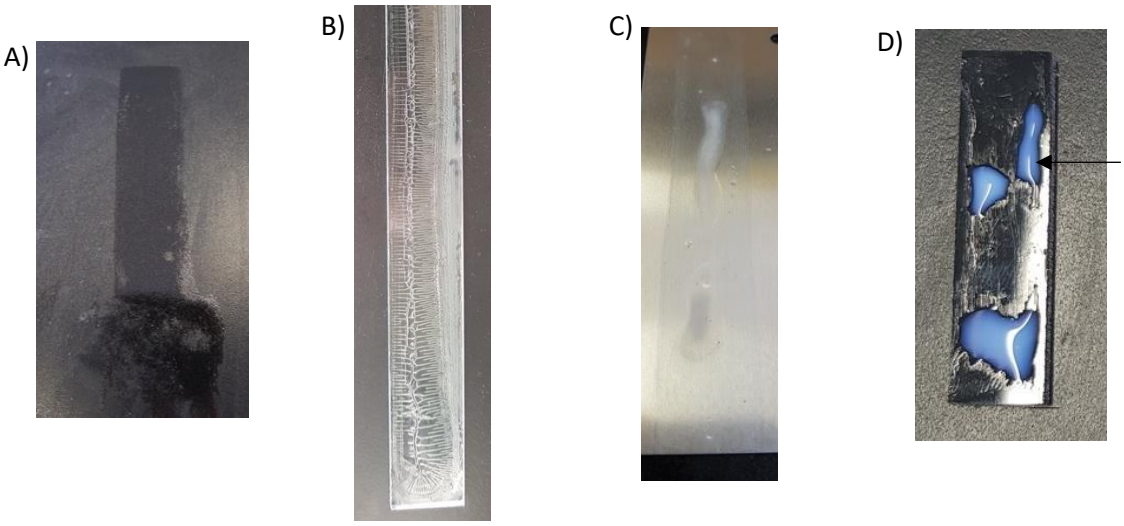

Figure 3.2.3- Co-polymer coated surfaces. Foamed PVC (A), glass (B), aluminium (C) and Perspex (D) (black arrows indicate surface pooling).

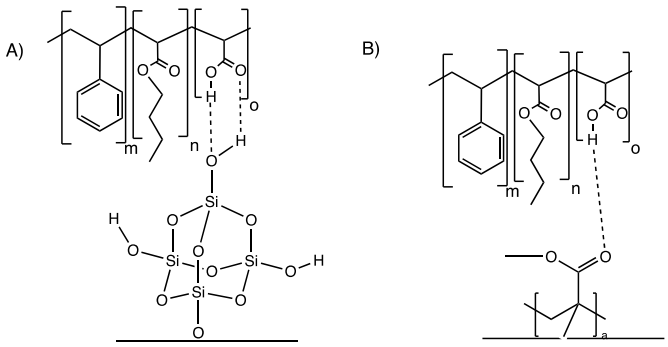

Figure 3.2.4- Potential glass (A) and Perspex (B) surface interactions with the polymer latex.

A polymer's hydrophobicity influences the surface-latex interactions. A factor in determining surface-latex compatibility lies with the surface's ability to be hydrophilic. Since 50 % of the contents in latex is water, it seems logical to conclude that a material's hydrophobicity also determines why some materials prove to be better scaffolds for surface compatibility regardless of their inherent functionality. Therefore, an ideal target material would have high hydrophilic properties to ensure surface covering and prevent pooling. In addition, the target material would possess functionality to adhere to the latex particles once evaporation of water had occurred.

3.2.3 Drying time

Drying time is the time required for the loss of volatile components so that the material is no longer adversely affected by weather conditions and is a vital component in the ability to create a practical polymer latex film. The drying time can contribute to determining the mechanical and physical properties of the coating and can be influenced by temperature, solvent, coating thickness, monomer composition and humidity. When studying drying time, the total duration is broken into 5 stages of drying (Figure 3.2.5). In this investigation, analysis was performed on the synthesised polymer latex using a drying time recorder which enabled identification of each drying stage by dragging a steel needle through the coating over a time duration. A 30 cm glass slide was coated using a 100 µm draw down cube and placed the slide onto the drying platform. In the case of this polymer latex, the total dry time from stage 1 to stage 5 was 2 hours. The polymer coating showed a similar pattern to most acrylic paints used in industry (drying time usually two to three hours depending on coating thickness). Stage 1 was the start of the process which involves the levelling of the needle once motion through the coating has started. Stage 2 (set-to-touch time) was seen around 4 minutes, which involves the evaporation of the water from the system. This leads to stage 3 in which a sol-gel transition was seen to begin 15 minutes into the drying. The sol-gel period is the point at which the coating moves from a liquid, where the polymer chains are dispersed and free to move within the system, to a gel state with restricted movement. This transition is heavily dependable upon the rate at which the solvent can evaporate and is determined by the distribution of the gels porosity. This technique is a popular way to create a free-floating polymer network through the evaporation of a solvent. For this polymer coating, drying time is reduced due to its high porosity properties. The sol-gel transition is also a vital stage in which polymer particles begin to create a uniform polymer network structure capable of forming a coalesced film. The time taken for this stage could be reduced by increasing drying temperature, however this can lead to problems in films such as cracking, through the rapid evaporation of water (Figure 3.2.6). After the gel transition, the coating enters a surface dry stage whereby polymer chains have formed and the majority of

solvent has evaporated, creating a dry surface. At this point surface adhesion is reduced when compared to the final dry time, hence a thin scratch is made by the needle. The surface dry period was found to be the longest with a period of about 90 minutes. After this period, scratches were negligible, and the coating was considered to be in the final dry stage.

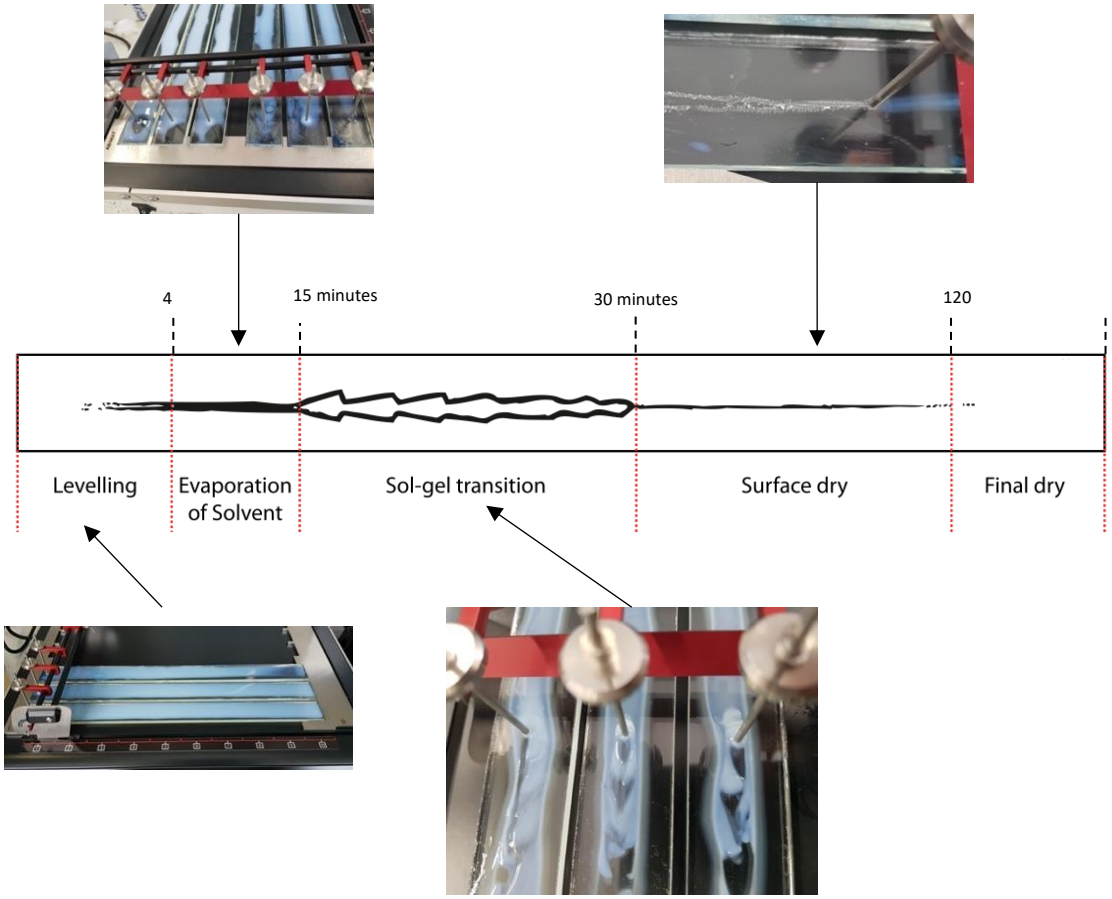

Figure 3.2.5- Drying time stages associated with a polymer latex.

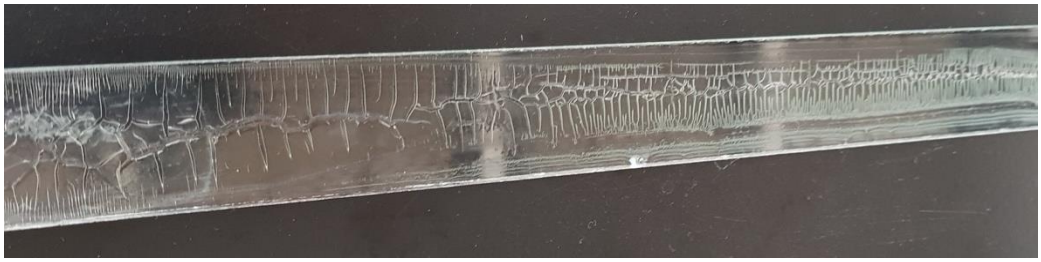

Figure 3.2.6- Example of cracking in a latex polymer film due to high drying temperatures.

3.2.4 Particle size using dynamic light scattering

Latex polymers consist of small (<400 nm) particles suspended in water. Following the evaporation of water, these particles form an environment which dictate the coating's mechanical properties and hence the coatings habitability for microorganisms (Figure 3.2.7). It is therefore essential to measure the size of these particles.

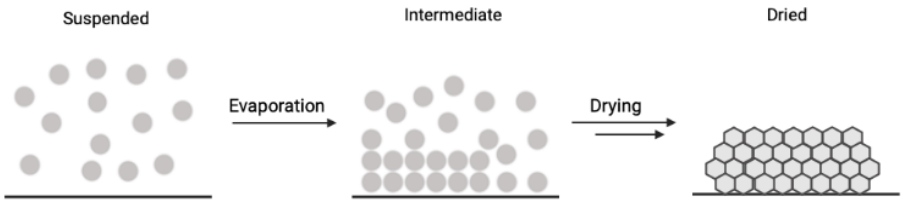

Figure 3.2.7- Latex polymer particle transition from suspended to dried particles.

Polymer particles were measured using dynamic light scattering, a non-invasive method which measures the size and size distribution of molecules and particles typically in the sub micrometre region whilst in suspension within a liquid. This suspension undergoes Brownian motion (the random motion of particles resulting from collisions with solvent molecules) and the rate Brownian motion is quantified by the translational diffusion coefficient (D). In a suspension, smaller particles diffuse quickly, and larger particles diffuse slowly as they are less influenced by solvent molecules. Particles are illuminated with a laser, which scatters the light that hits them. Because the polymer particles are in a dispersion, the scattered light fluctuates and is detected to create a random fluctuation intensity signal. This signal can vary depending on the size of the particle and following autocorrelation, this enabled the translational diffusion coefficient to be calculated. The Stokes-Einstein equation (Equation 3.2.1) can then be used to calculate the hydrodynamic diameter of the particles. Using this method, it was assumed throughout this investigation that polymer particles do not change size following the drying process and remain consistent once the formation of a polymer film is established.

$$d_H = \frac{kT}{3\pi\eta D}$$

d_H = hydrodynamic diameter

k = Boltzmann's constant

T = absolute temperature

η = viscosity

D = diffusion coefficient

Equation 3.2.1- Stokes-Einstein Equation.

Figure 3.2.8 shows the Particle size distribution for the latex polymer suspension. Size distribution was found to be between 0.036 and 0.252 µm. The highest abundant size was found to be 0.089 µm (11 %). However, the majority of particles (59 %) were found to be within 0.071 to 0.126 µm. When compared to previous research, polymer particles have found to be measured around 250 nm in size, larger than those discussed here. [63, 64] Reasons for this are most likely due to the species of monomers involved and their concentration, the stability of the initiator and the temperature at which polymerisation is held.

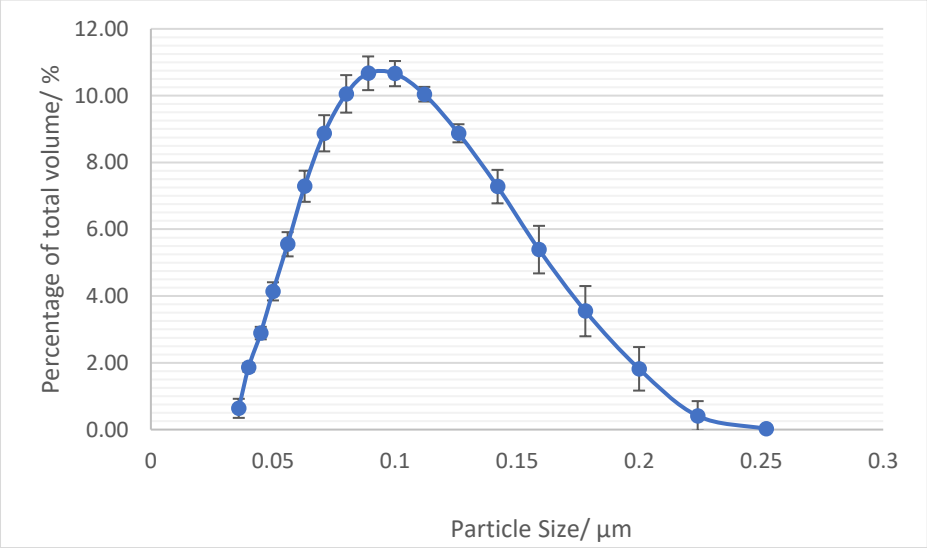

Figure 3.2.8- Particle size distribution for polymer latex using dynamic light scattering

From this work, numerous materials were found to show potential as scaffolds for the deposition of this latex polymer, with glass reporting the most promising regarding adhesion and surface coating. Drying time investigations reported latex coatings were capable of final drying after just 2 hours of

casting. Although there was a large distribution in particle size, the majority of particles reported sizes from 71 - 126 µm.

3.2.5 Chain properties

It is important to analyse chain properties to determine the degree of polymerisation. Molecular weights were determined using gel permeation chromatography, a size exclusion technique enabling molecular chains to be separated during passage through a porous column. Values in number average molecular weight (M_n), weight average molecular weight (M_w), molecular weight of the peak maxima (M_p), and polydispersity index (PDI) were determined. A total of five latex polymers with varying compositions of monomer ratios were synthesised. Monomer components that were altered were butyl acrylate and styrene. Acrylic acid contents were not changed for two reasons; the original formulation only contained 1 % acrylic acid of the total mass and hence changing this percentage by small amounts is unlikely to change polymer physical properties, secondly, acrylic acid can affect the polymers' ability to absorb water (swell). [151] Changing this would create further complications in future work when introducing the coating into a solution. To avoid this, acrylic acid masses remained unchanged. Once the synthesis of the five samples were complete, each were placed into a crucible and allowed to dry at room temperature for 48 hours. Once dry, the sample was dissolved in tetrahydrofuran (THF) (1 mg mL^{-1}).

Polymer samples will be named using their BA percentage composition for the foreseeable work. Table 3.2.3 shows the molecular chain properties. Polymer samples 12 %, 24 % and 36 % were somewhat similar in properties regarding molecular weight. However, 18 % and 30 % differed greatly to this with molecular weights reporting values far higher than that found in previous latexes 12 %, 24 % and 36 %. The reasons for this are not understood, as changes in formulation should not give rise to large differences in chain lengths. One suggestion is that the chain length is affected by the formulation method, rather than the formulation itself. If small changes such as reaction time, injection rate and mixing speed are adjusted, this could lead to vast changes in polymer chain

properties. One characteristic reported in all samples was a large polydispersity index. Ideally when building a polymer, a desired molecular weight is targeted. It is therefore important to not only get a molecular weight close to the target weight, but a low polydispersity (as PD = 1 would mean all chain lengths are the same). PD values ranged from 3.8 to 6.8, much larger than the ideal value of 1. Peak tailing is a characteristic feature of acrylic polymers and was also present in these samples (Figure 3.2.9). During the chain measurements, analysis software was introduced to implement a tailing factor (Figure 3.2.9). This took the surface area of the curve and eliminated anything under 5 % of the maximum peak height, reducing the impact of tailing on the overall calculation.

Butyl acrylate/ %	Styrene/ %	Mw	Mn	Mp	PDI
12.0	37.5	27600	5300	25500	6.8
18.0	31.2	94400	6500	90000	4.9
24.0	25.0	22500	5800	18000	3.8
30.0	18.8	113700	4600	109000	6.4
36.0	12.0	33600	6700	24900	4.3

Table 3.2.3- Monomer composition, Mw, Mn, Mp, and PDI for latex polymer samples.

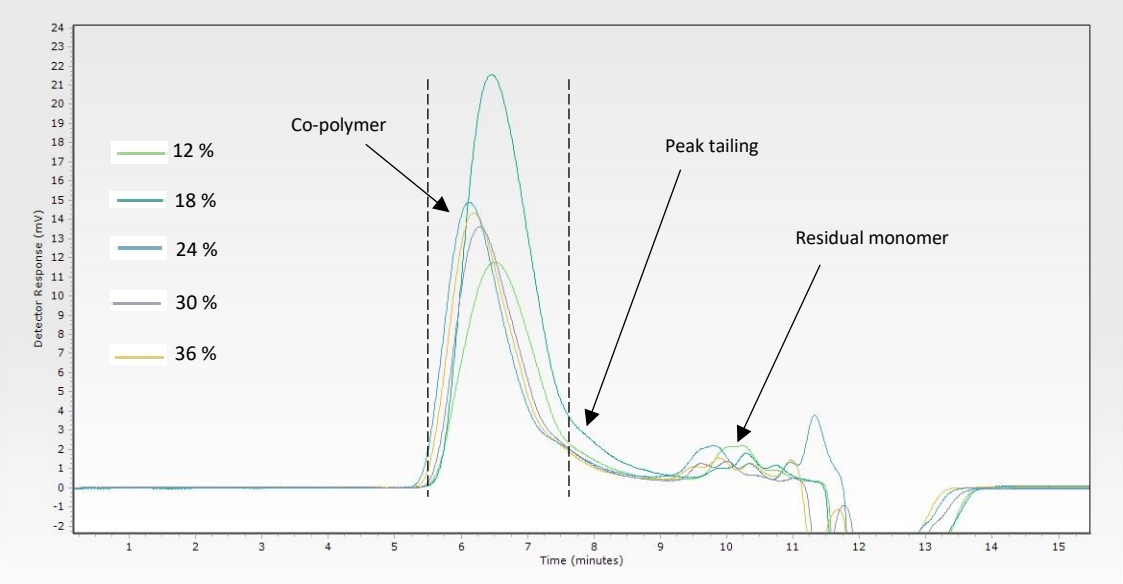

Figure 3.2.9- A gel permeation chromatography graph for the 5 acrylic latex polymer samples (dashed lines indicate tailing factor).

3.2.6 Glass transition temperature

Glass transition temperature (T_g) is the temperature at which amorphous regions change from a rigid glassy state to a soft flexible state and is typically detected by observing changes in dielectric, mechanical and thermodynamic properties of amorphous materials. Below the T_g the polymer structure is rigid and glassy with limited motion in polymer chains. Above T_g, the chains become mobile to move and rotate, creating a flexible rubbery state. There are three main ways to measure T_g: Differential scanning calorimetry (DSC), dynamic mechanical analysis (DMA), and thermomechanical analysis (TMA). The most common method to observe glass transition temperature is DSC. DSC measures small changes in heat capacity using temperature accelerations. All five formulations from section 3.2.5 were analysed using this method to identify any changes in T_g when altering monomer ratio.

Each monomer incorporated into the co-polymer chain has an identifiable glass transition temperature. In this case, the T_g of styrene is 100 °C, butyl acrylate -54 °C, and acrylic acid 101 °C. Each monomer incorporated into the polymer influences the polymer T_g and hence the amorphous state at room temperature. In the case of this polymer, styrene volumes can be increased to create a higher T_g (harder and rigid) or if a soft flexible coating is required butyl acrylate masses can be increased to lower the polymer T_g (soft and flexible). A theoretical glass transition temperature can be calculated enabling us to predict a T_g for each of these polymer formulations. Equations such as the Fox equation enable us to achieve this with the aid of monomer molecular weight and T_g. Experimental glass transition temperatures were investigated in parallel to establish differences between theoretical and experimental values. Although there are differences between theoretical and experimental values from Table 3.2.4, the graph (Figure 3.2.10) reports similar trends in increasing butyl acrylate percentage creates a lower glass transition temperature, providing styrene is equally adjusted in order to keep the latex's 50:50 solid to water ratio. Alternatively, if styrene content is increased and subsequently butyl acrylate decreased, glass transition temperature rises. The sample containing 12 % BA gave a glass transition temperature of 55.1 °C. When this styrene

content was reduced by 12.5 % the T_g dropped to 20 °C, a reduction of 35 °C. The styrene content was reduced further by 12 % and the glass transition temperature lessened to -13.1 °C, a difference in 35 °C. The same correlation is seen in 30 % BA which was synthesised as an intermediate point between 24 and 36 % BA.

% Butyl acrylate	Theoretical T_g/ °C	Experimental T_g/ °C	Difference/ °C
12	46.7	55.1 ± 0.6	+8
18	25.0	45.7 ± 1.1	+21
24	5.9	20.3 ± 1.1	+14
30	-10.9	4.1 ± 1.8	+15
36	-28.0	-13.1 ± 0.2	+15

Table 3.2.4- Theoretical and experimental T_g for latex polymer samples 1-5

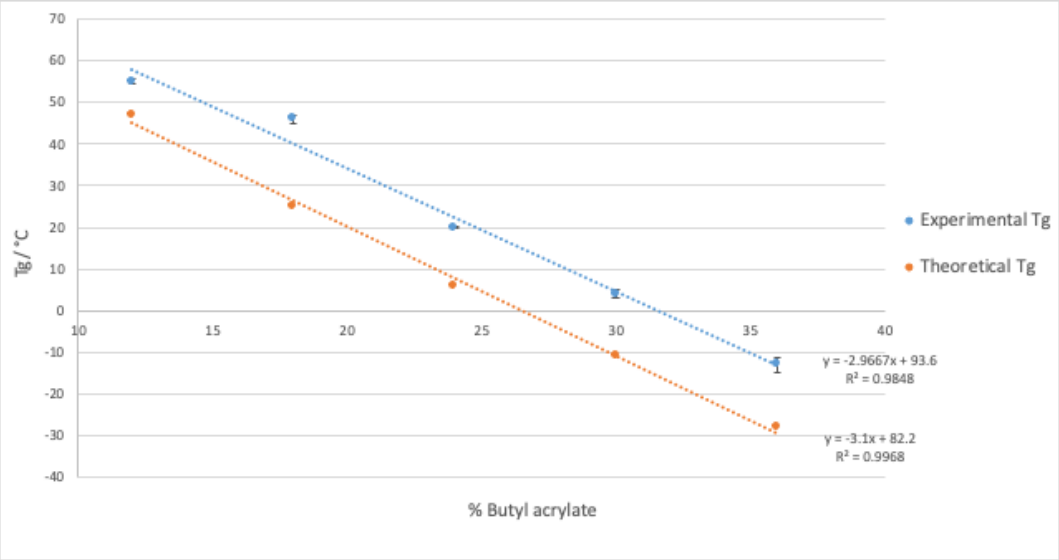

Figure 3.2.10- Experimental and theoretical glass transition temperature with increasing butyl acrylate composition

The data above is most likely explained by intermolecular forces between chains. Styrene's high T_g is due to its ability to form π - π stacking interactions between neighbouring polymers' styrene rings. The structured stacking of these rings creates strong forces that give polystyrene its high T_g. Increasing the ratio of styrene within a latex polymer would thereby increase the occurrence of styrene rings and the number of interactions between chains. This is why monomers such as

styrene, acenaphthylene and phenol monomers such as bisphenol terephthalate (T_g 205 °C) all have high glass transition temperatures. Other monomers involved in the synthesis of these latex examples include BA which characteristically has a low T_g of -54 °C due to its long flexible alkyl chain. BA is often used as a cost-effective soft monomer to balance hardness, flexibility, strength and durability because of the weak interactions between polymer units. Because glass transition temperatures were found to be highly influenced by monomer ratio formulations, polymer formulations can be tailored to meet a target T_g (depending on the organism immobilised).

3.3 Addition of coalescence agents

The coatings industry often applies additives such as coalescing agents to formulations to enhance film formation through the coalescence of latex particles. This additional additive is often used in the paints industry to enhance the coating's smooth finish by softening the polymer particles to increase their potential for coalescence. The effects of a coalescing agent were investigated on the polymer latex described in section 3.2.6 to create 15 different compositions of latex samples (Table 3.3.1). Each sample was weighed before and after the evaporation of water to calculate the percentage of solid mass in each sample (recorded in Table 3.3.1). 2,2,4 trimethyl-1,3-pentanediol monoisobutyrate (Texanol™), an ester alcohol-based agent, which is a popular additive to enhance film formation. This was added after the latex formulation method to allow increased coating coalescence in films. In this section of work, samples were abbreviated to H (12 % BA), N (24 % BA) and S (36 % BA).

Latex Sample	Sample Abbreviation	% Texanol ™ Weight	Acrylic Acid /g	Styrene /g	Butyl Acrylate /g	% Solids
Hard (Sty:BA 25:75)	0H	0 %	10	375	120	40.9 ± 0.4
	4H	4 %	10	375	120	42.2 ± 0.3
	8H	8 %	10	375	120	43.5 ± 0.4
	12H	12 %	10	375	120	43.7 ± 0.6
	16H	16 %	10	375	120	44.9 ± 0.4

Medium (Sty:BA 50:50)	0N	0 %	10	250	240	39.9 ± 0.3
	4N	4 %	10	250	240	39.9 ± 0.4
	8N	8 %	10	250	240	40.3 ± 0.5
	12N	12 %	10	250	240	40.7 ± 0.2
	16N	16 %	10	250	240	41.4 ± 0.3
Soft (Sty:BA 75:25)	0S	0 %	10	125	360	41.8 ± 0.1
	4S	4 %	10	125	360	42.3 ± 0.4
	8S	8 %	10	125	360	42.9 ± 0.2
	12S	12 %	10	125	360	44.8 ± 0.7
	16S	16 %	10	125	360	44.9 ± 0.5

Table 3.3.1- Latex sample formulations and their abbreviations

3.3.1 Glass transition Temperature

The inclusion of Texanol™ was analysed using DSC to identify any changes in coating properties. When compared to original DSC samples, all Texanol™ induced polymers reported small decreases in T_g. Figure 3.3.1 shows a clear patten in which Texanol™ can be used to alter T_g of a latex polymer coating. Altering these two factors now enable any specific T_g to be achieved within the monomer glass transition temperatures. Although increasing the mass of Texanol™ per sample decreased T_g, this reduction wasn't to the extremes found when altering monomer composition. It was also found that the effect of adding Texanol™ to softer latex samples had less of an influence on the T_g than in harder samples. From these results, not only do large adjustments in monomer composition affect T_g, but this can be further refined by the secondary addition of Texanol™. However, this change in T_g is expected to be a short-term effect. The agent is designed to be added directly to the coating before being applied to the surface. Once coated, Texanol™ slowly evaporates away from the coating leaving a hard and smooth finish.[152] This is also to be expected in samples analysed in this section containing Texanol™.

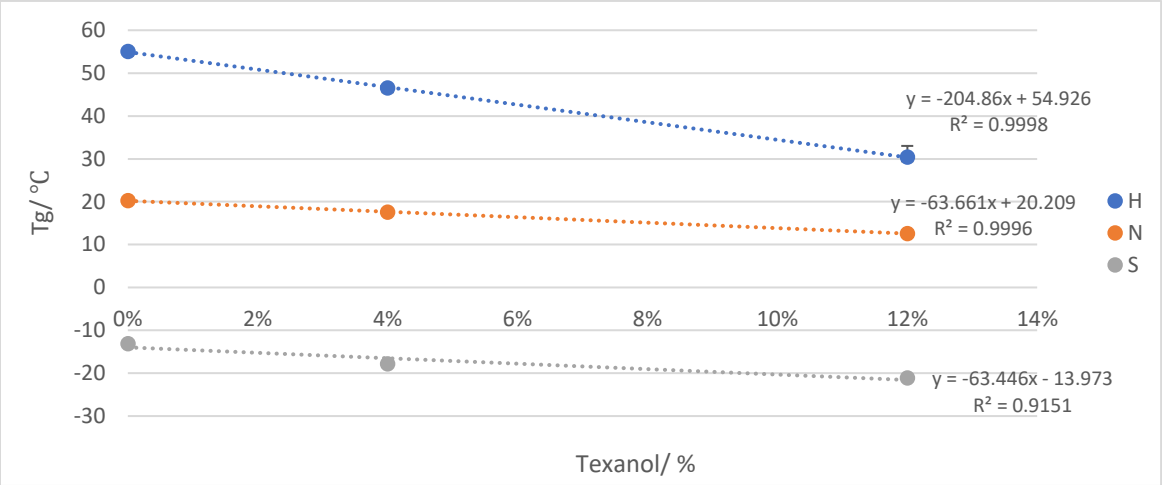

Figure 3.3.1- Addition of 4 % and 12 % Texanol™ coalescing agent on H, N and S polymer latexes

3.3.2 Wet vs Dry Tg

Following the trends found in glass transition data, procedures were replicated to obtain a glass transition temperature of a wet polymer sample. This is because the majority of future work would involve the coating to be submerged in buffer or aqueous solutions. Samples previously analysed in Table 3.3.1 were compared with identical wet samples. Wet samples were submerged in water for 2 hours prior to analysis. Polymer samples 0S, 4S and 12S were unable to be analysed as the low temperature ramps required to assess the T_g would freeze the water in the samples damaging the machine. This was also the case with sample 12N as the original T_g was too close to 0 °C.

Figure 3.3.2 shows the wet and dry glass transition temperature for samples 0H, 4H, 12H, 0N and 4N. Wet samples report small decreases in glass transition temperature when compared to the equivalent dry sample. However, when comparing this to monomer composition or Texanol™ addition, changes are very small. On average, a decrease of 2.2 °C was seen across the five formulations. Higher changes in T_g were found in samples containing 0 % Texanol™. The data suggests that the addition of excess water softens polymer particles to a 'wet minimum' T_g.

From this investigation glass transition temperatures of samples are slightly decreased through the absorbance of water. However, this change is small and found to have a negligible effect on polymer properties.

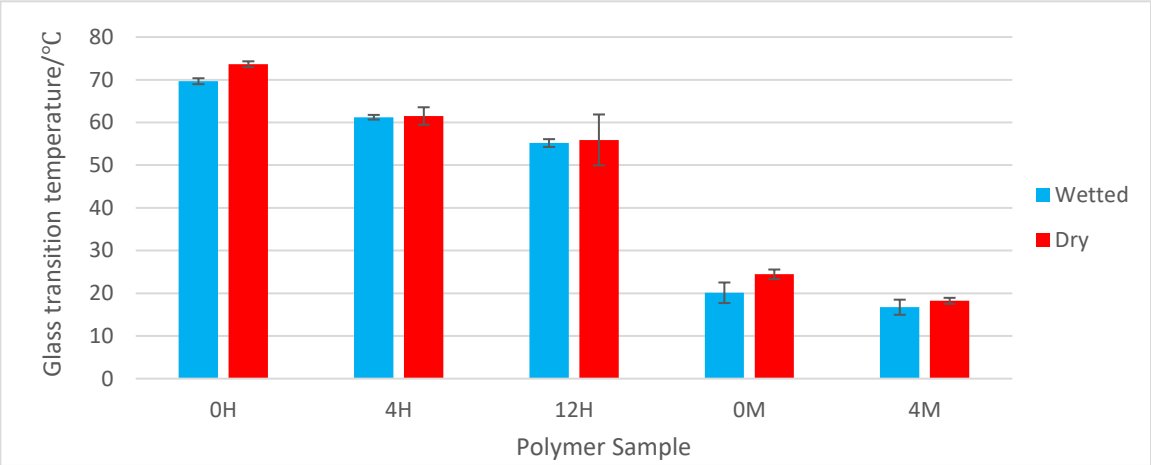

Figure 3.3.2 Glass transition temperature of wet and dry polymer latex samples.

3.3.3 Vickers Hardness Testing

The hardness of a coating is an important property in deciding its application. To determine the hardness of the five polymer latex coatings a standardized hardness testing method was implemented - the Vickers hardness test. This method is popular in metallurgy and can be adjusted for harder or softer samples. This involved the sample being subject to a diamond pressing indentation into the surface. This indentation was to be measured using microscope software and a hardness value calculated to create a Vickers Pyramid Number (HV). Each material has a unique HV and can be used to compare hardness in relation to other materials. This method is often easier to use than other hardness tests since the required calculations are independent of the size of the indenter.

Soft samples were unable to be analysed through diamond indentation due to their sample texture being too sticky. Results in Figure 3.3.3 showed a clear trend, similar to that found in glass transition temperature testing. Increasing butyl acrylate percentage decreases HV. Greater changes in hardness were found when changing monomer composition rather than Texanol™ addition. Sample N showed 30 % of the hardness to that of H latex polymers. Changing the volume of Texanol™ showed no statistical difference in hardness in N samples. However small deteriorations in hardness were found in H samples.

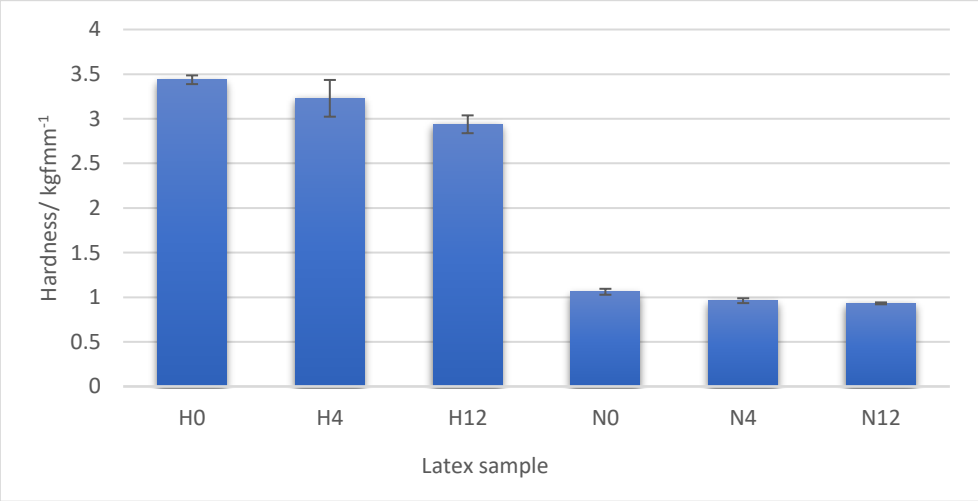

Figure 3.3.3- Vickers hardness testing of polymer latex coatings

3.4 Hydrophobicity using contact angle

3.4.1 Hydrophobicity of latex polymer coatings

Hydrophobicity refers to a molecules affinity for water and is an important property in coating applications. The hydrophobicity of a material or coating is often estimated using contact angle, a technique that involves the deposition of a water droplet onto the surface. The droplet is measured using camera software to accurately measure the left and right angles of the droplet (Figure 3.4.1).

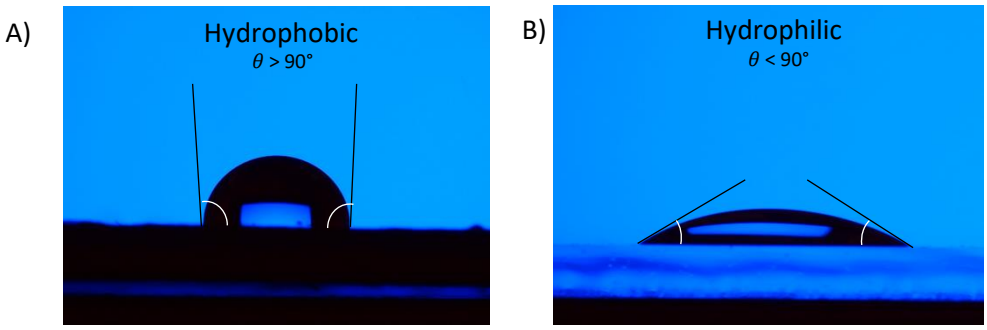

Figure 3.4.1- Hydrophobic (A) and hydrophilic (B) droplets of water on a Polystyrene (A) and Glass (B) surfaces.

To examine the level of hydrophobicity in these polymer coatings, contact angles were measured on glass and polystyrene surfaces. Higher droplet angles correlated to increased hydrophobic properties and reduced wetting. All samples were analysed alongside a blank equivalent with no coating applied. Materials were coated in latex by gentle surface wiping of latex using a sponge. This was to ensure a fully covered surface to allow a higher number of droplets to be examined.

All 5 of the synthesised latex polymers (from Table 3.2.4) were investigated in the hope to establish a trend. Prior to analysis, the assumption was made that higher styrene content would report more hydrophobic contact angles. Figure 3.4.2 represents water droplet contact angles for latex coated surfaces for glass and polystyrene materials. These materials were compared to acrylic equivalents consisting of a black acrylic-based primer before the addition of the latex coating. This was to identify if the use of primers influenced coating hydrophobicity.

The addition of 12 % BA latex on glass surfaces created a substantially more hydrophobic surface. Although uncoated polystyrene and glass reported vastly different contact angles, when coated, contact angles were much similar, proving this coating technique ensured full coverage of the material and that the material did not influence the contact angle.

It appears that surface properties (in this case hydrophobicity) of surfaces can be changed with the incorporation of the polymer latex coating. Depending on the formulation, materials can be created to be more hydrophobic, or more hydrophilic depending on the application.

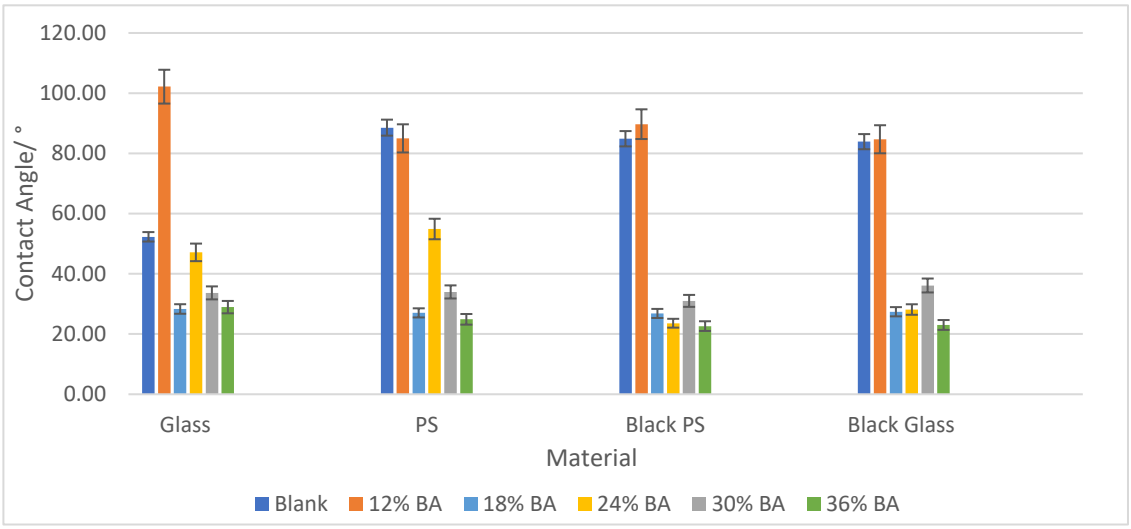

Figure 3.4.2-Contact angles for latex polymer coated glass and polystyrene.

3.4.2 Hydrophobicity of additive infused latex polymer coatings

Texanol™ coalescing agent was added to 3 latex polymers samples (H, N, S) in 5, 10 and 20 % (w/w). The infused samples were coated onto glass and polystyrene substrates and analysed. Figure 3.4.3 shows the contact angle for each polymer composite. Results were similar to section 3.4.1, where H samples reported higher contact angles than N and S samples. The addition of Texanol™ into latex samples created changes specific to each polymer. A slight decrease in contact angle was reported in H samples when Texanol™ was increased in higher volumes. In N and S, no correlations were found between coatings due to fluctuations of increasing and decreasing angle trends.

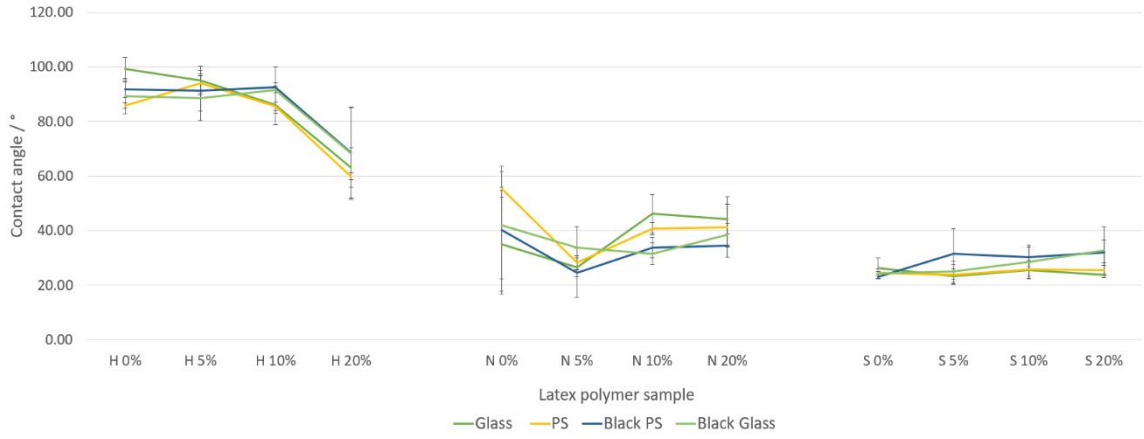

Figure 3.4.3- Contact angle for Texanol™ latex polymer composites.

From results reported in section 3.4 it can be concluded that hydrophobicity can be influenced by not only substrate choice but the polymer coating itself. Reasons for this is most likely due to monomer abundancy. Polymer coatings consisting of high contents of styrene have been shown to give hydrophobic properties. Maximum ratios of styrene content synthesised consisted of a 75:25 monomer composition. This complex resulted in a contact angle of up to 99 ° suggesting higher ratios of styrene could exceed contact angles of over 100 ° and in extreme ratios, the potential of creating polymers latexes with superhydrophobic tendencies (>150 °). Previously superhydrophobic latex polymers have been created using the addition of dodecyltriethoxysilane uniformly adsorbing it on the surface of emulsion latex particles. [153]

The addition of Texanol™ created slight fluctuations in contact angle most likely due to changes in increased particle film formation. The results found in this experiment could be due to a number of factors. This change in particle property could influence coating hydrophobicity due to Texanol's hydrophobic properties (although in some cases the opposite was reported). It is also worth considering Texanol™ is a slow evaporating agent, in which overtime (post film formation) concentrations will be significantly reduced and latex particles will eventually harden. The effects this would have upon contact angle and hydrophobicity is not known and would require further investigation.

3.5 Summary

In this chapter a polymer latex consisting of styrene, butyl acrylate and acrylic acid was synthesised. Polymers physical and molecular properties were analysed, and further formulations of the latex were also created through increasing and decreasing monomer compositions. The effects of these changes were predictable alterations in physical film properties opening possibilities to create custom coatings for required applications. The aim is now to assemble the data found in chapter 2 and chapter 3 to investigate living microorganisms immobilised into the polymer latex films to create biocomposite materials that can live and still sustain their microbial processes.

4 Incorporation of microorganisms into latex coatings

4.1 Introduction

Evolution has given organisms the ability to develop their own natural biofilm and has become a successful strategy to protect, adhere, and improve mechanical properties. Many different bacteria form biofilms including gram-positive, (eg *Bacillus spp, Staphylococcus spp, Listeria monocytogenes)* lactic acid bacteria (*Lactobacillus okantarum* and *Lactococcus lactis)* and gram-negative species (*Escherichia coli and Pseudomonas aeruginosa*). [154] Cyanobacteria also form biofilms in aquatic environments. [155]

However, not all bacteria can form biofilms. Recent research has shown how natural biofilms can be replicated by synthetic systems. Synthetic polymer latexes have shown particular success in their ability to host living microorganisms and use their community for a biotechnological purpose. [62] Latex coatings provide a particularly suitable environment for a microorganism because they provide a porous support structure which offers suitable levels of protection from mechanical damage whilst allowing high levels of and nutrient gas exchange. [72, 88]

This chapter describes work to immobilise organisms into synthetic polymer latexes to develop biocomposite materials capable of sustaining and improving cell activity. To analyse cell activity, Baker's yeast (*Saccharomyces cerevisiae*), isolated lipase (*Thermomyces Lamguinos*), cyanobacteria (*Synechococcus elongatus*), and *Escherichia Coli* are to be immobilised into a latex polymer coating. Furthermore, this study aims to analyse microorganism activity through chromogenic assays and CO_2 absorption while analysing adhesion to surfaces, toxicity, and distribution.

4.2 Reduction of 3, 4-Dinitrobenzoic acid using Baker's Yeast

In chapter 2 this assay was found to be a good reaction to follow enzymatic activity of an organism. As there is already a successful protocol for this reaction, this was replicated using identical

enzymes, except in this chapter Baker's yeast will be immobilised into the latex polymer coating developed in chapter 3.

4.2.1 3, 4-Dinitrobenzoic acid reduction using Baker's yeast embedded into latex coatings

As shown previously in section 2.1.1, Baker's yeast can reduce 3, 4-dinitrobenzoic acid to a mixture of 3-nitro-4-amino benzoic acid and 3-amino-4-nitrobenzoic acid. This chromogenic assay provided a simple indication for enzymatic activity. To achieve the immobilisation of cells into polymer samples a new method is necessary to embed yeast cells ensuring that they are evenly distributed and can be coated onto surfaces using similar techniques previously used. Based on previous work made by Flickinger *et al,* 6 different coatings were formulated. [156] A total of 6 formulations were synthesised using the latex formulation 24 % BA shown in (Table 4.2.1). Sucrose was added to samples 3, 4 and 6 and glycerol to samples 1, 2, 3, 4 and 6, to generate nanopores previously reported by Flickinger *et al*. Each formulation was diluted in different quantities to study the effects of particle concentration. Each formulation was cast onto a glass slide using a 100 µm draw down cube. Once dry each glass slide was placed inside a beaker containing buffer and 3, 4-dinitrobenzoic acid. Each beaker was placed into a water bath at 30 °C and swirled at 100 rpm to ensure mixing. Reactions were analysed over a 48-hour period and samples measured using UV-vis (wavelength 410 nm).

	Formulation					
	1	**2**	**3**	**4**	**5**	**6**
Baker's yeast/g	1.2	1.2	1.2	1.2	-	1.2
Latex (pH 7)/ mL (24 % BA)	1.0	1.0	1.0	1.0	1.0	-
Sucrose (0.58g/mL) / µL	-	-	350	350	-	350
Glycerol (50 % w/w) / µL	300	300	650	-	-	-
Glycerol 100 % / µL	-	-	-	150	-	150
Distilled water / µL (of total volume)	8x	4x	7850 µL	3x	4000 µL	3x

Table 4.2.1- Formulations 1-6 for biocomposite samples [156]

Figure 4.2.1 shows the absorbance for each formulation over 48 hours. From these results, it can be confirmed that yeast activity is still present when immobilised into a polymer coating. The highest absorbance reported was formulation 3, which had both sucrose and glycerol present, suggesting both components are important for yeast activity. Both formulation 2 and 3 reported higher final absorbance than the suspension formulation. In the majority of formulations, yeast activity started to drop after 24 hours with the exception of formulations 3 and 6. This could be due to sucrose acting as additional nutrition for yeast cells in which sucrose is cleaved to produce glucose and fructose (the main sources of food). [157] Interestingly, a latex polymer coating containing no immobilised yeast (formulation 5) demonstrated a reaction profile significantly more pronounced than blank samples (uncoated glass slide). Reasons for this are not known.

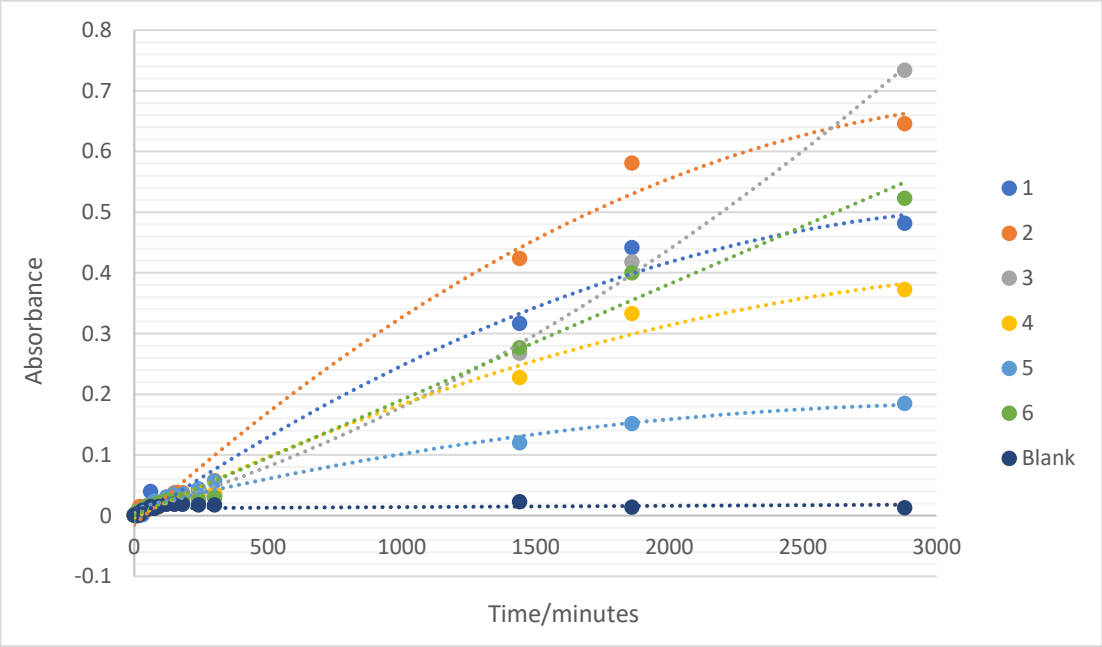

Figure 4.2.1- Absorbance over time for each component onto glass surfaces

From the above data two conclusions can be made; Firstly, Baker's yeast was active in coatings through this enzymatic assay and able to perform reductions over a period of at least 2 days (potentially more with the aid of further work). Secondly, a range of reaction additives could be implemented, though they lead to differing levels of reactivity. The effects of coating formulations

on this enzymatic assay have been investigated however, the choice of surface material can also contribute to cell activity.

4.2.2 The effect of underlying material on Baker's yeast activity

The compatibility of a wide range of materials with the latex/Baker's yeast biocomposite were analysed to assess the coating's activity. Surfaces were chosen to represent potential materials which could benefit from active coatings or materials which are used to form reactors, fermenters, and flow apparatus. This investigation analysed a series of potential materials in the form of a microscope slide (soda lime glass), foamed polyvinyl chloride (PVC) and an aluminum sheet. The best performing biocomposite formulations were taken from section 4.2.1 (formulations 1, 2 and 3). These formulations were cast, dried and assessed using the reduction of 3, 4-dinitrobenzoic acid over a 7-day period (Figure 4.2.2).

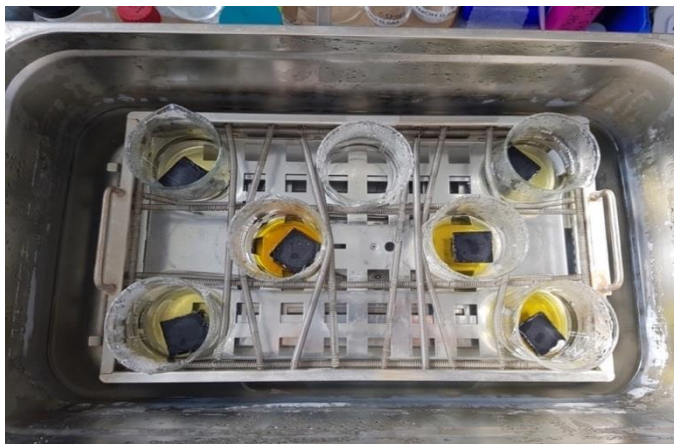

Figure 4.2.2- Reduction of 3, 4-dinitrobenzoic acid using different 100 µm coated latex formulations on 3 x 3 cm PVC surfaces in a 30 °C water bath

From Figure 4.2.3, surface materials had a higher influence on final absorbance than coating formulations. More interestingly, this data suggests aluminium surfaces (regardless of coating formulation) provided the best scaffold in this reduction assay after a 7-day period. The main factor for this difference in cell activity is most likely due to material properties such as coating adhesion and surface coverage. Adhesion is not only essential when combining a coating to a surface but is also important in deciding the efficiency and effectiveness of an immobilised system. Poor adhesion can cause peeling of the coating, which leads to the coating crumbling or cracking. This creates potential for embedded organisms to be removed from the coating and decrease the rate of cell activity. Although coating damage was not observed in this experiment, it remains a key factor in future investigations. Other potential factors responsible for decreased activity is the porosity of the coating, which is vital in dictating the rates at which bioactive components can move in and out of the biocomposite. Future work would include an experimental method to analyse and calculate this to dictate how influential this is to reaction rates.

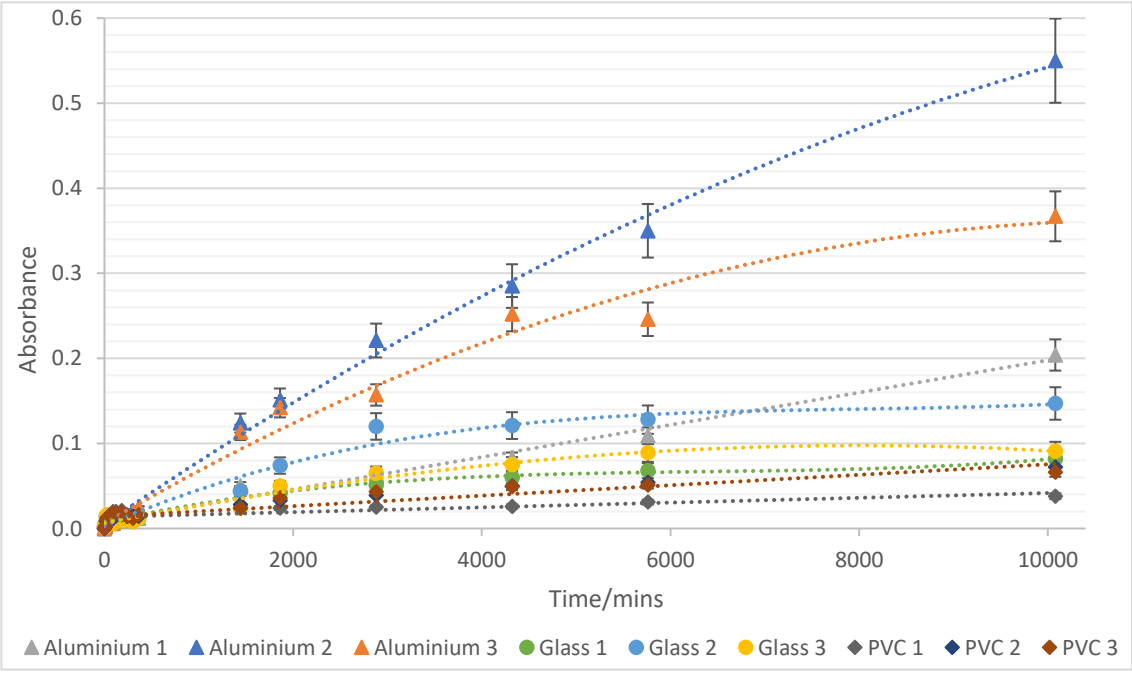

Figure 4.2.3- 3, 4-dinitrobenzoic acid reduction using Baker's yeast on aluminium, PVC, and glass.

From the results acquired in this work several conclusions can be drawn. Formulations 2 and 3 reported the highest activity absorbances on glass surfaces, most likely due to the presence of sucrose and glycerol increasing porosity and acting as a source of nutrients for yeast fermentation. The increase in film porosity helps diffusion pathways for gas exchange and substrate turnover. The foamed polyvinyl chloride support showed poor cell activity. This is most likely due to its surface morphology. Although surface porosity is an attractive feature to allow transport within a polymer, porous surfaces can make a polymer coating less well adhered. A poorly bonded material surface may hinder the evaporation of solvent from the polymer suspension regardless of good adhesion as the coatings keys into the surface roughness. [158]

4.3 Hydrophobicity in yeast embedded coatings

4.3.1 Contact angle in yeast polymer coatings

In this investigation, latex coatings in different monomer compositions with immobilised Baker's yeast were analysed to determine the effects of immobilised cells on coating hydrophobicity. Biocomposites were investigated using a 1:1 (w/w) of yeast and latex deposited on a glass slide and polystyrene. Figure 4.3.1 describes the difference in contact angle using three compositions of latex polymer. Each latex composition (12 %, 24 % and 36 % BA) was subject to 1, 2, and 3 g of yeast (Mauri Pinnacle yeast). Previous contact angles measured in section 3.4 reported a correlation whereby increasing coating glass transition temperature increased contact angle. In this section of work, the immobilisation of Baker's yeast into a biocomposite coating influenced changes in surface properties through contact angle measurements.

The addition of immobilised yeast into polymer coatings created significant alterations in contact angle when compared to the original coatings. From Figure 4.3.1 the addition of yeast into 12 % and 24 % BA coatings caused minor changes to surface properties. Generally, the addition of the yeast to a well-coalesced polymer coating increases its surface tension, though not significantly with the harder coatings. It is possible that the inclusion of yeast into the coatings may inhibit the

coalescence of the latex particles into a well-connected surface, or it may increase the surface roughness, and both may individually or together alter the surface properties, as indicated by a changed contact angle. The addition of yeast to 36 % polymer samples saw the biggest change in surface properties. This is most likely because without yeast, surface properties are more hydrophilic, and the polymer is flexible at room temperature. The addition of yeast disrupts the movement of polymer particles creating a stiffer, more rigid structure (Figure 4.3.2). Furthermore, soft latex particles are expected to show the highest coalesced film surface out of the polymer latexes tested. The addition of yeast to the surface of the film will most likely hinder surface coalescence and hence change surface roughness. It is this change in surface roughness that is thought to alter the contact angle when incorporating yeast into the polymer film. The contact angle was also measured with 3 different masses of yeast (1, 2, and 3 g). It was found that increasing the mass of yeast have little effect on the coating's hydrophobicity after 1 g (Figure 4.3.3).

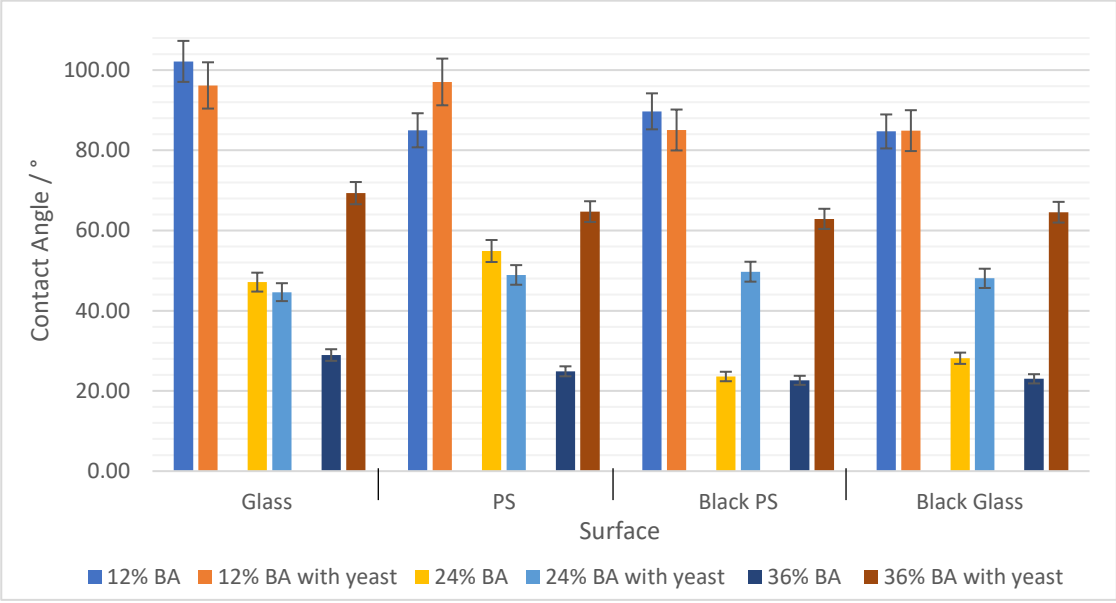

Figure 4.3.1- Contact angles for samples containing immobilised yeast (1g) in biocomposite samples and latex coatings with no immobilised yeast.

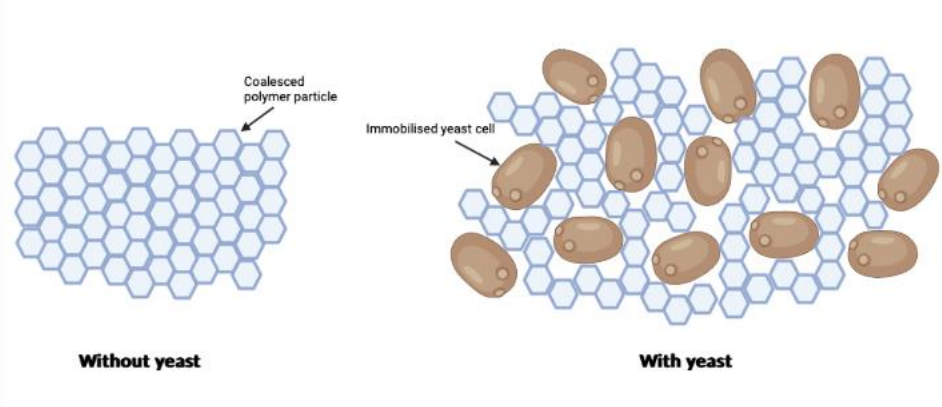

Figure 4.3.2- Increased surface area and surface roughness with the immobilisation of yeast cells into polymer films.

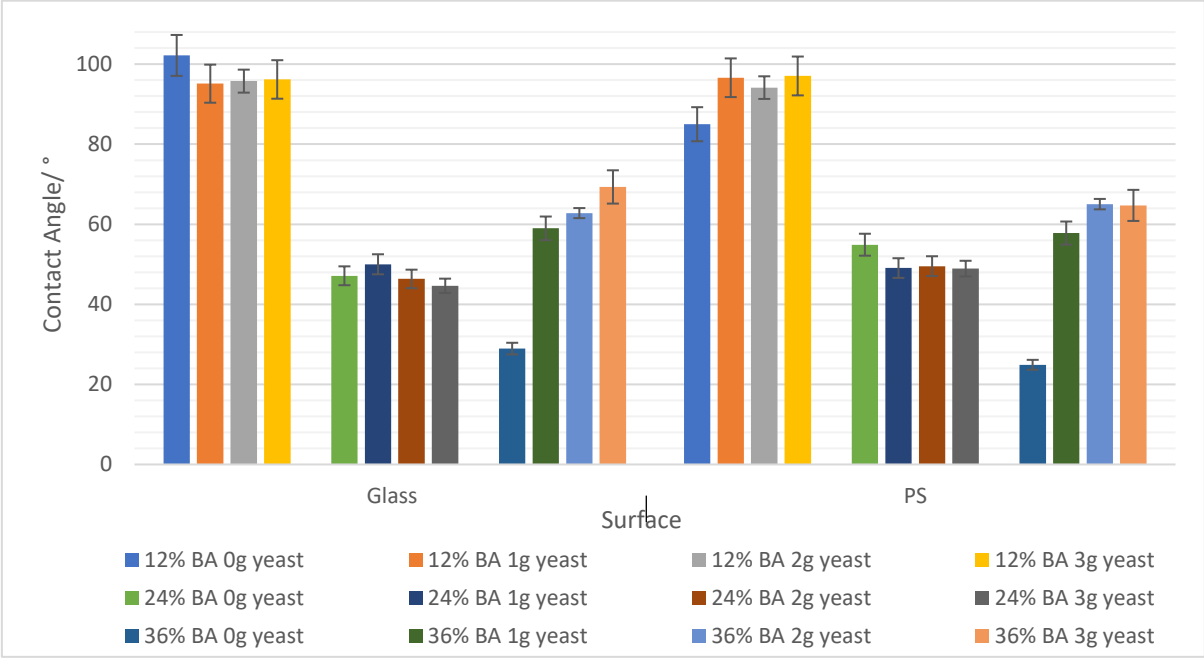

Figure 4.3.3- Contact angle for hard, medium, and soft polymer latex coatings each containing 1, 2 and 3 g of Baker's yeast.

Conclusions can be drawn that the incorporation of yeast cells into a polymer latex film can influence coating hydrophobicity. However, this highly depends on the monomer composition. Interestingly samples with higher T_g's reported no significant change in contact angle regardless of the mass of yeast immobilised.

4.3.2 Immobilisation of lipase for the catalysis of 4-nitrophenyl octanoate

Lipase enzymes (triacylglycerol acylhydrolase) are the most used enzymes in synthetic organic chemistry catalysing the chemo-, regio- and/or stereoselective hydrolysis of carboxylic acid esters.[159, 160, 161, 162, 163] Chapter 2 reported a method for the hydrolysis of 4-nitrophenyl octanoate using suspended lipase. In this section, a similar method to measure the immobilised enzyme activity within a polymer latex coating is attempted.

Lipase (*Thermomyces Lamuginosa)* was taken as an isolated lipozyme® (Novozymes) and immobilised in sodium alginate using two methods. One method involved the lipase-alginate being mixed and encapsulated using a hand syringe in $CaCO_3$, producing droplet capsules of 0.5 - 1 cm in diameter. The other method involved using a piezoelectric printer which printed capsules of 70 µm in diameter. Both methods used the same concentration of lipase-alginate solutions and were taken into the following 4-nitrophenyl octanoate assay alongside a blank buffer solution and a suspended lipase as a comparison. Samples were initially monitored for 2 days; however, sufficient activity was reported after 5 hours. Because of this, reactions were monitored for a period of 6 hours to ensure catalysts were responsible for changes in absorbance. Samples (750 µl) were taken and analysed using UV-Vis spectrometry.

All samples showed varying levels of activity including the buffer agent which naturally hydrolyses 4-nitrophenyl octanoate (shown in Figure 4.3.4). From this data, the average absorbance of suspended lipase exceeded that of both alginate encapsulated lipase methods after 6 hours. This could be due to limitations in diffusion across the alginate membrane. Jetted alginate reported lower absorbance values to that of the syringe method. Although jetted equivalents would, by mass be subject to larger surface area, the resulting data proves that surface area might be shadowed by other factors. Not only can lipase concentration per capsule vary when jetting a mixed solution, the printing itself

can be hindered by blockages, surface tension and viscosity. Inconsistency in jetting can therefore lead to problems when quantifying enzyme volumes and concentrations.

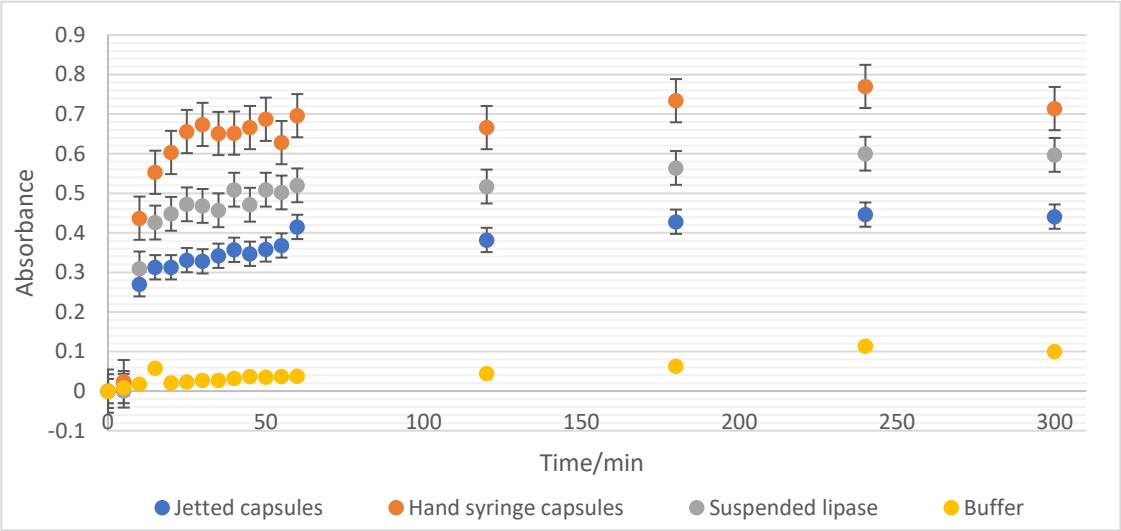

Figure 4.3.4- Hydrolysis of 4-nitrophenyl octanoate to 4-nitrophenol using alginate encapsulated lipase.

The second investigation saw the immobilisation of lipase into a polymer latex coating. The coating would be analysed alongside a suspended lipase solution (a solution containing buffer solution, substrate, and free-floating lipase enzyme) and a latex coating containing no lipase. Since this lipase was a viscous solution, potential problems could arise once immobilised and submerged in aqueous buffer. To reduce this risk, lipase was immobilised using a two-coating procedure. The first coating involved a standard biocomposite coating consisting of lipase and polymer latex. Once dried a protective second coating of polymer latex and glycerol. This was to reduce the leaching of lipase from the biocomposite. Glycerol was added in the protecting layer along with the polymer latex to ensure the coating was porous enough to maintain a high diffusion pathway. Figure 4.3.5 reports the absorbance after 6 hours of lipase systems. Although the immobilised system was subject to two coatings, final absorbances exceeded that of suspended enzymes. Furthermore, despite the suspended system having a significantly greater (providing the lipase was equally distributed throughout the latex) mass of lipase compared to the biocomposite, the improved activity in immobilised systems suggested an additional protective coating did not hinder diffusion. Hydrolysis

activity was present in bare latex coatings with no immobilised enzyme (similar to chapter 2), most likely due to the hydrolysis from water rather than the presence of the latex coating, however further investigations would need to be done to confirm this.

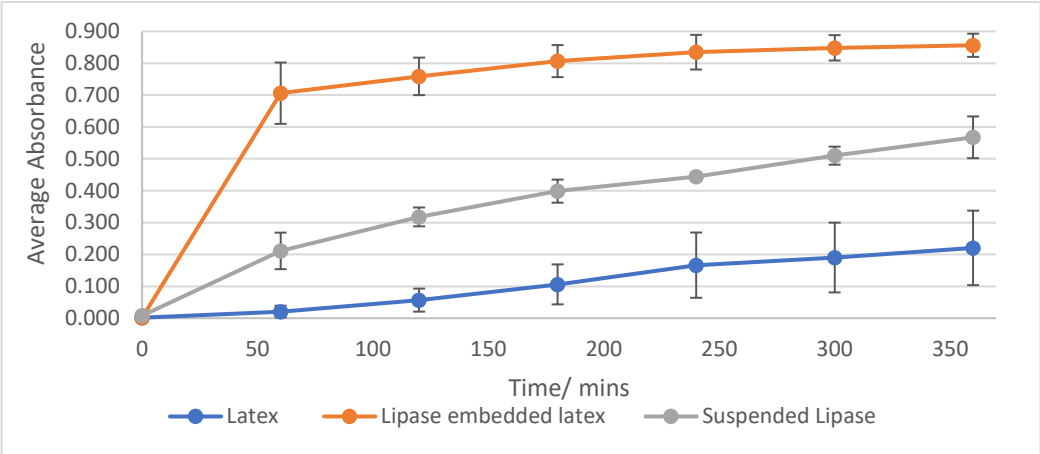

Figure 4.3.5-Average absorbance against time for lipase embedded samples.

From the data collected from this investigation, two conclusions can be made: encapsulating lipase into sodium alginate is a viable immobilisation method that can (in the case of hand syringe alginate capsules) increase the enzymatic activity of lipase in the production of 4-nitrophenol. Although this was not observed in jetted alginate, this might be due to jetting inconsistencies, rather than lower activity. Secondly, when immobilised, lipase in a latex coating increases activity compared to lipase in suspension. This is likely due to a better suited environment for the enzyme. The two coatings enable two protective layers that prevent the potential for enzymes to be damaged and causing denaturation during a reaction. Furthermore, these coatings reported suitable levels of porosity for the enzyme to interact with reagents while immobilised allowing high absorbance rates to be achieved.

4.4 Fluorescein diacetate hydrolysis using immobilised Baker's yeast

The hydrolysis of fluorescein diacetate is a well-known cell viability test which yields a highly fluorescent compound capable of being accurately measured by fluorescence spectroscopy. In chapter 2, suspended Baker's yeast was used to hydrolyse this ester bond to create fluorescein. In this section the aim is to immobilise Baker's yeast in a polymer latex film to not only show cell survival, but to investigate potential increases in cell activity.

4.4.1 Batch testing

Firstly, an investigation into immobilised yeast activity was assessed using different surfaces. From previous work with immobilising Baker's yeast, glass and aluminium surfaces reported good adhesion and surface coverage, however for this investigation, materials that can be easily cut and sized without the need for special equipment were preferred. The first was polystyrene, a material that is cheap and common in modern day appliances, and polyethylene, specifically polyethylene balls measuring 1.2 cm in diameter. Polyethylene balls were coated by dipping into a known mass of polymer-yeast mixture. Once removed the change in weight of this mixture was then recorded, this mass was cast onto a polystyrene sample using a draw down cube to make sure equal amounts of biocomposite were present on each surface. Once dry, each material was placed into a falcon tube containing buffer solution and FDA (Figure 4.4.1). Each tube was sealed, placed into a water bath at 37 °C, and swirled at 95 rpm. FDA experiments were run alongside a buffer solution containing no

yeast to ensure buffer solutions were not contributing to the hydrolysis of FDA. This fluorescence activity was negligible and found to be insignificant in comparison to yeast catalysed results.

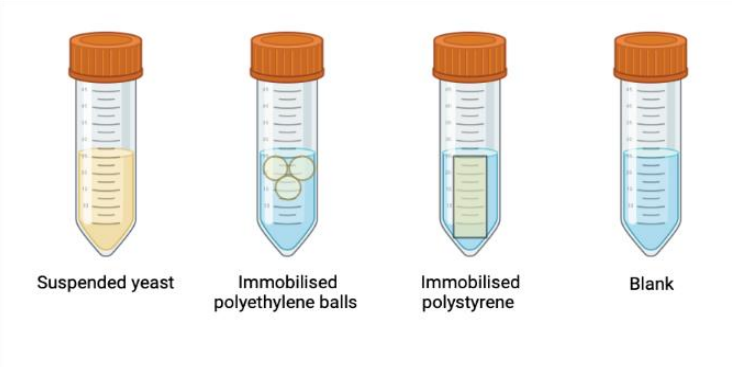

Figure 4.4.1- Falcon tubes containing immobilised yeast, suspended yeast and buffer samples.

Table 4.4.1 shows fluorescence for the suspension and two types of immobilised surfaces. Both immobilised samples reported higher rates of fluorescence than suspended yeast, however polyethylene achieved the highest fluorescence values after 24 hours. An important factor to consider is the surface area of each biocomposite material. The total surface area of the polyethylene balls was 13.56 cm^2 compared to polystyrene surface area of 15 cm^2. With this information it would be expected the larger surface area to exhibit higher fluorescence, however in this investigation it was the opposite. When considering fluorescence per cm^2 of surface, polystyrene reported fluorescence of 5 per cm^2 and polyethylene 11 per cm^2. To confirm leaching of cells was not present in immobilised samples, remaining solutions were analysed using a suspended solids procedure.

Table 4.4.1 reports the number of suspended solids per litre in each sample set. The results reported similar levels of suspended solids for both the immobilised systems. Although immobilised samples showed marginally higher levels of suspended solids when compared to buffer controls, masses were far lower than suspended samples. From this data, significant cell leaching was not present in immobilised samples.

Following this, samples were frozen for 24 hours. This would allow us to see any loss of yeast activity after this period. Immobilised and suspended samples were extracted from buffer solutions and

frozen at -20 °C. After 24 hours samples were defrosted and resubmerged in fresh buffer and FDA was added. An identical reaction procedure was used. Similar yeast activity was reported in immobilised and suspended samples, each one showing marginal decreases in fluorescence when compared to their initial assays. Both pre and post freezing samples were converted to a percentage conversion (Figure 4.4.2).

	Blank	Immobilised Polyethylene Balls Total Surface Area 13.56 cm^2	Immobilised Polystyrene Surface Area 15.0 cm^2	Suspension (0.1 g)
Fluorescence after 24 hours	1 ± 1	143 ± 10 (11 per cm^2)	70 ± 16 (5 per cm^2)	27 ± 6
Conversion (%)	0.1	11	6	2
Suspended solids (mg/L)	2 ± 1	11 ± 3	18 ± 4	560 ± 38
Post freezing fluorescence	0 ± 1	108 ± 5 (8 per cm^2)	53 ± 17 (4 per cm^2)	14 ± 1
Conversion (%)	0	8	4	1
Suspended solids (mg/L)	1 ± 1	10 ± 2	15 ± 5	504 ± 29

Table 4.4.1- Suspended solids, fluorescence and percentage conversion comparing suspended and immobilised yeast in batch reactions pre and post freezing

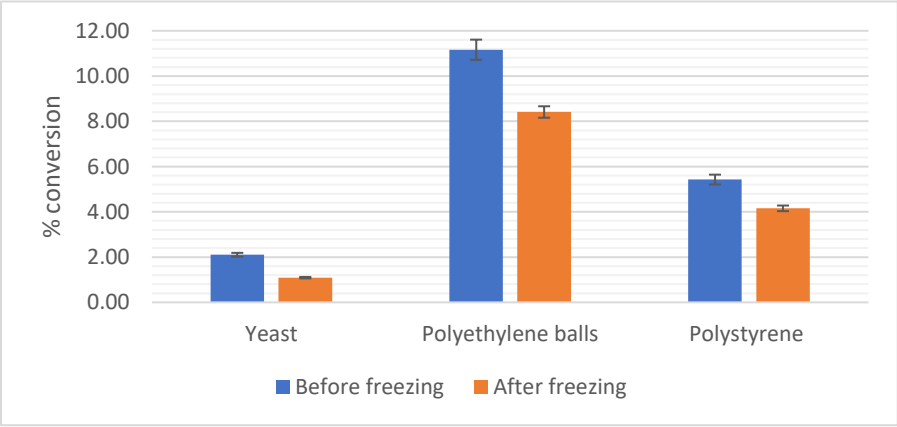

Figure 4.4.2- Percentage activity retained between pre and post freezing immobilised Baker's yeast onto polystyrene, polyethylene, and suspended yeast reactions.

Investigations into the immobilising of yeast into latex coatings proved to be an effective method for cell activity. Immobilised cells did not only show low levels of cell leaching, but dramatically increased activity rates compared to equivalent suspended cells.

4.4.2 Continuous Flow System

Following the success of section 4.4.1, the aim was to repeat the FDA assay using a continuous flow circuit to compare yeast activity using 3D printed pipelines. This investigation was designed to mimic a potential industry reaction procedure. A 10 cm 3D printed pipe was designed made of polylactic acid (PLA) and coated the inside of the pipe with the immobilised yeast biocomposite coating. Following drying, the pipe was attached to a flow circuit consisting of a pump and flask containing buffer solution and FDA (Figure 4.4.3). This was compared to a yeast suspension which flowed through tubing without passing through the pipeline. The pump initiated a flow from the beaker through the pipe back to the beaker. A sample was taken from the beaker after 24 hours and analysed by fluorescence spectroscopy.

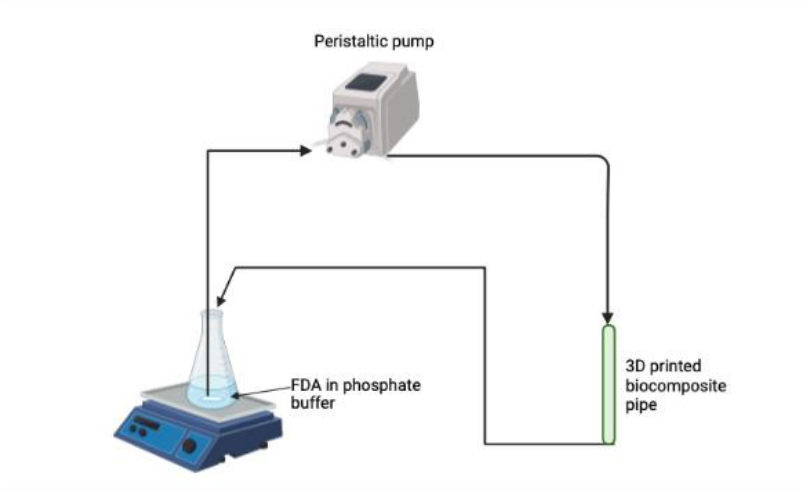

Figure 4.4.3- Continuous flow reaction for FDA hydrolysis using a 3D printed biocomposite pipe.

The data in Table 4.4.2 reported the flow system generated a higher average fluorescence for both suspended and immobilised yeast, most likely due to stirring methods. Similar to batch testing,

immobilised samples reported a far higher fluorescence than suspended systems. This is most likely due to extensive stirring which may damage and hence reduce activity of suspended cells. Equivalent immobilised cells are preserved within the polymer matrix protected from inhibitors or potentially cell damaging or toxic pollutants. Biocomposite suspended solids data provided evidence to suggest that similar to section 4.4.1, the polymer latex sufficiently retains the cells with little cell leaching and high cell adhesion. In addition, fluorescence results suggest the coatings provide a sufficiently porous environment with suitable gas exchange and diffusion pathways for cells to maintain short term (24 hours) activity. The fluorescence activity of both batch and flow samples over periods of up to 24 hours also suggest coatings were non-toxic to embedded cells. However, further investigations will be necessary to confirm this for longer durations.

	Blank	3D Printed Pipe (Surface area: 69 cm^2)	Yeast Suspension (0.1 g)
Fluorescence after 24 hours	11 ± 6	887 ± 58 (13 per cm^2)	51 ± 33
Conversion / %	0.9	69.1	4.0
Suspended solids (mg/L)	17 ± 4	38 ± 7	541 ± 71
Post freezing fluorescence	10 ± 4	714 ± 12 (10 per cm^2)	32 ± 19
Conversion / %	0.78	55.6	2.52
Suspended solids (mg/L)	14 ± 3	28 ± 6	486 ± 12

Table 4.4.2- Turbidity, fluorescence and percentage conversion comparing suspended and immobilised yeast in continuous flow reactions pre and post freezing

From this investigation, a continuous reaction procedure was created and implimented. The resulting data reported far greater absorbances using immobilised cells than a comparative suspension technique. Not only this, but immobilised samples also reported minimal cell leaching and higher activity post freezing.

4.5 Confocal and SEM Imaging Analysis of E. coli 10G pQE(-)ilux

Bacteria was cultured with the aid of Dr Lynn Dover at Northumbria University.

E. coli 10G pQE(-)ilux is a fluorescent bacterium that can be analysed using confocal microscopy. Figure 4.5.1 shows SEM screening of a 100 µm thick *E. coli* embedded latex surface after 3 hours. *E. coli* cells were measured to be 1 - 2 µm in length and 0.2 - 0.5 µm in width. Cells were found to be evenly distributed, covering all areas of the material surface. The image reported strong coalescence of the latex particles as only surface organisms could be visualised. To visualise embedded bacteria below the coating surface other microscopy techniques were used.

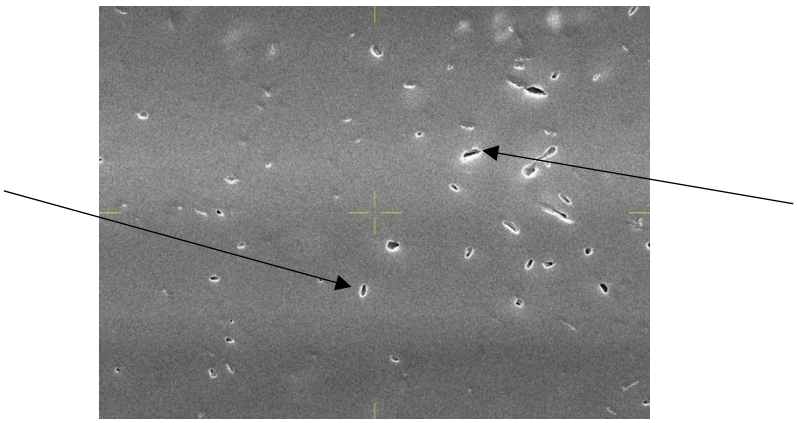

Figure 4.5.1- SEM surface imaging of immobilised E. coli 10G pQE(-)ilux in a latex film. (Black arrows indicate E.Coli cells).

Figure 4.5.2 shows images obtained from a confocal microscope using a Z layered scan under a DAPI filter. The scan takes multiple layered photos through the sample allowing a detailed 3D image from the base of the coating to the surface regardless of coating thickness. Confocal Z scanning confirmed previous SEM imaging in which *E. coli* was randomly dispersed throughout the coating. Although highly fluorescent areas measured in the range of 1 - 4 µm, their shape, particularly in 3D images were unlike typical *E. coli*. There are two possible explanations for this: Firstly, the latex polymer particles used to immobilise the bacteria are hydrophobic (to prevent them dissolving into water), this creates a problem as *E. coli* contains water. During the mixing process *E. coli* are more likely to clump together than be in contact with hydrophobic polymer particles, showing larger sized cells

under microscopes. Secondly, refractive light could manipulate the size and shape of cells, especially in 3D images whereby most *E. coli* found in Figure 4.5.2 were shown subject to tailing (blue arrows).

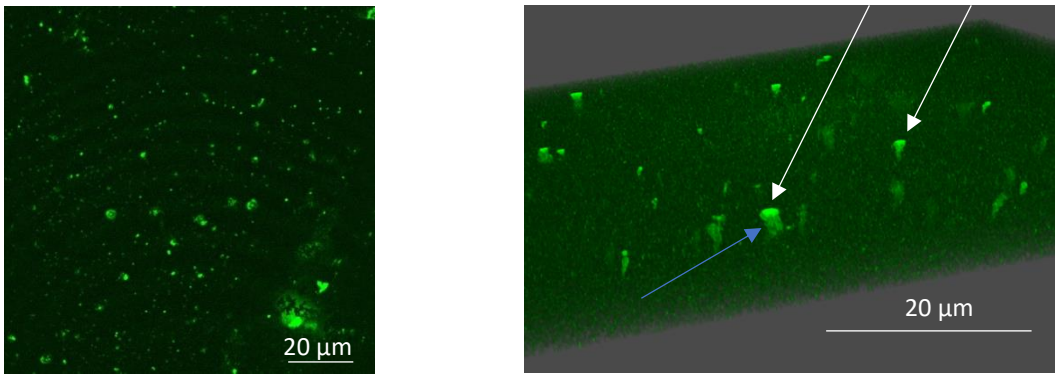

Figure 4.5.2- Confocal microscope Imaging of E. coli 10G pQE(-)ilux immobilised into a latex polymer coating onto a glass slide (white arrows indicating immobilised E. coli, blue arrows indicate image tailing)

The images discussed showed a randomised distribution of *E. coli* embedded throughout the polymer coating. Although cells remained fluorescent while embedded within the polymer coating, this did not indicate cell survival as fluorescence was present in living or dead cells. Therefore, these samples were examined for distribution of bacteria within the polymer coating, not cell sustainability, toxicity, or adhesion. To test cell survival an alternative bacterium that has the characteristics to be fluorescent only when alive would be required.

4.6 Immobilisation of *E. coli* producing N-terminally His-tagged eGFP proteins

This work was aided by Gregory Pollard at Bristol University.

BL21 (DE3) competent *E. coli* cells were investigated containing a pOPINF plasmid with a cloned eGFP gene so that it produces an N-terminally His-tagged eGFP protein (green fluorescent protein). Once bacteria are expressed with ITPG (isopropyl-beta-D-thiogalactopyranoside) solution, the fluorescent protein is produced and can be analysed using fluorescence microscopy. To investigate coating toxicity, *E. coli* were immobilised into the coating and expressed at controlled time points to measure cell activity. Time points consisted of short term (2, 4, and 6 hours) and long term (1, 3, 5 and 7 days). Each sample was viewed under a confocal microscope to assess if cells were alive.

Immobilised bacteria were analysed alongside two controls, one containing immobilised non-expressed *E. coli* and the other with no *E. coli* immobilised (Figure 4.6.1). *E. coli* cells remained fluorescent (alive) and active for a minimum of 7 days once expressed. However, notable reductions in fluorescence were reported between days 1 and 7 suggesting cell mortality (Figure 4.6.2). Although fluorescence was reported from cells after 7 days, accurately quantifying this between time points proved challenging. Furthermore, once cells were expressed and producing the GFP, cell death could no longer be assessed as the GFP would remain present regardless of cell death.

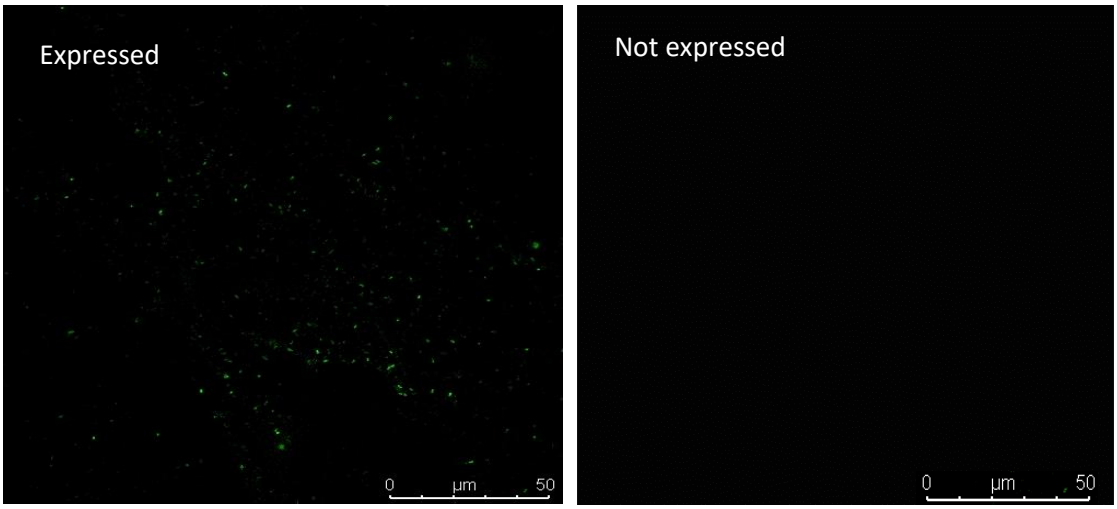

Table 4.6.1- Confocal imaging of immobilised E. coli BL21 (DE3) cells containing a pOPINF plasmid with a cloned eGFP gene to produce an N-terminally His-tagged eGFP protein expressed after 7 days in the coating (left). Confocal imaging of non-expressed E. coli BL21.

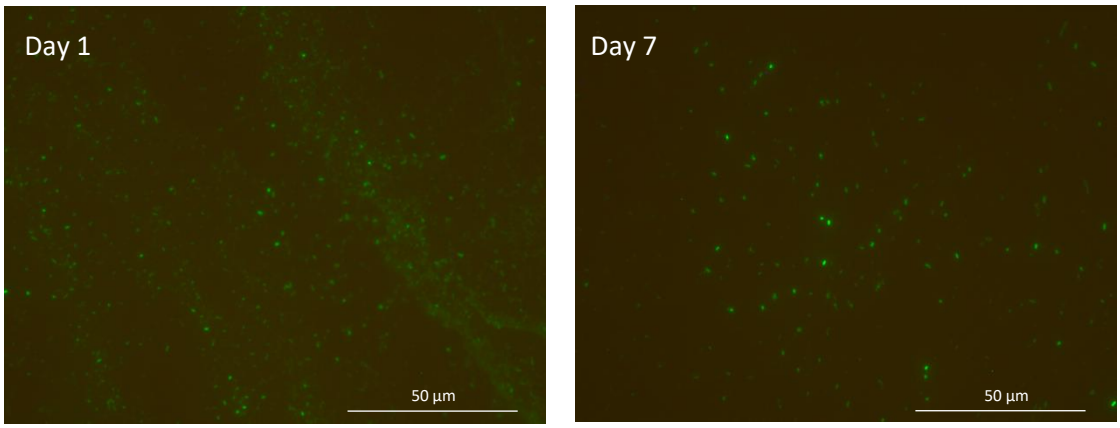

Figure 4.6.2- Immobilised E. coli BL21 (DE3) cells after expression during day 1 and day 7

The immobilisation of this fluorescent E. coli into a polymer latex film can be analysed through simple microscopic techniques. Furthermore, the immobilised cells not only survived within the coating but maintained their ability to produce their GFP once expressed after a minimum of 7 days. Further optimisation of this method would be necessary to obtain a numerical value to compare time points.

4.7 Immobilising cyanobacteria on loofah sponge surface using latex binders [164]

This work was investigated with the aid of Dr Warm In-Na from Newcastle University.

The majority of a microalgae and cyanobacteria cultivation system focuses on maintaining the cells as a suspension, free floating within the water column to minimise cell-cell or cell-surface interactions. However, the immobilisation of microalgae into engineered biofilms has enabled reductions in energy and resources while maintaining the system. [65] Cyanobacteria are single-celled organisms whose habitat can be fresh or marine water. [165] Under sunlight they can multiply quickly to create foam, scum, or mat-like films. Because of their ability to grow in extreme habitats, they have developed remarkable adaptability to varying environmental conditions. [166] Furthermore, their applications include the production of bioactive compounds, biofuels, biofertilizers, and detoxification agents. [155, 167] An increasing number of compounds from cyanobacteria have been isolated and identified as antimicrobial, antiviral, anticancer and antiprotozoal. [168, 169]
In this section, two species of cyanobacteria are immobilised into the latex coatings described in Chapter 3 to determine adhesion, toxicity, and carbon dioxide fixation. Biocomposite samples were named as stated in Table 3.3.1 (reported in *In-na et al*).[164]

4.7.1 Toxicity testing

A total of 9 latex additive compositions were tested for toxicity and adhesion with two cyanobacteria strains. The 9 samples were separated into 3 different polymer blends (S, N, and H) each with 0, 4 and 12 % (w/w) of Texanol™. The two cyanobacteria strains examined for cell growth are *S. elongatus PCC 7942* (PCC) and *S. elongatus CCAP 1479/1A* (CCAP). Approximately 1 mL of each cyanobacteria culture was mixed with 1 mL of 5 % (w/w) latex and left for 7 days. Cells were then counted to assess toxicity.

Figure 4.7.1 shows the normalised growth of each polymer alongside each glass transition temperature for both strains tested. Each strain proved to be influenced by changing polymer blends and increases in Texanol™ concentration. The ideal cell growth in this experiment would be 0 %, as this means the latex polymer is non-toxic, does not promote cell replication (or cell death rates are equal to cell replication rates). Each cell type reported different toxicities to each biocomposite. PCC showed S and H samples to be toxic towards cells (indicated by negative growth). The N biocomposites showed promising results, specifically 12N that showed -2 % growth. Like PCC, CCAP also reported high toxicity towards H biocomposites. However, S polymers promoted growth substantially. When plotting this toxicity data with the glass transition temperature of each latex, it was found that optimum T_g's for cell toxicity were in the range of 16 – 18 °C for CCAP and 11 – 13 °C for PCC.

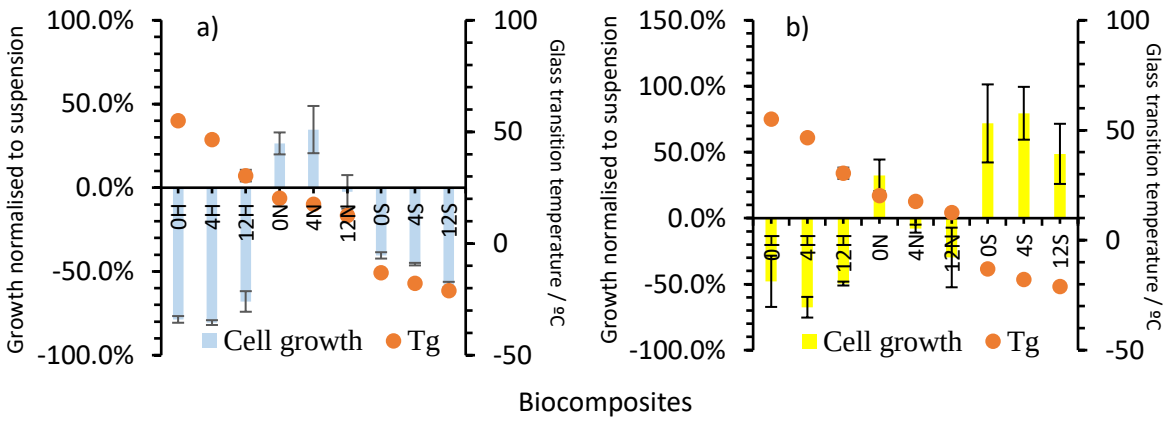

Figure 4.7.1- Cell toxicity to suspension controls with polymer glass transition temperature for a) S. elongates PCC 7942 and b) CCAP 1479/1A.

4.7.2 Adhesion testing

Loofahs are plant-based materials that are biodegradable, compostable and have been reported to be promising substrates for microorganism immobilisation. [65] To measure cell adhesion to surfaces, 1 cm loofah sponges were coated with each of the 9 biocomposites tested previously in section 4.7.1. Each loofah was shaken in darkness at 80 rpm for 1, 24, 48 and 72 hours. Any cells that were released were counted using a haemocytometer.

All binders reported a strong affinity for cell holding for both CCAP and PCC (Figure 4.7.2, Figure 4.7.3). All strains and binder combinations showed no more than 0.5 % of cells being released after 72 hours of testing. Increasing concentrations of Texanol™ was shown to marginally increase cell adhesion for both CCAP and PCC.

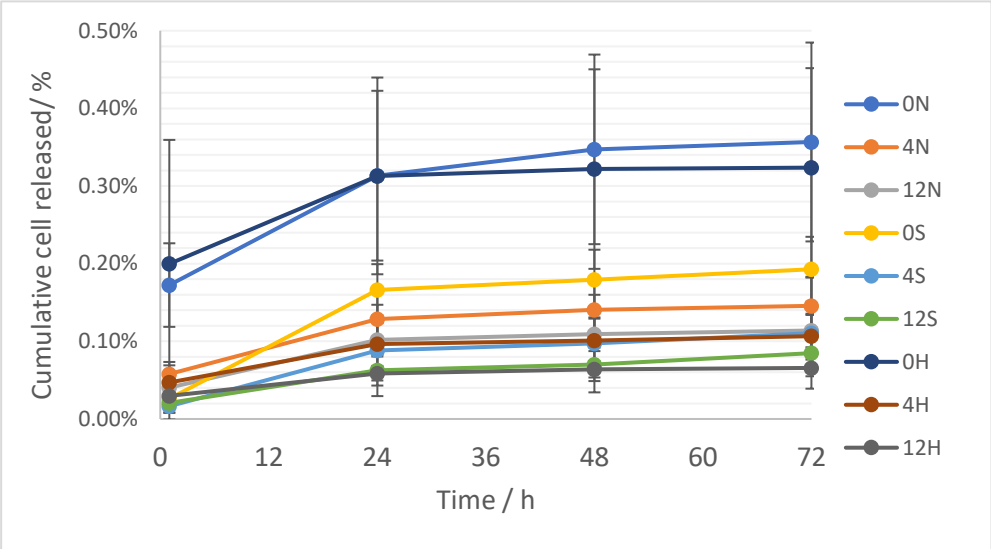

Figure 4.7.2- Cumulative cells released from adhesion testing for S. elongatus PCC 7942.

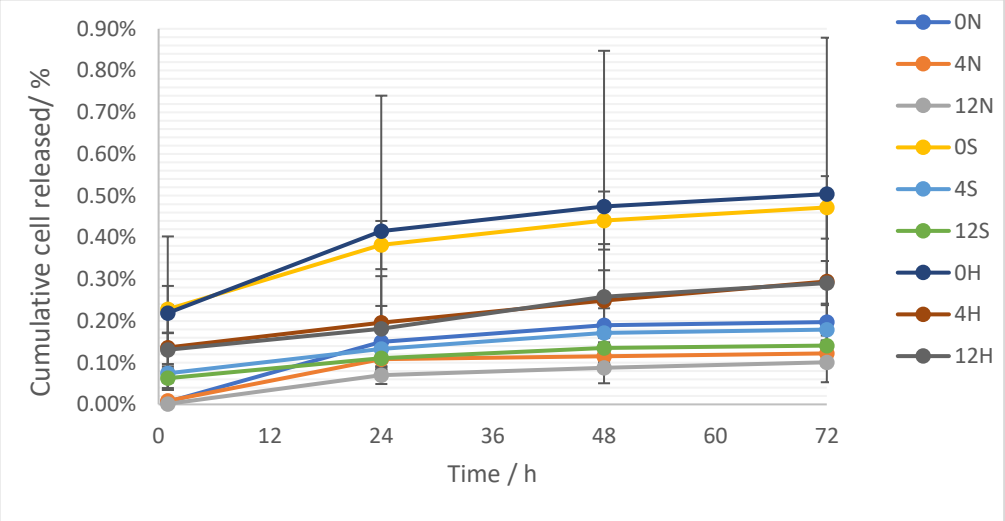

Figure 4.7.3- Cumulative cells released from adhesion testing for S. elongatus CCAP 1479/1A.

A decision matrix was derived from the previous toxicity and adhesion data (Figure 4.7.4). This was used to determine the best performing biocomposites for each cyanobacterium and to decide which biocomposites would be taken through into future testing. Each biocomposite was ranked (highest performing biocomposite was given the highest number) from adhesion and toxicity testing. Toxicity data was rated higher in a ratio of 3:2 as this was decided to be of higher importance. The best performing biocomposites will have both a high adhesion score and toxicity score (located in the top right corner of the matrix). From Figure 4.7.4, the best performing biocomposites were 4N and 12N for *S. elongatus* PCC and 4S and 12S for *S. elongatus* CCAP. These formulations were selected and carried forward to semi-batch net CO_2 adsorption testing.

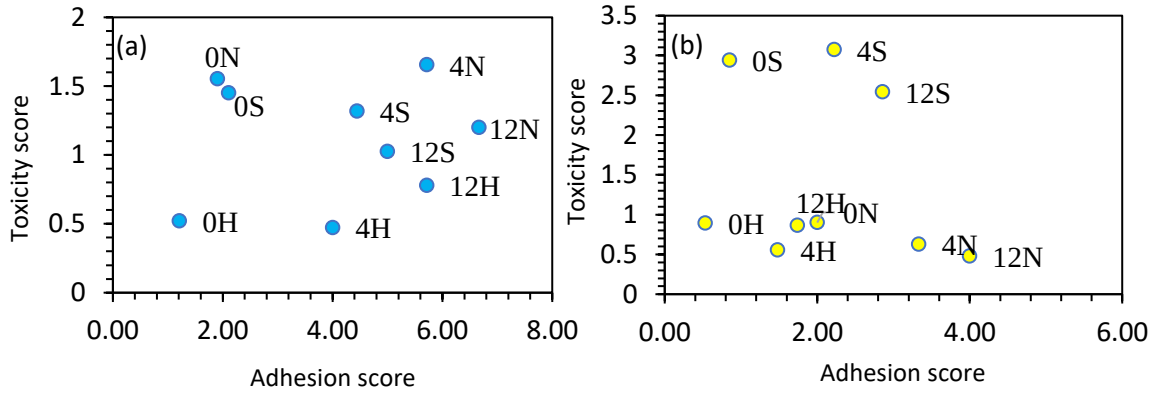

Figure 4.7.4- Decision matrix derived from toxicity and adhesion data for a) S. elongatus PCC 7942 and b) CCAP 1479/1A.

4.7.3 Biological responses to biocomposites

To investigate further into the sustainability of immobilised cyanobacteria within the biocomposite, the rate of photosynthesis needs to be examined. To do this PAM (Pulse amplitude modulation) analysis was used. PAM measures the apparent rate of photosynthesis (PS) which is used to calculate an estimation of the effective quantum yield of photosynthesis (Fv/Fm) (the proportion of photons of incident light that are used to drive the photochemistry in photosynthesis). [170] Each sample consisted of a latex polymer (1 mL) combined with concentrated cell mixture (1 mL) to form a biocoating (2.5 % v/v cells/sterile dH_2O) in individual wells of a 24-multiwell plate. These samples

were analysed alongside a corresponding latex control. All samples were monitored daily for seven days and gently mixed via reverse pipetting and left in darkness for 30 mins before taking results. Figure 4.7.5 and Figure 4.7.6 show the apparent rate of photosynthesis, while Figure 4.7.7 and Figure 4.7.8 show the maximum quantum yield for PCC and CCAP using the 9 biocomposites. The general correlation found that in PCC biocomposites, both the rate of photosynthesis and the maximum PSII quantum yield decreased from 0 to 7 days. However, for the rate of photosynthesis the PCC suspension control remained consistent around 4 μphoton m^{-2} s^{-1}. PCC cells suspended in the 12N biocomposite had the lowest PS and Fv/Fm indicating high toxicity towards the polymer. CCAP biocomposites reported similar negative trends in the rate of photosynthesis to the suspension control. H and N polymers reduced PS for CCAP cells below that of the suspension controls. The 0S and 4S samples reported PS levels similar to the suspension control including an improved PS response on days 2-4 suggesting an improvement in photo transport. More interestingly, nearly all samples showed a secondary peak in which photosynthesis increases, usually at 3 - 5 days. This increase is also seen in the suspension control but not to the same extent. Reasons behind this are unknown.

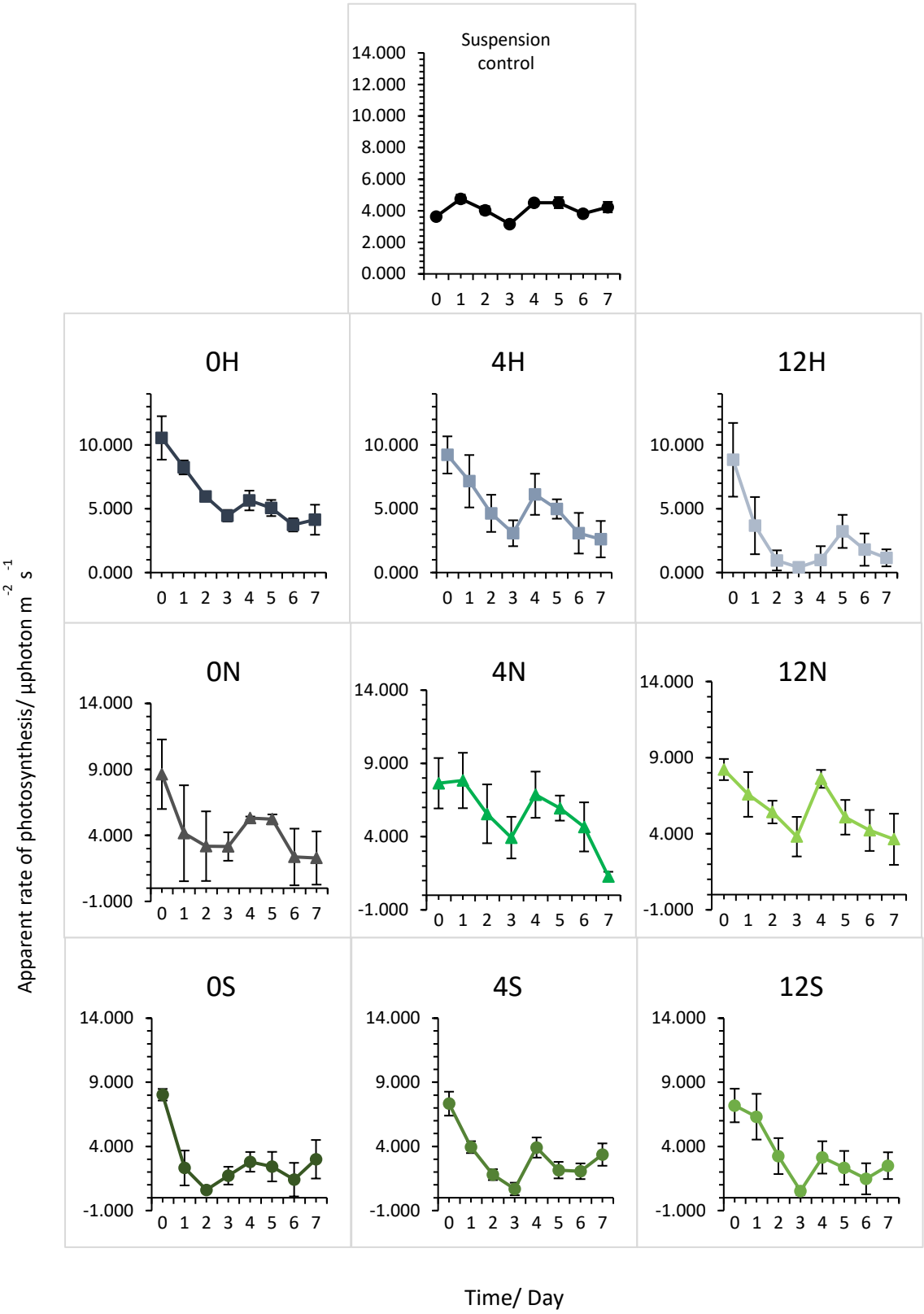

Figure 4.7.5- Apparent rate of photosynthesis of S. elongatus PCC 7942 in response to latex polymers.

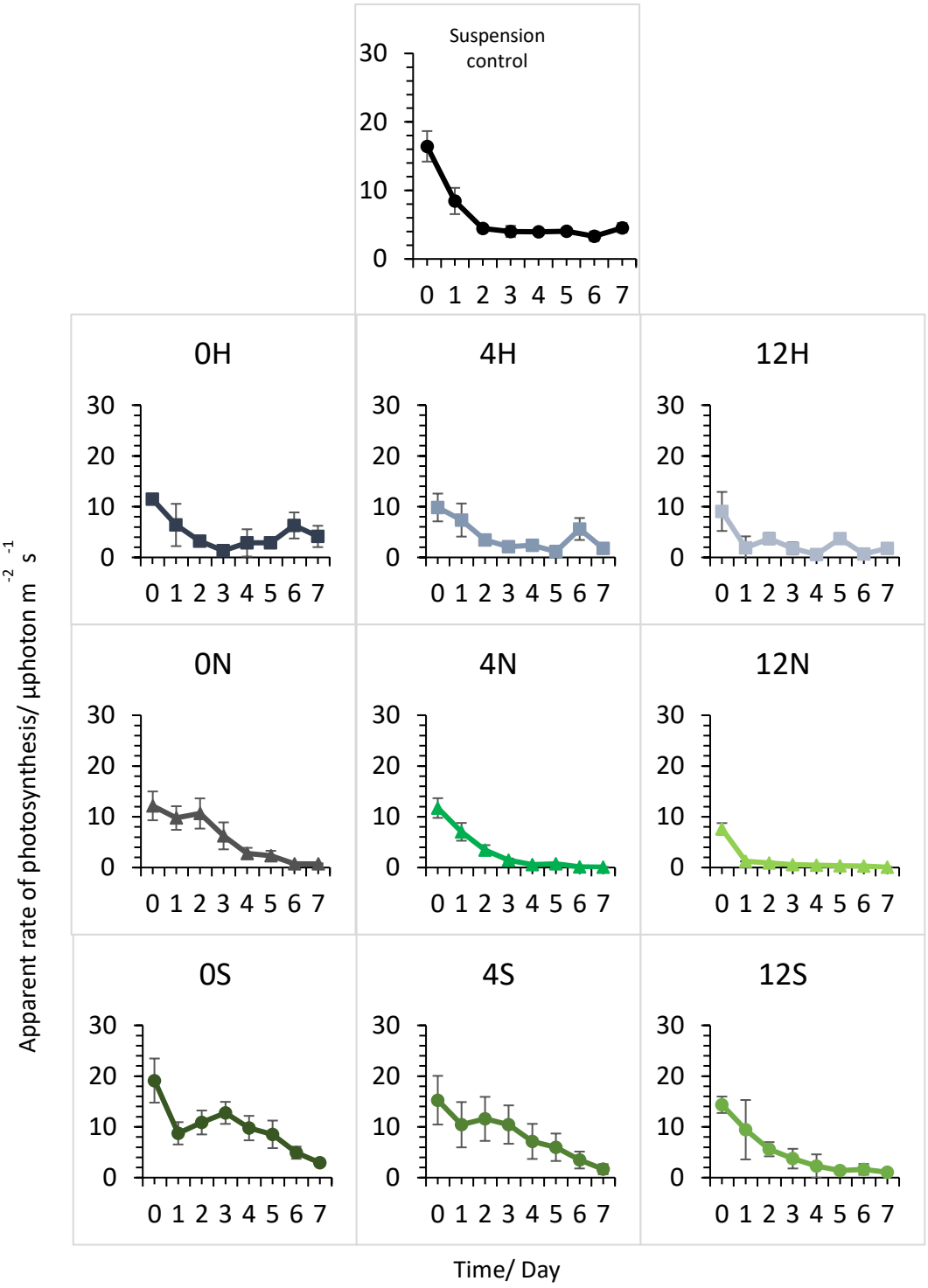

Figure 4.7.6- Apparent rate of photosynthesis of S. elongatus CCAP 1479/1A in response to latex polymers.

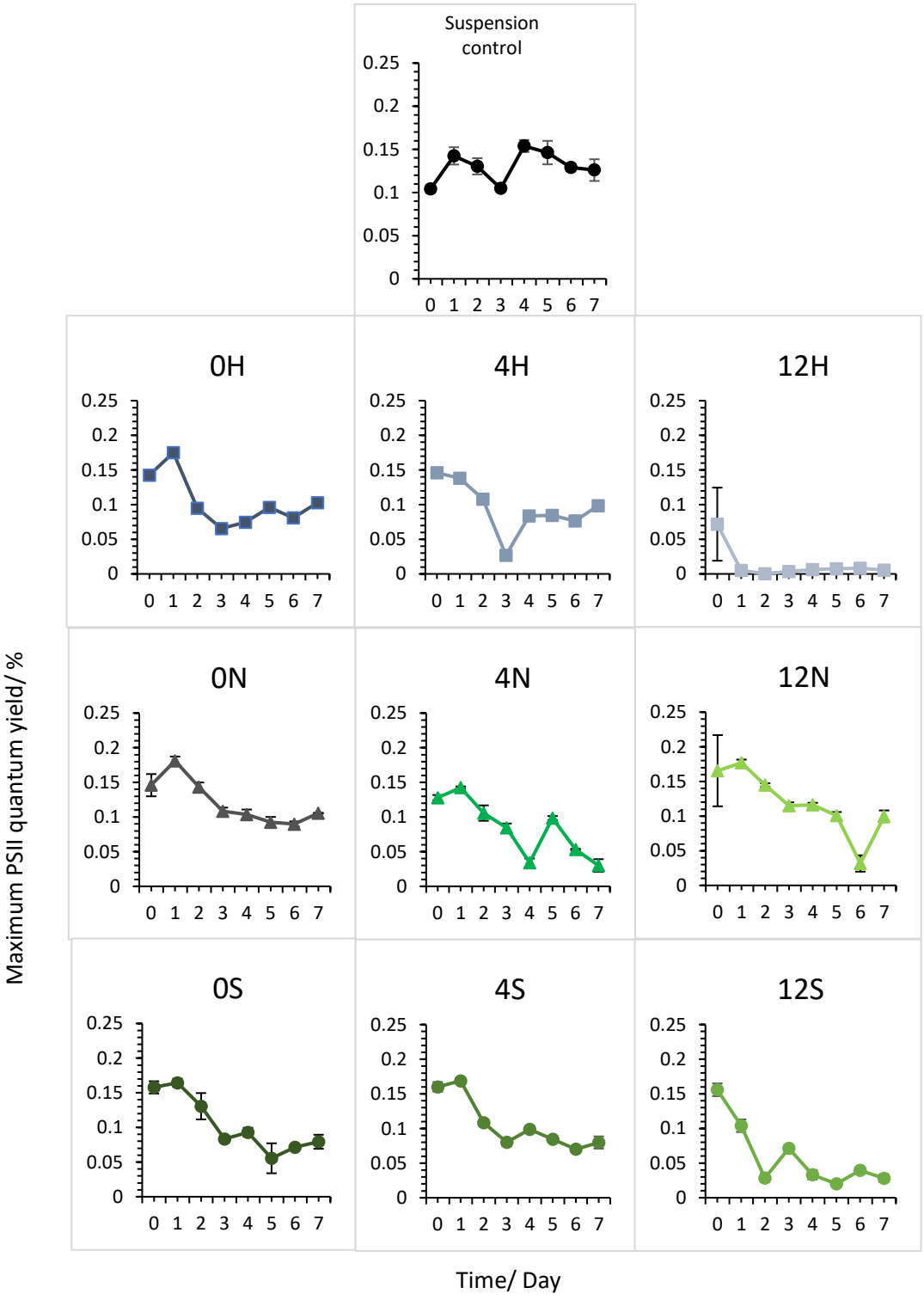

Figure 4.7.7- Maximum PSII quantum yield of S. elongatus PCC 7942 in response to latex polymers.

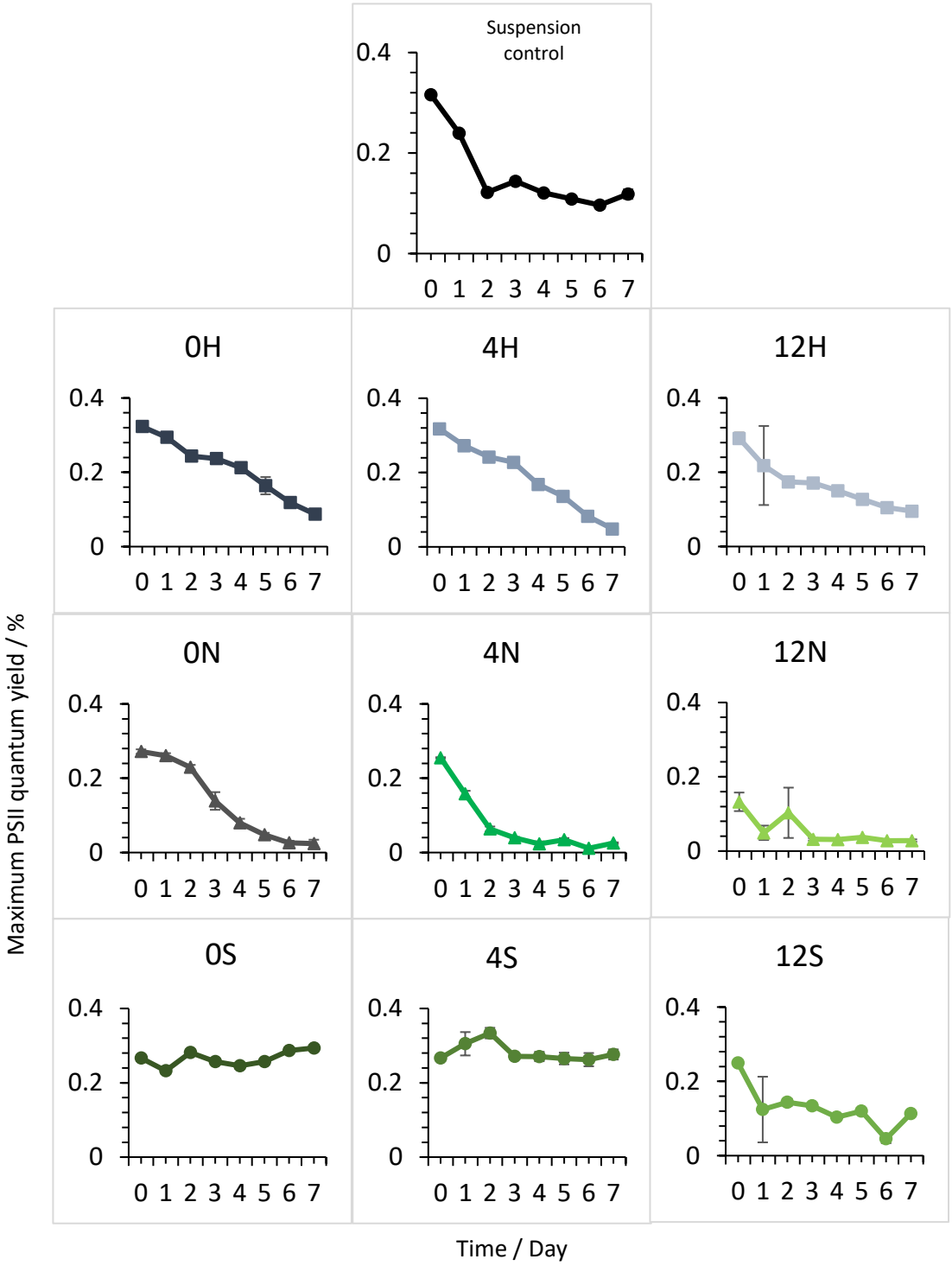

Figure 4.7.8- Maximum PSII quantum yield of S. elongatus CCAP 1479/1A in response to latex polymers.

The same investigation was repeated using different concentrations of latex (2.5 and 5 %) and additives (10 % glycerol and aloe vera) and run alongside suspension controls (Figure 4.7.9). In 2.5 and 5 % biocomposite samples, reductions in the apparent rate of photosynthesis was reported from days 1 to 7, whereas the equivalent suspension control remained stable. PCC (Figure 4.7.9 (a)) reported similar responses to photosynthesis with or without the presence of aloe vera and glycerol. The same trends can be seen in the concentration of latex with no significant difference between the two samples. For CCAP 1479/1A biocomposites with 2.5 % latex concentration reported significantly higher responses, exceeding that of suspension controls from days 2-7. The addition of glycerol and aloe vera (there due to its known hydrating properties [171]) reduced rates of photosynthesis dramatically from days 1 to 2 for CCAP 1479/1A, as did increasing concentrations of the latex concentration.

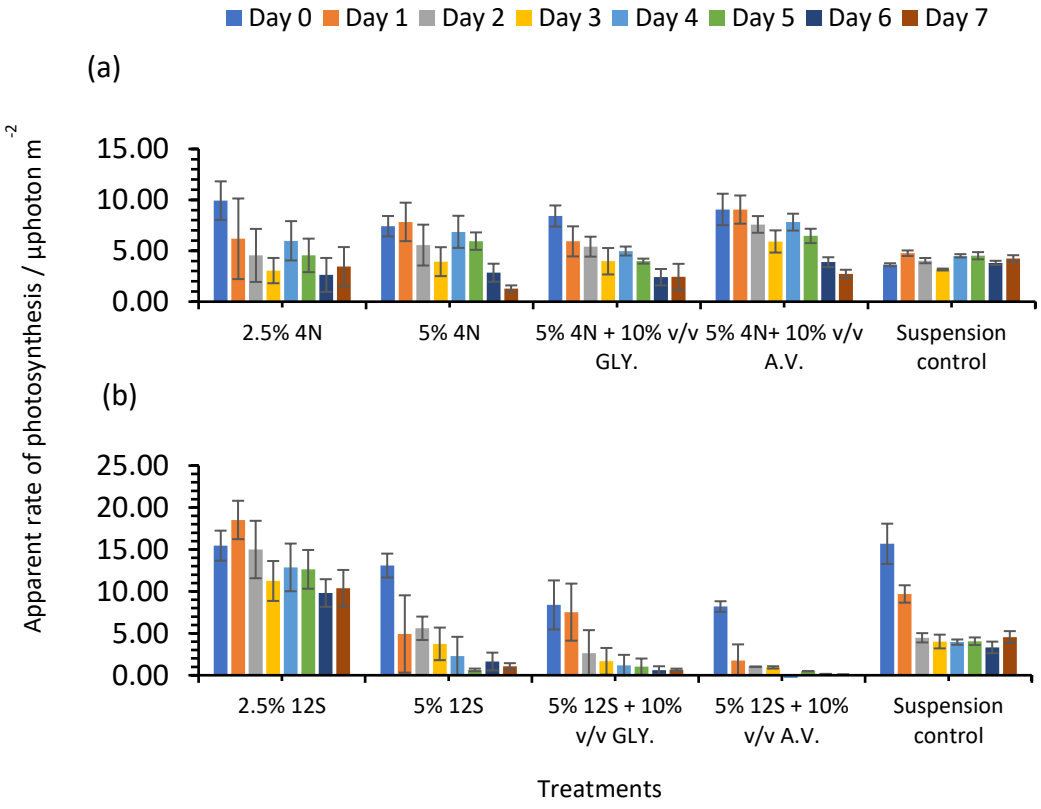

Figure 4.7.9- Apparent rate of photosynthesis for S. elongatus a) PCC 7942 and b) CCAP 1479/1A with the addition of 4 and 12 % Texanol, glycerol (GLY) and aloe vera (AV).

4.7.4 Net CO_2 fixation rates

Another method that can be used to identify the wellbeing of bacteria is CO_2 fixation testing. Cyanobacteria use carbon dioxide in processes that synthesise sugars and other useful compounds. This method continuously analyses CO_2 levels in a closed atmosphere. In this investigation a 2.5 % latex concentration was used for each biocomposite. Each cyanobacterium was tested with the same biocomposites as described in section 4.7.3 using a loofah surface. Loofahs were coated, dried, and placed into a glass chamber. These containers were flushed with 45 mL of 5 % CO_2 air and sealed. Carbon dioxide levels were measured by extracting the headspace with an airtight syringe and injecting it into an infrared absorption CO_2 meter. After analysis, the equivalent volume of CO_2 gas mixture was replenished.

Biocomposites containing PCC 7942 showed significant cell leaching (seen by the increasing colour of green) in the first four weeks of testing (Figure 4.7.10 (a)). Both samples containing 4 % and 12 % Texanol™ reported CO_2 adsorption in the first 4 days (Figure 4.7.10 (b)). After this period biocomposites containing the 12N biocomposite were found to release CO_2 from days 4 - 16 (indicated by the decrease in cumulative net CO_2). This corresponds to the photos found in Figure 4.7.10 that suggest pigment bleaching. This could be due to the high levels of Texanol™ found within this biocomposite as this trend was less pronounced in the 4N biocomposite. When introducing this to cyanobacteria, naturally there is potential for this compound to be toxic to living organisms and hence could be responsible for the deterioration of CO_2 absorption. Furthermore, the slow evaporation of Texanol™ can also be responsible for the increase in CO_2 absorption reported after 16 days. Despite Texanol™ being potentially toxic to these cyanobacteria, it appears necessary for the optimum mechanical properties for the polymer. Despite this, the 12N biocomposite accumulated 0.2 – 0.7 mol CO_2 / g biomass and 4N accumulated 0.7 – 1.1 mol CO_2 / g biomass by day 28. Both biocomposites gained a higher accumulation of CO_2 than the suspension control. Although analysis was not recorded after 28 days (due to cells growing out of the loofah), from Figure 4.7.10

predictions can be made to suggest the biocomposites would continue to increase in cumulative net CO_2 fixation for a longer duration of time however, this would require further investigations. Although PCC showed a marginally higher total net CO_2 fixation than CCAP after 28 days, CCAP showed no bleaching or overgrowing within the loofah (Figure 4.7.11(a)). Because of this, analysis was continued up to 84 days. Throughout this 84-day period, both 4S and 12S showed final net CO_2 fixation levels to be 7 - 15 times and 14 - 17 times higher than the suspension control. Interestingly, higher concentrations of Texanol™ were found to promote CCAP net CO_2 fixation tests, reasons behind this are unknown (Figure 4.7.11(b)). Both 4N and 12N binders before PCC CO_2 testing showed cells were embedded within the latex coating (Figure 4.7.12). Biocomposites used for CCAP despite cell growth, maintained strong adhesion to the biocomposite (Figure 4.7.13).

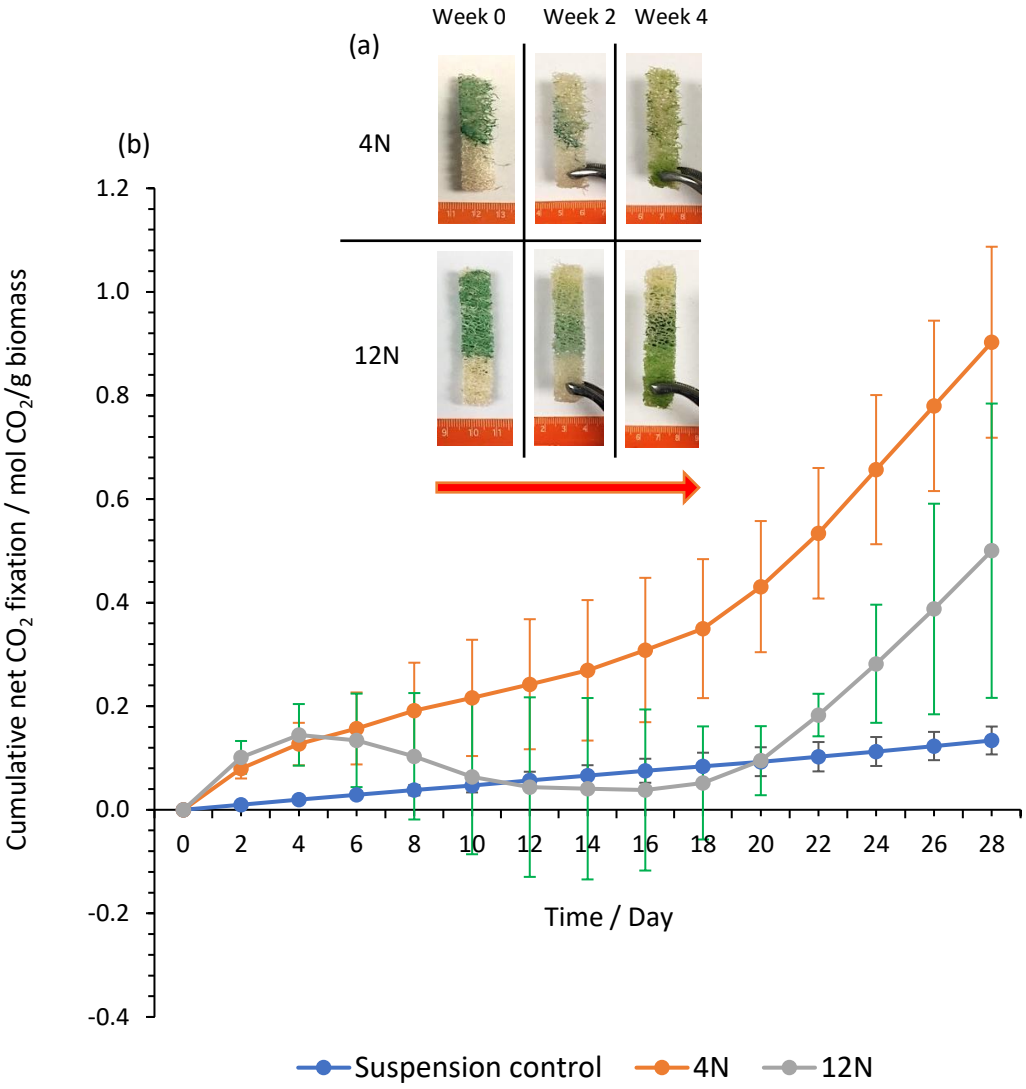

Figure 4.7.10- Semi-batch CO_2 absorption tests on a) S. elongatus PCC 7942 biocomposites with the 4N and 12N latex polymers. a) cell release and pigment bleaching b) Cumulative net CO_2 absorption over four weeks.

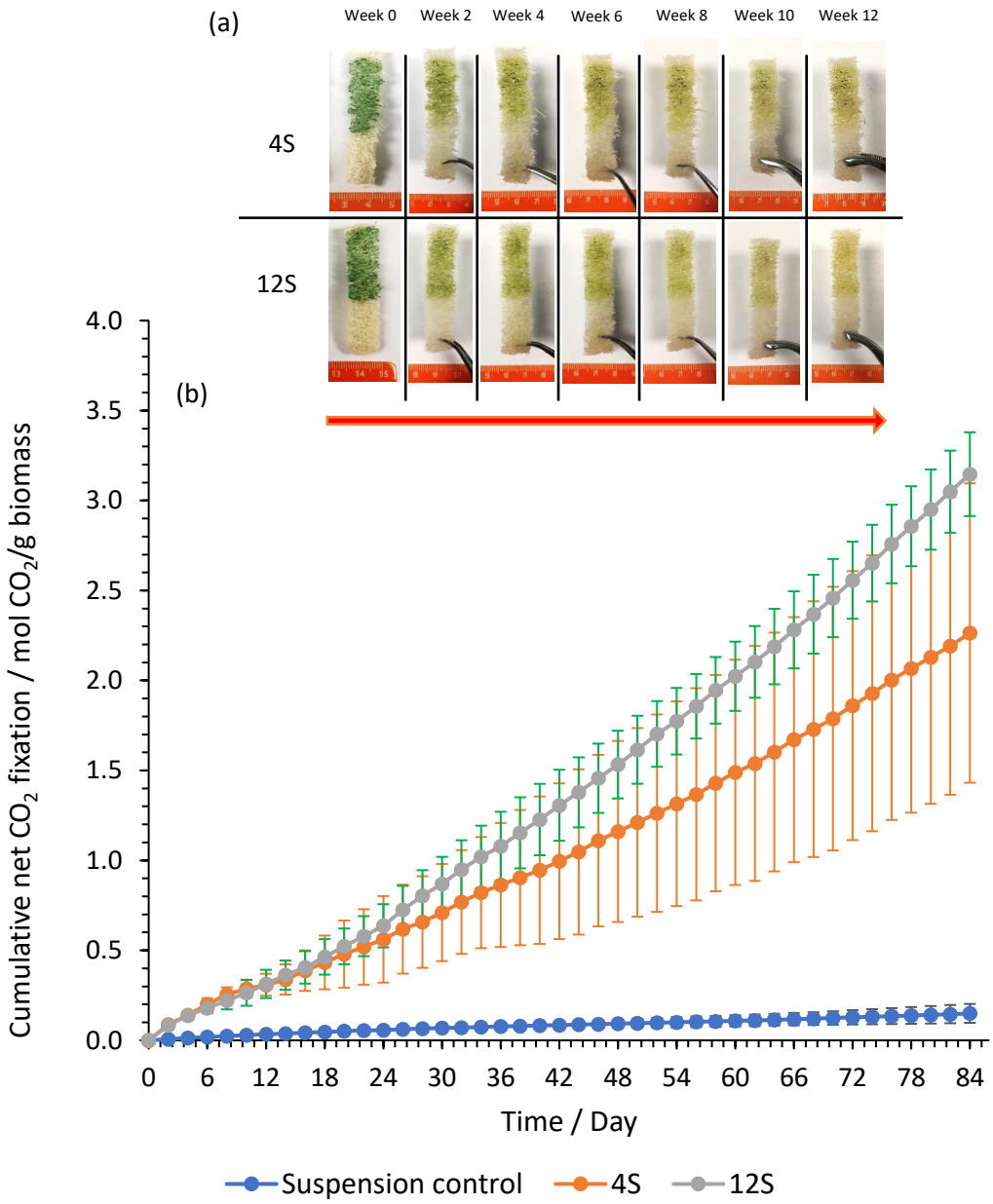

Figure 4.7.11- Semi-batch CO_2 absorption tests on a) S. elongatus CCAP 1479/1A biocomposites with polymers 4S and 12S. a) Cell release and pigment bleaching b) Cumulative net CO_2 absorption over the 12-week period.

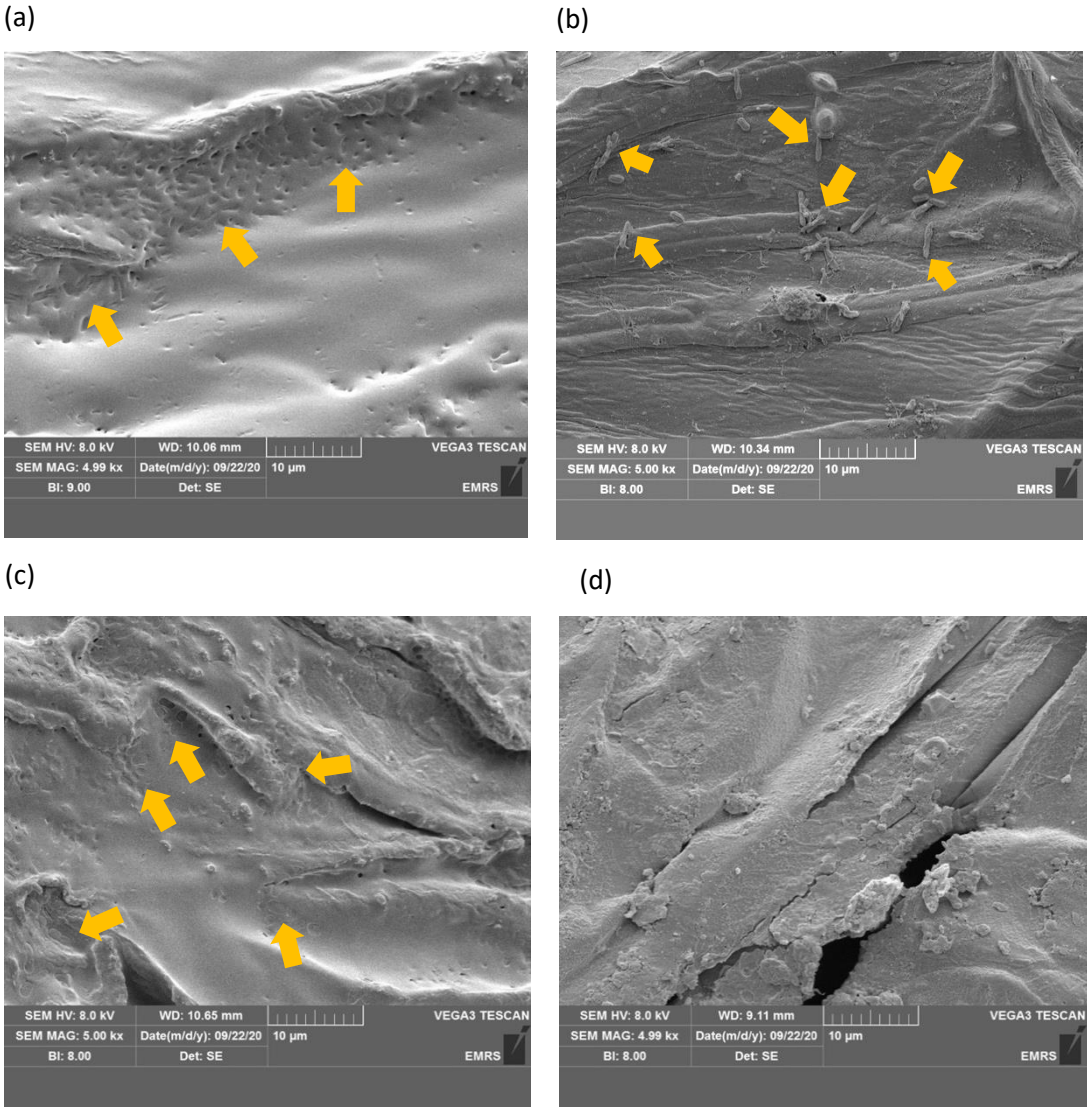

Figure 4.7.12-SEM images of S. elongatus PCC 7942 biocomposites before a) 4N and c) 12N and after b) 4N and d) 12N semi-batch CO2 absorption tests. Yellow arrows indicate where cells were deposited on the biocomposites.

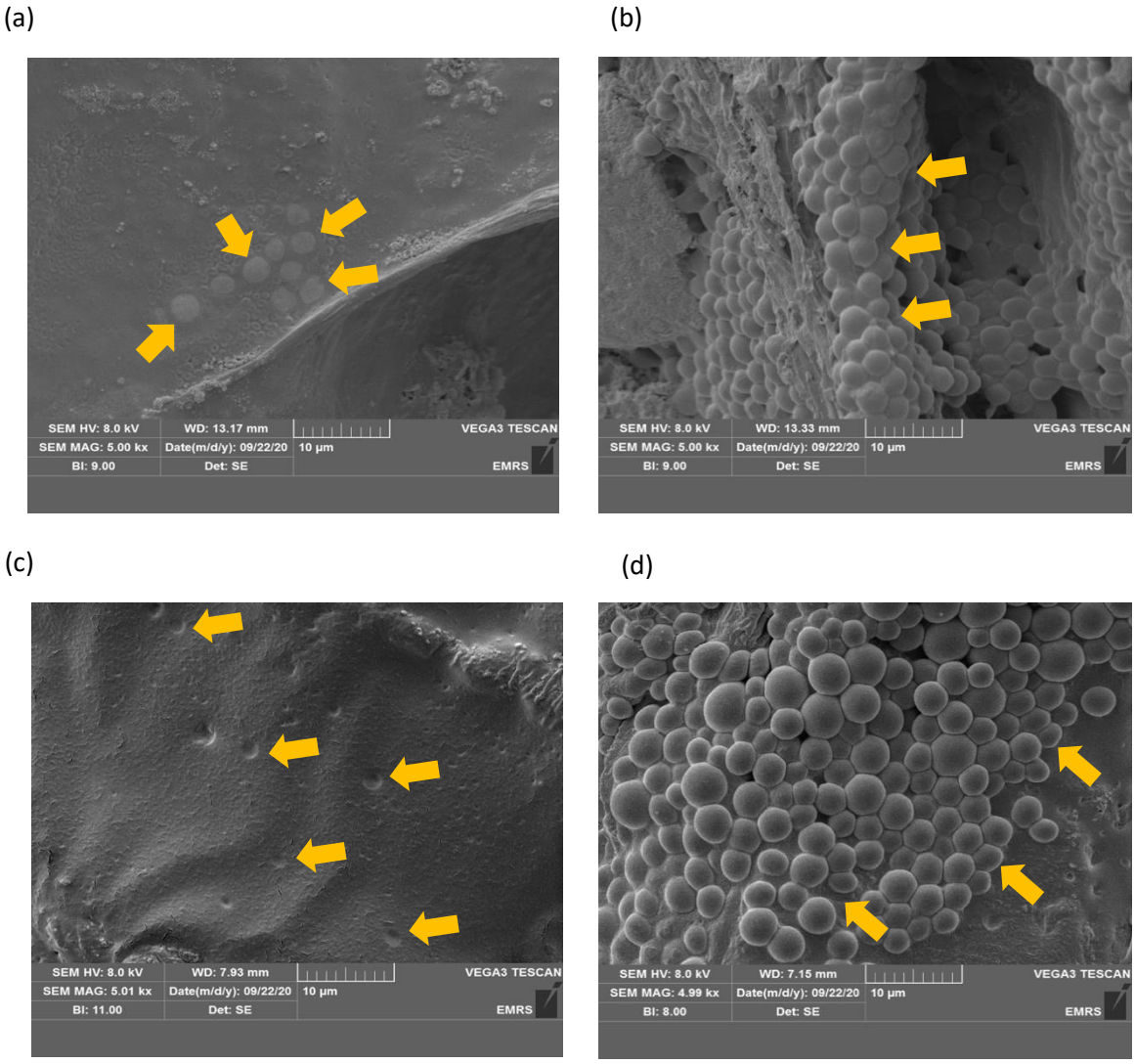

Figure 4.7.13- SEM images of S. elongatus CCAP 1479/1A biocomposites before a) 4S, c) 12S and after b) 4S, d) 12S semi-batch CO_2 absorption tests. Yellow arrows indicate where cells were deposited on the biocomposites.

The above CO_2 fixation testing results were compared to selected literature for related cell species (Table 4.7.1). The results reported in this study compared favourably with recent studies when adjusting for cell loading rate showing the highest CO_2 fixation rate from relevant literature. The cells in this study remained operational over much longer periods (84 days) versus 15 hours [172] or 3 weeks [90].

Species and Strain	Type	System description	CO_2 fixation rate		Ref
			mmol CO2 $m^{-2}d^{-1}$	g CO_2 $g^{-1}_{biomass}d^{-1}$	
Synechococcus PCC 7002	Cyanophyte	Paper-based biocomposites with 20% v/v CO2 at 25 °C; light: 100 µmol m^{-2} s^{-1} in batch for 500 h.	136	0.22	90
Chlorella vulgaris	Freshwater chlorophyte	Biopolymer porous paper pulp in microfiber cellulose mixed with chitosan matrix in BG11 and fixed onto spinning disk reactor for 15 h at 300 rpm with 5% v/v CO2.	110.64	1.38	172
Chlorella vulgaris	Freshwater chlorophyte	Immobilized to loofah at 18 °C; light: 16:8 photoperiod at 30.5 µmol m^{-2} s^{-1} with continuous 5% v/v CO2 at day 42.	2.38	0.17	65
Dunaliella salina	Marine chlorophyte	Immobilized to loofah at 18 °C; light: 16:8 photoperiod at 30.5 µmol m^{-2} s^{-1} with continuous 5% v/v CO2 at day 42.	3.44	0.25	65
S. elongatus CCAP 1479/1A	Cyanophyte	Immobilized to loofah at 18 °C; light: 16:8 photoperiod at 30.5 µmol m^{-2} s^{-1} with 5% v/v CO2 in semi-batch at day 56.	6.15	0.93	65
S. elongatus CCAP 1479/1A	Cyanophyte	Immobilized to loofah with 12S latex at 18 °C; light: 16:8 photoperiod at 30.5 µmol m^{-2} s^{-1} with 5% v/v CO2 in semibatch at day 84.	9.57	1.57	This study

Table 4.7.1- Comparison of the highest CO2 absorption rates with biocomposites relative to related literature.

4.7.5 Carbohydrate production in biocomposites

Following CO_2 adsorption testing, carbohydrate content of the dried cyanobacteria biomass (normalised to the carbohydrate content of the loofah scaffolds with binders) was tested against suspension controls. The binders remained the same for each cyanobacteria used previously in CO_2 adsorption testing (PCC 7942 - 4N/12N) (CCAP 1479-1A - 4S/12S). Samples were dried and grounded before being homogenised with H_2SO_4. Each sample was mixed with phenol solution and was analysed using a UV/Vis spectrometer at 485 nm. Samples were taken at 0, 2, 4 for PCC and 0, 2 ,4, 6 and 12 weeks for CCAP.

From Figure 4.7.14 it was found for PCC in weeks 0 and 2, total carbohydrate extraction was higher than in suspension controls, however in the final week all samples showed similar carbohydrate content. This trend was also found in CCAP whereby biocomposites reported higher total carbohydrate up to week 4. Following this period all samples remained consistent till week 12.

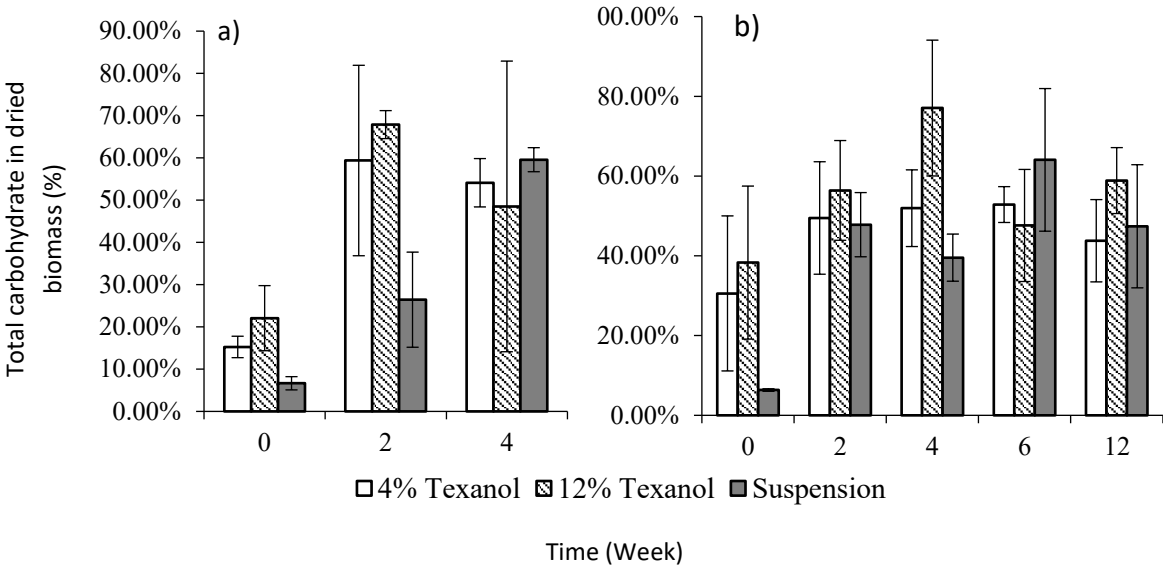

Figure 4.7.14- Total carbohydrate content extracted from a) S. elongatus PCC 7942 4N, 12N and b) CCAP 1479/1A 4S, 12S biocomposites during the CO_2 absorption test.

4.8 Summary

In chapter 3 a total of 9 acrylic-styrene based latex polymers ranging in different variations of monomer and Texanol™ composition was synthesised and characterised to identify possible sustainable environments of microorganism immobilisation. These water-borne polymer coatings were chosen due to their cost-effective synthesis and optimum glass transition close to room temperature. In this chapter, Baker's yeast was immobilised to catalyse numerous biocatalytic reactions while within a polymer coating. Reaction rates far exceeded those of suspended yeast equivalents with minimal cell leaching. With the aid of microscope imaging, the positioning of fluorescent *E. coli* cells was determined within a polymer film to confirm uniform and random distribution throughout the coating. *E. coli* capable of producing a GFP were assessed and reported to maintain cell metabolic activity while within a polymer film after 7 days once expressed.

The incorporation of cyanobacteria to these 9 latexes was analysed using toxicity testing, adhesion testing and CO_2 absorption techniques. Although residual monomer was not examined in this investigation, it is assumed that small levels of both styrene and butyl acrylate monomer are

present. The composition of these latex coatings proved to be essential for the toxicity towards cyanobacteria. The harder latex (75 Sty:25 BA) when tested for toxicity in both cyanobacteria proved highly toxic, reducing growth up to 80 %. This would support previous research on styrene's detrimental impacts on aquatic life and high toxicity to living organisms. [173] However, higher ratios of butyl acrylate, despite being harmful upon adsorption, inhalation, and to aquatic life did not have any growth reducing effects upon either cyanobacterium tested. This is most likely due to its low levels of bioaccumulation. Each latex polymer responded very differently in correspondence to the two cyanobacteria tested. *S. elongatus* PCC 7942 showed positive growth in only two samples tested, none of which contained extreme quantities of one monomer suggesting two things; the T_g of the polymer sample can affect the levels of toxicity, and hence development in cell growth. Secondly, the composition of the coating can highly influence cell toxicity and sustainability in the presence of harmful monomers. In the case of CCAP 1479/1A higher butyl acrylate ratios were favoured over styrene for unwanted cell toxicity. However, PCC 7942 rates proved detrimental to any extreme ratios of BA or styrene monomer.

The objective of this chapter was to create a biohybrid system using the integration of microorganisms embedded within a polymer film coating. Biohybrid systems were constructed which enabled yeast, *E. Coli,* and cyanobacteria to successfully survive and remain metabolically active for a period of days to months.

5 Self-healing polymers

5.1 Introduction to self-healing materials

Previously, materials that had reached their approved lifetime, or had received mechanical damage had to be discarded and replaced with new materials. Whilst a grossly damaged part is probably impossible to do anything with but replace, the growth and merging of microcracks, which would also result in the reduction of the service life of the materials is a more tractable problem for material science. It is possible to imagine a material that can detect and mend these cracks, and recover to its original properties, allowing the material to continue in its role with an extended lifetime. One way in which this could be achieved would be to develop materials which can self-heal. Polymer materials have since become some of the most widely investigated materials for self-healing capability due to their high intrinsic polymer chain potential. Despite this, issues are still present in creating materials with efficient self-healing whilst keeping their original physical properties. Approaches such as weaker reversible bonds or dynamic interactions are susceptible to weak mechanical properties when stretching. [174] It is therefore important to ensure these properties are not hindered while developing self-healing methods.

In this chapter a polyurethane (PU) material composed of four monomer components is investigated: poly(tetramethylene ether) glycol (PTMG), methylene diphenyl diisocyanate (MDI), 1,6 hexandiol (HDO), and 2, 2- bis(hydroxymethyl)propanoic acid (DMPA). In addition, the aim is to investigate polymer properties by creating a range of polyurethanes through alterations in monomer composition. Formulated polymers will be analysed for intrinsic self-healing through a preliminary cut and stick procedure. Following this, further analysis will be made using tensile strength testing whereby an optimum formulation can be established, and conclusions to potential origins for the polymers healing capabilities are analysed.

5.1.1 Polyurethane synthesis

This work was aided by Dr Robert Downs, Northumbria University (PDRA on the Immortality Manufacturing project).

A polyurethane can be regarded as a linear alternating copolymer formed by the reaction of an isocyanate rigid monomer in addition with a flexible polyol. In PUs, soft segments are composed of polyether, polyester or polycarbonate-based glycols and hard segments made from diisocyanate and diols of low molecular weight. This allows polyurethanes to exist with a range of performance from flexible soft polymers to hard rigid plastics as determined by the components exhibiting chain entanglement, crosslinking, and intermolecular forces between chains. [175] Hard segments chains can occasionally be in the crystalline state due to the formation of hydrogen bonded arrays creating highly rigid structures.

The synthesis followed a two-step procedure (Scheme 5.1.1). PTMG and MDI were placed into a beaker under heat using an oil bath and mixed slowly for 2 hours. The temperature was increased and HDO and DMPA were added together in small batches under stirring. After addition the mixture was cured for 2 hours at 190 °C.

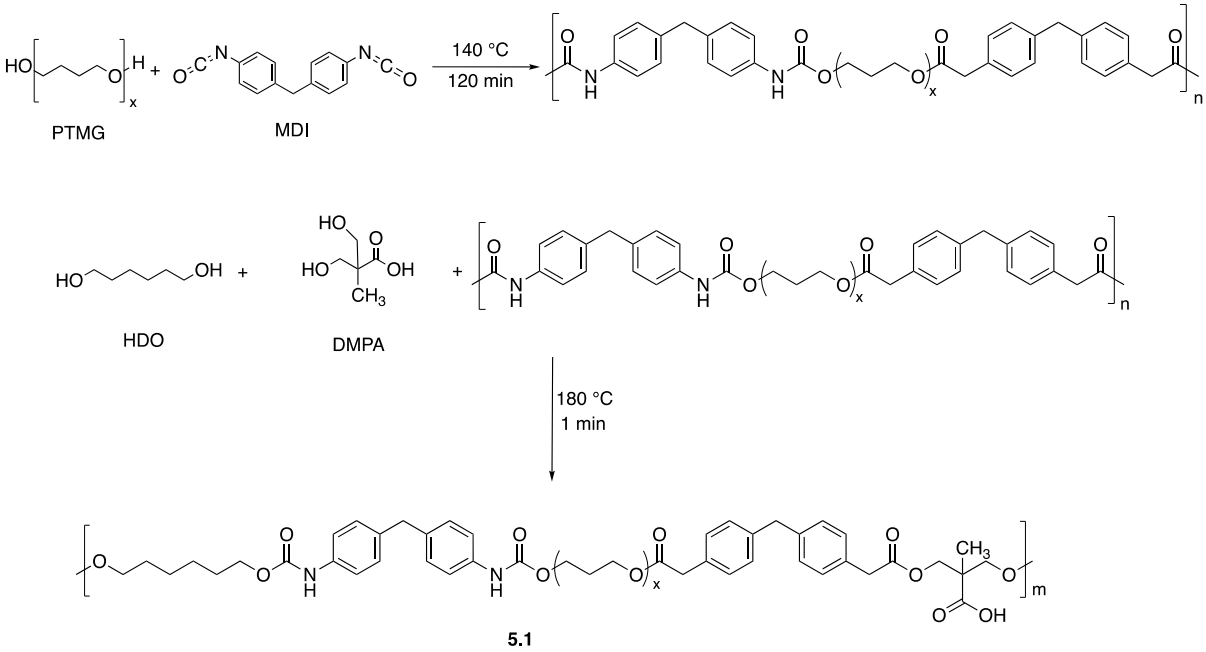

Scheme 5.1.1- Two-step polyurethane synthesis.

5.2 Optimisation of polymerisation of polyurethanes

Following the synthesis of the first PU sample (PU 1.0) ratios of OH : NCO functional groups were kept at 1.11 : 1.00 to minimise harmful residual isocyanate. Three different molecular weights of PTMG were used, 650, 1000, and 2900 to investigate the importance of chain length on physical polymer properties. Each formulation was cured for 24 hours in dog bone moulds following synthesis and cut into two separate parts directly in the centre of the dog bone. Each part was manually pushed back together so that cut areas were re-joined. Samples were held together for 3 seconds and left overnight. A total of 30 formulations were synthesised using varying quantities of HDO and DMPA with each PTMG. After 24 hours, small forces were applied to the joint to test material strength. If there was resistance between the joint section, the material was marked as being a potential self-healing polyurethane formulation (Y). If the material did not show any signs of healing, resistance or strength in the cut area it was marked as not self-healing (N). Table 5.2.1 shows the composition of each PU sample.

	Mass / g							
PU Sample	**HDO**	**PTMG**			**DMPA**	**MDI**	**Mol eq. OH : NCO**	**Self-healing**
		650	1000	2900				
1.0	1.560	-	11.800	-	1.780	26.000	1.00 : 3.36	N
2.0	1.560	-	26.000	-	1.780	11.800	1.13 : 1.00	Y
3.0	1.560	-	39.000	-	1.870	11.800	1.39 : 1.00	Y
4.0	1.560	-	26.000	-	1.780	11.800	1.11 : 1.00	Y
5.0	1.872	-	31.200	-	2.136	11.800	1.34 : 1.00	Y
6.0	2.184	-	36.400	-	2.492	11.800	1.56 : 1.00	Y
7.0	2.496	-	41.600	-	2.848	11.800	1.78 : 1.00	Y
8.0	2.350	-	26.000	-	0.890	11.800	1.11 : 1.00	N
9.0	2.440	-	26.000	-	0.780	11.800	1.11 : 1.00	N
10.0	3.125	-	26.000	-	0.000	11.800	1.11 : 1.00	N
11.0	0.000	-	26.000	-	3.550	11.800	1.11 : 1.00	Y
12.0	1.560	-	-	75.400	1.780	11.800	1.11 : 1.00	N
13.0	1.560	16.900	-	-	1.780	11.800	1.11 : 1.00	N/a
14.0	0.000	-	-	75.400	3.550	11.800	1.11 : 1.00	Y
15.0	0.780	-	-	75.400	2.660	11.800	1.11 : 1.00	Y
16.0	2.440	-	-	75.400	0.780	11.800	1.11 : 1.00	N
17.0	3.125	-	-	75.400	0.000	11.800	1.11 : 1.00	N
18.0	1.850	-	26.000	-	1.450	11.800	1.11 : 1.00	N
19.0	2.150	-	26.000	-	1.100	11.800	1.11 : 1.00	N
20.0	2.250	-	26.000	-	1.000	11.800	1.11 : 1.00	N
21.0	1.765	-	26.000	-	1.550	11.800	1.11 : 1.00	N
22.0	1.675	-	26.000	-	1.650	11.800	1.11 : 1.00	N
23.0	1.365	-	-	75.400	2.000	11.800	1.11 : 1.00	N

24.0	1.015	-	-	75.400	2.400	11.800	1.11 : 1.00	N
25.0	1.632	-	26.000	-	1.700	11.800	1.11 : 1.00	Y
26.0	0.925	-	-	75.400	2.500	11.800	1.11 : 1.00	N
27.0	2.540	16.900	-	-	0.890	11.800	1.11 : 1.00	N/a
28.0	3.045	16.900	-	-	0.445	11.800	1.11 : 1.00	N/a
29.0	3.130	16.900	-	-	0.000	11.800	1.11 : 1.00	N/a
30.0	0.000	16.900	-	-	3.550	11.800	1.11 : 1.00	N/a

Table 5.2.1-Polyurethane formulations (samples highlighted yellow indicated samples showing healing, samples highlighted blue could not be synthesised)

A great diversity in physical characteristics was observed when adjusting molecular weight of the PTMG component. As expected, higher molecular weight polyol chains (PTMG-2900) lead to polymers that were flexible and viscid throughout the polymer, while shorter molecular weight polyols generated polymers that are rigid and stiff. Polymers with PTMG-650 were unable to be synthesised due to rapid polymerisation of the first step involving PTMG with MDI. Because of this, any samples containing PTMG-650 were dropped from investigations. When HDO molar equivalents were reduced, DMPA were increased accordingly to maintain a constant OH : NCO ratio. In this investigation DMPA content was adjusted from 0 to 8.6 % for PTMG-1000 and from 0 to 4.0 % of the total PU mass for PTMG-2900. PUs report a sudden change in self-healing responses on increasing DMPA content past a threshold point. It should be noted that, to initiate self-healing properties, each PTMG variant required different masses of DMPA. In the case of PTMG-1000 self-healing thresholds were found to be between 4.0 - 4.1 % DMPA of the total polymer mass. A similar trend was found in PTMG-2900 with thresholds ranging from 2.6 - 2.9 % DMPA of the total mass. These results suggest DMPA is responsible, or at least a contributing factor to the materials ability to self-heal. Therefore, two assumptions are made; DMPA is necessary in this formulation in order to maintain self-healing properties, and in order to show self-healing properties, the proportion of DMPA in the material is required to be more than a defined threshold value. Although these formulations gave a clear indication into key factors contributing towards the polyurethanes self-healing, determining a quantitative method would require more complex analysis.

5.2.1 Tensile strength testing

Tensile testing is one of the most popular destructive methods for testing material strength and can be used on any material from flexible rubbers to strong alloys. [176, 177, 178] The process involves a defined shape (usually a dog bone) made of the test material being placed under a gradual increase in applied force until the material fails, either by tearing or rapid breakage.

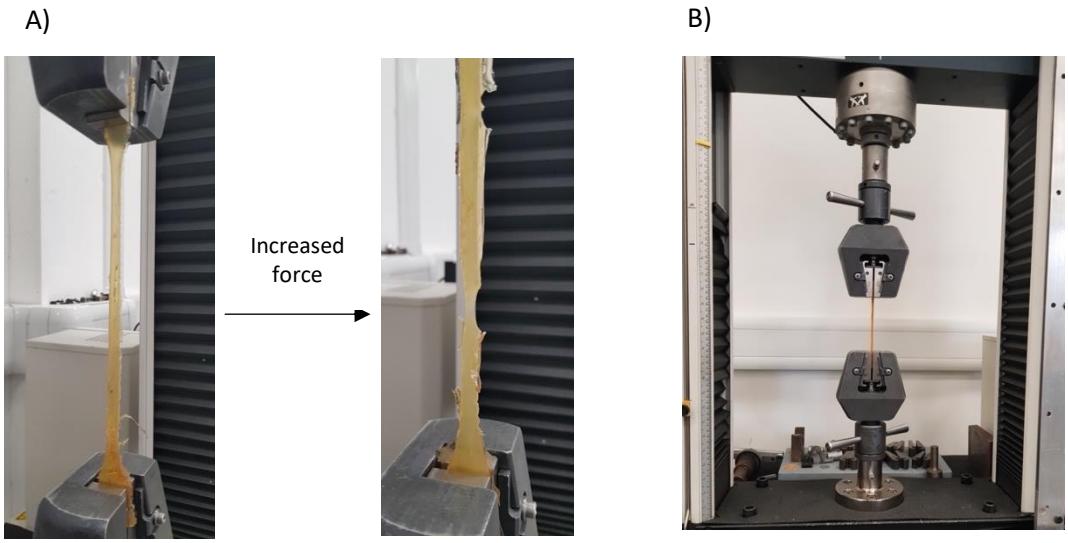

Figure 5.2.1- A) A polyurethane dog bone sample under increasing force before snapping, B) A tensile testing machine.

This technique can provide material properties such as yield strength, ultimate tensile strength, ductility and Young's modulus. This section of work aimed to use tensile strength testing to address two objectives. First, the maximum load of an uncut sample before breaking point to test formulation strength. Second, the load required to break a sample after 1 hour and 24 hours healing time, to calculate a recovery strength for each formulation. To calculate a recovery percentage relative to the polymer's original strength, each batch was made of three identical samples. Two samples were cut in the centre of the dog bone using scissors and left to heal. One sample was left for 24 hours, and the other left for 1 hour. The remaining sample was left uncut to analyse the

maximum tensile strength properties for the polymer formulation. Following this, the tensile strength testing was operated by measuring load in newtons N (force applied on material) against displacement in millimetres (the deformation of a material from its original size). Figure 5.2.2 shows the tensile strength run (fresh, 24 h and 1 h samples) for sample PU 2.0. Tensile results from samples showed on average, increased healing time led to an increase in recovery strength. Uncut samples for PU 2.0 were found to withstand loads of up to 20 N before failure, whereas cut samples possessing long term healing (24 hours) could be subject to loads of up to 16 N before breaking point. The recovery strength was calculated to be ranging from 63 – 98 % of the material's original strength. Samples cut and subject to healing of just 1 hour were found to regain between 33 – 61 % of the uncut strength.

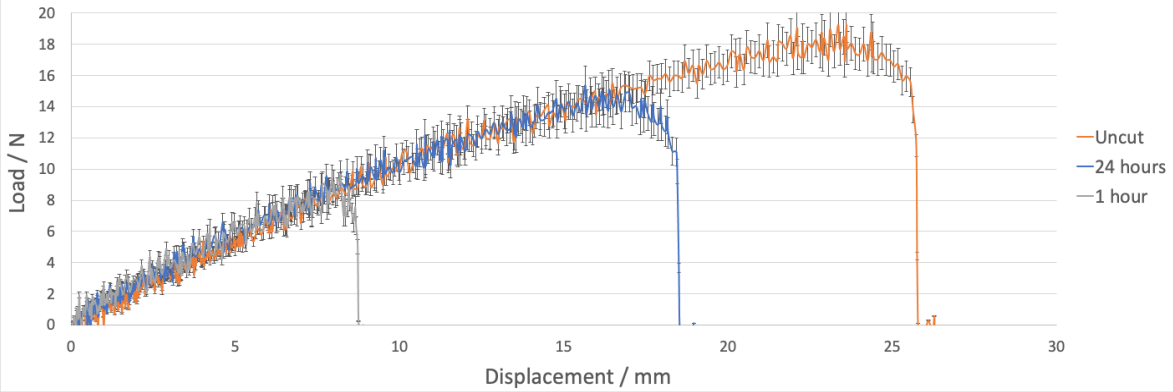

Figure 5.2.2- Tensile strength testing for uncut (orange), 24 hours healing (blue) and 1 hour healing (grey) of polyurethane sample 2.0.

After the cutting of a sample, an inspection of the self-healing process was analysed using a USB spotlight camera taking a time-lapse photograph every 6 hours over a duration of 5 days. The pictures taken during this time (Figure 5.2.3) show the stages of material healing. After 5 days a visible scar can be seen on the surface of the material.

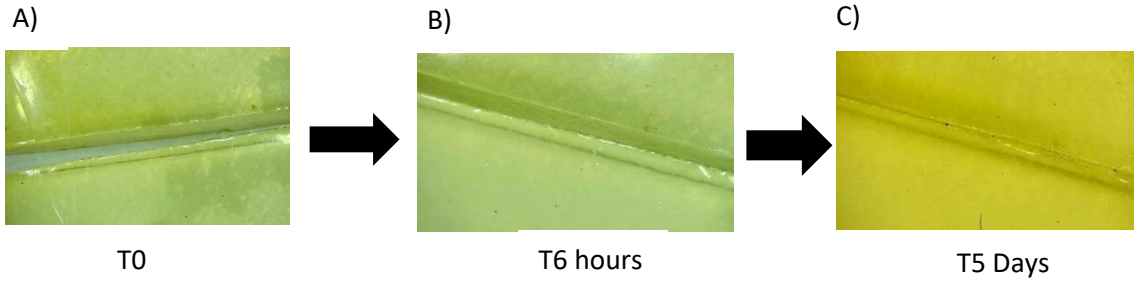

Figure 5.2.3- Snapshots of the healing process of PU 2.0 over a 5-day period.

The integration of tensile testing to investigate the material properties of multiple polyurethane formulations proved effective. Preliminary methods came with challenges in procedure, equipment, and sample handling. However, solutions to these problems enabled a reliable and time efficient tensile strength process which allowed a representative comparison between both formulations and strength recovery.

5.2.2 Formulating DMPA into polyurethane

This work was aided by Bradley Thomas, Northumbria University (RA on the Immortality Manufacturing project).

In this section the proportions of DMPA, chain length of PTMG, and 3 different chain extenders were assessed for changes in tensile recovery strength (Table 5.2.2). Whilst it would have been optimal to do tensile testing on all future samples, due to the time-consuming nature of the tensile testing process, a compromise between the number of samples and analysis time was necessary. To solve this, a method was needed to design an array of samples that covered the criteria using the smallest sample size possible. To ensure this, a L9 Taguchi array was proposed (

Table 5.2.3). The array consisted of a total of 9 samples consisting of 3 different PTMG polyol chains (1000, 2000, 2900 m_w), 3 chain extenders 2-Methyl-1,3-propanediol, 1,4-butanediol and 1,6-hexanediol, and 3 concentrations of DMPA (0, 0.03, 0.06 mol).

Run	Moles of DMPA	Chain Extender	PTMG M_n
1	0	2-Methyl-1,3-propanediol	1000
2	0	1,4-butanediol	2000
3	0	1,6-hexanediol	2900
4	0.03	2-Methyl-1,3-propanediol	2000
5	0.03	1,4-butanediol	2900
6	0.03	1,6-hexanediol	1000
7	0.06	2-Methyl-1,3-propanediol	2900
8	0.06	1,4-butanediol	1000
9	0.06	1,6-hexanediol	2000

Table 5.2.2- Moles of DMPA, type of chain extender and PTMG.

Run	DMPA / %	Chain Extender / %	PTMG / %	MDI / %	Total mass / g
1	0	3.25	72.42	24.40	35.9
2	0	1.90	88.87	14.13	31.0
3	0	1.79	87.84	10.21	29.6
4	3.00	1.75	77.15	18.01	33.7
5	2.20	1.28	83.07	13.35	31.3
6	4.82	3.69	62.35	29.09	41.7
7	4.20	1.21	78.55	16.13	33.1
8	8.60	2.51	55.67	33.19	46.7
9	5.51	2.11	71.23	21.23	36.5

Table 5.2.3- L9 Taguchi orthogonal array for polyurethane formulations.

Contradicting previous results found in Table 5.2.1, all nine formulations were found to self-heal to different extents. Figure 5.2.4 reports the maximum load prior to breaking point for each polyurethane sample. The graph suggests, similar to previous results, healing time strongly influences recovery tensile strength. Exceptions to this were found in formulations 1 and 8 where cut samples were reported to be over 100 % of the uncut material strength. Samples that withstood

the highest loads were formulations 3 and 5 both containing PTMG-2900. This suggests the incorporation of higher molecular weight polyols promote greater material strength; however this is more likely to be creating materials that are stretching due to increasing flexibility, rather than increasing material strength. Small increases in 24-hour recovery strength was reported when increasing DMPA content, however a higher sample number would be necessary to confirm this. No correlations between chain extender recovery strength were found.

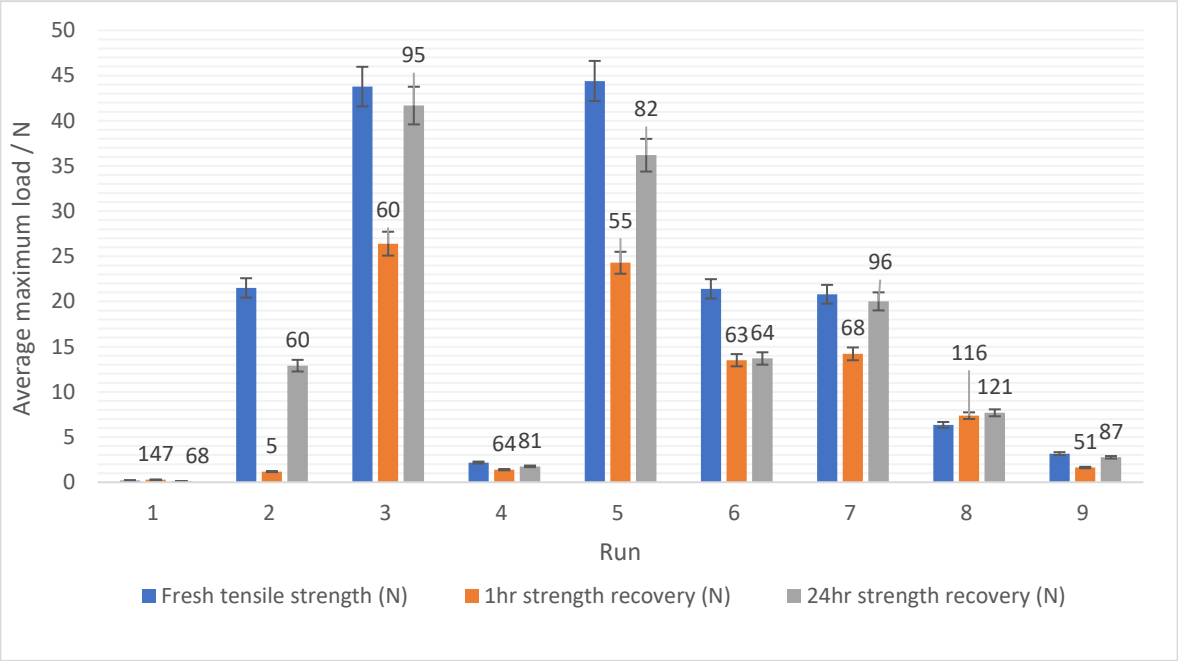

Figure 5.2.4- Average maximum tensile load for polyurethane runs 1 – 9.

Figure 5.2.5 reports the average displacement for each run for uncut, short term and long-term healing. Interestingly in contradiction to previous results, runs 4, 6 and 9 had the highest displacement before breakage. This data suggested molecular weight may not be directly linked to polymer flexibility as none of these samples possessed the longest molecular weight chain. Furthermore, these results indicate high molecular weight may even hinder maximum displacement as all samples containing PTMG-2900 were found to have the lowest values. Other variables such as chain extender and moles of DMPA did not appear to be influential in displacement analysis. To confirm this, additional analysis of these polyurethanes with extensive ranges in chain lengths, chain extenders and DMPA would be necessary.

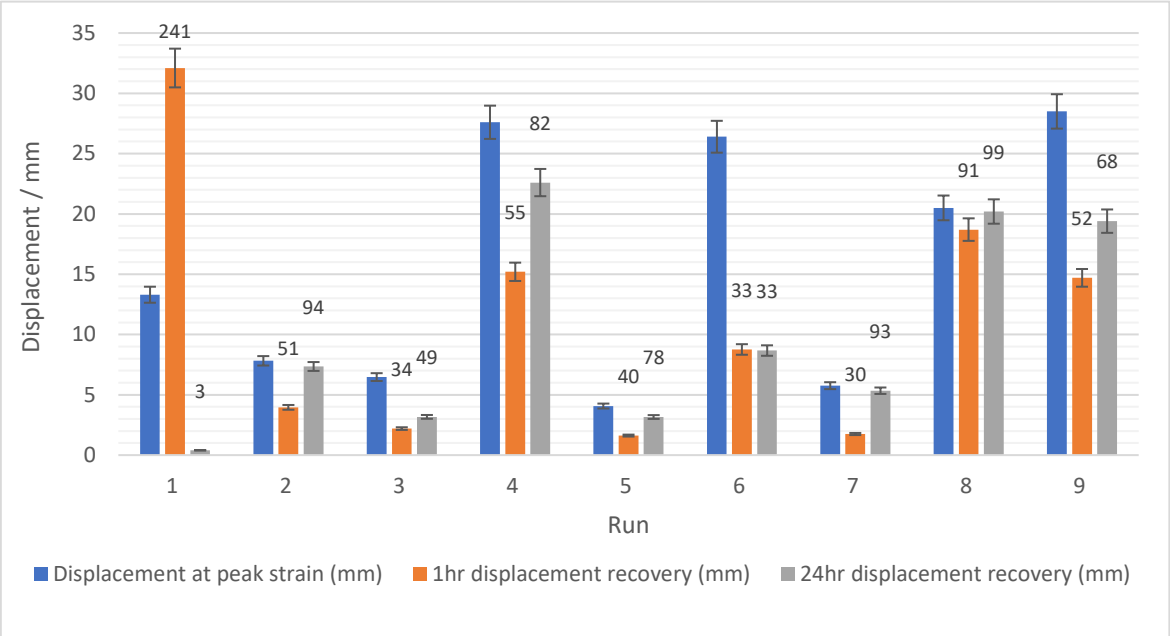

Figure 5.2.5- Average displacement for polyurethane samples runs 1- 9.

It appears the sources responsible for self-healing in these polyurethane samples might be more complex than just one factor. From the results found in section 5.2.2 three conclusions can be made. Firstly, no monomer is responsible for the self-healing capabilities after 1 hour. Secondly, increasing DMPA in polyurethane formulations marginally increases the self-healing recovery after 24 hours. Thirdly, increasing PTMG molecular chain length increases the strength of the material prior to cutting, however has no effect on recovery strength.

In order to understand the results above, the structure of polyurethane was investigated. DMPA's structure has a high affinity for hydrogen bonding through its carboxylic acid groups. Between polymer chains, the extent of potential hydrogen bonding is identified in Figure 5.2.6. One potential route is the bonding between acid-carbamate and acid-acid groups. The change in DMPA proportions would directly impact this factor. Results obtained from this investigation would see this as the most viable explanation. Other interactions include Van der Waals between the hydrocarbon chains of the PTMG which could be responsible for the higher uncut material strength seen in this section. Furthermore, π - π stacking between the isocyanate groups could also contribute to

potential bonding between chains although MDI was not assessed in this investigation. To further aid understanding of chain interactions computational modelling will be implemented.

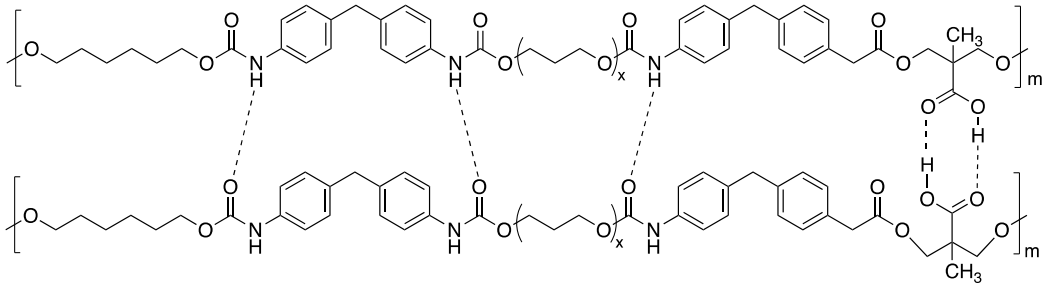

Figure 5.2.6- Potential hydrogen bonding between carbamate and acid groups in polyurethane chains.

5.2.3 Molecular dynamic to polyurethane systems using computational chemistry

This work was completed by Kristian Poll, Northumbria University.

To assist the self-healing characteristics found in previous work, additional computational methods were applied to explore molecular dynamics to polyurethane systems previously discussed in section 5.2.1. A computational method was derived from work previously reported by Chen *et al*. that analyses the healing mechanism of a self-healing polyurethane elastomer using Equation 5.2.1. [179] A uniaxial deformation method was used to analyse a 16-chain polyurethane system (Figure 5.2.7). This involved expanding the simulation box at a constant rate (at a constant temperature and pressure) along a single dimension until the system was completely pulled apart and the pressure along the direction of deformation was zero (indicating the sample had broken). During this period, pressure and box dimensions were measured at each frame throughout the simulation (250 in total). From these properties, the dependence of the stress (σ) on the relative strain (ε) can be calculated:

$$\sigma = -P_i$$

$$\varepsilon = (L_i - L_{0i})/L_{0i}$$

P_i – Pressure tensor

L_i – Simulation cell size at time t

L_{oi} – initial simulation cell size at t=0

i – x, y z

Equation 5.2.1- Equations used to calculate the relative strain and dependence of stress.

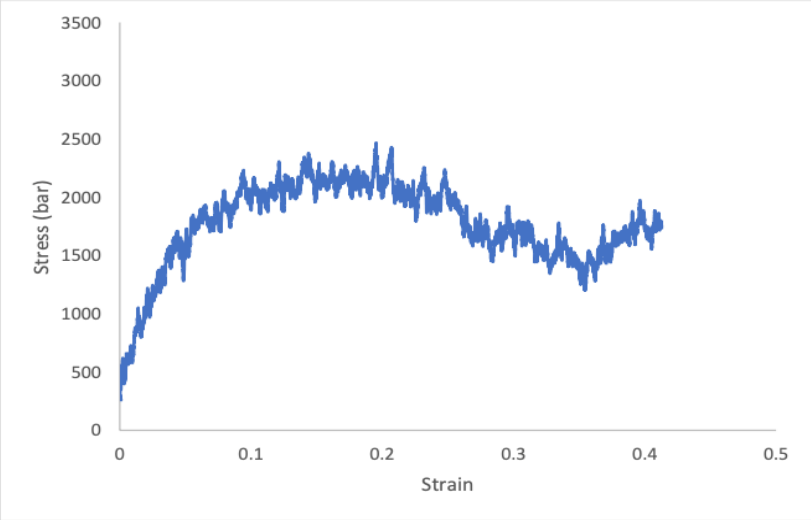

Figure 5.2.7- Plot of stress-strain dependence for an uncut 16-chain polyurethane system from 250 data points.

To measure self-healing capabilities, a micro-fracture was inserted into the polymer system by extending the polymer in the z axis direction and was analysed using the same uniaxial deformation method previously used. A simulation was run to analyse the development of the damaged polyurethane at 300 K, 1 bar. Several snapshots were taken to visualize this process. Figure 5.2.8 shows the rapid formation of two 8-chain polyurethanes reforming to form a 16-chain polymer. This subsequent polymer was then reassessed using the same uniaxial deformation method previously described. The results, found in Figure 5.2.9 show that the maximum stress value before breaking was parallel to that of the original sample and that the material properties remain largely

uninfluenced by previous damage. Although the atomistic simulation of chains coming together is most likely due to a mixture of H-bonding and Van der Waals interactions, no evidence was found that stated H-bonding was the primary driving force for the self-healing. To determine this, more complex computational methods will be required.

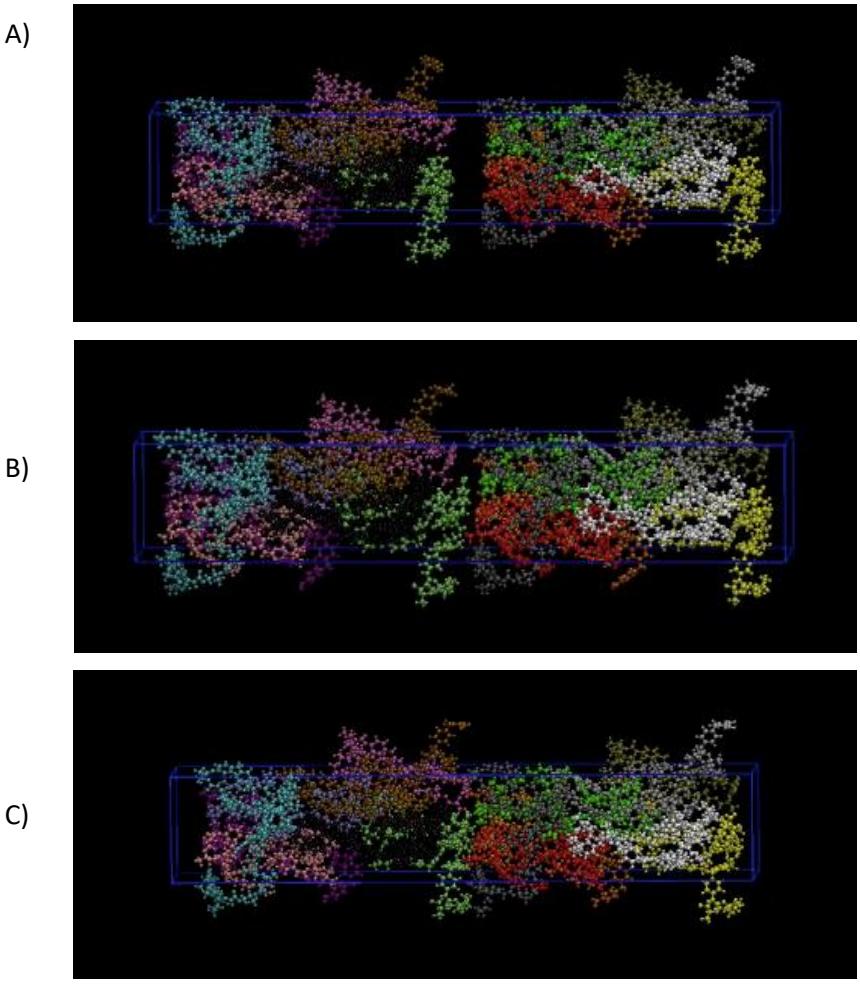

Figure 5.2.8- Visualisation of a 16-chain polyurethane system containing a micro fracture self-healing at 0 ps (A), 10 ps (B) and 50 ps (C) of an NPT simulation

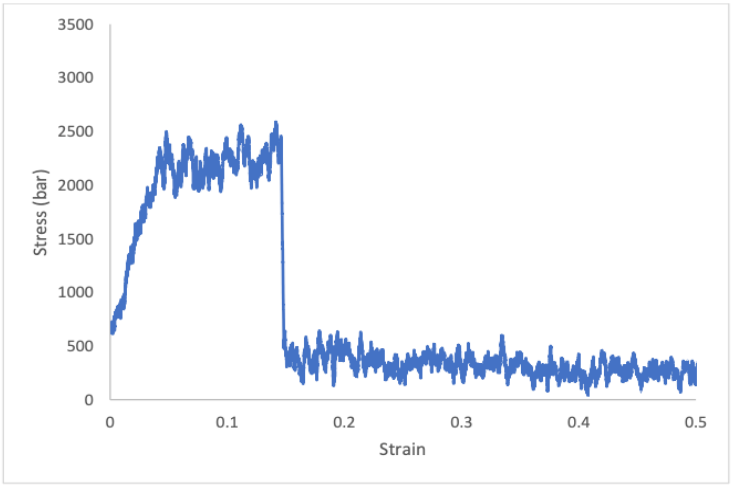

Figure 5.2.9- Uniaxial deformation for a 64-chain polyurethane after self-healing

The work performed above provides a basic methodology that may be valuable for the further application of simulation techniques to polymer systems, and in particular those that exhibit self-healing behaviour. Other areas of interest may be the computational modelling of polymers at a non-atomistic resolution, exploring if the properties of polyurethanes, which are thought to be largely dependent on hydrogen bonding between different sections of the chain structure, can be accurately captured at a singular atom.

5.3 Summary

In this chapter the synthesis of a polyurethane formulation that has potential to exhibit intrinsic self-healing was reported. It was clear that self-healing was time dependent through the integration of a tensile testing method. Determining factors that contribute to the polymers self-healing deemed challenging due to polymer viscidity when using higher molecular weight polyols. No differentiation in tensile strength was found when substituting different chain extenders, however in prior work, higher molecular weight PTMG reagents reported increases in uncut material strength and decreases in maximum displacement. Further work will be necessary to find the factors responsible for the short-term healing properties as results in this investigation were inconclusive. However, long term healing appeared to be influenced by DMPA content. Computational methods gave

inconclusive data regarding the primary driving force for self-healing properties. Although further work is essential in establishing the materials characteristics, this work provides a steppingstone to developing a material that can potentially show self-healing properties for modern day applications.

6 Deposition of biocoatings using inkjet printing technology

6.1 Introduction

Inkjet printing is a printing technique that generates small droplets of solution onto a surface, generating a high-quality image. In the past century, ink-jet printing has surpassed other printing methods due to its high resolution and low cost and is now the most widely used printing technique in home and workplace environments. Advancements in printing technology have developed inkjet systems that perform high resolution printing by ejecting a stream of small (<100 μm) droplets using a computer defined pattern. One of the latest advancements is the Jetlab 4 system (Figure 6.1.1). This advanced instrument has a 210 x 260 mm printing platform with a jetting device that can print up to 50 mm s^{-1} and printing accuracy of ± 30 μm. Although most printers are used to deposit ink-based solutions, systems such as the Jetlab are capable of printing any solutions within a surface tension of 20 - 70 dynes cm^{-1} and viscosity <20 cPs.

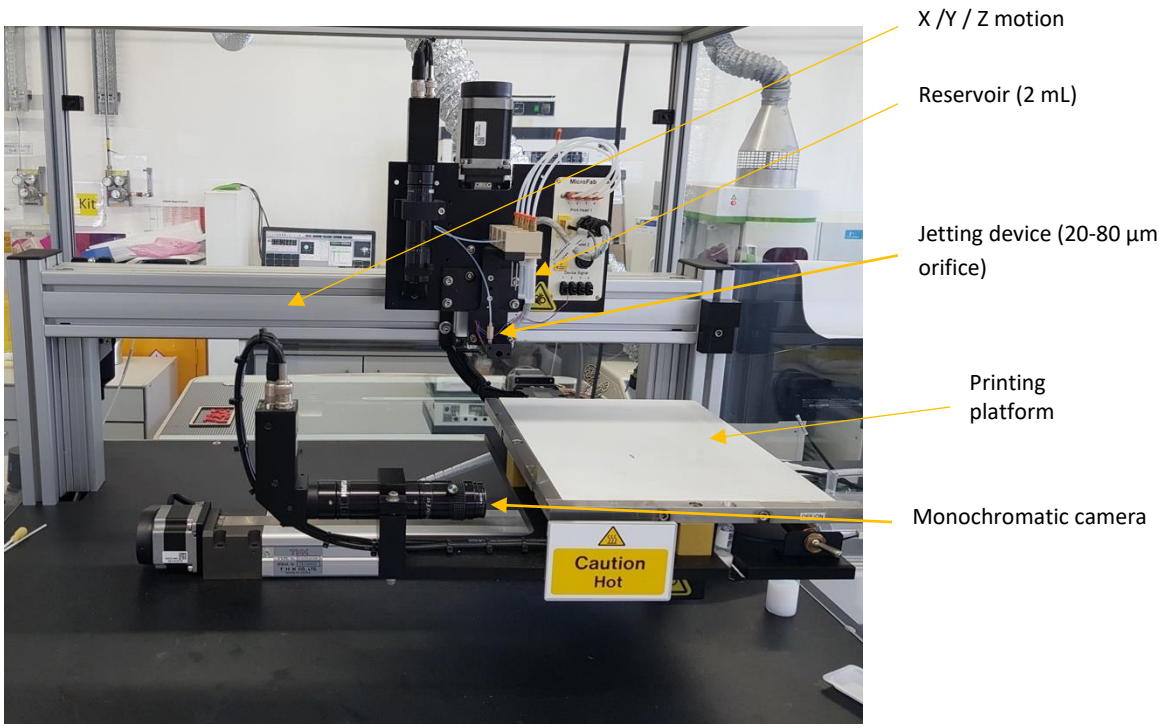

Figure 6.1.1- Jetlab 4 inkjet printing system.

Inkjet printing is now considered an attractive route to printing biomolecules and even prokaryotic and eukaryotic cells because the process temperatures are typically in the range 23 – 50 °C.
This established printing technology offers a printed multilayer 3D structure using a repeated pattern with a layer-by-layer construction of a 3D, textured, functional coating. Furthermore, the advancements of inkjet printing now make it possible to print on any surface whether flat or 3D by overflying the surface on a predetermined trajectory. The ability to use multiple print heads, enables synchronized printing of solutions containing bioactive and synthetic components. This includes any co-factors (metal or small organic molecules able to assist in enzyme production) such as the NADP (nicotinamide adenine dinucleotide), a co-enzyme that functions as a reducing agent in cellular respiration, can all be printed in the same process. In the case of printing biologically sensitive solutions, the printing provides a non-contact and potentially sterile process which reduces the risk of contamination and the potential of harming cells through rough handling.

In this chapter, a Jetlab 4 ink-jet system was used to create viable methods for the deposition of dyes, polymer latexes and immobilised cells with bioactive properties. Printing patterns were created using in depth scripts and bitmap imaging. Ultimately, this chapter describes how to perform jetting of low concentration polymer latexes and biologically active cell-polymer complexes in patterns on three dimensional surfaces.

6.2 Droplet formation using preliminary solutions

Prior to printing, all fluids were filtered using a syringe filter to remove all particulate matter.
A total of 5 (20, 40, 50, 60 and 80 µm) jetting devices (print heads) were investigated using isopropyl alcohol (IPA), water, and fluorescein to establish and optimise printing parameters. In this research, it was found the voltage required to generate droplet formation exceeded what was recommended by the manufacturer.
Isopropyl alcohol was used to visually examine droplet formation (Figure 6.2.1(a)). This ensured no blockages were present within the device prior to jetting. If blockages were present formation of secondary droplets could form. This was clear in smaller printing devices that were prone to be blocked more readily (Figure 6.2.1(b)).

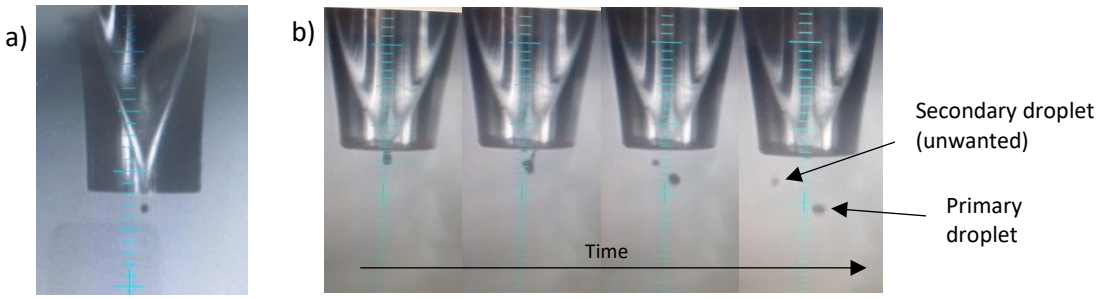

Figure 6.2.1- a) A desired isopropyl alcohol droplet dispensed from a 50 µm device. b) Secondary droplet formation using a 20 µm printing device.

Depositing water onto water sensitive paper (a change of yellow to blue) would provide a reliable method in creating and optimising printing patterns. Once parameters were altered, droplets were produced consistently to print patterns defined by programmed sequences called “scripts”. A script

was generated consisting of 4 squares measuring 0.5, 1, 1.5 and 2 cm wide (Figure 6.2.2 (a)) (an example of a jetting script can be found in 9.4 of the appendix). More complex images (such as the water molecule in Figure 6.2.2 (b) were printed using bitmap images (images that can be incorporated into the script). Images below 1 cm were challenging due to large surface wetting between water and the sensitive paper. For higher resolution images other solution-substrate combinations were required. Nevertheless, this method proved useful in the development of scripting, imaging and printing techniques because of its clear and instant colour change.

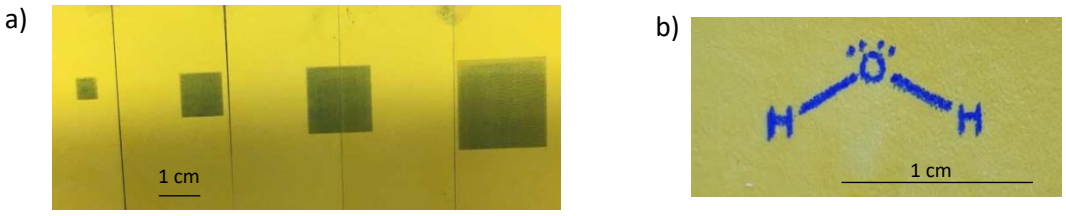

Figure 6.2.2- Water printed onto water sensitive paper using a script file (left) and a bitmap image (right).

Prior to printing, fluorescein was dissolved in distilled water (0.05 %) and filtered to remove suspended solids. Printing fluorescein was not only easy to print because of its very similar jetting parameters to water, but because of its vibrant fluorescence, it could be printed onto any material and analysed under a UV lamp. This was noticeable even when attempting to see small or hard to see images such as Figure 6.2.3 (a). Scripts could also be inverted to create an image which saw the deposition of fluid around the bitmap image (Figure 6.2.3 (b)). This could be especially useful in future work when printing superhydrophobic areas onto surfaces to create channeled networks.

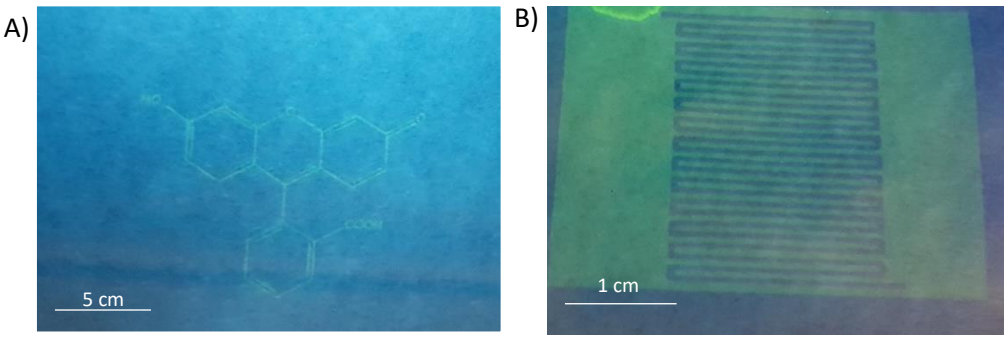

Figure 6.2.3- A) Corresponding fluorescein molecule (left) and B) Fluorescein printed networks (right).

After preliminary printing trails using 3 solutions with different viscosities and surface tensions, a 50 µm device was concluded as the best compromise for droplet size, printing speed, and resolution.

6.2.1 Click chemistry of iridium complexes using ink-jet printing [180]

VNK 591 was synthesised and donated by Valery Kozhevnikov, Northumbria University.

To expand the range of fluids that can be jetted by this method the deposition of an iridium complex onto a paper surface was investigated. The printing of this complex would perform an Inverse Electron Demand Diels Alder (IEDDA) reaction using 1,2,4,5-tetrazines with strained alkynes. Metal ions often catalyse IEDDA reactions. [181] In this section the aim was to perform a click IEDDA reaction with the compound VNK-591 onto bicyclo[6.1.0]nona-4-yne (BCN-C10) coated filter paper. The click chemistry allows the fast production of VNK-593, a highly luminescent compound (excitation 438 nm, emission 562 nm). [180]

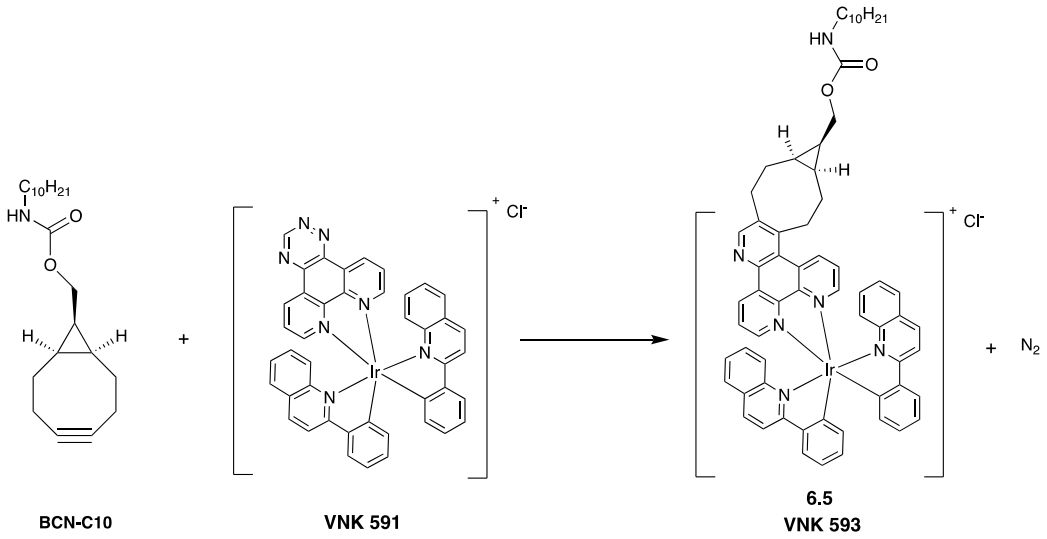

Scheme 6.2.1-Reaction of iridium (III) complex VNK-591 with BCN-C10.

The iridium complex VNK-591 was synthesised and dissolved in isopropyl alcohol (5 mg mL^{-1}) and inserted into the jetting reservoir. Prior to printing, the filter paper was coated by dipping into BCN-C10 solution. Prints were analysed under a UV lamp (254 nm). VNK-593 required one coating onto treated filter paper to be seen under UV by the naked eye (Figure 6.2.4).

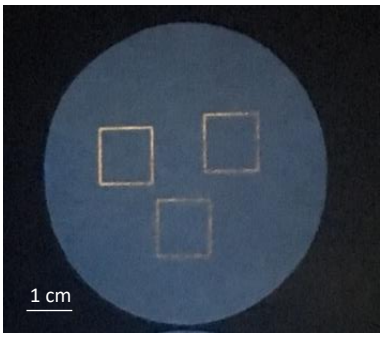

Figure 6.2.4- One coating print of an iridium (III) complex ion (VNK-593) onto filter paper surface treated with BCN-C10.

A successful IEDDA reaction of a non-luminescent 1,2,3-triazine metal complex was preformed using ink-jet printing to form a luminescent iridium (III) ion. This presents new opportunities to develop alternative reaction methods for this novel class of click reagents whereby metal-based functionalisation is required.

6.2.2 Deposition of superhydrophobic solutions

Soft99 Ultra Glaco solution (Glaco) is an IPA based reagent that contains silica nanoparticles capable of conferring superhydrophobic surfaces to materials. The aim of this investigation was to establish a printing method for Glaco solution with the advancement to incorporate a double headed printhead system to print both Glaco reagent alongside a biocomposite to create a surface coating consisting of hydrophobic and hydrophilic areas.

Once printing conditions were optimised, 1 coat of Glaco was printed onto a glass slide and analysed measuring the contact angle of a water droplet. Samples were compared to a glaco aerosol spray and an uncoated glass slide. Table 6.2.1 reports the contact angle for samples. As expected, uncoated glass was found to have an average contact angle of 56 °, in line with previous research which reports around 55 °. [182] Glaco coated glass (sprayed directly onto the slide and wiped into the material using cloth) developed contact angles of 86 ° and was found the be the most hydrophobic from the samples tested. In comparison, a jetted Glaco solution at 1 % concentration gave a contact angle of 67 ° indicating it could create an increase in hydrophobic surface properties despite its low concentration and coating thickness.

Material	**Contact angle / °**
Glass	56 ± 3
Glaco (100 %) coated glass	85 ± 4
Glaco (1 %) jetted glass	67 ± 4

Table 6.2.1- Contact angles for Glaco coated, Glaco printed, and uncoated glass

The results above suggest jetting Glaco onto glass substrates can generate more pronounced hydrophobic areas. Although these areas are less hydrophobic (most likely due to their thin coating) than other coating methods, ink-jet printing provides a high level of accuracy when dealing with small or complex substrate coverage.

6.3 Droplet size formation using fluorescence

As previously described in chapter 4, the Jetlab could be used to create alginate beads as an immobilised form of a biocatalyst. One factor yet to be established when using the Jetlab is the size of droplets ejected in relation to the print head. The size of the droplet has a drastic effect on the coating and surface properties and is essential for high resolution and maximising surface properties. A printing procedure was developed whereby alginate (0.15 g mL^{-1}) and fluorescein (0.05 g mL^{-1}) were mixed and loaded into the jetting reservoir. A jetting procedure was created to generate singular droplets in a petri dish containing 20 % calcium chloride solution (ionic cross-linking agent). To reduce blockages, an 80 µm jetting device was used. Once all alginate solution had been consumed, the suspended capsules were carefully transported and filtered using filter paper. After washing the filter paper, capsules were analysed using a USB microscope and a UV lamp (254 nm). Measurements were taken using live camera imaging and a scale bar.

Fluorescein's high UV fluorescence enhances droplet visibility coupled with camera and imaging software allows droplets to be isolated easily (Figure 6.3.1). All beads ranged between 70 - 80 µm with a mean diameter of 72 µm. Future work would perhaps use more advanced techniques such as light scattering to avoid the unnecessary transportation and filtration of capsules.

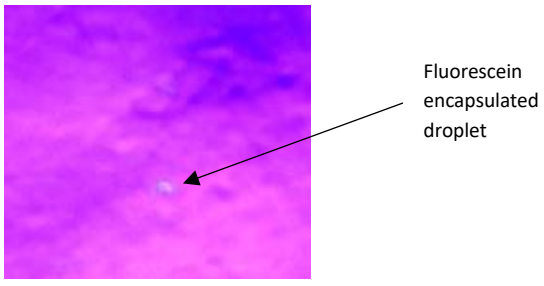

Figure 6.3.1- Fluorescein encapsulated alginate droplet (72 µm) on filter paper using an 80 µm jetting device under a microscope and UV lamp (254 nm).

6.4 Deposition of latex polymer

A crucial part of this project was to develop a method to be able to print a biolatex solution by jetting. In order to achieve this, samples of polymer latex (with no microorganisms present) were jetted and parameters optimised.

A high dilution factor (0.5 % latex concentration) was used to achieve high resolution printing of a synthetic polymer latex. Due to this low latex concentration in water, it was found to have similar jetting parameters to water. This enabled the use of water sensitive paper as a useful indicator for the presence of latex (Figure 6.4.1). Concentrations which gave successful printing performance were in the range of 0.5 – 1 %. Concentrations greater than 1 % led to blockages and deviation in jetting parameters. Droplet spacing was kept low to improve picture quality. Differences in print quality can be seen in Figure 6.4.2 where 0.5 mm (a) and 0.1 mm (b) spacing was implemented. Similar print patterns will be used in future work to print into 3D channeled surfaces.

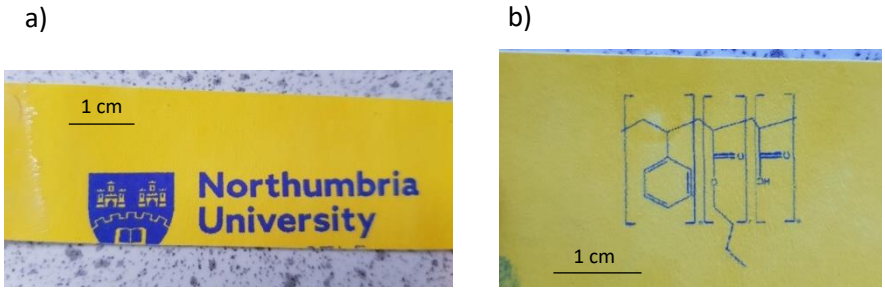

Figure 6.4.1- 0.5 % concentration acrylate polymer suspended in water using a single print a) Northumbria University crest b) Structure of the synthetic co-polymer printed on water sensitive paper.

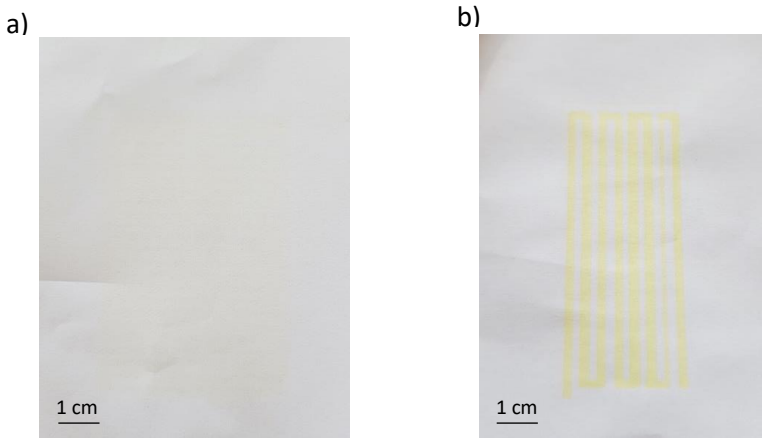

Figure 6.4.2- a) Fluorescein printed with 0.5 mm x / y axis spacing b) Fluorescein printed using 0.1 mm x / y axis spacing.

6.5 Immobilising cells into 3D laser cut scaffolds using ink-jet technology

Low concentrations of Baker's yeast (5 mg / mL) were immobilised into a 0.5 % (w/w %) diluted polymer latex. Due to yeast and latex concentrations remaining low, jetting parameters were similar to water. To reduce blockages an 80 µm device was used. The solution was successfully jetted onto water-sensitive paper using the method described in section 7.6.5.1 and observations were identical to that found in section 6.4.

The printing method was replicated onto 3D surfaces. In order to achieve this, the design and construction of a custom 3D scaffold was necessary. There were two ways to do this; the first involving 3D printing a substrate (used in section 4.4.2) and the other using laser cutting to engrave materials. One advantage to using laser cutting over 3D printing was that it allowed to cut very precise patterns onto a range of materials such as wood and plastics. In comparison, 3D printing only allowed scaffolds to be designed using polylactic acid (PLA). Although acrylic showed poor surface adhesion in thicker coatings (most likely due to the substrate being a mixture of plastics), with the selection of surfaces available, it was decided acrylic was to be selected because as a thin coating the

latex would more likely adhere to the surface. One significant advantage of using laser cutting produced a ridged surface, creating a higher surface area seen on Figure 6.5.1 (b).

Once a successful engraving of a channelled network onto an acrylic scaffold was made, a bitmap image pattern scaled to the size of the engraved channels was designed. The biocomposite was deposited into the cut channels with two coats. This was repeated with another identical acrylic scaffold. Following this, the two identical coated acrylic scaffolds were glued together (facing each other) to create a tunnel network (Figure 6.5.1 (a)). Plastic tubing was sealed into each end of the acrylic tunnel using bathroom sealant. This was a cheap and effective solution to prevent water leaking out of the scaffold.

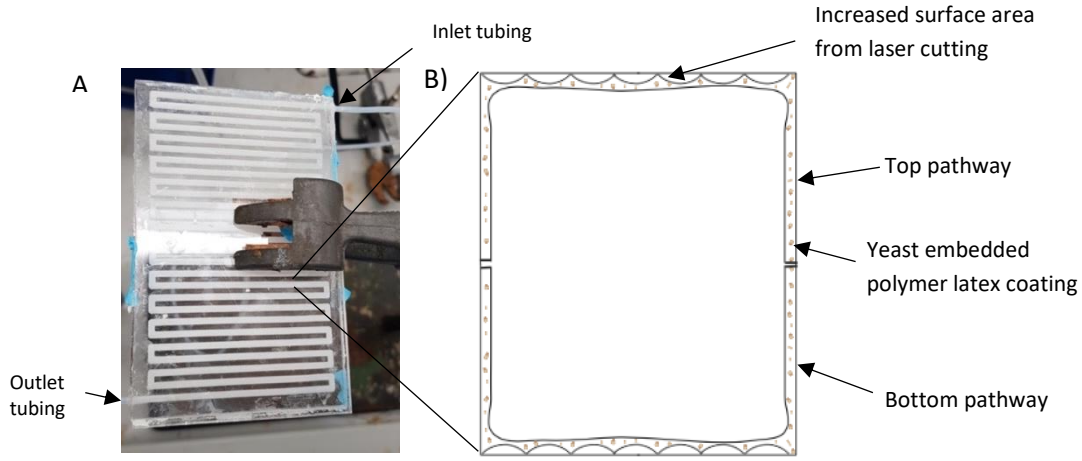

Figure 6.5.1- A) 3D laser cut acrylic scaffold B) Cross-sectional area of acrylic scaffold pathway.

6.5.1 Fluorescein diacetate hydrolysis using a 3D laser cut ink-jet coated reactor

To investigate cell activity, the hydrolysis of fluorescein diacetate was repeated from section 4.4. A continuous flow circuit was set up consisting of a pump, silicone tubing, coated channelled reactor, and flask. Tubing connecting the pump, flask, and scaffold transported the buffer / FDA solution through the scaffold back into the flask. Fluorescence readings were taken from the flask throughout the reaction with a final 24-hour fluorescence. After 24 hours the solution was analysed for suspended solids to assess cell leaching. These readings were compared to previous results where the same reaction was recorded using suspended and immobilised yeast with different deposition techniques on multiple surfaces (Table 6.5.1).

The 3D bioreactor proved an effective method to show enzymatic catalysis. The fluorescence reading after 24 hours was lower than most of the immobilised and suspended systems investigated however, when considering the total mass of immobilised yeast and thickness of coating, the fluorescence per gram of yeast was far higher. In addition to this, the sample showed the lowest levels of cell leaching and significantly reduced volumes of latex.

Baker's yeast Sample	**Total Yeast / g**	**Total Latex / g**	**Latex solid / %**	**Coating thickness / µm**	**Fluorescence (24 hr)**	**Fluorescence per g yeast**	**Suspended solids/ mg / L**	**Ref Chapter**
Suspended	0.1	-	-	-	97 ± 6	970	541 ± 71	2
	0.3	-	-	-	119 ± 9	397	675 ± 88	2
	1.0	-	-	-	139 ± 8	139	887 ± 56	2
	2.0	-	-	-	208 ± 47	104	1093 ± 121	2
Immobilised Polyethylene Balls	0.25	0.25	50	100	143 ± 10	572	11 ± 3	4
Immobilised Polystyrene	0.30	0.30	50	100*	70 ± 16	233	18 ± 4	4
PLA 3D tube	1.0	3.0	50	500*	887 ± 58	887	38 ± 7	4
Ink-jet printed 3D bioreactor	0.01	0.1	1	<50*	85 ± 14	8500	7 ± 2	6

*Table 6.5.1- Fluorescein diacetate hydrolysis results for suspended and immobilised methods. (*Estimation based on total biocomposite mass and surface area.)*

6.6 Summary

In this chapter an ink-jet printing method was established enabling the jetting of a large variety of fluids onto a range of materials. Ink-jet enables the generation of microdroplets in a variety of sizes (20 - 80 µm) depending on the jetting device selected. Through the deposit of these droplets, an Inverse Electron Demand Diels Alder (IEDDA) reaction using 1,2,4,5-tetrazines with strained alkynes was successfully achieved.

Coupling ink-jet printing with 3D laser cutting provided an alternative method for the deposition of a biocomposite onto an acrylic scaffold. Although only one material was analysed for yeast cell activity, this technique can be moulded to other materials to create bioactive surfaces (proved in previous chapters using other coating techniques). Furthermore, providing microorganisms survive ink-jet printing (with their activity intact), this method becomes an attractive alternative to generate a thin biocomposite coating which enables a non-contact, sterile environment.

The future of this work allows endless possibilities in surface-biocomposite combinations. Advancements in printing patterns and optimisation in biocomposites have the potential to transform any non-active surface into a 3D bioreactor capable of biocatalysis on an industrial scale. In addition to this, the evolution of a single channelled network into a multichannel scaffold enables a number of different transformations to be established all within one continuous biocomposite network.

7 Experimental

NMR spectra were recorded using a JEOL ECS400 Delta spectrometer at frequencies of 399.78 MHz for ^{1}H NMR and 100.53 MHz for ^{13}C NMR. All chemical shifts are quoted as parts per million (ppm) relative to tetramethylsilane (TMS) as an internal standard in either deuterated dimethyl sulfoxide (DMSO-d_6) or deuterated chloroform ($CDCl_3$).

Infra-red spectra were recorded *via* a SensIR Technologies Durascope diamond anvil cell mounted on a Perkin-Elmer Paragon 1000FT-IR Spectrometer. Wavenumbers are reported in cm^{-1}.

Fluorescence spectra were recorded using a Biotek Synergy HT and Gen5 1.06 software.

Ultraviolet spectra were recorded using dilute solutions *via* a Varian Cary 50 Bio UV-Visible Spectrophotometer. Sample placed into a UV Quartz Suprasil rectangular Micro Cell, PerkinElmer.

Gel permeation chromatography were recorded using a Agilent 1260 Infinity II with Agilent GCP/SEC software. All samples were dissolved in HPLC grade tetrahydrofuran prior to analysis.

Differential scanning colorimetry were recorded using a PerkinElmer DSC 8500 and Intercooler 2 with Pyris Data Analysis software.

Scanning electron microscope imaging was taken using a Tescan Mira 3 scanning electron microscope with Tescan Alicona 3D imaging. Samples were subject to the resolution mode using the backscattered electrons (BSE) in-beam detector. Samples were prepared using a 4 nm platinum coating *via a* Quorum Q150R ES spray chamber.

Scanning electron microscope imagining for biocomposite cell growth was taken using a Tescan Vega 3LMU microscope with Tescan Alicona 3D imaging.

Pulse amplitude modulated-fluorometer analysis was taken using a M-Series MAXI Version; Walz GmbH.

Contact angle analysis was analysed using a Ossila Contact angle goniometer attached to Ossila software.

Dynamic light scattering was recorded using a Malvern Mastersizer 2000 using Malvern Mastersizer 5.12 software. Data was processed using Malvern Mastersizer 5.12 software.

Drying time was recorded using a TQC sheen drying time recorder AB3600 using the BK (Beck Koller) method.

Turbidity was recorded using a Hach DR1900 and glass 20 mL cells.

Confocal imaging was taken using a Lecia BMi8 confocal microscope, Lecia TCS SPE fluorescence source and a Leica EL6000 compact light source. Lecia LAS X software was used.

3D printing was processed using a Rise 3D N1 3D printer and Ideamaker software. All designed were created using Sketchup software.

Ink-jet printing was processed by a Jetlab 4 printer system attached to a Thomas VTE 6 pump, Ibamini silent compressor, Microfab CT-PT-4 pressure control system. The system was control by the Jetlab 4 software, version 4.1.2.3050, 2016.

Hardness analysis was recorded using a Buehler Micromet II for indentation and a Burker Aliconer microscope for indentation analysis and measurements.

Tensile strength testing analysis was recorded using a Instron 3382 tensile tester and Series IX v8.33.00 software.

Surface materials were purchased from Bay plastics Ltd, Tyne and Wear.

Reagents were purchased from Sigma-Aldrich, Solvay, Fisher Scientific, Tokyo Chemical Industry, and Apollo Scientific and were used without further purification unless otherwise noted.

Solvents were obtained from Fisher Scientific and were either reagent or HPLC grade.

All results were made in triplicate and averaged with standard deviation.

7.1 Preliminary whole-cell biocatalysis

7.1.1 Reduction of 3, 4-dinitrobenzoic acid using suspended Baker's yeast

7.1.1.1 Preliminary

Three conical flasks were filled with phosphate buffer (0.1 M, 100 mL, pH 7). 3,4-dinitrobenzoic acid (DNB) (0.1 g, 4.72 x 10^{-4} M, Tokyo Chemical Company) was dissolved in ethanol (100 %, 5 mL) and added to one of the beakers. 3,4-dinitrobenzoic acid (0.1 g) was added directly to the buffer solution. In addition, Baker's yeast (1 g, Mauri Pinnacle yeast) was added to the beaker containing ethanol, DNB and buffer, and one of the beakers containing buffer and DNB. All three beakers were heated via a Grant OLS 200 water bath at 30 °C. The reaction was recorded over a 48-hour period using UV-Vis spectrometry with samples taken every 30 minutes for 2 hours and every hour for a further 4 hours with an additional 24 hour reading. Samples were frozen immediately after extraction. Samples were defrosted at room temperature for 30 minutes and filtered using a 0.02 µm syringe filter (Fisher scientific). Absorbance readings were measured using a UV-Vis spectrometer (wavelength 480 nm) using a 700 µL quartz cell.

Sample	3,4 Dinitrobenzoic acid	Yeast	Ethanol (100 %)	Phosphate Buffer (0.1 M)
A	0.1 g	1 g	5 mL	100 mL
B	0.1 g	0 g	0 mL	100 mL
C	0.1 g	1 g	0 mL	100 mL

Table 7.1.1-Preliminary 3, 4-dinitrobenzoic acid reduction set up.

7.1.1.2 Yeast calibration

Baker's yeast (0.1 - 2.0 g) (Mauri Pinnacle yeast) was suspended in phosphate buffer (100 mL, 0.1 M, pH 7) and heated via a Grant OLS 200 water bath at 30 °C. 3,4-dinitrobenzoic acid (0.1 g, 4.72 x 10^{-4} M, Tokyo Chemical Company) was added to the flask. The reaction was recorded over a 24-hour period with samples taken every 30 minutes for 2 hours and every hour for a further 4 hours. Samples were frozen immediately after extraction. Samples were defrosted at room temperature

and filtered using a 0.02 µm syringe filter (Fisher scientific) and absorbance readings were measured using a Varian Cary 50 UV-Vis spectrometer (wavelength 480 nm) using a 700 µL quartz cell

7.1.2 Lipase catalysis of 4-nitrophenyl octanoate

4-Nitrophenyl octanoate (0.1 g, 3.77 x 10^{-4} M) was added to a beaker containing phosphate buffer (100 mL, 0.2 M, pH 7) and 1 % (w/w %) lipase (*Thermomyces lamuginosa*) solution at 30 °C. Each beaker was swirled at 100 rpm using a Grant OLS 200 water bath and samples taken every 5 minutes for the first hour, every hour for the next 3 hours and each 24 hours after. Samples were frozen and absorbance readings were measured using a Varian Cary 50 UV Vis spectrometer (wavelength 400 nm).

7.1.3 Reduction of ethyl acetoacetate using Baker's yeast [128]

A three-neck 500 mL round bottomed flask was set up with a thermometer, bubbler and magnetic stirrer (3rd neck stoppered), in an oil bath on a stirrer hotplate. Tap water (50 mL), sucrose (7 g) and dried Baker's yeast (6 g, Mauri Pinnacle yeast) were added to the flask and stirred for 1 hour at 30 °C to induce fermentation. Ethyl acetoacetate (0.5 g, 3.84 x 10^{-3} M) was added dropwise and then stirred for a further 24 hours at 30 °C. Sucrose (7 g) was dissolved in tap water (40 °C, 50 mL) and added to the mixture in the flask. More yeast (6 g) was added to the flask and stirred for 1 hour. Another 0.5 g ethyl acetoacetate was added and stirred for a further 72 hours. Celite (2 g) was then added to the suspension and stirred. The mixture was filtered in a large Buchner funnel (lined with wet filter paper) through a layer of sand and washed with distilled water. The filtrate was then saturated with sodium chloride. The aqueous mixture was extracted with 5 x 75 mL dichloromethane (DCM). The organic layer (DCM) was combined and dried over magnesium sulphate. The drying agent was filtered off with fluted filter paper in a funnel. The filtrate was then evaporated to dryness and product assessed *via* NMR.

Ethyl acetoacetate

Colourless liquid (1 g, 7.68 x 10^{-3} M), 1H-NMR (400 MHz, DMSO-D6) δ 4.05 (quart, J = 7.0 Hz, 2H), 3.55 (s, 2H), 2.13 (s, 3H), 1.15 (t, J = 7.3 Hz, 3H).

(S/R)-ethyl 3-hydroxybutyrate

Yellow oil (59 %, 5.22 x 10^{-3} M), 1H-NMR (400 MHz, DMSO-D6) δ 4.69 (s, 1H), 4.02 - 3.94 (m, 3H), 2.28 (d, J = 6.4 Hz, 3H), 1.13 (t, J = 7.1 Hz, 3H), 1.04 (d, J = 6.0 Hz, 3H).

7.1.4 Lipase encapsulation using sodium alginate

Sodium alginate (1.5 g) was dissolved overnight in distilled water (100 mL). Lipase solution (1 mL) was added to distilled water (9 mL). The alginate solution (37 °C, 5 mL) was added to diluted lipase solution (5 mL) and mixed thoroughly using a spatula. The lipase-alginate solution (2 mL) was added dropwise using a bulb pipette into calcium chloride solution (2 %, 20 mL). While doing this, swirling was encouraged to encapsulate alginate balls. These were filtered through a Buckner funnel and washed with distilled water (3 x 10 mL). Beads along with the filter paper used were inserted directly into a conical flask inside the water bath previously heated to 30 °C.

7.1.5 Lipase encapsulation using Jetting technology

Sodium alginate (1.5 g) was dissolved overnight in distilled water (100 mL). Lipase solution (1 mL) was added to distilled water (10 mL). The alginate solution (37 °C, 5 mL) was added to diluted lipase solution (5 mL) using 5 ml syringes and mixed thoroughly using a spatula. The Jetlab 4 was flushed with IPA solution (2 mL) for cleaning purposes. Lipase-alginate solution was inserted into the Jetlab solution reservoir (2 mL). The Jetlab 4 was calibrated using the lipase-alginate solution under zeroed parameters. Calcium chloride (20 %) was placed into a glass petri dish below the orifice and the jetting parameters were set to the following: Jetting device orifice size: 50 µm, Rise Time: 16 µs, Drift

Time: 18 µs, Fall Time: 12 µs, Echo, Time: 30 µs, Rise Time $_2$: 4 µs, Idle Voltage: 0, Dwell Voltage: 30 V, Echo Voltage: -30 V.

Lipase solution was then jetted in a continuous rectangular array measuring 2 cm x 2 cm using a on the flow script. Once jetted balls were filtered and cleaned with distilled water. Beads were directly added to buffer and lipase solutions described in section 7.3.2.

7.1.6 Fluorescein diacetate hydrolysis using suspended Baker's yeast [140]

A 250 mL conical flask containing fluorescein diacetate (0.0208 g, 1 mM) (Sigma Aldrich) in potassium phosphate buffer (0.1 M, pH 7, 50 mL) was warmed to 37 °C and stirred at 200 rpm using a magnetic stirrer. Baker's yeast (Mauri Pinnacle Yeast) was defrosted for 20 minutes prior to weighing. Yeast (0.1 - 2.0 g) was directly added to the conical flask and allowed to suspend within the buffer. Sample assays (50 µL) were taken every hour for 7 hours and a final sample at 24 hours. Readings were recorded using a fluorescence spectrometer. Assay samples (50 µL) were analysed under 485 nm absorption and 530 nm emission using a polystyrene black 96-well plate (Corning Incorporated, USA).

7.2 Latex formulation synthesis

7.2.1 Synthesis of Poly (butyl acrylate-co-styrene-co-acrylic acid)

The formulation reagents were taken from Solvay chemical company using their RUS18 formulation. A 1 L beaker was filled with distilled water (174 g), sodium hydrogen carbonate (0.5 g, 5.9x10^{-3} M) (fisher scientific) and Rhodapex Ab/20 (30.92 g, Solvay). The mixture was stirred via Heidolph Hei-TORQUE value 100 overhead stirrer at 100 rpm. Styrene (250 g, Sigma Aldrich), butyl acrylate (240 g, Sigma Aldrich) and acrylic acid (10 g, 0.139 M, Sigma Aldrich) was added dropwise via a Cole Palmer syringe injector using a 100 mL Scientific Glass Engineering syringe. As the monomer solution was added the resulting solution thickened into a bright white emulsion. This emulsion was continuously

stirred to ensure suspension was kept and was covered with foil to ensure reduced evaporation overnight.

Distilled water (206 g), sodium hydrogen carbonate (1 g, 0.01 M) and Rhodapex Ab/20 (4.42 g) was placed into a 1 L jacketed vessel and heated via a VWR scientific 1137P to 82 °C. Contents of vessel was stirred with a 12 cm overhead stainless-steel propeller at 150 rpm. Initiator solution was made using ammonium peroxide sulphate (3.0 g, 0.013 M, Fischer scientific) and distilled water (100 mL). Initiator (20.60 g) and emulsion (28.21 g) seeds were added slowly while mixing and left for 20 minutes. The remainder of initiator and emulsion solutions were added dropwise using a syringe pump. Emulsion drop rate was 144 mL/hr and initiator 20.6 mL/h. Both solutions were added over a time period of 4 hours. Once added vessel temperature was increased to 85 °C and allowed to mix for 30 minutes at 600 rpm. Temperature was then decreased to 65 °C. A chaser solution containing distilled water (5 g) and tert-Butyl hydroperoxide (t-BHP, 70 %) (0.71 g, 7.87×10^{-3} M, Tokyo Chemical Industry) was added dropwise using a glass pipette and allowed 15 minutes to mix. A second chaser solution of distilled water (5.0 g) and isoacorbic acid (0.5 g, 2.84×10^{-3} M) was added over 1 hour via syringe pump (injection rate 5 mL/hr). Once added the mixture was allowed to be stirred for a further 30 minutes. The resulting solution was then cooled to room temperature and filtered through a steel sieve into a sealed glass container.

Latex samples were diluted with 10 % of total volume with distilled water (103 mL) and pH adjusted to 7 using sodium hydroxide (13 mL, 0.1 M).

7.2.2 Drying time

Glass slides were coated in the required latex polymer solution and drawn down using a 100 µm stainless steel draw down cube (Sheen). The polymer side was immediately placed carefully into the 1 of 6 slide holders available and stainless-steel needles were lowered into the coating. A total travel duration of 5 hours was set and started immediately.

7.2.3 2, 2, 4 trimethyl 1, 3- pentanediol monoisobutyrate (Eastman Texanol ™ ester alcohol) addition

Following section 7.2.1, the synthetic latex polymer was poured into a 250 mL flask (100 ml) and stirrer at 100 rpm via overhead stirrer. A mixture of 2, 2, 4 trimethyl 1, 3- pentanediol monoisobutyrate (Texanol ™ ester alcohol) isomers were added to the required weight percentage using a chemyx Inc Fusion 100 syringe pump and a Heidolph Hei-TORQUE value 100 overhead stirrer at a rate of 4 mL/h and 150 rpm respectively.

7.2.4 Glass transition temperature

All glass transition temperatures (T_g) were taken using differential scanning colorimetry. Samples were prepped using Perkin Elmer aluminium sample pan and crimper press. Each sample was ran alongside an empty sample pan. The acrylic polymer T_g method consisted of two temperature ramps at 20 °C /min. Both ramps starting at -50 °C to a maximum temperature of 220 °C. At the end and beginning of each ramp a temperature hold of 1 minute was inserted into the method to ensure sample temperatures were aligned with oven temperatures. At the end of the run the oven temperature was programed back to 30 °C.

7.2.5 Molecular Weight

Molecular weight (M_w), molecular number (M_n) and dispersity index were all measured using Gel permeation Chromatography. Oven columns consisted of an Agilent PL gel 5 µm MiniMIX-D and an Agilent PL gel 3µm MiniMIX-E at 40 °C with a 0.6 mL/min flow rate. Pressure limit ranged from 5 - 150 bar with an injection volume of 100 µL. All latex samples were dried and dissolved in tetrahydrofuran (1 mg/mL).

7.2.6 Hardness Testing

Dried latex polymer samples were placed onto a steel mantle under a 10x microscope lens. Samples were subjected to forces ranging from 100 - 200 g with a set 7 seconds of loading time creating a diamond indentation within the sample (Figure 7.2.1). This indent was analysed using a Burker Aliconer x10 microscope lens with the additional shape measuring software. A measurement was taken for both height and width of the indent and this value was averaged to create a mean value d. This value, along with the known force applied was used to calculate a hardness measurement using the Vickers Hardness equation (Equation 7.2.1).

Figure 7.2.1- A lens view diamond indentation (black circle) on a latex polymer surface using a microhardness tester.

$$HV = 1.854 \frac{F}{d^2}$$

HV: Vickers Hardness (Kgf/ mm)

F: Test Load (Kgf)

d: Mean value of the diagonals of the indentation (mm)

Equation 7.2.1- Vickers Hardness equation.

7.2.7 Latex Polymer Particle size using dynamic light scattering

Particle size was analysed using a 0.04 % volume latex solution in distilled water. The Mastersizer was ran in single narrow mode under enhanced sensitivity in dispersed water. Polymer solution (50

% w/w) was added dropwise to the dispersion unit (hydro 2000SM (A)) until saturation limits were achieved. Particle size ranges were set from 0.02 to 2000 µm and sample runs consisted of 6 individual runs and averaged. After each run the sample chamber was flushed 3 times with distilled water to ensure thorough cleaning.

7.2.8 Contact Angle

Glass and polystyrene substrates were cut (3 cm x 3 cm) and cleaned with distilled water and dried with nitrogen. A total of 3 polymer latex solutions were used ranging in hardness (hard, normal and soft compositions). Half of all substrates were prepared using an acrylic based black primer coating (chaos black primer spray, Games Workshop). This was applied in two coatings and allowed to dry for 24 hours. Latex coatings were applied first with a primary base layer. This was applied using tissue whilst rubbing the surface of the substrate and was dried over 1 hour. This primer ensured an even distribution of coating throughout the substrate and prevented pooling when applying the secondary coating. A draw down cube (100 µm) was used to deposit the second coating and was dried over 24 hours. Each coated substrate was then placed onto the Ossila platform to accurately calculate contact angles using water droplets deposited by a Hamilation glass 50 µL syringe (Figure 7.2.2). A total of 10 water droplets were deposited per substrate with the 2 highest and 2 lowest angles deducted from the sample set. Any anomalies found within the data set were discarded from the sample set. The remaining 6 angles were analysed and averaged providing each left and right angle calculated were within 5 degrees of each other.

A) 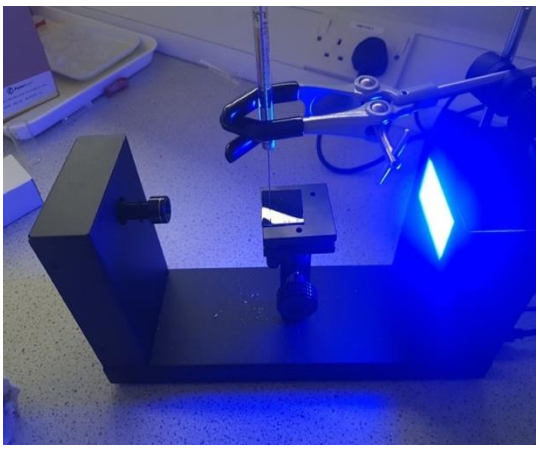 B) 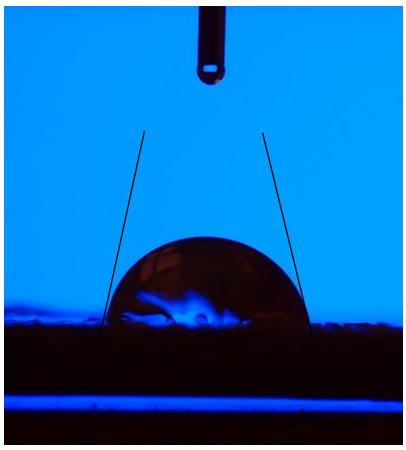

Figure 7.2.2- A) Contact angle set up consisting of a camera, platform, syringe holder, syringe and backlight. B) Software analysis measuring a water droplet contact angle deposited via syringe onto a glass surface.

7.3 Incorporation of microorganisms into latex coatings [157]

7.3.1 3, 4-Dinitrobenzoic acid reduction using Baker's yeast embedded latex coatings

Baker's yeast (1.2 g) (Mauri Pinnacle yeast) was taken and used as a direct replacement for wet cell paste. Sucrose (350 µL, 0.58 g/ mL) and glycerol (300 - 650 µL, 50 % in H_2O) were added directly to the yeast in the ratio stated in Table 4.2.1 *via* Gilson pipette and gently mixed with a spatula. Latex emulsion was then added *via* Gilson pipette and components were swirled for a further 10 minutes. Components were then pipetted into a draw down cube onto a chosen surface with a thickness of 100 µm. Materials chosen were glass, aluminium and PVC (polyvinylchloride). Each slide was left for 2 hours to dry at room temperature. 6 x 250 mL beakers were placed into a water bath at 30 °C filled with 0.1 M Phosphate buffer (100 mL, pH 6.5) with the material slide inserted facedown. 3, 4-dinitrobenzoic acid (0.1 g, 0.47 mM) was dissolved in absolute ethanol (5 mL) and added to each of the 250 mL beaker. Samples (1 mL) were taken and subjected to a calorimetry assay every 10 minutes over a 1-hour period then taken every 30 minutes for a further 2.5 hours, and every 1 hour for a further 5 hours. All samples were frozen immediately after extraction. Reactions were left for a further 48 hours. Future materials were tested using the same method as stated above. All assay

samples were unfrozen at room temperature and analysed using a UV Visible spectrophotometer using a quartz 1 mL cell (wavelength 410 nm).

7.3.2 Lipase embedded latex coatings for the catalysis of 4-nitrophenyl octanoate

Glass microscope slides were coated in a primary 100 µm layer of latex and lipase solution (4 drops from a 5 mL latex and 1 mL lipase mixture). These slides were left to dry for 2 hours at 2 – 8 °C. Once dry, slides were coated in a secondary 100 µm coating of latex with 12 % by weight Texanol ™ and 10 % glycerol solution. Slides were then placed into fridge at 2 - 8 °C for 24 hours. Another set of slides were coated with latex as a primary layer and contained the same additional secondary layer as previously made. 3 sets of 3 x 250 mL beakers were set up within a 30 °C water bath, each containing 100 mL of phosphate buffer (pH 7, 0.5 M). Each set contained 3 of the same coated slides. Set 1 containing both latex and lipase together, set 2 containing latex with no lipase, set 3 suspended lipase with no latex covered glass slide. 2 drops of 4-nitrophenyl octanoate was added to all samples and immediately started rotation at 100 rpm in the water bath. Samples (750 µL) were taken from 0 to 360 minutes and taken Samples taken were immediately placed within the fridge to stop the reaction progressing any further (2 - 8 °C). Samples were measured for absorbance using a UV Visible spectrophotometer (wavelength 400 nm).

7.3.3 Immobilised Baker's yeast fluorescein diacetate hydrolysis batch chemistry

An acrylate-styrene (50:50) based polymer latex (50 % solid) was combined with the yeast in a 1:1 ratio (w/w). This mixture was gently stirred with a steel spatula to ensure even yeast dispersion. Polyethylene spheres (1.5 cm diameter) were dip coated into the polymer-yeast mixture and polystyrene surfaces were cut (5 cm x 3 cm) and coated using a stainless-steel draw down cube (100 µm). To ensure equal masses of coating the total mass of polymer-yeast mixture was weight pre and post dipping. The different in weight was recorded and cast onto the polystyrene surface. Surfaces were allowed to dry for 4 hours before being submerged in phosphate buffer (50 mL, pH 7, 0.1 M)

using falcon tubes. Each tube was sealed and placed into a water bath at 37 °C that consisted of buffer, yeast (immobilised or suspended) and FDA (0.0208 g, 1 mM) (Sigma Aldrich). Solutions rotated at a speed of 90 rpm within the water bath. Samples were recorded every 15 minutes for the first hour, 30 mins for the following hour, every hour for a further 4 hours and 24 hours. All assay samples were frozen immediately following extraction to avoid further progression. Prior to analysis samples were filtered using a syringe and 0.02 µm syringe filter. Fluorescence spectroscopy (excitation 470 nm, emission 520 nm) was used to analyse colour change and was compared to a previous calibration of fluorescein ranging from 0.2 mM to 1.4 mM.

7.3.4 Immobilised Baker's yeast fluorescein diacetate hydrolysis using continuous flow chemistry

An acrylate-styrene (50:50 monomer composition) based polymer latex (50 % solid) was combined with the yeast in a 1:1 ratio (w/w). This mixture was gently stirred with a steel spatula to ensure even yeast dispersion. Using a 3D printer (Ender 3 Pro), polylactic acid (PLA) tubes (length 150 mm, diameter 5 mm) were printed.

Figure 7.3.1- Polylactic acid 3D printed tube.

Using a glass pipette, the biocoating solution was deposited onto the 3D printed tube and the tube was rotated to ensure full covering of the surface. The tube was then dried under nitrogen gas for 2 hours and a further 24 hours under room temperature to ensure a fully dry coating. A 250 mL conical flask containing fluorescein diacetate (0.0208 g, 1 mM) (Sigma Aldrich) in potassium phosphate buffer (0.1 M, pH 7, 50 mL) was warmed to 37 °C and stirred at 200 rpm using a magnetic stirrer. A peristaltic pump (L100-1E, premier control technologies) was attached using silicone tubing in a

circuit with the conical flask while flowing through the coated pipe. The pump was set to 100 rpm and the reaction was assessed for 24 hours. Sample assays were taken every hour for the first 7 hours and 24 hours. Samples were frozen immediately after extraction. All assay samples were analysed under fluorescence spectroscopy (excitation wavelength 470 nm, 520 nm emission).

7.3.5 Suspended solids of biocatalysed reaction systems

A 10 mL sample was taken immediately post reaction and placed into a 10 mL sample cuvette. No dilution factor was required. The suspended solid method (5 - 750 mg/L detection limit) was selected and three consecutive measurements were taken and averaged.

7.3.6 Scanning electron microscope analysis of E. coli 10G pQE(-)ilux

Before analysis, all samples were pre coated in a 4 nm thick coating of platinum using a Quorum Q150R ES spray chamber. Once coated all samples were placed onto a double-sided adhesive carbon tab mounted onto a SEM specimen stub (agar scientific). Samples were subject to the resolution mode using the backscattered electrons (BSE) in-beam detector. Control panel was as follows: Scan Mode: Resolution, HV: 4.00 kV, Magnification 47.10 kx, View Field: 16.68 µm, Speed: 5 (10 µs/pxl), WD: 3.719 mm, Depth of focus: 0.71 µm , Stigmator: 8.4 % / 2.9 %, Image Shift: 0.0 µm / -0.0 µm , Rotation: 0.00 °, Beam Intensity: 7.78 , Absorption Curr: 33 pA , Spot Size: 4.2 nm.

7.3.7 Confocal analysis of E. coli 10G pQE(-)ilux

Biocoatings were formulated as stated in 7.2.1 and allowed to cool at room temperature. Fluorescent *E. coli* (*E. coli 10G pQE(-)ilux*) was cultured and directly added to the latex and gently stirred to ensure even distribution. The biolatex was coated onto a glass microscope slide using a 100 µm draw down cube and allowed to dry for 2 hours at room temperature. Slides were covered with cover slips, sealed using nail varnish and allowed to dry for 1 hour. Leica LAS X imaging software was used using the fluorescence FITC filter setting (excitation 485 nm, emission 530 nm).

7.3.8 Immobilisation of Mcherry and eGFP E. coli

This section of work was completed alongside Gregory Pollard, PhD student at Bristol University.

GFP and *Mcherry E. coli* cells were taken from frozen and streaked onto separate agar (Difo™ Agar Bacteriological) plates and incubated for 24 hours at 37 °C. A single colony was extracted and placed into cell media (1 L, LB media) with carbenicillin antibiotic (10 µL) and incubated for 4 hours at 37 °C. Solutions were centrifuged for 15 minutes and majority of media decanted to leave a small volume of cells and media (5 mL). Suspended cells were submerged into PBS buffer (0.137 M, 2 mL) and stored at 2 – 8 °C for 2 hours. Buffer was decanted and cells were added to 1 % latex solution (5 mL, pH 7) and shaken to ensure even suspension. Solutions were drawn down onto glass slides using a 100 µm draw down cube and left to dry for 1 - 24 hours at room temperature. Cells were expressed from 1 to 24 hours with ITPG (2 mL, 1 mM) using a pressure spray to ensure full coverage. Expressed slides were incubated at 37 °C for 4 hours. Analysis of cell activity was investigated using confocal and fluorescence microscopy (see section 7.3.7 for confocal method).

7.4 Immobilising algae on loofah sponge substrate using latex binders [164]

This section of worked was completed alongside Pichaya-In-Na, PhD student at Newcastle University.

7.4.1 Cyanobacteria growth

Synechococcus elongatus CCAP 1479/1A and PCC 7942 (freshwater cyanobacteria) were studied and combined with latex binder to produce biocomposites. Both CCAP and PCC were cultivated in BG11 medium and JM medium respectively. Cultures were grown in 10 L polycarbonate carboys (Nalgene) with a constant HEPA filtered aeration using a KOI AIR 50 Blagdon aquarium pump. Conditions were maintained at 18 ± 2 °C with a 16:8 hour light:dark cycle with 2500 lux (≈30.5 µM m^{-2} s^{-1}) of illumination provided by 30 W daylight-type fluorescent tubes.

7.4.2 Loofah Analysis

Loofah sponges were purchased from retail outlets, a sample (5 x 1 x 1 cm) was embedded in an epoxy resin within a silicon mould and cured for 48 hours at 20 °C (100 parts EpoxiCure 2 to 23 parts hardener by weight, containing five drops of black acrylic liquid pigment to enhance contrast). sections were cut (1 mm thick) using a Buehler IosMet Low Speed Saw at 100 rpm. Loofah sections were imaged using a digital HD camera (canon EOS M10 fitted with an EF-M 15 - 45 mm 1:3.5 - 6.3 IS STM Canon zoom lens). The loofah strand perimeter per area (mm mm^{-2}) was determined using Image J software. Loofah samples were measured for light penetration (transmitted photosynthetic active radiation, PAR) through different sections (whole loofah vertical orientation 100.8 ± 0.27 mm height; horizontal orientation 54.63 ± 0.72 mm dimeter, half loofah vertical orientation 13.01 ± 0.43 mm diameter) and was measured using a Skye PAR Quantum Sensor under natural sunlight (1500 hrs BST, July 3rd, 2019). A lightproof tube was used to hold the sensor to prevent peripheral light from distorting the readings. Ambient sunlight PAR (mean ± StDev = 1902 ± 39 µM $m^{-2}s^{-1}$) was recorded before and after each loofah sample.

7.4.3 Cell adhesion test

All cyanobacteria strains were centrifuged for 30 mins at 1717 RCF to obtain wet cell paste from 2 L of culture of known cell density. Loofah materials were autoclaved and dried at 105 °C for 3 hours. Once dry, loofah was stored overnight in a desiccator before immobilisation. Loofah was cut into 1 x 1 x 1 cm cubes and placed in 24-multiwell plates. Synthetic latex polymers were formulated as describes in section 7.2.1 .Each polymer was mixed with 2.5 % wet cell paste and vortexed for 10 to 20 seconds (Vortex Genie 2, Scientific Industries Inc.) until uniform. Each latex biocomposite (1 mL) was pipetted onto each loofah cube and dried at 30 °C for 24 hours. Cells within the mixture were counted and dried separately and hence the number of immobilised cells could be calculated. Each biocomposite was submerged in growth medium (2 mL) and shaken in darkness at 80 rpm for 1, 24,

48 and 72 hours. At each of these time intervals growth medium was remade and any cells that were released from the loofah were counted using a haemocytometer.

7.4.4 Cell toxicity testing

All polymers were diluted to 5 % w/w solid content using deionized water. Approximately 1 mL of each latex was mixed with 1 mL of cell culture in 24-multiwell plates. The biocomposites were cultured for 7 days (20 °C, 16:8 light:dark photoperiod at 2500 lux). After 7 days samples were diluted (by a factor of 20) using sterile dH_2O and cell counts analysed using a Neubauer Hawksely haemocytometer comparative to suspension controls.

To identify the most suitable binders for each cyanobacteria, a weighted decision matrix was used from the toxicity and adhesion data collected. Toxicity was given a higher ranking (ratio 3:2) as the maintenance of cell viability was deemed a higher priority.

7.4.5 Biological response analysis using I-PAM

To measure photosynthetic metabolic responses of cyanobacteria exposed to different latex biocomposites through quantification of chlorophyll fluorescence levels, an imaging pulse amplitude modulated-fluorometer (Imaging PAM) was used. Each sample consisted of a latex polymer (1 mL) combined with concentrated cell mixture (1 mL) to form a biocoating (2.5 % v/v cells/sterile dH_2O) in individual wells of a 24-multiwell plate. These samples were analysed alongside a corresponding latex control. All samples were monitored daily for seven days and gently mixed via reverse pipetting and left in darkness for 30 mins before taking results. IPAM settings were altered to gain values of 20 to 25 depending on the base intensity and low saturation pulse intensity of 1 to compensate for the high phycocyanin pigment content in cyanobacteria. The maximum photosystem II (PSII) quantum yield (Fv/Fm) was determined from the dark florescence yield (Fo) and maximum florescence yielded (Fm) (Equation 7.4.1). The apparent rate of photosynthesis (PS) was calculated from the measured

effective PSII quantum yield (Y(II)), the incident photon flux density (PAR) which was fixed at 370 µM photon $m^{-2}s^{-1}$ and the measured absorptivity (Abs.) (Equation 7.4.2). In calculation 50 % of the absorbed PAR was assumed to be distributed to PSII.

$$\frac{F_v}{F_m} = \frac{F_m - F_o}{F_m}$$

Equation 7.4.1- Calculation for quantum yield.

$$PS = 0.5 \times Y(II) \times PAR \times Abs.$$

Equation 7.4.2-Apparent rate of photosynthesis.

7.4.6 CO_2 absorption test (Semi-batch) [66]

Loofah material was cut into 1 x 1 x 5 cm strips and weighed. Using previous results, the best corresponding partnerships between the latex and *S. elongatus* CCPA 1479/1A (4S and 12S) and PCC 7942 (4N and 12N) cyanobacteria were used. Biocoating consisting of latex polymer and suspended cyanobacteria (2.5 % w/v Wet cell paste and 2.5 % solid binder) were pipetted onto each loofah strip covering 1x1x3 cm and dried in an oven at 20 °C for 24 hours in darkness. Cell loading efficiency upon the loofah was found to be under 100 % due to the nanoporous structure of the loofah meaning some formulation flowing to waste. To combat this reduction in cell count, a dried formulation was made as a new reference. Abiotic controls consisting of loofah, latex and sterile growth medium were similarly set up. For batch testing, tests were run over a 8 week period. Biocomposites deposited onto loofah were placed into glass bottles (50 mL) containing growth medium (5 mL) (Figure 7.4.1). Bottles were sealed using 20 mm butyl rubber stoppers and crimped using silver aluminum caps. A gas mixture (45 mL of 5 % CO_2/air) was injected using an airtight syringe into each glass bottle. Samples were studied alongside two control bottles containing a latex

coated loofah with no immobilised cells and a bottle containing an appropriate liquid cell suspension equivalent to the cell loading found within the biocomposite sample. Samples and controls were made in triplicate and maintained at 18 ± 2 °C with a 16:8 light and dark photoperiod at 2500 lux. Every 2 days, the extraction of headspace with an airtight syringe and injecting into a GEOTech G100 infrared absorption CO_2 meter was used to measure the percentage of CO_2 fixation. After analysis the equivalent volume of CO_2 gas mixture was replenished.

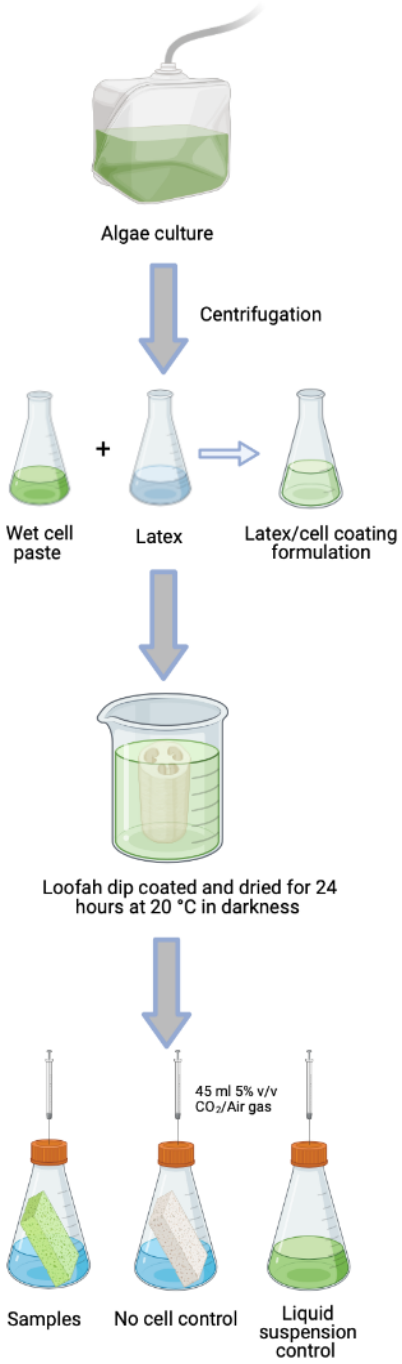

Figure 7.4.1- Process of CO2 Semi-batch testing using immobilised microalgae and cyanobacteria on loofah sponge.

Direct cell counts were found to be impractical due to the complex loofah shape and transparency of latex coatings. To solve this, growth was estimated based on changes in mass. The net quantity of CO_2 fixed by immobilised cells was calculated using the total immobilised biomass. Biomass was determined from the difference in loofah mass pre and post immobilisation. Net CO_2 fixation rates were calculated using Equation 7.4.3. When calculating the CO_2 fixation rate per unit surface area, assumptions regarding void area was considered the same throughout the structure. Other assumptions made were that the loofah does not consume CO_2, the cell biocomposite formulation was uniformly distributed across the loofah surface, and that there was no outgrowth of cells beyond the estimated surface area.

$$\text{net } CO_2 \text{ fixation rate (mol } CO_2\ g^{-1}_{biomass}\ day^{-1}) = \frac{\%\ CO_2 \text{ fixed x } \frac{PV}{RT}}{IDW \text{ x 2 days}}$$

P- Gas Pressure (kPa)
V- Gas volume (l)
R- Ideal gas constant
T- Temperature (K)
IDW- Immobilised dry weight of biomass (g)

Equation 7.4.3- Net CO_2 fixation rate equation [66]

7.4.7 Biocomposite cell growth analysis using SEM

Biocomposites were analysed using SEM imaging before and after CO_2 absorption testing with a voltage of 8 kV. Prior to analysis, all biocomposite samples were dried at 105 °C for 3 hours and stored in a desiccator for at least 24 hours. Samples were prepped using a 5 mm coating of gold to enhance conductivity and attached to a 12 mm pin stub using carbon tape. Analysis was conducted using a 5000x magnification.

7.4.8 Total carbohydrate extraction

This total carbohydrate extraction method was altered from Mohemimani *et al*. [183] Before extraction, semi-batch CO_2 absorption samples were frozen at -20 °C, freeze dried for 48 hours

(Martin Christ 1-1 LD Plus) and ground (Cookworks coffee and Herb Grinder). Samples were homogenised with H_2SO_4 (1 mL, 1M) in a 45 mL acid resistance centrifuge tube. A further 10 mL of the identical acid solution was added to each sample. All samples were then incubated using a water bath at 100 °C for 1 hour and allowed to cool at room temperature (20 °C). Acid solution was separated from each samples using a centrifuge (Sigma Laboratory Centrifuges 3K18 C) at 2000 RCF (3333 RPM) for 10 mins. Without disturbing solid residues, 2 mL from each sample was removed and transferred into another centrifuge tube. The isolated extract was mixed with 1 mL of phenol solution (50 g L^{-1}) before 5 mL H_2SO_4 (>95 %) was added. Both solutions were vortexed for 10 to 20 seconds (Vortex Genie 2, Scientific Industries Inc) and were left to cool to room temperature. Cooled samples (1 mL) were then placed into a 1.5 mL cuvette and analysed in a UV/Vis spectrometer at a wavelength of 485 nm. Total carbohydrate content was calculated using a known glucose concentration calibration curve. Biocomposites were analysed at weeks 2, 4, 6 and 12 weeks of the absorption tests. Carbohydrate extraction was also conducted alongside abiotic controls (no immobilised cells) to normalise biocomposites. Results were presented as a percentage of total carbohydrate content in immobilised dried weight biomass.

7.5 Self-healing Polyurethane

7.5.1 Polyurethane Synthesis

Polytetrahydrofuran-1000 (PTMG) (26.0 g, 0.0520 M) was placed into a 250 mL beaker and heated using a hot plate and oil bath at 140 °C for 10 minutes accompanied by an overhead stirrer (Heidolph Hei-TORQUE value 100) and PTFE blade shaft (Fisher Scientific) rotating at 100 rpm. Methylene diphenyl diisocyanate (MDI) (11.80 g, 0.094 M) was added to the reaction flask in small batches. The mixture was allowed to stir for 2 hours after the addition at 70 rpm. The temperature was increased to 180 °C. 1, 6-Hexanediol (HDO) (1.56 g, 0.035 M) and 2, 2-Bishydroxymethyl propionic acid (DMPA) (1.78 g, 0.0266 M) were mixed and added slowly in small batches to the flask. The resulting polymer

was transferred into a Technico vacuum oven attached to a Vacuuband 2C pump and was cured for 2 hours under vacuum.

7.5.2 Alterations in polymer composites

Polyurethane samples were constructed using the same method described in section 7.5.1. PTMG, HDO and DMPA were altered in numerous compositions to create varying ratios of alcohol to cyanide (OH : NCO) functional groups. Following this, individual composites were then altered within the alcohol functional groups. Overall functional group ratios remained constant by increasing or decreasing other alcohol contributing constituents.

7.5.3 Impacts of DMPA on self-healing

This work was aided by Bradley Thomas, Northumbria University (RA on the Immortal Manufacturing project).

To assess the impact of DMPA on the self-healing efficacy, and the effect of other formulation components, an L9 Taguchi orthogonal array was produced. The array alters the type of chain extender and molecular weight of the PTMG, whilst keeping the concentration of hydroxyl groups constant. Only the concentration of DMPA contributing to the OH functionalization is altered.

To maintain comparable amounts of material produced, the mass of PTMG within the formulations is kept fixed to 26 g, all other component masses are altered to maintain a constant ratio of reactive functional groups within the final materials.

PUs were synthesised using a solvent-free two step polymerisation procedure, all masses of materials used were in accordance with the run within the L9 array. Poly(tetramethylene ether) glycol (PTMG) was added to a 250 mL beaker and heated in an oil bath at 140 °C for 10 minutes, accompanied by overhead stirring at 50 rpm. Methylene diphenyl diisocyanate (MDI) was added to

the reaction flask in small batches. The mixture was allowed to stir for 2 hours after the addition at 50 rpm. The oil bath temperature was increased to 160 °C and the chain extender and DMPA (where used) were added slowly to the flask over a minute. Once the reaction mixture thickened the beaker was placed into a vacuum oven and air was evacuated at 2kPa and 190 °C for 1 hour. The material was then poured into silicone moulds and allowed to set at RTP for 24 hours before being released.

7.5.4 Self-healing tensile strength testing

Following polymer synthesis described in 7.5.1, 7.5.2, and 7.5.3, the contents of cured polymer was transferred at 190 °C into a heated silicone dog bone mould. The mould was placed into the oven at 180 °C for 2 hours to allow the polymer to melt evenly into shape. The silicone moulds were then cooled at room temperature and allowed to set for 24 hours (Figure 7.5.1). Dog bones were cut via scissors directly in the centre of the mould. The two sections were then manually pushed together for 3 seconds and left at room temperature and pressure for a timed duration (1 hour and 24 hours). Dog bones were clamped in place using an aluminium plate to prevent sample sticking to the clamp (Figure 7.5.2). Before starting the procedure, sample slack was reduced until the sample was flat to ensure tensile results were reflective to the material properties. Parameters for testing were as follows: Geometry: Rectangular, Machine Control: Standard, Data Rate: 10.00 pts/sec, Crosshead Speed: 15.00 mm/min.

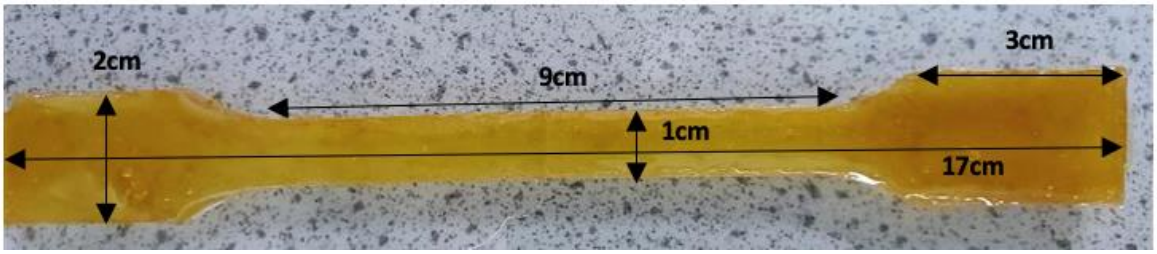

Figure 7.5.1-Polyurethane dog bone sample post curing.

Figure 7.5.2-Tensile Strength testing using an Instron Series IX version 8.33.00.

7.5.5 Polyurethane self-healing analysis using a USB microscope

Three polyurethane samples were synthesised and moulded into identical dog bone structures as described in section 7.5.4. Samples were cut using scissors in the middle of the dog bone and immediately pushed together. To analyse self-healing characteristics each sample was recorded via a Jiusion F210 wireless portable microscope camera. The camera was programed to take photos every 12 hours over a 7-day period.

7.6 Deposition of solutions using Ink-Jet technology

7.6.1 Jetlab 4 system set up

All printing was performed using a single print head and achieved at 23 °C (room temperature). Prior to printing, the jetting system was purged with 2 mL isopropyl alcohol (IPA) to inspect for any blemishes and to flush the device. If a clean jetting stream was observed the reservoir was filled with 2 mL of jetting solution. The solution was purged (0.1 mL) to ensure tubing and devices were filled. Devices were then inspected via the monochromatic camera to ensure the correct back pressure was applied. Continuous jetting was applied to the system and parameters altered to create one

stable, small and consistent droplet with the correct trajectory. Factors such as surface tension, viscosity and jetting temperature were all closely monitored during jetting procedures to ensure consistent parameters. Two methods of printing scripting were used. Both scripts were jetted using on the fly mode. A directly coordinated shape which manually inserts each step using coordinates was used in the initial stages of printing patterns:

Set fly on 30.0

Move to 10.0 10.0

Array 0.15 20 0.25 10 0.0 1

Later stages of printing involved more advanced printing patterns. In order to do this a bitmap method was used. All bitmap images were created on Microsoft Paint and saved as a monochromatic file and scripted such as:

Set fly on 30.0

Bitmap 0.0 0.0 0.0 1 1 <bitmap file name>

7.6.2 Electron spray droplet size determination using fluorescein encapsulate alginate

Sodium alginate (1.5 g) was dissolved overnight in distilled water (100 mL). The alginate solution (37 °C, 5 mL) was added to fluorescein in 10 mL water (0.5 g, 1.5 x 10^{-3} M) and mixed thoroughly using a spatula. This mixture (2 mL) was added directly to the reservoir and parameters were adjusted: Jetting device orifice size: 50 µm, Rise Time: 16 µs, Drift Time: 18 µs, Fall Time: 12 µs, Echo Time: 30 µs, Rise Time $_2$: 4 µs, Idle Voltage: 0 V, Dwell Voltage: 30 V, Echo Voltage: -30 V. The alginate solution was jetted using a on the fly jetting in a rectangular array directly into a petri dish containing calcium chloride solution (20 %). While doing this, swirling of the calcium chloride solution was encouraged to encapsulate alginate balls. Once the reservoir was empty the solution was collected and filtered using a Buchner funnel, filter paper (Fisher Scientific, 0.16 mm) and washed with distilled water (10 mL). Filter paper was analysed using a DM USB microscope and compatible DM wifi app software. To

enable fluorescein to be visible at this small scale, a UV torch (Winzwon UV torch) was directed over the filter paper to enhance droplets. Alginate balls were measured using callipers.

7.6.3 Preliminary printing

7.6.3.1 Isopropyl Alcohol

Isopropyl alcohol was printed using the same procedure in 7.6.1. Backpressure was set to -6 using a standard wave pulse. A strobe delay was set to 180 µs and a frequency of 280 Hz. A bipolar wave was created using the following parameters. Rise time 5.0 µs, dwell time 40 µs, fall time 5.0 µs, echo time 45 µs, rise time 2 4.0 µs, idle voltage 0 V, dwell voltage 35 V, echo voltage -35 V.

7.6.3.2 Distilled water jetting

Distilled water was printed using the same procedure in 7.6.1. A standard wave with a strobe delay of 200 µs and a frequency of 250 Hz was used. Back pressure was set to -14 and a bipolar waveform was created using the following parameters. Rise time 5.0 µs, dwell time 70 µs, fall time 5.0 µs, echo time 65 µs, rise time 2 4.0 µs, idle voltage -30 V, dwell voltage 35 V, echo voltage -30 V. Once droplet formation was achieved, distilled water was printed onto water sensitive paper (Teejet water and oil sensitive paper, 76 x 26 mm) indicating a yellow to blue colour change. A range of patterns and shapes were printed using scripts on both drop demand functions and bitmap imaging.

7.6.3.3 Glaco spray jetting

Glaco 99 spray was purchased from an online distributor and diluted to 1 % concentration using IPA. Glaco spray was printed using the same procedure in 7.6.1. A standard wave with a strobe delay of 220 µs and a frequency of 220 Hz was used. Back pressure was set to -4 and a bipolar waveform was created using the following parameters. Rise time 5.0 µs, dwell time 50 µs, fall time 5.0 µs, echo time 45 µs, rise time 2 4.0 µs, idle voltage -10 V, dwell voltage 15 V, echo voltage -10 V. Glass and polystyrene surfaces were sprayed using a bitmap image containing alternate 20 cm lines varying in width (Figure 7.6.1).

Figure 7.6.1-Bitmap print pattern (white) using varying widths of print widths (black)

7.6.3.4 Click chemistry of iridium complexes [180]

The iridium complex was synthesised by Valery Kozhevnikov, Northumbria University.

Backpressure was set to -6 using a standard wave pulse. A strobe delay was set to 180 µs and a frequency of 280 Hz. A bipolar wave was created using the following parameters. Rise time 5.0 µs, dwell time 40 µs, fall time 5.0 µs, echo time 45 µs, rise time 2 4.0 µs, idle voltage 0 V, dwell voltage 37 V, echo voltage -37 V. Prints were analysed under a UV lamp (254 nm).

7.6.3.5 Polymer latex jetting

Latex polymers were formulated and synthesised using procedure 7.2.1. Solutions were neutralized using sodium hydroxide (0.1 M) and diluted to 0.5 % concentration using distilled water and mixed using an overhead stirrer. Polymer latex solution was printed using the same procedure in 7.6.1 using a bitmap script. A standard wave with a strobe delay of 240 µs and a frequency of 250 Hz was used. Back pressure was set to -14 and a bipolar waveform was created using the following parameters. Rise time 5.0 µs, dwell time 60 µs, fall time 5.0 µs, echo time 50 µs, rise time 2 4.0 µs, idle voltage -30 V, dwell voltage 40 V, echo voltage -30 V. Polymer solutions were printed onto glass using 'on the fly' setting under a continuous drop formation. Due to the high contents of water in the solution the polymer was able to be printed onto water sensitive paper to confirm consistent jetting.

7.6.3.6 Fluorescein jetting

Fluorescein (0.05 %) was dissolved in 20 mL of distilled water and sonicated for 1 minute. The solution was filtered through filter paper (Fisher Scientific 70 mm) and filtered again through a syringe filter (0.2 µm). This solution was placed directly into the printing reservoir and was printed using the same procedure in 7.6.1 using a bitmap script. A standard wave with a strobe delay of 240 µs and a frequency of 250 Hz was used. Back pressure was set to -12 and a bipolar waveform was created using the following parameters. Rise time 5.0 µs, dwell time 20 µs, fall time 5.0 µs, echo time 25 µs, rise time 2 4.0 µs, idle voltage -30 V, dwell voltage 35 V, echo voltage -35 V. Fluorescein solutions were printed onto filter paper (Fisher Scientific 150 mm) using 'on the fly' setting under a continuous drop formation. Printing patterns were analysed under UV light (wavelength 254 nm).

7.6.4 Printing onto 3D scaffold systems using laser cutting technology

Medium clear acrylic (Glowforge, USA) was purchased and cut using a Glowforge 3D laser printer. Images were created using Inkscape software. Laser settings were set to default acrylic cutting parameters (laser cutting power full, cutting speed 800). Quality settings were set to maximum quality and auto focus height. In order to print onto the 3D acrylic scaffolds previously discussed, files were converted into image files and further converted to bitmaps using Microsoft Paint. Files were scaled to the acrylic surface via pixel formatting. In order to determine the correct size, angles and patterns, fluorescein (0.05 %, 2 mL) was printed onto the engraved surfaces and analysed under UV (wavelength 254 nm) to confirm printing accuracy. Two symmetrical patterns were engraved and cut as seen in Figure 7.6.2 (9.6 x 6.2 cm).

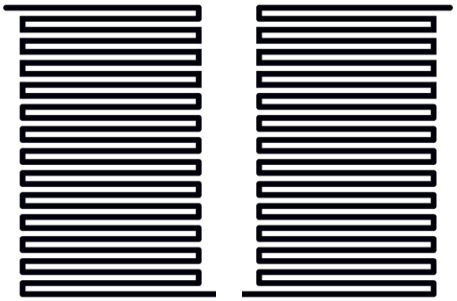

Figure 7.6.2- Bitmap imaging of two symmetrical laser cut networks onto 3D acrylic materials

7.6.5 Microorganism embedded polymer jetting

7.6.5.1 Baker's Yeast

Identical procedures were used from previous jetting methods to successfully print a polymer-bacteria blend. Latex polymer solutions were diluted to 0.5 % polymer concentration using distilled water (20 mL) and Baker's yeast (0.1 g) were directly added to the polymer. Solutions were kept at a minimum concentration to avoid potential blocking of the jetting orifice from cell accumulation (0.005 g mL^{-1}). The solution was stirred gently to disperse cells and a sample taken and placed into the jetting reservoir (2 mL). Solutions were printed using the same procedure in 7.6.1 using a bitmap script. A standard wave with a strobe delay of 240 µs and a frequency of 250 Hz was used. Back pressure was set to -12 and a bipolar waveform was created using the following parameters. Rise time 5.0 µs, dwell time 65 µs, fall time 5.0 µs, echo time 50 µs, rise time 2 4.0 µs, idle voltage -30 V, dwell voltage 30 V, echo voltage -30 V.

7.7 Jetting embedded cells using polymer latexes onto 3D laser cut scaffolds

Two separate medium clear acrylic surfaces (10 x 5 cm, Glowforge, USA) were cut using a laser cutter under the same method found in 7.6.4. Trenches were engraved three times to create a deeper channel (3 mm). Scaffolds were later subject to printing using the method described in 7.6.5.1 and were dried for 2 hours at room temperature. Silicone tubing (1.6 mm diameter, tubing 14, premier

control technologies) was inserted and glued into the inlet and outlet ports (Loctite super glue). Acrylic surfaces were then lined up to ensure networks were in line and glued together using super glue (Loctite super glue). Bathroom sealant (wilko bathroom sealant, UK) was used around the borders of the plastic to maintain a watertight seal and was dried for 24 hours. Fluorescein diacetate (0.0208 g, 1 mM) was inserted into a beaker containing 50 mL of phosphate buffer (0.1 M, pH 7) as described in method 7.3.4. The circuit was attached via a silicone line feeding back into the beaker to create a flow circuit. The peristaltic pump (L100-1E, premier control technologies) was set to 100 rpm (10 mL min^{-1}) and the reaction was monitored via assay as described in method 7.3.4.

8 Future work

The work reported in this thesis contributes to several areas of research. Firstly, regarding synthesised latex polymer formulations, further analysis such as quantifying residual monomer would be essential to understand the extent of coating toxicity on immobilised cells. Formulating different monomers (various methacrylate-based monomers and styrene derivatives) into the polymer and investigating how their compositions enable a wider range of physical and chemical properties. Further alterations in coating properties could be investigated through the addition of additives to change its porosity, coalescence and film formation. The synthesis of these monomer and additive compositions would see the start of a sample library whereby cell environments can be tailored to optimise the biocomposite and enhance its enzymatic activity.

Currently a diverse range of procedures are reported for the immobilisation of cells into polymer latexes. Simplifying these methods and developing a universal technique capable of sustaining a diverse range of microorganisms will see rapid advancements in the evolution of polymer latex immobilisation. In this thesis, several techniques to measure immobilised cell activity were used, in particular, a green fluorescent protein (GFP) as in indicator to distinguish between living and dead cells. However, the GFP required expression after a duration of time, and once expressed could not be further analysed. One method to investigate is the immobilisation of bioluminescent *E. coli*. This genetically modified bacteria consist of a recombinant firefly gene which when metabolically active presents bioluminescence. This would provide a rapid analysis method to measure cell degradation while immobilised in a polymer coating and further evidence to this coatings capability to sustain microorganisms. Although this synthetic latex polymer was tested on numerous enzyme and cell species, further investigations into polymer microorganism composites would not only see the involvement of a wider range of species, but the addition of a collection of bacteria, isolated enzymes and even mammalian cells incorporated into a single polymer coating to provide a multibiocatalytic coating.

In chapter 5 the synthesis of a polyurethane that had the potential to self-heal was analysed. Although numerous monomer formulations of polyurethane were synthesised, additional investigations into short term healing would be necessary to determine factors contributing to tensile recovery. The most challenging aspect of this research would be the optimisation in recovery strength to create a material whereby the uncut maximum load is equivalent to healed maximum load. Additionally, quantifying the interactions and mechanisms responsible for this healing behavior is adamant in developing this material further. To achieve this, highly complex computational methods will be necessary to identify sites of interest.

Chapter 6 creates an effective method to print living bacteria within a polymer formulated solution which can be expanded to other microorganisms with the aid of alterations in polymer composition and jetting parameters. With further jetting experience, the addition of multiple print heads would see double or treble synchronized printing to effectively create high resolution areas with numerous bacteria functions. Additionally, advancements in 3D printing and 3D laser cutting could see the development of channeled networks whereby each channel has a carefully selected immobilised microorganism capable of a singular function. The controlled movement of reagents could not only create an efficient way of catalysing reactions, but able to process a multistep reaction all within a smart network just through the precise placement and flow of components.

9 Appendix

9.1 Synthesis of acrylic latex polymer

9.1.1 Infra-red

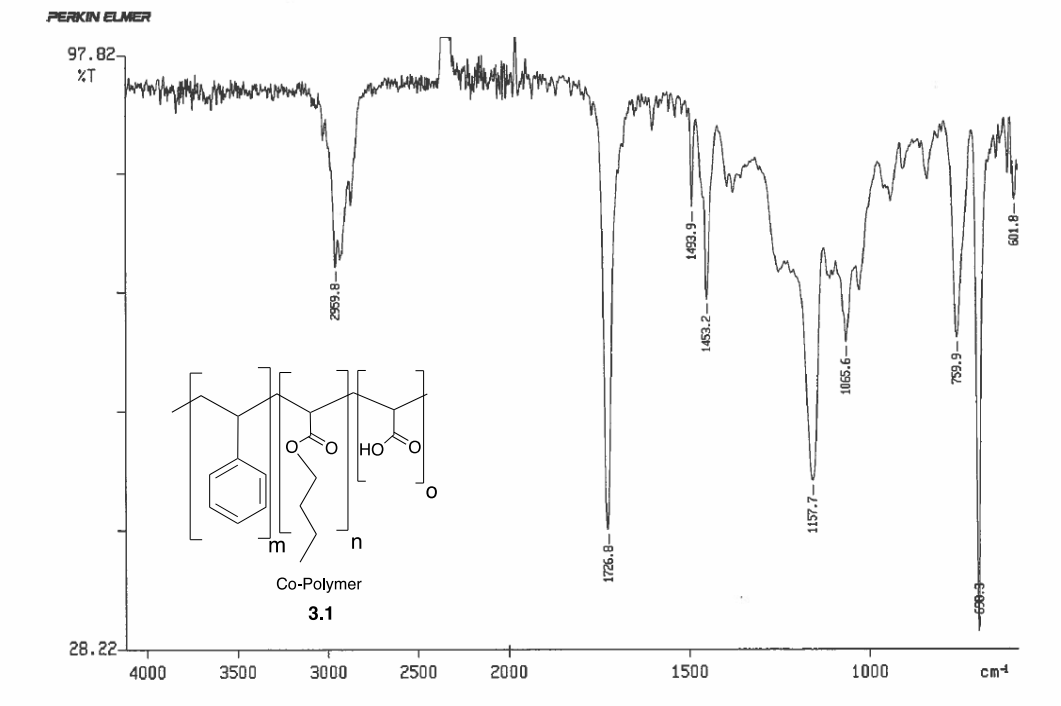

Figure 9.1.1- IR spectrum of Co-polymer 3.1

2850-3050 (C-H), 1726 (C=O), 1157 (C-O), 1065 (C-H)

9.2 SEM imaging of a latex polymer coating surface

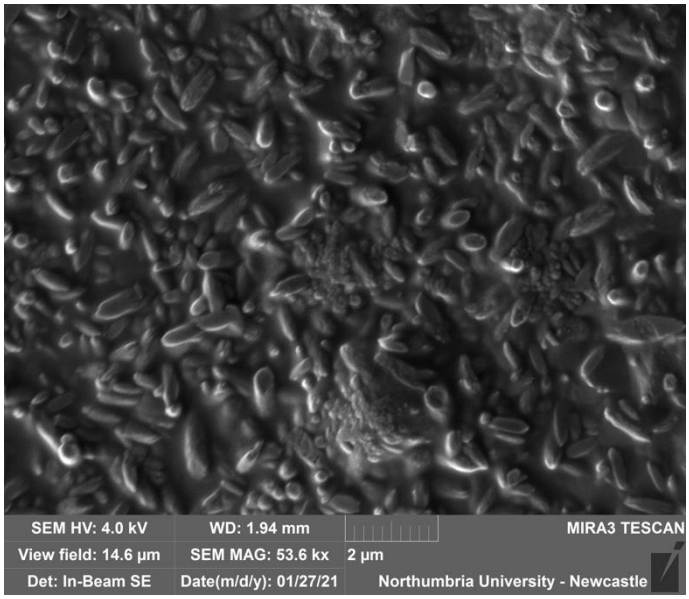

Figure 9.2.1- Surface of a dried coalesced latex polymer coating

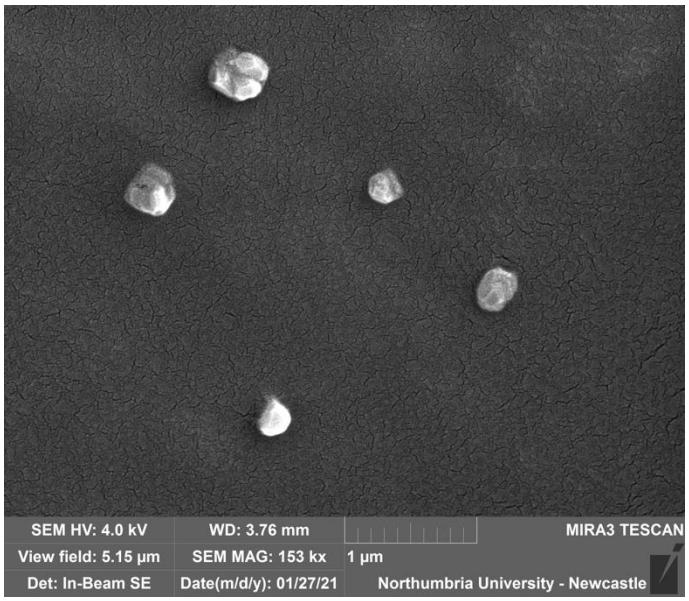

Figure 9.2.2- Latex particles on a coalesced surface coating

9.3 Particle size analysis

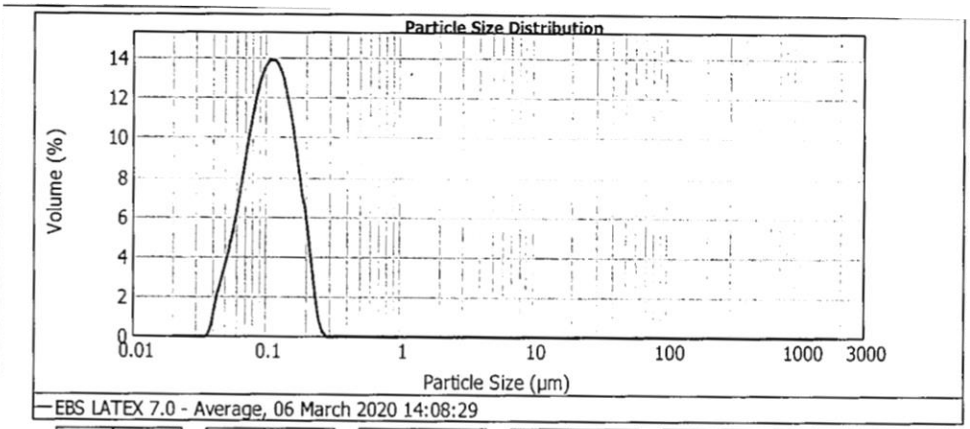

Size (µm)	Volume In %
0.020	0.00
0.022	0.00
0.025	0.00
0.028	0.00
0.032	0.00
0.036	0.01
0.040	1.31
0.045	2.19
0.050	3.21
0.056	4.36
0.063	5.88
0.071	7.45
0.080	8.81
0.089	9.83
0.100	10.39
0.112	10.44
0.126	9.95
0.142	

Size (µm)	Volume In %
0.142	8.90
0.159	7.33
0.178	5.43
0.200	3.28
0.224	1.18
0.252	0.08
0.283	0.00
0.317	0.00
0.356	0.00
0.399	0.00
0.448	0.00
0.502	0.00
0.564	0.00
0.632	0.00
0.710	0.00
0.796	0.00
0.893	0.00
1.002	

Size (µm)	Volume In %
1.002	0.00
1.125	0.00
1.262	0.00
1.416	0.00
1.589	0.00
1.783	0.00
2.000	0.00
2.244	0.00
2.518	0.00
2.825	0.00
3.170	0.00
3.557	0.00
3.991	0.00
4.477	0.00
5.024	0.00
5.637	0.00
6.325	0.00
7.096	

Size (µm)	Volume In %
7.096	0.00
7.962	0.00
8.934	0.00
10.024	0.00
11.247	0.00
12.619	0.00
14.159	0.00
15.887	0.00
17.825	0.00
20.000	0.00
22.440	0.00
25.179	0.00
28.251	0.00
31.698	0.00
35.566	0.00
39.905	0.00
44.774	0.00
50.238	

Size (µm)	Volume In %
50.238	0.00
56.368	0.00
63.246	0.00
70.963	0.00
79.621	0.00
89.337	0.00
100.237	0.00
112.468	0.00
126.191	0.00
141.589	0.00
158.866	0.00
178.250	0.00
200.000	0.00
224.404	0.00
251.785	0.00
282.508	0.00
316.979	0.00
355.658	

Size (µm)	Volume In %
355.656	0.00
399.052	0.00
447.744	0.00
502.377	0.00
563.677	0.00
632.456	0.00
709.627	0.00
796.214	0.00
893.367	0.00
1002.374	0.00
1124.683	0.00
1261.915	0.00
1415.892	0.00
1588.656	0.00
1782.502	0.00
2000.000	

Figure 9.3.9.2.1- Particle size analysis report for latex polymer 24 % BA

9.4 Jetting scripts

9.4.1 Three squares jetting script

4 Squares 2.0,1.5,1.0,0.5 cm

;

;Script file to print 4 squares parrellel to the x axis decreasing in size 2.0 cm - 0.5 cm with 2 cm spacing between.

;

set fly on 30.0

;

moveall 0.0 0.0 - 45.0

;

rotation - rotation is CCW starting at 0 parallel to x axis

;

array 0.2 101 0.2 101 0.0 1

;

0.0

moveto 40.0 0.0

array 0.2 76 0.2 76 0.0 1

;

moveto 75.0 0.0

array 0.2 51 0.2 51 0.0 1

;

moveto 105.0 0.0

array 0.2 26 0.2 26 0.0 1

10 References

1 J. O. Rich, P. C. Michels and Y. L. Khmelnitsky, Combinatorial biocatalysis, *Curr. Opin. Chem. Biol.*, 2002, **6**, 161–167.

2 J. M. Woodlley, Microbial Biocatalytic Processes and Their Development, *Adv. Appl. Microbiol.*, 2006, **60**, 1–15.

3 N. C. Goodwin, J. P. Morrison, D. E. Fuerst and T. Hadi, Biocatalysis in Medicinal Chemistry: Challenges to Access and Drivers for Adoption, *ACS Med. Chem. Lett.*, 2019, **10**, 1363–1366.

4 S. L. Neidleman, Applications of Biocatalysis to Biotechnology, *Biotechnol. Genet. Eng. Rev.*, 1984, **1**, 1–38.

5 A. Basso and S. Serban, Industrial applications of immobilized enzymes—A review, *Mol. Catal.*, 2019, **479**, 110607.

6 B. A. Cheba, T. I. Zaghloul, A. R. EL-Mahdy and M. H. EL-Massry, Affinity Purification and Immobilization of Chitinase from Bacillus sp.R2, *Procedia Technol.*, 2015, **19**, 958–964.

7 M. A. A.Khan, Recent Advances and Applications of Immobilized Enzyme Technologies, *Res. J. Biol. Sci.*, 2010, **5**, 565–575.

8 R. Di Cosimo, J. Mc Auliffe, A. J. Poulose and G. Bohlmann, Industrial use of immobilized enzymes, *Chem. Soc. Rev.*, 2013, **42**, 6437–6474.

9 U. Hanefeld, L. Gardossi and E. Magner, Understanding enzyme immobilisation, *Chem. Soc. Rev.*, 2009, **38**, 453–468.

10 E. M. M. Abdelraheem, H. Busch, U. Hanefeld and F. Tonin, Biocatalysis explained: From pharmaceutical to bulk chemical production, *React. Chem. Eng.*, 2019, **4**, 1878–1894.

11 J. J. Dong, E. Fernández-Fueyo, F. Hollmann, C. E. Paul, M. Pesic, S. Schmidt, Y. Wang, S. Younes and W. Zhang, Biocatalytic Oxidation Reactions: A Chemist's Perspective, *Angew. Chemie - Int. Ed.*, 2018, **57**, 9238–9261.

12 R. A. Sheldon, D. Brady and M. L. Bode, The Hitchhiker's guide to biocatalysis: Recent advances in the use of enzymes in organic synthesis, *Chem. Sci.*, 2020, **11**, 2587–2605.

13 A. Fryszkowska and P. N. Devine, Biocatalysis in drug discovery and development, *Curr. Opin. Chem. Biol.*, 2020, **55**, 151–160.

14 S. Galanie, D. Entwistle and J. Lalonde, Engineering biosynthetic enzymes for industrial natural product synthesis, *Nat. Prod. Rep.*, 2020, **37**, 1122–1143.

15 E. E. Ferrandi and D. Monti, Amine transaminases in chiral amines synthesis: recent advances and challenges, *World J. Microbiol. Biotechnol.*, 2018, **34**, 1–10.

16 T. C. Nugent and M. El-Shazly, Chiral amine synthesis - Recent developments and trends for enamide reduction, reductive amination, and imine reduction, *Adv. Synth. Catal.*, 2010, **352**, 753–819.

17 C. E. Paul, M. Rodríguez-Mata, E. Busto, I. Lavandera, V. Gotor-Fernández, V. Gotor, S. García-Cerrada, J. Mendiola, Ó. De Frutos and I. Collado, Transaminases applied to the synthesis of high added-value enantiopure amines, *Org. Process Res. Dev.*, 2014, **18**, 788–792.

18 D. J. C. Constable, P. J. Dunn, J. D. Hayler, G. R. Humphrey, J. L. Leazer, R. J. Linderman, K. Lorenz, J. Manley, B. A. Pearlman, A. Wells, A. Zaks and T. Y. Zhang, Key green chemistry research areas—a perspective from pharmaceutical manufacturers, *Green Chem.*, 2007, **9**, 411–42.

19 A. Nobili, F. Steffen-Munsberg, H. Kohls, I. Trentin, C. Schulzke, M. Höhne and U. T. Bornscheuer, Engineering the active site of the amine transaminase from vibrio fluvialis for the asymmetric synthesis of aryl-alkyl amines and amino alcohols, *ChemCatChem*, 2015, **7**, 757–760.

20 J. Kress, R. Zanaletti, A. Amour, M. Ladlow, J. G. Frey and M. Bradley, Enzyme accessibility and solid supports: Which molecular weight enzymes can be used on solid supports? An investigation using confocal raman microscopy, *Chem. - A Eur. J.*, 2002, **8**, 3769–3772.

21 C. Mateo, O. Abian, R. Fernandez-Lafuente and J. M. Guisan, Reversible enzyme immobilization via a very strong and nondistorting ionic adsorption on support-polyethylenimine composites, *Biotechnol. Bioeng.*, 2000, **68**, 98–105.

22 K. Ovsejevi, C. Manta and F. Batista-Viera, Reversible covalent immobilization of enzymes via disulfide bonds, *Methods Mol. Biol.*, 2013, **1051**, 89–116.

23 R. A. Sheldon, Cross-Linked Enzyme Aggregates as Industrial Biocatalysts, *Pharm. Process Chem.*, 2010, 159–181.

24 R. M. Donlan, Biofilms: Microbial life on surfaces, *Emerg. Infect. Dis.*, 2002, **8**, 881–890.

25 P. D. Marsh, Dental plaque as a microbial biofilm, *Caries Res.*, 2004, **38**, 204–211.

26 Z. L. J. William Costerton, Microbial Biofilms, *Annu. Rev.Microbiol.*, 1995, **49**, 711–45.

27 B. Halan, K. Buehler and A. Schmid, Biofilms as living catalysts in continuous chemical syntheses, *Trends Biotechnol.*, 2012, **30**, 453–465.

28 B. Díaz-Reinoso, I. Rodríguez-González and H. Domínguez, Towards greener approaches in the extraction of bioactives from lichens, *Rev. Environ. Sci. Biotechnol.*, 2021, **20**, 917–942.

29 W.-F. Su, Radical Chain Polymerization, *Princ. Polym. Des. Synth.*, 2013, **82**, 137–183.

30 J. Y. F.Wang, L.Guo, T.Qiu, A direct polymerization approach toward hindered phenol / polymer composite latex and its application for waterborne damping coating, *Prog. Org. Coatings*, 2019, **130**, 1–7.

31 P. A. Lovell and F. J. Schork, Fundamentals of Emulsion Polymerization, *Biomacromolecules*, 2020, **21**, 4396–4441.

32 A. Guyot, Advances in reactive surfactants, *Adv. Colloid Interface Sci.*, 2004, **108**–**109**, 3–22.

33 M. Danková, A. Kalendová and J. Machotová, Waterborne coatings based on acrylic latex containing nanostructured ZnO as an active additive, *J. Coatings Technol. Res.*, 2020, **17**, 517–529.

34 D. Ahn, K. A. Wier, T. P. Mitchell and P. A. Olney, Applications of Fast , Facile , Radiation-Free Radical Polymerization Techniques Enabled by Room Temperature Alkylborane Chemistry, *Appl. Mater. Interfaces*, 2015, **7**, 23902–23911.

35 L. López De Arbina, M. J. Barandiaran, L. M. Gugliotta and J. M. Asua, Emulsion polymerization: Particle growth kinetics, *Polymer (Guildf).*, 1996, **37**, 5907–5916.

36 S. Krishnan, A. Klein, M. S. El-Aasser and E. D. Sudol, Effect of surfactant concentration on particle nucleation in emulsion polymerization of n-butyl methacrylate, *Macromolecules*, 2003, **36**, 3152–3159.

37 D. Distler, W. S. Neto and F. Machado, Emulsion Polymerization, *Encycl. Mater. Sci. Technol.*, 2001, 2769–2774.

38 S. Cortez, A. Nicolau, M. C. Flickinger and M. Mota, Biocoatings: A new challenge for environmental biotechnology, *Biochem. Eng. J.*, 2017, **121**, 25–37.

39 D. Colombini, H. Hassander, O. J. Karlsson and F. H. J. Maurer, Influence of the particle size and particle size ratio on the morphology and viscoelastic properties of bimodal hard/soft latex blends, *Macromolecules*, 2004, **37**, 6865–6873.

40 M. L. W. Knetsch and L. H. Koole, New strategies in the development of antimicrobial coatings: The example of increasing usage of silver and silver nanoparticles, *Polymers (Basel).*, 2011, **3**, 340–366.

41 M. Zielecka, E. Bujnowska, B. Kępska, M. Wenda and M. Piotrowska, Antimicrobial additives for architectural paints and impregnates, *Prog. Org. Coatings*, 2011, **72**, 193–201.

42 N. Bellotti, R. Romagnoli, C. Quintero, C. Domínguez-Wong, F. Ruiz and C. Deyá, Nanoparticles as antifungal additives for indoor water borne paints, *Prog. Org. Coatings*, 2015, **86**, 33–40.

43 T. J. Bunning, C. W. Lawton, H. E. Klei and D. W. Sundstrom, Physical property improvements of a pellicular biocatalyst, *Bioprocess Eng.*, 1991, **7**, 71–75.

44 M. C. Flickinger, O. I. Bernal, M. J. Schulte, J. J. Broglie, C. J. Duran, A. Wallace, C. B. Mooney and O. D. Velev, Biocoatings : challenges to expanding the functionality of waterborne latex coatings by incorporating concentrated living microorganisms, *J. Coatings Technol. Res.*, 2017, **14**, 791–808.

45 M. Fidaleo, N. Bortone, M. Schulte and M. Flickinger, Ink-Jet Printing of Gluconobacter oxydans: Micropatterned Coatings As High Surface-to-Volume Ratio Bio-Reactive Coatings, *Coatings*, 2014, **4**, 1–17.

46 W. P. Flanagan, H. E. Klei, D. W. Sundstrom and C. W. Lawton, Optimization of a pellicular biocatalyst for penicillin G production by Penicillium chrysogenum, *Biotechnol. Bioeng.*, 1990, **36**, 608–616.

47 N. Martens and E. A. H. Hall, Immobilisation of photosynthetic cells based on film-forming emulsion polymers, *Anal. Chim. Acta*, 1994, **292**, 49–63.

48 R. P. Wool, Pressure-Sensitive Adhesives, Elastomers and Coatings from Plant Oil, *Handb. Biopolym. Biodegrad. Plast. Prop. Process. Appl.*, 2013, 265–294.

49 B. H. S.Eckersley, Mechanistic Considerations of Particle Size Effects on Film Properties of Hard / Soft, *J. Coatings Technol. Res.*, 1997, **69**, 97–107.

50 A. Zosel and G. Ley, Influence of Cross-Linking on Structure, Mechanical Properties, and Stength of Latex films, *Macromolecules*, 1993, **26**, 2222–2227.

51 L. Chen and F. Wu, Properties of polyacrylate latex prepared under different emulsified systems, *J. Wuhan Univ. Technol. Mater. Sci. Ed.*, 2012, **27**, 134–137.

52 J. L. K. A. Tzitxinou, Film Formation of Latex Blends with Bimodal Particle Size Distributions: Consideration of Particle Deformability and Continuity of the Dispersed Phase, *Macromolecules*, 2000, **33**, 2695–2708.

53 E. Macchi and L. A. Felton, Influence of relative humidity during coating on polymer deposition and film formation, *Int. J. Pharm.*, 2016, **510**, 116–124.

54 B. Mesic, M. Cairns, L. Järnstrom, M. Joo Le Guen and R. Parr, Film formation and barrier performance of latex based coating: Impact of drying temperature in a flexographic process, *Prog. Org. Coatings*, 2019, **129**, 43–51.

55 H. N. L.Kornum, Surface defects in drying paint films, *Prog. Org. Coatings*, 1980, **8**, 275–324.

56 A. Kalendová, Methods for testing and evaluating the flash corrosion, *Prog. Org. Coatings*, 2002, **44**, 201–209.

57 J. F. R. Pontes, E. V. Bendinelli, C. da Costa Amorim, M. M. de Sá and A. P. Ordine, Effect of Corrosion Inhibitor Used in Surface Treatment on the Anticorrosive Performance of an Epoxy

Paint System, *Mater. Sci. Appl.*, 2016, **07**, 593–609.

58 A. Barranco, A. Borras, A. R. Gonzalez-Elipe and A. Palmero, Perspectives on oblique angle deposition of thin films: From fundamentals to devices, *Prog. Mater. Sci.*, 2016, **76**, 59–153.

59 J. Livage and D. Ganguli, Sol-gel electrochromic coatings and devices: A review, *Sol. Energy Mater. Sol. Cells*, 2001, **68**, 365–381.

60 O. I. Bernal, B. Bharti, M. C. Flickinger and O. D. Velev, Fabrication of Photoreactive Biocomposite Coatings via Electric Field-Assisted Assembly of Cyanobacteria, *Langmuir*, 2017, **33**, 5304–5313.

61 O. K. Lyngberg, V. Thiagarajan, D. J. Stemke, J. L. Schottel, L. E. Scriven and M. C. Flickinger, A patch coating method for preparing biocatalytic films of Escherichia coli, *Biotechnol. Bioeng.*, 1999, **62**, 44–55.

62 O. K. Lyngberg, D. J. Stemke, J. L. Schottel and M. C. Flickinger, A single-use luciferase-based mercury biosensor using Escherichia coli HB101 immobilized in a latex copolymer film, *J. Ind. Microbiol. Biotechnol.*, 1999, **23**, 668–676.

63 O. K. Lyngberg, C. P. Ng, V. Thiagarajan, L. E. Scriven and M. C. Flickinger, Engineering the microstructure and permeability of thin multilayer latex biocatalytic coatings containing E. Coli, *Biotechnol. Prog.*, 2001, **17**, 1169–1179.

64 L. S. M.Flickinger, J.Schottel, D.Bond, A.Aksan, Painting and Printing Living Bacteria : Engineering Nanoporous Biocatalytic, *Biotechnol. Prog.*, 2007, **23**, 2–17.

65 P. In-Na, A. A. Umar, A. D. Wallace, M. C. Flickinger, G. S. Caldwell and J. G. M. Lee, Loofah-based microalgae and cyanobacteria biocomposites for intensifying carbon dioxide capture, *J. CO2 Util.*, 2020, **42**, 101348.

66 J. S. Jenkins, M. C. Flickinger and O. D. Velev, Deposition of composite coatings from particle-particle and particle-yeast blends by convective-sedimentation assembly, *J. Colloid Interface Sci.*, 2012, **380**, 192–200.

67 Z. Huang, V. S. Thiagarajan, O. K. Lyngberg, L. E. Scriven and M. C. Flickinger, Microstructure

evolution in polymer latex coatings for whole-cell biocatalyst application, *J. Colloid Interface Sci.*, 1999, **215**, 226–243.

68 M. Schneider and T. F. McKenna, Comparative study of methods for the measurement of particle size and size distribution of polymeric emulsions, *Part. Part. Syst. Charact.*, 2002, **19**, 28–37.

69 D. Weichart, R. Lange, N. Henneberg and R. Hengge-Aronis, Identification and characterization of stationary phase inducible genes in Escherichia coli, *Mol. Microbiol.*, 1993, **10**, 407–420.

70 D. A. Siegele and R. Kolter, Life After Log, *J. Bacteriol.*, 1992, **174**, 345–348.

71 A. T. Roberto Kolter, Deborah Siegele, The stationary phase of the bacterial life cycle, *Annu. Rev.Microbiol.*, 1993, 855–874.

72 J. L. Gosse, M. S. Chinn, A. M. Grunden, O. I. Bernal and M. C. Flickinger, A versatile method for preparation of hydrated microbial – latex biocatalytic coatings for gas absorption and gas evolution, *J. Ind. Microbiol. Biotechnol.*, 2012, **39**, 1269–1278.

73 V. B. M. Rosa, A.Gambacorta, L.Lama, B.Nicolaus, Immobilization of thermophilic microbial cells in crude egg white., *Biotechnol. Lett.*, 1981, **3**, 183–186.

74 S. Alka and B. N. Johri, Production of celluloytic enzymes by immobilized Sporotrichum thermophile, *Enzyme Microb. Technol.*, 1990, **12**, 464–468.

75 R. M. Worden, R. Subramanian and M. J. Bly, Growth kinetics of bacillus stearothermophilus BR219, *Appl. Biochem. Biotechnol.*, 1991, **28**, 267–275.

76 O. K. Lyngberg, Æ. C. Solheid, Æ. S. Charaniya and M. C. Flickinger, Permeability and reactivity of Thermotoga maritima in latex bimodal blend coatings at 80 ° C : a model high temperature biocatalytic coating, *Extremophiles*, 2005, **9**, 197–207.

77 M. J. Schulte, J. Wiltgen, J. Ritter, C. B. Mooney and M. C. Flickinger, A high gas fraction, reduced power, syngas bioprocessing method demonstrated with a Clostridium ljungdahlii OTA1 paper biocomposite, *Biotechnol. Bioeng.*, 2016, **113**, 1913–1923.

78 Y. Chen, S. Krings, J. R. Booth, S. A. F. Bon, S. Hingley-Wilson and J. L. Keddie, Introducing Porosity in Colloidal Biocoatings to Increase Bacterial Viability, *Biomacromolecules*, 2020, **21**, 4545–4558.

79 M. Mota, A. Yelshin, M. Fidaleo and M. C. Flickinger, Modelling diffusivity in porous polymeric membranes with an intermediate layer containing microbial cells, *Biochem. Eng. Jounral*, 2007, **37**, 285–293.

80 E. Limousin, N. Ballard and J. M. Asua, The influence of particle morphology on the structure and mechanical properties of films cast from hybrid latexes, *Prog. Org. Coatings*, 2019, **129**, 69–76.

81 X. Chen, S. Fischer and Y. Men, Temperature and relative humidity dependency of film formation of polymeric latex dispersions, *Langmuir*, 2011, **27**, 12807–12814.

82 J. D. P. Wang, M. Sergeeva, L. Lim, Biocatalytic plastics as active and stable materials for biotransformations, *Nat. Biotechnol.*, 1997, **15**, 739–793.

83 I. Gill and A. Ballesteros, Bioencapsulation within synthetic polymers (Part 1): sol-gel encapsulated biologicals., *Trends Biotechnol.*, 2000, **18**, 282–96.

84 S. J. Novick and J. S. Dordick, Investigating the effects of polymer chemistry on activity of biocatalytic plastic materials, *Biotechnol. Bioeng.*, 2000, **68**, 665–671.

85 Y. D. Kim, J. S. Dordick and D. S. Clark, Siloxane-based biocatalytic films and paints for use as reactive coatings, *Biotechnol. Bioeng.*, 2001, **72**, 475–482.

86 M. C. Flickinger and K. L. Swope, Activation and Regeneration of Whole Cell Biocatalysts : Initial and Periodic Induction Behavior in Starved Escherichia coIi after Immobilization in Thin Synthetic Films, *Biotechnol. Adv.*, 1996, **51**, 360–370.

87 J. S. Jenkins, M. C. Flickinger and O. D. Velev, Engineering cellular photocomposite materials using convective assembly, *Materials (Basel).*, 2013, **6**, 1803–1825.

88 O. Bernal, J. Pawlak and M. C. Flickinger, Microbial Paper: Cellulose Fiber-based Photo-Absorber Producing Hydrogen Gas from Acetate using Dry-Stabilized Rhodopseudomonas

palustris, *Bioresources*, 2017, **12**, 4013–4030.

89 O. I. Bernal, C. B. Mooney and M. C. Flickinger, Specific photosynthetic rate enhancement by cyanobacteria coated onto paper enables engineering of highly reactive cellular biocomposite 'leaves', *Biotechnol. Bioeng.*, 2014, **111**, 1993–2008.

90 J. L. Gosse and M. C. Flickinger, Nanoscale Biocatalysis, *Methods Mol. Biol.*, 2011, **743**, 213–222.

91 N. Banaei, E. Z. Kincaid, S. Y. G. Lin, E. Desmond, W. R. Jacobs and J. D. Ernst, Lipoprotein processing is essential for resistance of Mycobacterium tuberculosis to malachite green, *Antimicrob. Agents Chemother.*, 2009, **53**, 3799–3802.

92 S. A. Odom, S. Chayanupatkul, B. J. Blaiszik, O. Zhao, A. C. Jackson, P. V. Braun, N. R. Sottos, S. R. White and J. S. Moore, A self-healing conductive ink, *Adv. Mater.*, 2012, **24**, 2578–2581.

93 E. K. Gamstedt and R. Talreja, Fatigue damage mechanisms in unidirectional carbon-fibre-reinforced plastics, *J. Mater. Sci.*, 1999, **34**, 2535–2546.

94 B. J. Blaiszik, S. L. B. Kramer, S. C. Olugebefola, J. S. Moore, N. R. Sottos and S. R. White, Self-healing polymers and composites, *Annu. Rev. Mater. Res.*, 2010, **40**, 179–211.

95 P. Fratzl and R. Weinkamer, Nature's hierarchical materials, *Prog. Mater. Sci.*, 2007, **52**, 1263–1334.

96 R. P. Wool, Self-healing materials: A review, *Soft Matter*, 2008, **4**, 400–418.

97 X. Zhang and R. M. Waymouth, 1,2-Dithiolane-Derived Dynamic, Covalent Materials: Cooperative Self-Assembly and Reversible Cross-Linking, *J. Am. Chem. Soc.*, 2017, **139**, 3822–3833.

98 S. R. White, N. R. Sottos, P. H. Geubelle, J. S. Moore, M. R. Kessler, S. R. Sriram, E. N. Brown and S. Viswanathan, Autonomic Healing of Polymer Composites, *Nature*, 2001, **409**, 794–797.

99 T. Szabó, L. Molnár-Nagy, J. Bognár, L. Nyikos and J. Telegdi, Self-healing microcapsules and slow release microspheres in paints, *Prog. Org. Coatings*, 2011, **72**, 52–57.

100 F. Safaei, S. N. Khorasani, H. Rahnama, R. E. Neisiany and M. S. Koochaki, Single microcapsules

containing epoxy healing agent used for development in the fabrication of cost efficient self-healing epoxy coating, *Prog. Org. Coatings*, 2018, **114**, 40–46.

101 X. M. Na, F. Gao, L. Y. Zhang, Z. G. Su and G. H. Ma, Biodegradable microcapsules prepared by self-healing of porous microspheres, *ACS Macro Lett.*, 2012, **1**, 697–700.

102 K. S. Toohey, N. R. Sottos, J. A. Lewis, J. S. Moore and S. R. White, Self-healing materials with microvascular networks, *Nat. Mater.*, 2007, **6**, 581–585.

103 W. M. Huang, Z. Ding, C. C. Wang, J. Wei, Y. Zhao and H. Purnawali, Shape memory materials, *Mater. Today*, 2010, **13**, 54–61.

104 M. Behl, J. Zotzmann and A. Lendlein, Shape-Memory Polymers and Shape-Changing Polymers, *Adv. Polym. Sci.*, 2009, **226**, 1–40.

105 A. Kirillova and L. Ionov, Shape-changing polymers for biomedical applications, *J. Mater. Chem. B*, 2019, **7**, 1597–1624.

106 G. I. Peterson, M. B. Larsen and A. J. Boydston, Controlled depolymerization: Stimuli-responsive self-immolative polymers, *Macromolecules*, 2012, **45**, 7317–7328.

107 H. Tang, Y. Luan, L. Yang and H. Sun, A perspective on reversibility in controlled polymerization systems: Recent progress and new opportunities, *Molecules*, 2018, **23**, 2870.

108 J. Y. R. Silva, Y. G. Proenza, L. L. da Luz, S. de Sousa Araújo, M. A. G. Filho, S. A. Junior, T. A. Soares and R. L. Longo, A thermo-responsive adsorbent-heater-thermometer nanomaterial for controlled drug release: (ZIF-8,EuxTby)@AuNP core-shell, *Mater. Sci. Eng. C*, 2019, **102**, 578–588.

109 Y. Yang and M. W. Urban, Self-Repairable Polyurethane Networks by Atmospheric Carbon Dioxide and Water, *Angew. Chemie*, 2014, **53**, 12142–12147.

110 X. Chen, M. A. Dam, K. Ono, A. Mal, H. Shen, S. R. Nutt, K. Sheran and F. Wudl, A thermally Re-mendable Cross-Linked Polymeric Material, *Science (80-.).*, 2002, **295**, 1698–1702.

111 M. Burnworth, L. Tang, J. R. Kumpfer, A. J. Duncan, F. L. Beyer, G. L. Fiore, S. J. Rowan and C. Weder, Optically healable supramolecular polymers, *Nature*, 2011, **472**, 334–337.

112 C. H. Li, C. Wang, C. Keplinger, J. L. Zuo, L. Jin, Y. Sun, P. Zheng, Y. Cao, F. Lissel, C. Linder, X. Z. You and Z. Bao, A highly stretchable autonomous self-healing elastomer, *Nat. Chem.*, 2016, **8**, 618–624.

113 L. Huang, N. Yi, Y. Wu, Y. Zhang, Q. Zhang, Y. Huang, Y. Ma and Y. Chen, Multichannel and repeatable self-healing of mechanical enhanced graphene-thermoplastic polyurethane composites, *Adv. Mater.*, 2013, **25**, 2224–2228.

114 C. C. Corten, M. W. Urban and F. Shelby, Repairing polymers using an oscillating magnetic field, *Adv. Mater.*, 2009, **21**, 5011–5015.

115 Y. Yang, D. Davydovich, C. C. Hornat, X. Liu and M. W. Urban, Leaf-Inspired Self-Healing Polymers, *Chem*, 2018, **4**, 1928–1936.

116 H. M. Jonkers, A. Thijssen, G. Muyzer, O. Copuroglu and E. Schlangen, Application of bacteria as self-healing agent for the development of sustainable concrete, *Ecol. Eng.*, 2010, **36**, 230–235.

117 H. Chen, C. Qian and H. Huang, Self-healing cementitious materials based on bacteria and nutrients immobilized respectively, *Constr. Build. Mater.*, 2016, **126**, 297–303.

118 T. Xu, S. Petridou, E. H. Lee, E. A. Roth, N. R. Vyavahare, J. J. Hickman and T. Boland, Construction of High-Density Bacterial Colony Arrays and Patterns by the Ink-Jet Method, *Biotechnol. Bioeng.*, 2004, **85**, 29–33.

119 H. Y. Gan, X. Shan, T. Eriksson, B. K. Lok and Y. C. Lam, Reduction of droplet volume by controlling actuating waveforms in inkjet printing for micro-pattern formation, *J. Micromechanics Microengineering*, 2009, **19**, 55010–55019.

120 K. Yan, J. Li, L. Pan and Y. Shi, Inkjet printing for flexible and wearable electronics, *APL Mater.*, 2020, **8**, 120705.

121 R. D. Boehm, P. R. Miller, J. Daniels, S. Stafslien and R. J. Narayan, Inkjet printing for pharmaceutical applications, *Mater. Today*, 2014, **17**, 247–252.

122 R. E. Saunders and B. Derby, Inkjet printing biomaterials for tissue engineering: Bioprinting,

Int. Mater. Rev., 2014, **59**, 430–448.

123 T. Xu, J. Jin, C. Gregory, J. J. Hickman and T. Boland, Inkjet printing of viable mammalian cells, *Biomaterials*, 2005, **26**, 93–99.

124 L. Ning, H. Sun, T. Lelong, R. Guilloteau, N. Zhu, D. J. Schreyer and X. Chen, 3D bioprinting of scaffolds with living Schwann cells for potential nerve tissue engineering applications, *Biofabrication*, 2018, **10**, 035014.

125 A. Negro, T. Cherbuin and M. P. Lutolf, 3D Inkjet Printing of Complex, Cell-Laden Hydrogel Structures, *Sci. Rep.*, 2018, **8**, 1–9.

126 J. T. Delaney, P. J. Smith and U. S. Schubert, Inkjet printing of proteins, *Soft Matter*, 2009, **5**, 4866–4877.

127 C. Cui, D.-O. Kim, M. Y. Pack, B. Han, L. Han, Y. Sun and L.-H. Han, 4D printing of self-folding and cell-encapsulating 3D microstructures as scaffolds for tissue-engineering applications, *Biofabrication*, 2020, **12**, 045018.

128 M. Hamdani, B. De Jeso, H. Deleuze and B. Maillard, Derivatives of the product of Baker's yeast reduction of ethyl acetoacetate as precursors of free radical chirons of the 2(S)-hydroxypropyl moiety, *Tetrahedron: Asymmetry*, 1991, **2**, 867–870.

129 W. Baik, J. Lim Han, K. Chang Lee, N. Ho Lee, B. Hyo Kim and J. T. Hahn, Selective reduction of aromatic nitro compounds to aromatic amines by Baker's Yeast in basic solution, *Tetrahedron Lett.*, 1994, **35**, 3965–3966.

130 F. Li, J. Cui, X. Qian and R. Zhang, A novel strategy for the preparation of arylhydroxylamines: Chemoselective reduction of aromatic nitro compounds using bakers' yeast, *Chem. Commun.*, 2004, 2338–2339.

131 P. Soni and U. C. Banerjee, Enantioselective reduction of acetophenone and its derivatives with a new yeast isolate Candida tropicalis PBR-2 MTCC 5158, *Biotechnol. J.*, 2006, **1**, 80–85.

132 V. Waagen, V. Partali, I. Hollingsaeter, M. S. Huang and T. Anthonsen, Stereoselectivity of Baker's yeast reduction of 2-propanones: influence of substituents., *Acta Chem. Scand.*, 1994,

48, 506–510.

133 S. Rodríguez, M. Kayser and J. D. Stewart, Improving the stereoselectivity of bakers' yeast reductions by genetic engineering, *Org. Lett.*, 1999, **1**, 1153–1155.

134 E. P. Siqueira Filho, J. A. R. Rodrigues and P. J. S. Moran, Baker's yeast reduction of α-methyleneketones, *Tetrahedron Asymmetry*, 2001, **12**, 847–852.

135 A. J. Smallridge and M. A. Trewhella, Yeast-Mediated Reactions in Organic Solvents, *Enzym. Nonaqueous Solvents*, 2003, **15**, 417–422.

136 H. Alexandre, V. Ansanay-Galeote, S. Dequin and B. Blondin, Global gene expression during short-term ethanol stress in Saccharomyces cerevisiae, *FEBS Lett.*, 2001, **498**, 98–103.

137 A. Bryan, C. Hart, M. Wise and B. Roberts, Glucose Concentrations Effect on Rate of Fermentation in Yeast, *J. Undergrad. Biol. Lab. Investig.*, 2018, **1**, 1–4.

138 A. M. Klibanov, Asymmetric enzymatic oxidoreductions in organic solvents, *Curr. Opin. Biotechnol.*, 2003, **14**, 427–431.

139 V. Gotor-Fernández and C. E. Paul, Deep eutectic solvents for redox biocatalysis, *J. Biotechnol.*, 2019, **293**, 24–35.

140 V. S. Green, D. E. Stott and M. Diack, Assay for fluorescein diacetate hydrolytic activity: Optimization for soil samples, *Soil Biol. Biochem.*, 2006, **38**, 693–701.

141 P. Breeuwer, J. L. Drocourt, N. Bunschoten, M. H. Zwietering, F. M. Rombouts and T. Abee, Characterization of uptake and hydrolysis of fluorescein diacetate and carboxyfluorescein diacetate by intracellular esterases in Saccharomyces cerevisiae, which result in accumulation of fluorescent product, *Appl. Environ. Microbiol.*, 1995, **61**, 1614–1619.

142 M. Nikolova, I. Savova and M. Marinov, An Optimised Method For Investigation Of The Yeast Viability By Means of Fluorescent Microscopy, *J. Cult. Collect.*, 2000, **3**, 66–71.

143 U. Dittmer and H. C. Weltzien, A Rapid Viability Test for Sclerotia with Fluorescein Diacetate, *J. Phytopathol.*, 1990, **130**, 59–64.

144 V. Kumthekar and S. Kolekar, Attributes of the latex emulsion processing and its role in

morphology and performance in paints, *Prog. Org. Coatings*, 2011, **72**, 380–386.

145 C. Fang and Z. Lin, Effect of propyleneimine external cross-linker on the properties of acrylate latex pressure sensitive adhesives, *Int. J. Adhes. Adhes.*, 2015, **61**, 1–7.

146 A. Ouzas, E. Niinivaara, E. D. Cranston and M. A. Dubé, Synthesis of poly(isobutyl acrylate/n-butyl acrylate/methyl methacrylate)/CNC nanocomposites for adhesive applications via in situ semi-batch emulsion polymerization, *Polym. Compos.*, 2019, **40**, 1365–1377.

147 M. C. Flickinger, M. Fidaleo, J. Gosse, K. Polzin, S. Charaniya, C. Solheid, O. K. Lyngberg, M. Laudon, H. Ge, J. L. Schottel, D. R. Bond, A. Aksan and L. E. Scriven, Engineering Nanoporous Bioactive Smart Coatings Containing Microorganisms : Fundamentals and Emerging Applications, *ACS Symp. Ser.*, 2009, **1002**, 52–94.

148 J. L. Gosse, B. J. Engel, J. C.-H. Hui, C. S. Harwood and M. C. Flickinger, Progress toward a biomimetic leaf: 4,000 h of hydrogen production by coating-stabilized nongrowing photosynthetic Rhodopseudomonas palustris, *Biotechnol. Prog.*, 2010, **26**, 907–918.

149 C. Y. Kan, S. De Liu, X. Z. Kong and X. L. Zhu, Study on the preparation and properties of styrene-butyl acrylate - Silicone copolymer latices, *J. Appl. Polym. Sci.*, 2001, **82**, 3194–3200.

150 F. Ziaee and M. Nekoomanesh, Monomer reactivity ratios of styrene-butyl acrylate copolymers at low and high conversions, *Polymer (Guildf).*, 1998, **39**, 203–207.

151 W. M. Cheng, X. M. Hu, Y. Y. Zhao, M. Y. Wu, Z. X. Hu and X. T. Yu, Preparation and swelling properties of poly(acrylic acid-co-acrylamide) composite hydrogels, *E-Polymers*, 2017, **17**, 95–106.

152 M. Soleimani, J. C. Haley, W. Lau and M. A. Winnik, Effect of hydroplasticization on polymer diffusion in poly(butyl acrylate-co-methyl methacrylate) and poly(2-ethylhexyl acrylate-co-tert-butyl methacrylate) latex films, *Macromolecules*, 2010, **43**, 975–985.

153 J. Yang, H. Liang, L. Zeng, S. Liu and T. Guo, Facile Fabrication of Superhydrophobic Nanocomposite Coatings Based on Water-Based Emulsion Latex, *Adv. Mater. Interfaces*, 2018, **5**, 1–8.

154 T. Abee, Á. T. Kovács, O. P. Kuipers and S. van der Veen, Biofilm formation and dispersal in Gram-positive bacteria, *Curr. Opin. Biotechnol.*, 2011, **22**, 172–179.

155 A. M. Ruffing, Engineered cyanobacteria: Teaching an old bug new tricks, *Bioeng. Bugs*, 2011, **2**, 136–149.

156 M. C. Flickinger, O. K. Lyngberg, E. A. Freeman, C. R. Anderson and M. C. Laudon, Formulation of reactive nanostructured adhesive microbial ink-jet inks for miniature biosensors and biocatalysis, *ACS Symp. Ser.*, 2009, **1008**, 156–187.

157 W. L. Marques, V. Raghavendran, B. U. Stambuk and A. K. Gombert, Sucrose and Saccharomyces cerevisiae: A relationship most sweet, *FEMS Yeast Res.*, 2015, **16**, 1–16.

158 S. J. F. Erich, O. C. G. Adan, L. Pel, H. P. Huinink and K. Kopinga, NMR imaging of coatings on porous substrates, *Chem. Mater.*, 2006, **18**, 4500–4504.

159 F. D. Gunstone, Enzymes as biocatalysts in the modification of natural lipids, *J. Sci. Food Agric.*, 1999, **79**, 1535–1549.

160 V. M. Balcão and F. X. Malcata, Lipase catalyzed modification of milkfat, *Biotechnol. Adv.*, 1998, **16**, 309–341.

161 D. Otzen, Protein-surfactant interactions: A tale of many states, *Biochim. Biophys. Acta - Proteins Proteomics*, 2011, **1814**, 562–591.

162 R. D. Schmid and R. Verger, Lipases : Interfacial Enzymes with Attractive Applications, *Analysis*, 1998, **37**, 1608–1633.

163 J. Y. Park, J. Ha, Y. Choi, P. S. Chang and K. M. Park, Optimization of Spectrophotometric and Fluorometric Assays Using Alternative Substrates for the High-Throughput Screening of Lipase Activity, *J. Chem.*, 2021, **2021**, 1–10.

164 P. In-na, E. B. Sharp, G. S. Caldwell, M. G. Unthank, J. J. Perry and J. G. M. Lee, Engineered living photosynthetic biocomposites for intensified biological carbon capture, *Sci. Rep.*, 2022, **12**, 1–15.

165 S. Mazard, A. Penesyan, M. Ostrowski, I. T. Paulsen and S. Egan, Tiny Microbes with a Big

Impact: The role of cyanobacteria and Their Metabolites in Shaping Our Future, *Mar. Drugs*, 2016, **14**, 1–19.

166 M. Bozan, A. Schmid and K. Bühler, Evaluation of self-sustaining cyanobacterial biofilms for technical applications, *Biofilm*, 2022, **4**, 100073.

167 D. C. Ducat, G. Sachdeva and P. A. Silver, Rewiring hydrogenase-dependent redox circuits in cyanobacteria, *Proc. Natl. Acad. Sci. U. S. A.*, 2011, **108**, 3941–3946.

168 E. Chrapusta, A. Kaminski, K. Duchnik, B. Bober, M. Adamski and J. Bialczyk, Mycosporine-Like Amino Acids: Potential health and beauty ingredients, *Mar. Drugs*, 2017, **15**, 1–29.

169 J. Kumar, D. Singh, M. B. Tyagi and A. Kumar, Cyanobacteria: Applications in Biotechnology, *Cyanobacteria*, 2018, **7421**, 327–346.

170 W. Schrimpf, A. Barth, J. Hendrix and D. C. Lamb, PAM: A Framework for Integrated Analysis of Imaging, Single-Molecule, and Ensemble Fluorescence Data, *Biophys. J.*, 2018, **114**, 1518–1528.

171 P. C. S. Dal'Belo, L. Gasper, Moisturizing effect of cosmetic formulations containing Aloe vera extract, *Ski. Res. Technol.*, 2006, **12**, 241–246.

172 T. Ekins-coward, K. V. K. Boodhoo, S. Velasquez-orta, G. Caldwell, A. Wallace, R. Barton and M. C. Flickinger, A Microalgae Biocomposite-Integrated Spinning Disk Bioreactor (SDBR): Toward a Scalable Engineering Approach for Bioprocess Intensi fi cation in Light-Driven CO2 Absorption Applications, *Ind. Eng. Chem. Res.*, 2019, **58**, 5936-59–49.

173 B. F. Gibbs and C. N. Mulligan, Styrene toxicity: An ecotoxicological assessment, *Ecotoxicol. Environ. Saf.*, 1997, **38**, 181–194.

174 J. Hu, R. Mo, X. Sheng and X. Zhang, A self-healing polyurethane elastomer with excellent mechanical properties based on phase-locked dynamic imine bonds, *Polym. Chem.*, 2020, **11**, 2585–2594.

175 G. Sinawang, M. Osaki, Y. Takashima, H. Yamaguchi and A. Harada, Supramolecular self-healing materials from non-covalent cross-linking host-guest interactions, *Chem. Commun.*,

2020, **56**, 4381–4395.

176 J. Angst, R. Sellar and K. R. Merikangas, On the tensile strength and hardness relation for metals, *J. Mater. Eng. Perform.*, 2001, **10**, 718–722.

177 G. I. Kanel, Rate and temperature effects on the flow stress and tensile strength of metals, *AIP Conf. Proc.*, 2012, **1426**, 939–944.

178 A. V. Tobolsky and P. F. Lyons, Tensile strength of rubbers, *J. Polym. Sci. Part A-2 Polym. Phys.*, 1968, **6**, 1561–1566.

179 X. Chen, J. Zhu, Y. Luo, J. Chen, X. Ma, D. Bukhvalov, H. Liu, M. Zhang and Z. Luo, Molecular dynamics simulation insight into the temperature dependence and healing mechanism of an intrinsic self-healing polyurethane elastomer, *Phys. Chem. Chem. Phys.*, 2020, **22**, 17620–17631.

180 V. N. Kozhevnikov, M. E. Deary, T. Mantso, M. I. Panayiotidis and M. T. Sims, Iridium(iii) complexes of 1,2,4-triazines as potential bioorthogonal reagents: metal coordination facilitates luminogenic reaction with strained cyclooctynes, *Chem. Commun.*, 2019, **55**, 14283–14286.

181 T. S. M. Tang, H. W. Liu and K. K. W. Lo, Monochromophoric iridium(III) pyridyl-tetrazine complexes as a unique design strategy for bioorthogonal probes with luminogenic behavior, *Chem. Commun.*, 2017, **53**, 3299–3302.

182 H. Mohsin, U. Sultan, Y. F. Joya, S. Ahmed, M. S. Awan and S. N. Arshad, Development and characterization of cobalt based nanostructured super hydrophobic coating, *IOP Conf. Ser. Mater. Sci. Eng.*, 2016, **146**, 2–8.

183 N. R. Moheimani and M. A. Borowitzka, Standard Methods for Measuring Growth of Algae and Their Composition, *Algae for Biofuels and Energy*, 2013, **5**, 265–284.